

Structure of binary mixed polymer Langmuir layers

Cecilia Bernardini

Thesis committee

Thesis supervisors

Prof. dr. M.A. Cohen Stuart
Professor of Physical Chemistry and Colloid Science
Wageningen University

Prof. dr. F.A.M. Leermakers
Personal chair at the Laboratory of Physical Chemistry and Colloid Science
Wageningen University

Other members

Prof. dr. C.J.M. van Rijn, Wageningen University

Prof. dr. A.J. Schouten, University of Groningen

Dr. P. Guenoun, Laboratoire Interdisciplinaire sur l'Organisation Nanométrique et Supramoléculaire (LIONS), C.E.A. Saclay, France

Prof. dr. ir. J. Vermant, Catholic University of Leuven, Belgium

This research was conducted under the auspices of the Graduate School VLAG

Structure of binary mixed polymer Langmuir layers

Cecilia Bernardini

Thesis

submitted in fulfillment of the requirements for the degree of doctor

at Wageningen University

by the authority of the Rector Magnificus

Prof. dr. M.J. Kropff,

in the presence of the

Thesis Committee appointed by the Academic Board

to be defended in public

on Friday 27th April 2012

at 1:30 p.m. in the Aula.

Cecilia Bernardini

Structure of binary mixed polymer Langmuir layers

208 pages

Thesis, Wageningen University, Wageningen, NL (2012)

With references, with summaries in Dutch and English

ISBN 978-94-6173-214-9

Table of contents

Chapter 1	General Introduction	1
Chapter 2	Two–Dimensional Colloids: Preparation, Characterization and Research Perspectives	9
Chapter 3	Polymers at the Water/Air Interface: Surface Pressure Isotherms and Molecularly Detailed Modeling	65
Chapter 4	PMMA Highlights the Layering Transition of PDMS in Langmuir Films	103
Chapter 5	Polymer Compatibility in Two Dimensions: Modeling of Phase Behavior of Mixed Polymethacrylate Langmuir Films	135
Chapter 6	Summary and General Discussion	163
	Samenvatting	177
	Riassunto	181
	Curriculum Vitae	187
	List of publications	189
	Afterword	191
	Overview of completed training activities	199

The very fact that a Line is visible implies that it possesses yet another Dimension.

E. A. Abbott, *Flatland*

Chapter 1

General Introduction

1. Langmuir monolayers through human history

The subject of spreading and observing the behavior of immiscible liquids seems to have fascinated humankind since the beginning of historical accounts. One of the earliest civilizations, the Sumerians, credited with having devised the oldest script, were also the first to report on the spreading of oil on top of water¹. This ancient culture practiced a poorly known form of divination by pouring oil onto water (or water onto oil) and observing the ensuing behavior to infer future destiny of individuals, as well as reigns. During the 19th and 20th century archaeologists found written accounts on this practice: "if from the middle of the oil a drop appears towards the sun (i.e., eastward) and remains stationary: if one proceeds on a campaign he will enjoy a share in the booty: for the sick there will be recovery." This text dates back to the first Babylonian dynasty (1894–1595 B.C.). Other texts have been translated and contain descriptions of several phenomena relevant to the surface science domain: spreading and retraction, the formation of fingers of oil, of droplets, of globules, the attachment of the oil to the edge of the bowl, a shiny or dull appearance in the oil film, interference colors and black films. It is absolutely amazing to discover how much developed was the perception of such phenomena so long ago. A thousand years later, this practice was adopted by the Greeks, who named it lecanomancy (from the words *λεκάνη* = bowl, and *μαντεία* = divination).

The most cited records of monolayers regard dampening of waves on the sea surface, caused by spreading of oil, which was already observed by sailors in ancient times and described by Plutarch, Aristotle and Plinius² "...hieme mare calidius esse, autumnale salsius; omne oleo tranquillari, et ob id urinantes ore spargere, quoniam mitiget naturam asperam lucemque deportet...". In the V century A.D. Costantius of Lyon³ described the storm that almost sunk the ship on which St. Germanus, bishop in Auxerre, was travelling. Despite the mystic account, which evokes Christian rituals and resembles a miracle operated by faith, the facts remind of this practical knowledge, common among sailors that was not lost during transition to medieval time, but kept to be exploited over the centuries.

However, the first scientific investigation of this phenomenon is much more recent, and dates back only to 1774, when Benjamin Franklin made his famous Clapham Pond experiment⁴, where he reported that "...the oil, though not more than a teaspoonful... spread amazingly... making all that quarter of the pond, perhaps half an acre, as smooth as a looking glass...". The first quantitative account on the effect of spreading oil on the water surface is due to Lord Rayleigh, who measured a lowering of the surface tension of the water⁵. This experiment is

also the first one in which an estimation of the dimensions of molecules has been practically obtained (although this would have been understood only later on by Rayleigh himself): the thickness of the oil film formed on water was calculated to be 16 Å, on the basis of density values and area measurements. Modern study of spread molecular films clearly began with the experiments of Agnes Pockels in Germany, around 1882, carried out in the family kitchen, when she was only 18 years old. In a systematic study⁶, published after she wrote to Lord Rayleigh about her accomplishments, she described experiments where she compressed layers containing different amounts of oil on the water surface with ‘barriers’, thus observing that very small amounts of oil on the surface of water have no appreciable effect on the surface tension, but that the surface tension begins to decrease suddenly when the amount of oil per unit area is increased beyond a certain sharp limit. By that time she had invented many of the techniques which are now standard “tools of the trade”: in addition to the trough technique, she introduced the use of volatile solvents to assist, and quantify, spreading. What we now call surface pressure/area curves were first published by her in a paper from 1893. While most of the substances she worked with were not well-defined chemical compounds, it is amazing to note that, if the data in her 1892 notes are converted to modern terms, the molecular area⁷ she obtained for stearic acid was 22 Å²! Basing his reasoning on these experimental accounts, later on Lord Rayleigh hypothesized that, at this area, the oil molecules were closely packed, forming a monomolecular film, and deduced the dimensions of oil molecules⁸.

The pioneer of modern surface science in the XX century has been undoubtedly Irving Langmuir. Using pure substances, he elaborated on the dimensions of molecules, by calculating the cross-section area and film thickness of various pure substances spread at the air/water interface, deducing that molecules are not spherical objects, and display an orientation at the interface. He hypothesized that spreading of films on surfaces is determined by the shapes of molecules and the relative activities of the different portions of the molecules⁹. He was also the first to report how these monomolecular films could be transferred from the water surface, to a solid substrate¹⁰, but the one who undoubtedly proved the possibility to transfer monomolecular films in a sequential way, forming multilayered films, was Katharine Blodgett¹¹, in 1935, a scientist who collaborated with Langmuir to the investigation of this topic since the 1920s. The development of this technique opens up the opportunity of technological exploitation of monolayers, bringing us to the most modern advances achieved in surface science nowadays.

2. Langmuir monolayers in modern science

The development of advanced materials for technological applications is a highly pursued goal of today scientists. One of the most important factors in their synthesis and fabrication is the control of their structure at the nanoscale, in order to maximize their performance. The most recent achievements in this area have been obtained through the so called “top–down” approach, by using microfabrication techniques to shape well–defined microstructures. All silicon–based technologies rely on this approach. However, scientists are well aware of intrinsic limitations of top–down approaches, such as Moore’s law, and are actively investigating novel strategies to overcome this issue. The new approach, now widely investigated, is called “bottom–up”, since it relies on the spontaneous ability of molecules to self–assemble, driven by physical and chemical forces, into hierarchical, well–defined structures at the nanoscale level, up to macroscopic dimensions. Some self–assembly processes can be designed to get structures that have a predefined morphology: very often in this case interfacial processes are involved. Langmuir–Blodgett films are among these self–assembled structures, and are obtained through the preparation of Langmuir monolayers. The medium used to prepare Langmuir films is the air/water interface. This interface has several interesting features as a medium: it is a molecularly flat environment; it is a boundary region between two phases with different dielectric constants; it is a highly dynamic medium within the two–dimensional plane of the interface, which allows mobility of the molecules inside the horizontal plane; finally, it provides an access point between hydrophobic and hydrophilic compounds. For all these reasons, the air/water interface offers a unique opportunity to investigate self–assembly of molecules, disclosing wide opportunities to scientists that pursue both fundamental studies (such as the origin of cell membrane formation, and consequently, the beginning of life) and more applied investigations (biophysics, biomineralisation studies, molecular recognition at interfaces, chiral recognition, synthesis of nanostructured materials)¹².

3. Nanostructuring in surface science: new approaches based on Langmuir monolayers and outline of this thesis

The renewed interest of scientists in the applications of the LB technique over the last two decades has resulted in the production of a large body of literature: an ample amount of studies covers not only the spreading behavior and properties of conventional amphiphiles, but also that one of carbon nanotubes, inorganic nanomaterials, organic nanocrystals and several polymers. Nowadays the palette

available to the scientist who wants to prepare nanostructured thin films is huge and varied, offering several opportunities to tune both chemical properties and self-assembly behavior of thin films at the micro and nanoscale level. Particularly interesting is the application of polymers to the buildup of nanostructured films: these molecules are available through a vast amount of standard synthesis procedures, and can be prepared with a complete and wide range of functional chemical groups, according to the properties that the scientist wishes to introduce in the new material. In order to achieve the control over the patterning of several polymers in a thin film, a widely pursued strategy is the use of block copolymers, which self-assemble over scales from a few nanometers up to several micrometers¹³. Patterns (dot, stripes etc.) can be manipulated by changing length and type of block copolymers used. Though this strategy is promising and versatile, it requires an *ad hoc* synthesis of the block copolymers, which must be carried out in adequately controlled conditions (the so-called “living”, or controlled polymerization techniques). The molecular architecture embodies the self-assembly characteristics, and so it has to be precisely determined and controlled. The quest for even simpler strategies, therefore, never ends. The possibility of the development of a new, suggestive approach has been investigated in this thesis. This approach is inspired by the observation of the phase behavior of Langmuir monolayers: analogously to every substance in bulk quantities, also Langmuir films form two-dimensional gases, liquids, and solids, by changing the lateral pressure and concentration of molecules. They also form 2D mixtures, which respond to changes of lateral pressure and concentration thanks to the lateral mobility of molecules allowed by the fluid/fluid interface. When two compounds are mixed, analogously to the 3D bulk case, they might interact favorably or unfavorably. In the former case a homogeneous mixture is obtained, while in the latter demixing is observed. The achievement of the dispersion and stabilization of immiscible compounds is the subject of investigation of colloid science: while in bulk conditions this issue has been fully explored, there are much less accounts on how to do the same in monomolecular films. The aim of this thesis is to explore the possibilities to prepare and stabilize 2D dispersions, focusing on polymer-based ones, due to their technological relevance for fabrication of “smart materials”. In order to do so, a combined experimental and theoretical approach has been developed, since fundamental knowledge of the type of interactions relevant to the creation of 2D colloids is scarce. The SCF (Self Consistent Field) approach has allowed to model the behavior of polymers in bulk systems successfully: here the aim is to apply this modeling technique to thin films, in order to describe the

behavior observed in parallel experiments more accurately, and to provide feedback on which materials are suitable to the preparation of a stable, polymer-based, 2D colloid.

A comprehensive review of the state of the art of the preparation and investigation of 2D colloids is the subject of **Chapter 2**. This chapter introduces to the field of research of this thesis, by providing a general definition of the concept of a 2D colloid, followed by a section that summarizes the most relevant instruments and experimental tools available for the investigation of these systems. The next sections present a comprehensive *excursus* of systems suitable to the preparation of a 2D colloid dispersion, ranging from lipid-based systems (the first and most widely investigated ones at the moment, also for the biological relevance of these studies), to short fluorinated amphiphiles and fluorinated and non-fluorinated polymer-based mixtures. This review of the field clearly brings out that the polymer-based mixtures are a poorly explored subject, compared to amphiphiles of natural origin, and so the following chapters have been devoted to the investigation of polymer Langmuir monolayers.

Chapter 3 deals with the setup of the SCF modeling of Langmuir monolayers made of a single pure homopolymer: four water-insoluble homopolymers, with an increasing amphiphilicity degree have been selected, and their pressure/area isotherms recorded. Then SCF calculations have been carried out, in order to reproduce qualitatively the results obtained from the experiments: parameters employed in the model have been varied and the calculated isotherms have been compared to the experimental ones, until a satisfactory match was achieved.

Two of the four polymers studied, poly(methylmethacrylate) (PMMA) and poly(dimethylsiloxane) (PDMS) have been selected, according to their properties, for the preparation of binary mixed Langmuir monolayers, which are dealt with in **Chapter 4**. In this chapter an experimental investigation of binary mixed Langmuir monolayers is carried out, by recording pressure/area isotherms and observing the film morphology with the Brewster Angle Microscope (BAM). Furthermore, ternary mixtures, in which a PMMA-*b*-PDMS diblock copolymer was added to the homopolymer blend, are also investigated: in case of formation of a 2D emulsion, the diblock copolymer is expected to adsorb at the contact line between phase-separated domains, lowering the tension of the three-phase line (line tension, the analog of the surface tension in bulk 3D systems) and allowing an efficient control of the size and shape of the homopolymer domains. In order to account for the experimental findings, an SCF model was developed, which builds on the conclusions of Chapter 3. This model provided insights into the 2D behavior of

both binary and ternary mixtures: in particular, experimental evidence shows that control and stabilization of 2D emulsions made of PDMS and PMMA is not achievable. The SCF calculations demonstrate that a complex interplay of interactions leads to a demixing of the two polymers along the direction *normal* to the air/water interface, rather than parallel. Since a successful emulsification process depends on a demixing occurring exclusively in the direction parallel to the interface, the layering phenomena observed in the SCF model explains effectively the outcome of the experiments.

Chapter 5 deals with the question of which are the suitable conditions for successful in-plane phase separation. Again, we utilize SCF modeling, and we investigate a series of polymethacrylate-based mixtures. It shows that in order to obtain a 2D emulsion the crucial parameter to control is the amphiphilicity of both the mixed homopolymers. In particular, sufficient matching of amphiphilicity of both the compounds is absolutely needed to observe the occurrence of demixing exclusively along a direction parallel to the air/water interface. This can be obtained by using two different types of polymethylmethacrylates, where the backbone structure is the same, but the lateral functional groups are different. It has been demonstrated that a sufficient mismatch in the length of pending alkyl groups allows the occurrence of a lateral phase separation, leading to the successful formation of a 2D emulsion. Results of the calculations are in good agreement with experimental evidence found in literature, which represents an independent proof of the validity of the developed model. Furthermore, calculations with ternary mixtures have been carried out. A diblock copolymer made from the two components of the binary mixtures was added: results evidenced that – as anticipated – the diblock adsorbs preferentially at the interfacial contact line between the two homopolymers, paralleling the behavior of a surfactant in bulk, 3D systems. Therefore the diblock copolymer acts as a “*lineactant*” and reduces the line tension at the domain boundaries. These results provide an insight into which system could be used successfully in experiments aimed at preparing a 2D emulsion.

Finally, in **Chapter 6**, a summary of the content of the thesis is provided, followed by a general discussion summarizing the fundamental insight into the behavior of 2D polymer-based colloids, and the implications for applied research, in particular the feasibility of a lineactant-based approach for the preparation of technologically-relevant materials.

Bibliography

- (1) *Journal of Colloid and Interface Science* **1980**, 75, 240.
- (2) Plinius the Elder *Naturalis Historia*; Vol. II.
- (3) Costantius of Lyon *Vita Sancti Germani Episcopi*; Vol. 13.
- (4) Franklin, B. *Philos. Trans. R. Soc. London*, 64, 445.
- (5) Lord Rayleigh *Proc. R. Soc. Ser. A* **1890**, 47, 364.
- (6) Pockels, A. *Nature (London)* **1891**, 43, 437.
- (7) Gaines, G. L. *Thin Solid Films* **1983**, 99, ix.
- (8) Lord Rayleigh *Phil. Mag.* **1899**, 48, 321.
- (9) Langmuir, I. *J. Am. Chem. Soc.* **1917**, 39, 1848.
- (10) Irving Langmuir et al. *Trans. Faraday Soc.* **1920**, 15, 62.
- (11) Katharine Blodgett et al. *J. Am. Chem. Soc.* **1935**, 57, 1007.
- (12) Katsuhiko Ariga and Jonathan P. Hill *The Chemical Record* **2011**, 11, 199.
- (13) S. Foerster and T. Plantenberg *Angew. Chem. Int. Ed.* **2002**, 41, 688.

Chapter 2

Two-Dimensional Colloids Preparation, Characterization and Research Perspectives

Abstract

This chapter presents to the reader the state of the art of the preparation and investigation of 2D colloids: a general definition of the concept of a 2D colloid is provided, followed by a section that summarizes the most relevant instrumental techniques and experimental tools available for the investigation of these systems. The next sections extensively summarize several systems suitable for preparing 2D colloid dispersions, ranging from lipid-based systems (the first and most widely investigated), to short fluorinated amphiphiles and fluorinated and non-fluorinated polymer-based mixtures. The concepts of line tension and “lineactant” are then introduced and several examples, both experimental and theoretical, are presented, regarding both the different techniques used to measure line tension and the compounds that proved to act as lineactants. This review clearly shows that the polymer-based mixtures are a poorly explored research topic, when compared to amphiphiles of natural origin, and therefore a very promising subject for further investigations.

1. General introduction

In 1861, Thomas Graham coined the term “colloid”, by which act a new field of science was born. The term colloid was derived from the Greek word “κόλλα”, meaning “gluten” or “glue”, it of course covered materials with glue-like properties (among which one finds hydrophilic macromolecules and clusters of these), but various kinds of particulate organic and inorganic materials were also – given their behavior in dialysis experiments – considered as colloids. Later on, the definition of colloids was generalized to all sorts of materials consisting of particles in a particular size range (typically 10^{-8} to 10^{-5} m) dispersed in a medium. Nowadays, the notion “colloid” is often used in a more restricted sense, referring to systems consisting of two immiscible phases, one of which is finely dispersed into the other. In the classification introduced by Kruijt, these are the “lyophobic colloids”, which must consist, at least, of a dispersed and a continuous phase. Research on colloids deals mostly with sols (solids dispersed in a liquid), emulsions (liquids dispersed in liquid), and foams (gas dispersed in a liquid).

Since lyophobic colloids are by definition biphasic, they feature an interface between the phases. Moreover, because the dispersed particles are small, there is a lot of interface per unit mass. Not surprisingly, therefore, the properties of the interface have often a decisive effect on the behavior of colloids. Forces between colloidal particles can often be treated as originating from the particle interfaces; one speaks of “surface forces” and the study of such forces is almost a field by itself. The very existence of colloidal dispersions is largely determined by surface forces: for colloidal systems to survive, repulsive contributions to surface forces are a prerequisite.

Given the importance of interfaces, it will come as no surprise that surface-active molecules, commonly called “surfactants” because they tend to accumulate or *adsorb* at interfaces, play a very important role in colloid science. The presence of these molecules at the interface, their shape, extension and mutual interaction affect the structure and free energy of the interface, and any perturbation of the structure by a second interface coming into close proximity will change the free energy and thereby induce a surface force. The study of interfaces, their structure and free energy (including the role of surfactants) is therefore considered as the logical counterpart of colloid science. Indeed, many textbooks discuss the combination of colloid science and interface science, e.g., the series “*Fundamentals of Interface and Colloid Science*”, by Lyklema.

Water-air interfaces have a special place in the domain of interface science, as they are so familiar to us. The water-air interface has a remarkably high tension (72

mN/m at room temperature) due to the strong tendency of water to self-associate. Many molecules which are not soluble in water can, nonetheless, spread on water, because they have at least some polar character, due to the presence of electronegative atoms. Given enough available area, the spreading goes on until a monolayer, a layer of one molecule thick, eventually remains. This was already concluded by Benjamin Franklin when he carried out his famous experiment with a teaspoon of oil on the Clapham Common pond in 1765. It was Irving Langmuir who gave such experiments a systematic basis, developing an instrument for measuring the 2D (two dimensional) *surface* pressure, but it was Agnes Pockels who reported, in 1893, the first measurement of surface pressure as a function of monolayer density. Such 2D pressure *isotherms*, just like those for (three dimensional) compressed gases and vapours, sometimes feature a constant pressure in a range of densities, signalling the occurrence of phase coexistence. Indeed, depending on temperature, chemical structure, and density, several 2D phases have been identified for such monolayers, like “gas”, “liquid expanded”, “liquid condensed”, and “solid”. There is a vast literature on the behavior of Langmuir layers; the multiphasic systems they make can nowadays be directly observed by means of sophisticated optical methods.

The central question of this review is whether 2D phases can also exist as colloidal systems, and what stabilizes the dispersed state in such systems. In particular, we shall consider the special role of molecules that tend to accumulate at the phase boundaries, that is, at the contact lines, which will therefore be denoted as “line-actants”.

2. Two-dimensional colloids: definition and peculiar characteristics

A system is commonly referred to as a colloid, when it consists of two immiscible phases, one of which is finely dispersed into the other. The composition of the two phases is either different (two chemically different components are mixed together) or identical (the same substance coexists in two different physical states). It is essential that the dispersed phase is stabilized by specific interaction forces, so that demixing is prevented on a reasonable timescale. Usually, thermodynamic stabilization is hardly achieved in colloid systems, however kinetically stabilized systems are obtained that can last over a significant period of time.

This definition is perfectly applicable to both standard colloids (in three dimensions) and 2D colloids.

Some physical peculiarities, however, distinguish 2D colloids from their counterparts in bulk systems: here follows a brief list.

- Gravitational forces are negligible in 2D colloids.
- The Rayleigh instability, that is, the tendency of liquid filaments to break up into (spherical) droplets, is commonly observed in 3D colloids, but is absent in 2D ones: it is possible, therefore, to elongate a domain of the dispersed phase into the continuous one indefinitely, without causing the rupture of the filament.
- Formation of a bicontinuous phase is topologically impossible in 2D¹.
- Molecules are strictly confined in the interfacial plane where they are adsorbed: the confinement between two different phases leads always to a preferred orientation of the molecules. In contrast, molecules distributed in a bulk colloid system do not necessarily have a preferred orientation and so the system as a whole is generally isotropic. Anisotropy in 2D colloids is exploited by some instrumental characterization tools (SFG, sum-frequency generation spectroscopy; SHG, second harmonic generation spectroscopy) in order to distinguish them from the bulk subphase and increase instrumental sensitivity.
- Dipolar repulsive forces in 2D colloids propagate over long distances, due to the anisotropy in their orientation. Electrostatic interaction among molecules are less screened than in common 3D aqueous bulk systems².

3. Instruments and techniques for characterization of phase separated systems

The investigation of phase separation in a constrained two-dimensional (2D) system poses several technical challenges, which require adequate instrumentation and experimental procedures, in order to guarantee a rigorous study and reliable results. Our aim here is to briefly expose a range of well-established characterization techniques and tools, now available to the interested experimentalist, without the ambition of covering all the detailed aspects of each technique. Several detailed reviews will be listed below on all the subjects covered in this section.

3.1 Langmuir Monolayer production and surface pressure/area isotherms

A comprehensive review on Langmuir Monolayer (LM) investigation tools and techniques is available³, and represents a valid starting point for the readers who wish to become familiar with all the aspects connected to the characterization of LM and preparation of Langmuir-Blodgett (LB) films.

The production and characterization of LM are usually performed in an apparatus called Langmuir trough: the most essential trough is usually made of a hydrophobic material (Teflon), easy to be cleaned, preferably resistant to acids and oxidising solutions, and equipped with movable barriers (usually of the same material used for the trough) and a sensor to measure the surface tension of the subphase. It is often possible to circulate water, coming from a thermostat, underneath the trough, in order to control the temperature of the subphase during the experiment. The equipment should be mounted on an anti-vibration table and be protected from dust and flow of air during experiments by using a suitable case. The cleanliness of water subphase, spreading solvents, materials and apparatus is crucial for the accuracy and reproducibility of the experiments. Extra accessories are a surface potential probe, to measure surface potential/area isotherms, and a dipping tool, to prepare LB films.

The monolayer is usually obtained by dissolving the substance of interest in a suitable, volatile, organic solvent, immiscible with the water subphase. The thermostated water subphase is cleaned from dust and floating impurities by suction of the surface, just before spreading of the material used to prepare the monolayer. Then, the solution is spread on top of the water using a microliter syringe, by carefully touching the water surface with the needle, and then gradually supplying the desired amount of solution. After some minutes, necessary to allow total evaporation of the spreading solvent, the monolayer is formed and equilibrated with the subphase. It is then ready to be compressed by the movable barriers to the desired surface pressure value. The compression rate is a parameter which might influence the experimental outcome, therefore its settings and variations are important in the context of data analysis, at the end of the experiment. Also extremely relevant are the concentration and total volume of the spreading solution, necessary to calculate the amount of molecules present in the monolayer and other experimental parameters, such as the area per molecule occupied at different compression stages.

The surface pressure/area isotherm is a plot of the change in surface pressure (defined as the difference between the surface tension of the pristine subphase and the actual tension measured in presence of the monolayer, i.e. the 2D analog of the pressure) as a function of the area occupied by the monolayer, usually expressed as area per molecule. The measurement is usually performed in pseudo-equilibrium conditions, by slowly and continuously compressing the LM, while recording the surface pressure value. Ideally it is possible to distinguish three different regions in the pressure/area diagram of a typical amphiphile. At large areas the monolayer

behaves as a 2D gas, since the molecules are far apart and have weak or vanishing interactions; at this stage almost no work is needed to perform the compression, therefore the surface pressure is almost unchanged. When the area is sufficiently reduced, the molecules start to interact, and form the so-called liquid state, marked on the isotherm by a change in the slope of the curve, which becomes steeper. Further compression allows to obtain a so-called solid or crystalline state, in which the molecules are closely packed, and (presumably) nearly vertically-oriented with respect to the surface; the transition is signalled by another change in the slope of the curve, which becomes very steep at this stage. If the monolayer is compressed beyond this state, it reaches a pressure value (collapse pressure) where it breaks apart and forms multilayered regions. Sometimes the states are subdivided into a liquid-expanded (LE) and liquid-condensed (LC) region, or a solid-condensed (SC) region, depending on the type of compound studied: these states are mainly determined by the molecular orientations, and are investigated by X-ray diffraction techniques^{4,5}. Since these topics are out of the scope of this review, we will not discuss any details.

In mixed LM, the way mean molecular areas depend on the composition of the mixture has been used to infer possible interactions in the mixed monolayer. A mixed LM shows non-ideal behavior when its properties, do not depend linearly on the monolayer composition. Deviations from ideality, such as minima or maxima in the studied function indicate significant molecular interactions. If the area per molecule is studied as a function of the composition of the LM, at a fixed pressure, information on the miscibility of the mixture components can be inferred, according to this criterion. The mean molecular area, weighed by the molar fraction of the components, is calculated and plotted versus the molar fraction of one component of the mixture, and measured at several compositions from the recorded pressure/area isotherm. When the measured data overlap with the values calculated assuming linear behavior, the monolayer behaves ideally; in this case two different scenarios can be equally hypothesized: either the mixture is ideally miscible, and the molecules do not interact with each other, or immiscibility is complete. When positive deviations are found (a maximum in the experimental curve), repulsive interactions are present between the molecules of the two different types, and segregation and partial miscibility can be hypothesized. If negative deviations are found (a minimum in the experimental curve), this indicates attractive interactions between the molecules of the two different types, which are stronger than the mutual attraction between molecules of the same type of substance. Ideality deviations can also be tested studying the dependence of surface pressure of a

mixed LM, at a given area, on its composition. Again, deviations from linearity indicate interactions, while linear behavior is a sign of either ideal 2D mixing or complete immiscibility. To distinguish between them, the analysis of isotherms at the collapse pressure is helpful. When the components are miscible, the collapse pressure depends on the molar fraction of the components; moreover, the collapse pressure of the mixed film (for all possible composition ratios) lies between the collapse pressures of pure components. In case of immiscible components, two distinct collapse pressures are found, corresponding to the values recorded for LM of the pure components. Until recently, LM investigations on miscibility were usually carried out exclusively by this indirect approach. However, nowadays several direct means of investigation (e.g. BAM and fluorescence microscopy) are available to test and verify these inferences. Such complementary test tools should be always used in combination with analysis based on surface pressure data.

Finally, it is possible to characterize the monolayer structure and morphology by several techniques, not applicable directly at the air/water interface, provided that the monolayer is transferred to a solid substrate. The transfer can be done on either hydrophobic or hydrophilic surfaces, by using the Langmuir-Blodgett (LB), or Langmuir-Schaefer (LS) technique. The LB technique is also referred to as vertical dipping method; the type of transfer performed is indicated as Y-type, when the LM is transferred to the substrate both during immersion and withdrawal, as Z-type, when the LM is transferred only during withdrawal, or as X-type, when the LM is transferred only during immersion. The LS technique is also referred to as horizontal touching method, and can be performed approaching the interface either from the air-side or from the water-side. In every case, the quality of the transfer can be assessed calculating the transfer ratio (TR), which is defined as the change in the area, at constant surface pressure, caused by barrier movement during transfer, divided by the area of the substrate coated with the monolayer. For optimal transfer, the TR should always be unity.

3.2 Optical techniques

The most relevant optical techniques available to the scientist who studies LM morphology are Brewster Angle Microscopy (BAM), Scanning Near Field Optical Microscopy (SNOM) and Fluorescence Microscopy. Here we will briefly summarize the working principles, the main advantages and the drawbacks related to these techniques, and provide adequate references for those who need to expand their knowledge of the issue. BAM allows in situ studies of LM, directly at the air/water interface, without addition of molecular probes: in this way the LM is not

altered by presence of impurities or transfer to a solid support. Fluorescence Microscopy is a widely used technique, much appreciated for the high sensitivity and selectivity of visualized objects, guaranteed by the fluorescence detection. Several sophisticated fluorescence-based instruments are becoming more common and provide further ways to investigate LM. Scanning Near Field Optical Microscopy has the advantage of greatly enhancing the resolution, far beyond the diffraction limit imposed by the use of visible light.

3.2.1 Brewster Angle Microscopy

Brewster Angle Microscopy is the most direct optical visualisation technique available to characterize *in situ* LM, probing the 2D organisation of films, showing heterogeneity, size and shape of domains on the micrometer scale^{6,7}. The microscope is based on a simple optical principle: when p-polarised light hits the surface of pure water at the so-called Brewster Angle \mathcal{J}_B (53,1 °), no reflected light is detected. The Brewster Angle is a physical parameter which depends on refractive indexes of both water and air ($\sin \mathcal{J}_B = n_A/n_W$). If a LM is spread on top of the water surface, the Brewster Angle of the compound surface changes. Therefore, if the angle of incidence of the polarised light is kept constant at 53,1 °, but an LM is spread on water, the LM-carrying surface reflects light, while the bare water surface does not and appears black. According to both the thickness and the chemical nature of the monolayer formed (both indeed affect the refractive index value), the reflected light will change in intensity, providing a way to distinguish different morphologies in the film. The polarisation of the incident light can be affected by the orientation of hydrophobic tails in the amphiphiles, with respect to the plane of incidence of light.

The technique is appreciated because there is no need to add labels, tracers, or any unnecessary compound to the LM in order to study it, and this eliminates any risk to obtain experimental artefacts due to (voluntarily introduced) impurities, which could affect the response of the monolayer components.

Disadvantages connected to the use of this technique are briefly illustrated below. The main drawback is caused by the tilted plane of incidence of light with respect to the water surface: this causes formation of a distorted image, in which only a thin stripe around the centre is focused. In order to overcome this problem the image is often digitally reconstructed by taking partial images at different focal depths and then gluing into a single picture all the parts of these images which are in focus. However, time resolution depends on the rapidity of scanning, and investigations on the dynamics of LM are limited. Lateral resolution down to 1 μm

is achievable, provided that the objective has a sufficient numerical aperture. The width of the strip in focus can be improved at the expense of the resolution, reducing the numerical aperture of the lens; in this simple way acceptable images can be obtained, at video frequency. A home-built BAM has been realised⁸, with special optics that remove the necessity of the scanning followed by digital reconstruction, without losing lateral resolution. However, no equipment that incorporates these features has been commercialised so far.

3.2.2 Fluorescence Microscopy

Fluorescence is an emission of light from an excited molecule, which occurs within nanoseconds after the absorption of an exciting photon of shorter wavelength. The difference in wavelength between the exciting and emitting light, known as the Stokes shift, makes fluorescence-based techniques so powerful: indeed, by filtering out all the exciting light and detecting only the emitted radiation, only fluorescent objects are visible. This detection mode is therefore much more sensitive than bright-field microscopy, where the difference in amount of absorbed light is only infinitesimally different from the background⁹. The preferred set-up is epi-illumination, in which the objective not only magnifies the specimen, but also serves as a condenser to illuminate it. The advantage of the epi-illumination mode over the common transmission microscope is that only the small percentage of exciting light reflected off the sample needs to be screened in the return-path.

The main issue, however, is that usually LM components are not fluorescent, and therefore a probe must be added to the monolayer. In principle, interferences due to the probe addition cannot be excluded, therefore a complementary characterization technique is required to do so. It is possible to distinguish phase transitions and structures caused by phase separation in LMs provided that a fluorescent probe is chosen which partitions preferentially in one of the phases under investigation^{10,11}. Interpretation of pictures should always be done with care: in cholesterol/phospholipid LM contrast inversion has been observed when the pressure was increased¹². The probe partitioned from one liquid phase into the other, when the system was sufficiently compressed, independently of the type of phospholipid studied. The widespread use of fluorescence microscopy in molecular biology studies has favoured fast and significant advancements in this field. New fluorescent sensors, responsive to local viscosity in lipid membranes, have been synthesized and applied for imaging¹³.

Several more sophisticated techniques have been developed: Fluorescence Lifetime Imaging Microscopy (FLIM)¹⁴ probes alterations in the environment in the immediate vicinity of the fluorescent molecule, and allows to assess molecular interactions between fluorescently-labelled molecules and interacting partners; Forster Energy Resonance Transfer (FRET)¹⁵ allows to assess changes in intermolecular distances far below the resolution of the light, thanks to the interaction between two neighbouring fluorophores, whose exciting and emission spectra are overlapping; Fluorescence Correlation Spectroscopy (FCS)¹⁶, which records temporal fluctuations in fluorescence emission, is used to measure lateral diffusion and dynamic parameters with great precision.

3.2.3 Scanning Near Field Optical Microscopy

Scanning near-field optical microscopy (SNOM) is a new methodology for achieving a spatial resolution beyond the theoretical limitation imposed by the wavelength of light¹⁷. When incident light illuminates an object smaller than its wavelength, a non-propagating electric field, restricted around the object, known as “optical near-field”, is generated. The non-propagating optical near-field contains information on the local structure (smaller than the wavelength used), and can be exploited to achieve spatial resolution beyond the diffraction limit. SNOM technique uses a probe (generally an optical fiber, mechanically or chemically sharpened) with an aperture much smaller than the wavelength of the incident beam. This allows to illuminate the specimen and to obtain an optical response from an area of a few nm², building up an image with a resolution as high as the aperture size. The gap between the SNOM probe and the sample surface must be kept constant, at a few nanometers, because the near-field intensity decays rapidly with increasing distance from the probe. This technique allows to obtain simultaneously also a topographic image of the sample. Furthermore, the instrument enables to do time-resolved measurements and polarization measurements of a single molecule with high sensitivity. The combination of SNOM and fluorescence provides detailed information of structure and dynamics of mixed polymer systems with a nanometric spatial resolution¹⁸⁻²⁰.

3.3 Atomic Force Microscopy

Atomic Force Microscopy has become the main standard investigation tool in LM studies²¹, able to yield information with a high lateral resolution (the order of nanometers) about not only monolayer topography, but also adhesion, friction and wear^{22,23}. The AFM image is created on the basis of the various forces acting

between a sharp cantilever tip and the sample surface; important forces are van der Waals, electrostatic, frictional (lateral), and magnetic forces. The force sensor of an AFM consists of a cantilever beam with a sharp tip at the end. The distance between the sample surface and the cantilever tip can be controlled by the piezo-driver on which the sample is mounted. When the surface approaches the cantilever tip, it experiences a (attractive or repulsive) force, the strength of which depends on the distance between the cantilever tip and the surface, thus resulting in a deflection of the cantilever. The force acting on the cantilever is obtained by multiplying the deflection of cantilever with its spring constant. The laser beam deflection method is used mostly for the detection of a cantilever displacement. In case of AFM, the forces perpendicular to the sample surface are used to assess the sample topography. During imaging, a suitable feedback system is used to guide the tip scan over the sample surface, keeping the bending of the cantilever constant. This mode is called constant-force mode. On the other hand, the image can be obtained by scanning at constant height. The image obtained in constant-height mode is a 2D distribution of the force. "Tapping mode" is a compromise between the contact and non-contact regimes - the cantilever is made to oscillate, so that the tip is very close to the sample for a very brief time and then far away for a brief time. The compromise between the two force regimes allows one to scan soft fragile materials with better resolution than in the non-contact regime, but with less interaction between the cantilever tip and material's surface. The tapping mode has been extensively applied to biological systems. When the cantilever is scanned over the sample surface in the repulsive-force region (contact region), a frictional (lateral) force parallel to the surface is observed²³. In the LFM mode the torsion of the cantilever, due to the frictional (lateral) force, is detected. The magnitude of frictional force depends on the surface chemistry of the sample (functional groups, molecular orientation, crystallinity etc.).

The main drawbacks connected to the use of AFM techniques are: the need to transfer the LM to a suitable support for observation. Transfer may be incomplete or introduce distortions in the original morphology. In addition, drift or other visualisation artefacts caused by the instrumental settings could be present.

EFM (Electrochemical Force Microscopy) is a type of noncontact atomic force microscopy (AFM) sensitive to variations in the potential difference between a probe and the sample surface²⁴, and represents an evolution of surface potential/area measurements carried out in the Langmuir trough. The probe is a metal tip at the end of an AFM cantilever. The sample surface topography is first traced while either contacting the tip with the sample, at an applied tip/sample

voltage of zero, or scanning the tip over the surface in intermittent contact (tapping) mode. The tip is then raised and scanned above the sample at a height of 25–75 nm, while retracing the topographic features. While in this “Lift Mode,” an ac voltage is applied between tip and substrate at the resonance frequency of the cantilever. As the cantilever is scanned across the surface, a deflection at the frequency of the applied voltage is produced, which is proportional to the average potential difference between the tip and sample surface. The ac deflection of the cantilever is sensed by an optical beam deflection technique. The electrostatic deflection signal (proportional to the average surface potential difference) is the parameter recorded by the microscope to produce an EFM image. The images can reach a lateral spatial resolution below 100 nm.

4. Phase-separated systems based on natural lipids and amphiphiles

The hydrophobic association that occurs among the alkyl chains is the driving force of lipid monolayers formation. A detailed account on the issue of domain and raft formation in model lipid bilayers, and its impact on biological systems, has been provided in an extensive review by W.H. Binder *et al*²⁵. Here we give a schematic summary of the main physical and chemical interactions existing in lipid monolayers that can be used to trigger lateral phase separation.

4.1 Principal categories of lipids

Several lipids are found in membranes: it is possible to group them according to common chemical architectures in three broad families: diacyl-glycerols and derived lipids, sphingolipids, and sterols.

Diacyl-glycerols are formed by two identical acyl tails (saturated or unsaturated), joined to the glycerol moiety, and a headgroup, which is constituted by the H- atom, or more complex, hydrophilic functional groups for the derived lipids (e.g. phosphatidylcholine or phosphatidylethanolamine). Diacyl-glycerols have cylindrical shapes (apart from phosphatidylethanolamines) and assemble spontaneously in planar layers. When they assemble below their melting transition temperature, they adopt an all-trans conformation and a crystalline hexagonal lattice, forming a solid state (gel). Upon their melting transition temperature, some bonds adopt a gauche conformation, and the layer expands into a liquid-crystalline state (fluid). Transition temperatures vary from –22 °C for dioleoylphosphatidylcholine, to 42 °C for dipalmitoylphosphatidylcholine, increasing with longer and saturated chain lengths.

Sphingolipids derive from the sphingosine base, which has an unsaturated backbone tail, connected by an amide bond to an acyl chain of variable length. The sphingolipid tails are asymmetrical, and headgroups can be of several types (phosphorylcholine for sphingomyelins, carbohydrates for cerebrosides). The melting transition temperatures are always higher than those of the corresponding diacyl-glycerol derivatives, and can exceed 60 °C.

Sterols have a characteristic, condensed-ring structure, and a very small headgroup (the 3-hydroxy moiety), which makes them highly hydrophobic and remarkably stiff.

When two different types of lipids (from the same family or not) are mixed in a monolayer, induction of lateral phase separation may be driven either by interactions between lipid headgroups, or by interactions between lipid tails. We elaborate on this below.

4.2 Phase-separated systems controlled by headgroup interactions

Interactions between headgroups respond to several parameters: pH of the subphase, electrostatic interactions with ions, mismatch between headgroup types, or pairing interactions between the same type of headgroup. Each of these variables can be tuned to trigger phase separation of binary lipid mixtures.

Monolayers made of stearic acid and dimyristoylphosphatidylcholine are sensitive to pH changes in the subphase²⁶: pure stearic acid monolayers are fully ionised (and thus water soluble) at pH 10 and neutral (insoluble) at pH 4, whereas the phosphatidylcholine heads are, of course, zwitterionic: as a result, the mixed monolayer in acidic condition is phase-separated over a wide concentration range, and the condensed, stearic acid domains change morphology, depending on the composition ratio and compression rate. When the fatty acid hydrophilic head is not charged, at pH 4, the molecules pack in a condensed monolayer, while the phospholipid molecules retain a liquid-expanded state; this situation leads to demixing. When the hydrophilic head is dissociated, at pH 10, both the stearic acid molecules and the phospholipid ones form a liquid-expanded monolayer, and their miscibility increases. The electrostatic interactions are not the determining factor for the phase separation phenomenon observed, however they contribute indirectly, affecting the density and, hence, the degree of disorder in the hydrocarbon chains of the monolayer components.

The presence of dissolved ions in the water subphase affects the physical characteristics of ionic lipid monolayers. Divalent ions, for instance, induce ordering of the lipids and cause phase transitions not observed on pure water: Ca^{2+}

ions exert a condensing effect on lipids²⁶, and form lipid complexes with the phosphate headgroup of phospholipids^{27,28}. A new phase transition is observed at low surface pressures, while chain reorientation effects are observed at higher surface pressures, and the lipid tails are more ordered and aligned along the direction normal to the interface²⁷. Cd²⁺ ions induce phase transitions in monolayers formed by phosphatidylcholine and arachidic acid, however the components remain partially miscible²⁹. Monovalent ions, such as Na⁺, have more subtle effects, since the ion-phosphate interaction is weaker and water-mediated²⁸; they induce an increased disorder in the monolayer structure^{27,29}.

Head-head dipolar interactions in mixtures are usually repulsive, because the normal component of the dipole moment has the same orientation; the positive lobe points towards the air phase, and the negative lobe points towards the water phase. This, in principle, favours the phase separation of the mixed components in a monolayer. Mismatch between two different types of headgroup³⁰ (charged/neutral, or neutral/neutral) can thus lead to immiscibility in solid systems, however it is more difficult to achieve phase separation in the fluid state. Several systems composed of combinations of phosphatidylethanolamines, phosphatidylserines, phosphatidic acid, and phosphatidylcholines with the same tail groups have been tested, and shown partial miscibility to different degrees. The phase separation achieved through this strategy, however, is not significant. The influence of headgroup mismatch on phase separation has been also tested in binary mixtures containing either (i) cholesteryl acetate and octyl cyano biphenyl, or (ii) cholesterol and octyl cyano biphenyl³¹. In the first case the ester moiety does not form a strong hydrogen bond with water in the subphase. Moreover, the ester has lateral interactions with the cyanide group, which stabilise the monolayer through dipole-induced dipole interactions, improving the miscibility. In the second case, the cyanide moiety destroys the network of hydrogen bonds formed by the cholesterol hydroxyl groups with the water subphase, reorienting the dipole of water molecules, and therefore destabilising the mixture. Immiscibility, therefore, is obtained in the latter system.

Interactions occurring among headgroups of the same type³²⁻³⁴ have been recognised as the driving force of phase separation in mixtures made of sphingolipids and phospholipids. Phase separation occurs in both solid/solid and liquid/liquid systems, and is due to a network of hydrogen bonds formed by the ceramide headgroups, which favours their clustering.

4.3 Phase-separated systems controlled by tail interactions

Interactions between lipid tails depend on the chain length and type, and are mainly of van der Waals type. It is well known that these (usually attractive) interactions are much stronger at the air/water interface than at the oil/water interface, due to refractive index mismatch between the polar tails and surrounding phase (oil or air)^{35,36}. The interactions between lipid tails depend strongly on their saturation degree and generally they mix non-ideally³⁷.

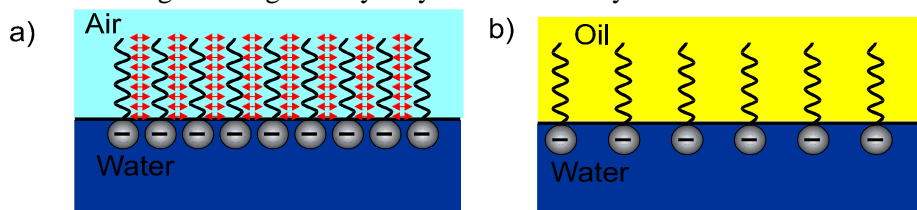


Figure 1. There is a considerable interaction (denoted by red arrows) between the lipid tails chains across air (a), whereas such an attraction is usually weak across oil (b). Adapted from ref. 35

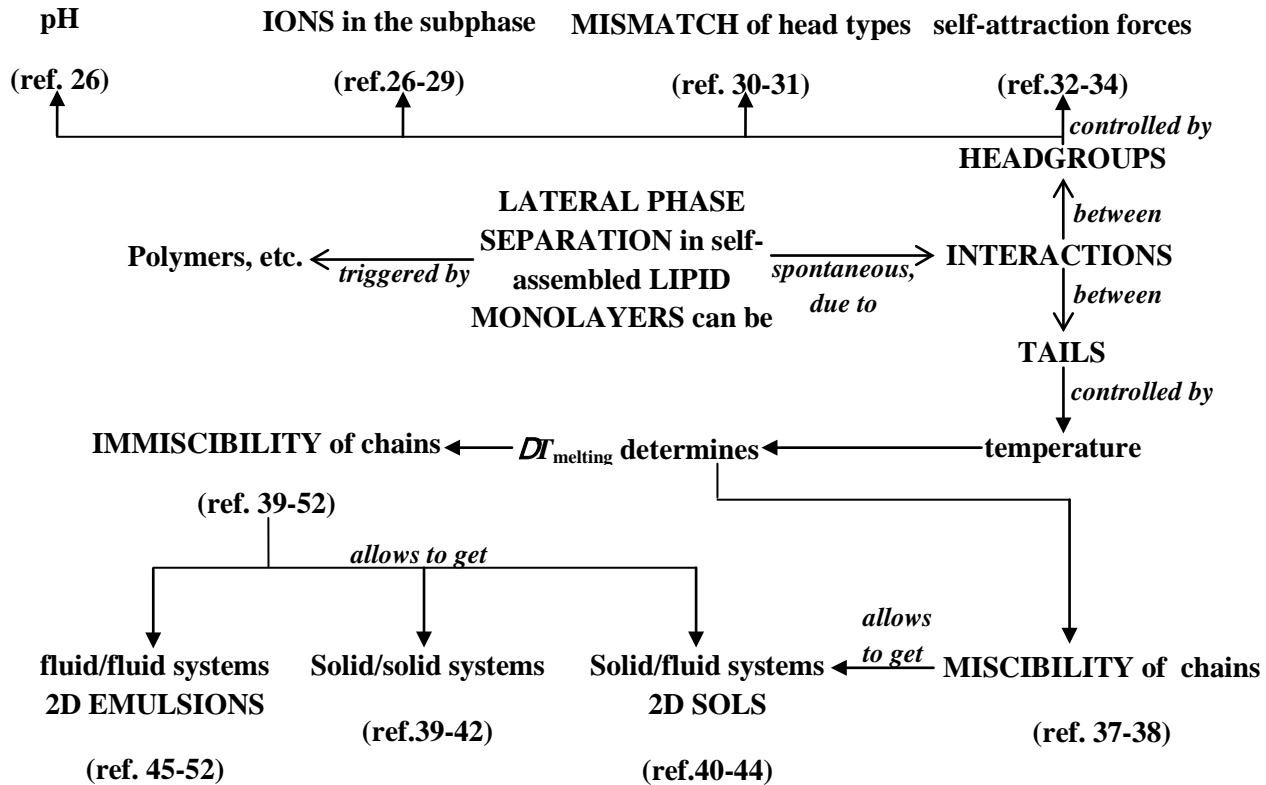
The miscibility of lipid tails is correlated with their melting transition temperature. Two scenarios are possible: the two lipids chosen are either miscible in both the solid and liquid state, or not miscible at all.

When the two lipids are miscible, it is possible to obtain a phase-separated system only in a range of temperatures bounded by the two different melting transition temperatures of the chosen compounds. The lipid with the lower melting transition temperature will be in a fluid state, while the other will be in a solid state: solid-like domains of the latter will float in a fluid-like layer, so that they can be seen as a 2D sol. Such systems have been observed when sphingolipids and phospholipids are mixed, since their respective melting transition temperatures are very different^{38,39}. Above the higher and below the lower melting transition temperature, a one-phase system is obtained, respectively of a liquid-like or solid-like nature.

When the two lipids are immiscible, several phase-separated systems can be obtained: solid/solid, solid/liquid, or liquid/liquid, depending on their melting transition temperatures and the actual temperature of the layer formed. The miscibility of myristic acid and 7-(2-anthryl)heptanoic acid in monolayers depends on both their relative molar ratio, and on the surface pressure: an increase in the amount of dye or in the surface pressure drives a progressive phase separation of the monolayer components, probably caused by the different packing of the respective two-dimensional crystalline lattices⁴⁰. Solid/solid and solid/liquid

phase-separated systems have been observed upon mixing phospholipids: the phase separation is induced by an alkyl chain mismatch of, at least, four $-\text{CH}_2-$ groups in phosphatidylcholines⁴¹⁻⁴³. Binary mixed monolayers made of triglycerides are also phase-separated: the demixing depends on the mismatch in the alkyl chain length. The most clear phase-separated monolayer is made of tripalmitin (C16) and triarachidin (C20) (4 C atoms of difference in alkyl chain length), while tristearin (C18) and triarachidin (C20) mix almost ideally⁴⁴. The interaction between fatty acids and phosphatidylcholines in mixed monolayers depends strongly on their saturation degree. Generally they mix non-ideally; saturated fatty acids display more repulsive interactions with unsaturated phospholipids than with saturated ones; unsaturated and saturated phospholipids are immiscible over a wide range of compositional ratios³⁷. Liquid/liquid phase-separated mixtures have been prepared mixing cholesterol with saturated phospholipids, up to 30% mol^{45,46}. The van der Waals interactions occurring between the sterol rings and the acyl chains induce a stiffening of the lipid layer, creating a liquid-ordered phase, richer in cholesterol, in coexistence with a liquid-disordered phase, richer in phospholipids. If the cholesterol molar fraction is increased above 30%, the whole layer becomes liquid-ordered and just one phase is observed. The effect of several types of sterols (cholesterol, sitosterol and stigmasterol) added to dipalmitoylphosphatidylcholine has been investigated, and condensation effects have been observed for all the mixtures, although the interaction of sitosterol and stigmasterol with the lipid is weaker than the interaction with cholesterol⁴⁷. An extensive review on the liquid-liquid immiscibility in cholesterol-phospholipid mixtures is available to the interested reader⁴⁸. Ternary phase diagrams of mixtures containing cholesterol have been reviewed extensively⁴⁹. Mixtures of cholesterol and sphingolipids are also phase-separated⁴⁶. The degree of condensation of the lipid layer affects the efficacy of cholesterol-induced phase separation. The condensing effect is increased by using lipids in an expanded state. Interaction of cholesterol is higher with sphingolipids that have longer *N*-alkyl chains⁵⁰: a review on this subject is available⁵¹. Polyunsaturated fatty acids increase the degree of disorder in the membrane, therefore they display high repulsion for cholesterol, and form highly disordered segregated domains: these domains are compositionally, and organizationally, the opposite of lipid rafts, and have been reviewed by Wassall and Stillwell⁵².

Scheme 1. On next page, schematic summary of all the possible interactions occurring among lipid amphiphiles, which cause phase separation in these systems.



5. Phase-separated systems based on fluorinated amphiphiles

5.1 Fluoroalkanes and partially fluorinated alcohols

Fluoroalkyl diblock amphiphiles are molecules formed by a fully fluorinated alkyl chain attached to an alkane: both moieties can be adjusted in their total length to change the fluorinated *vs.* hydrogenated composition ratio. They can be represented by the notation F_nH_m , where F_n stands for the fluorinated moiety of n C-atoms, and H_m stands for the alkane part of m C-atoms. Due to their structure these compounds have the following important properties: (i) amphiphilicity, thus able to adsorb preferentially at the air/water interface; (ii) amphidynamicity, the combination of a rigid moiety (fluorinated block) with a more flexible one (hydrogenated block); (iii) amphistericity, caused by the difference in cross-section, steric hindrance and conformation between the fluorinated block and the hydrogenated block. Another critical characteristic of fluoroalkyl-alkyl diblock amphiphiles is the strong dipole moment located at the CF_2-CH_2 junction, which is not present in the parent blocks. The CF_2-CH_2 bond is shorter and stronger than both the CF_2-CF_2 and the CH_2-CH_2 bonds, and connects two moieties with different physical and chemical properties. The hydrogenated (H) block has a 30% smaller cross-sectional area than the fluorinated (F) block, when hexagonally packed, and it is more disordered than the F block, especially if it is located at the end of the polymer chain, rather than in the middle. Both the C-H and the C-F bonds are polarised, but, since the fluorine atoms are strongly electronegative, the C-F bond is strongly polarised towards the F atom, whereas the electronegativity of C and H are comparable, so that the C-H bond is only slightly polarised towards the C atom. The dipolar components add up, conferring a strong anisotropy to the molecular chain: the molecular dipole is located at the CF_2-CH_2 junction, directed towards the F block, and oriented at a different angle with respect to the molecular axis.

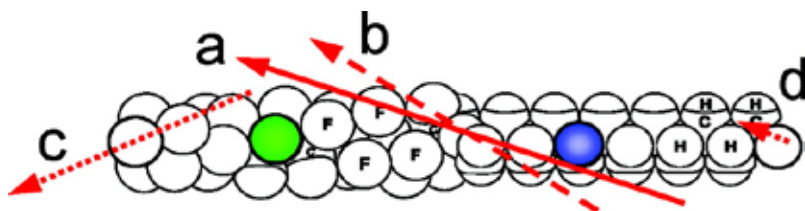


Figure 2. F -alkyl/ H -alkyl diblocks host a strong dipole (a), with components arising from (b) the F_n-H_m junction, (c) the terminal CF_3 , and (d), to a much lesser extent, the terminal CH_3 . Adapted from ref. 53(Scheme 4.1).

As a result, fluoroalkanes are surface-active compounds, even though they lack the hydrophilic moiety present in the classical surfactant-like molecules. The F block is fluorophilic, hydrophobic and lipophobic at the same time, while the H block is lipophilic, hydrophobic and fluorophobic at the same time. Fluoroalkanes, when spread at the air/water interface, lower the surface tension down to 15-25 mN/m, in contrast to long, hydrogenated alkanes, which in general do not spread at the water surface, but form lenses on top of it.

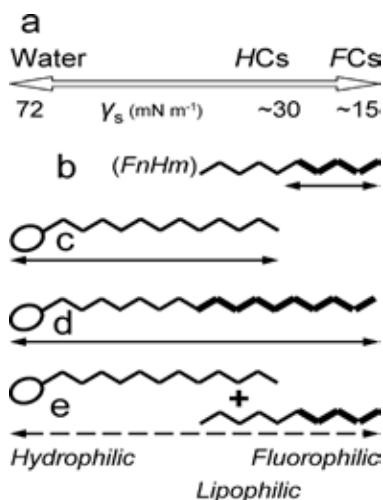


Figure 3. Schematically represented on the hydrophilic/fluorophilic (hydrophobic) scale (a), along with typical surface tension values γ_s , are the surface activity ranges of (b) a lipophilic/fluorophilic *FnHm* diblock, as compared to (c) a standard hydrophilic/lipophilic *H*-surfactant and (d) an *F*-surfactant with a hydrocarbon spacer. Part (e) depicts the co-surfactant effect anticipated between an appropriate *FnHm* diblock and a standard *H*-surfactant. Adapted from ref. 53(Scheme 4.2).

Fluorocarbon-hydrocarbon compounds have been extensively reviewed by Krafft and Riess⁵³: here we focus exclusively on systems which could be directly used to form 2D colloids. Several fluorocarbon-hydrocarbon amphiphiles (*FnHm*) form variously shaped surface micelles, when spread as Langmuir monolayers on top of water⁵³. Nanometer-sized, one-component hemimicelles are generally formed, with either elongated or circular morphology: the total length of the used diblocks affects the length of the elongated micelles, whereas the diameter of the circular micelles is affected only by the H block length⁵⁴. Langmuir monolayers often display *vertical* phase separation, rather than *lateral* phase separation^{53,55}, however at low surface pressures lateral phase separation has been observed in monolayers⁵⁶ of *F8H16* fluoroalkane hemimicelles and DPPE molecules, at pressure values

lower than 10 mN/m. The driving force for this phenomenon is the limited miscibility of fluorinated and hydrogenated chains, which favours the segregation of *F* chains into orderly, self-assembled domains. If the surface pressure is increased, however, the fluoroalkane chains are expelled from the monolayer: the driving force for the expulsion is the contribution to a further lowering of the surface tension, down to values which cannot be achieved with any alkyl surfactant alone. The absence of a hydrophilic headgroup in fluoroalkanes is crucial in favouring, at higher surface pressure, the occurrence of a vertical phase-separation, rather than the exclusive occurrence of lateral phase separation.

Fatty alcohols of several length ($n_C = 12, 14, 16$) have been mixed with *F8H14* in Langmuir monolayers: from pressure/area measurements, one can conclude that all the fluoroalkane/alcohol combinations are immiscible at high surface pressure values; at low pressure values, only alcohols with a hydrocarbon chain longer than the fluoroalkane *H* block are immiscible. Alcohols with a hydrocarbon chain shorter than the fluoroalkane *H* block become miscible⁵⁷. The repulsive forces between fluorinated blocks and hydrogenated blocks prevail only when the lateral compression of the chains reaches a critical value: below that value, attraction forces between hydrocarbon blocks prevail, if the length of the chains is properly matched. Two alcohols with very different tail length have been selected for further investigations: tetradecanol ($n_C = 14$) and docosanol ($n_C = 22$) have been mixed to four different fluoroalkanes, *iF3H20*, *F4H20*, *iF9H20* and *F10H20*⁵⁸ (the 'i' stands for *iso*- branched chain, rather than a linear one). Both pairs couples have same total number of atoms, but with different connectivity (in the first pair one chain is branched, with a terminal *iso*- group, while the other is linear), whereas the second pair has longer fluorinated moieties, connected in a parallel way to what has done in the first couple. The length of the *H* block is the same for all the four fluoroalkanes. Pressure/area measurements have been used to obtain phase diagrams for all the binary mixtures, and the characterization has been complemented with BAM observations. Very heterogeneous behaviors have been observed for all in the combinations with tetradecanol. The short, linear *F4H20* molecule has a two-phase coexistence region up to a composition of 0.7 molar fraction of alcohol, with fluorinated domains dispersed in the hydrogenated continuous phase. Above 0.7 in alcohol molar fraction, three phases are present at the interface, with a continuous phase constituted by the fluoroalkane, in which alcohol domains and fluoroalkane crystallites are dispersed. The *iF3H20* compound displays also full immiscibility with tetradecanol: at low pressure values, when the molar fraction of alcohol is below 0.5, two phases are observed,

with domains of fluoroalkane dispersed in the alcohol-continuous phase; above 0.5 molar fraction of alcohol, three phases coexist, with alcohol domains and fluoroalkane crystallites dispersed in a fluorinated continuous phase. The long, linear *F10H20* molecule is totally miscible and forms a homogeneous monolayer with tetradecanol in the range from 0 to 0.5 molar fraction of alcohol; above 0.5 molar fraction of alcohol, fluoroalkanes crystallites are found dispersed in the alcohol continuous phase. The branched *iF9H20* molecule has a pressure-dependent miscibility behavior. At very low pressure values and an alcohol molar fraction below 0.4, two phases are observed, with alcohol domains dispersed in the fluorinated continuous phase; above 8 mN/m three phases are present, with alcohol domains and fluoroalkane crystallites dispersed in the fluorinated continuous phase. Beyond 60 mN/m a fourth phase appears, consisting of multi-layered domains of alcohol. In the range of alcohol molar fractions between 0.4 and 0.8, the mixed monolayer is homogeneously mixed.

Docosanol phase diagrams show that *F4H20* is immiscible with the long alcohol when the content of the latter one is below 0.3 molar fraction, while above this value the two components are fully miscible. The branched, short *iF3H20* molecule mixes with docosanol when the molar fraction of the latter one is below 0.3 or above 0.6. In between these two values two phases are formed, with fluoroalkane crystallites in equilibrium with a homogeneously mixed, continuous, fluid phase: if the pressure is raised above 50 mN/m a third phase appears, made up of alcohol multi-layered domains. The long molecules *F10H20* and *iF9H20*, when mixed with docosanol, form homogeneous, single-phase monolayers. The interplay of van der Waals forces regulates the miscibility of these compounds: the attraction force between homogeneous moieties is higher than the one between heterogeneous moieties, therefore the balance between the length of the perfluorinated block and the length of the hydrogenated block determines the ultimate behavior observed in mixtures.

The behavior of a fluoroalkane molecule, *F10H20*, has been studied in lateral miscibility investigations conducted with three types of model alcohols: a fully hydrogenated alcohol, *n*-octanol (*HC8OH*), a perfluorinated equivalent one (*FC8OH*), and two partially fluorinated longer ones, perfluorooctyldecanol, *F8H10OH*, which is linear, and *iF9H10OH*, which is branched at the end of the fluorinated part⁵⁹. The fully hydrogenated alcohol is totally miscible with the fluoroalkane, whereas the perfluorinated analog is totally immiscible and forms aggregates in the continuous phase. The two partially fluorinated alcohols are miscible in low amounts, but demix at higher concentrations. The linear one,

F8H10OH is demixed in a molar fraction range between 0.6 and 1.0: below the collapse pressure domains of *F8H10OH* are present, in coexistence with a continuous phase of *F10H20*, and in equilibrium with 3D aggregates of *F10H20*. The branched *iF9H10OH* has a narrower miscibility range, from 0 molar fraction to 0.2. Above 0.2 molar fraction of partially fluorinated alcohol demixing occurs, and three phases are observed: separate domains of *F10H20* monolayer and a continuous phase of *iF9H10OH* in equilibrium with 3D aggregates of the alcohol. Above the collapse pressure, a fourth phase appears, made up of 3D aggregates of *F10H20*. The interaction of a fluoroaryl surfactant, 11,11-difluoro-11-(pentafluorophenyl)undecan-1-ol, with, respectively, a fluoroalkane (*F10H20*) and four alcohols, differing in the amount of fluorinated parts in their chains, has been investigated⁶⁰ by means of pressure/area isotherms and BAM. Mixed monolayers of fluoroaryl surfactant and fluoroalkane *F10H20* are fully miscible, and display strong attractions between the two types of molecules, higher than the attractions occurring between each molecule of the same type. Also the fully fluorinated alcohol, *FC18OH*, is completely miscible with the fluoroaryl surfactant. The monolayer made with octadecanol (*HC18OH*) has a contrasting behavior, because it is totally immiscible in the fluoroaryl surfactant. Monolayers containing the partially fluorinated alcohols display partial miscibility: homogeneous binary mixtures are formed below the collapse pressure, whereas above the collapse pressure both *F8H10OH* and *iF9H10OH* form 3D multilayers coexisting with a monolayer made of the pure partially fluorinated alcohol.

5.2 Fluorinated and partially fluorinated fatty acids

Short, amphiphilic molecules, such as partially or fully fluorinated fatty acids, have been widely studied in the context of mixed Langmuir monolayer preparation⁶¹.

One-component monolayers made of perfluorocarboxylic acids form nanometre-sized domains when spread on water subphase containing 2-propanol⁶². The size of the domains varies from 20 to 100 nm, depending on the amount of 2-propanol used in the subphase.

An early work by O. Shibata et al.⁶³ has characterized several Langmuir monolayers made by mixing tetradecanoic acid (*HC14A*) to a series of perfluorinated fatty acids ($n_C = 10, 12, 14, 16, 18$), using pressure/area isotherms and surface potential/area isotherms. Phase diagrams obtained from elaboration of the experimental data allow to divide the investigated binary mixtures into three different types: (i) a positive azeotropic type, (where components are miscible in

both the expanded and the condensed state) formed by perfluorodecanoic (*FC10A*) and perfluorododecanoic (*FC12A*) acids mixed to *HC14A*; (ii) a totally immiscible type, formed by perfluorotetradecanoic acid (*FC14A*) and *HC14A*; (iii) an eutectic type, formed by *HC14A* combined to either hexadecanoic (*FC16A*) or octadecanoic (*FC18A*) acid, in which a combination of expanded (*HC14A*) and condensed films (*FC16A*, *FC18A*) are present, and components are miscible when in the expanded state, but immiscible when in the condensed state.

More recently⁶⁴, mixed perfluorododecanoic acid Langmuir monolayers have been formed with either stearic acid ($n_C = 18$) or lauric acid ($n_C = 12$) mixtures. In the stearic acid case the pressure/area isotherm data, once analyzed, shown miscibility of the components, in agreement with earlier work by Shibata. The mixture of lauric acid and perfluorododecanoic acid, in contrast with Shibata's conclusions, is found totally miscible, however, the authors point out that their model system is not fully comparable to Shibata's one (pH of subphase is 5 instead of 1, the chain length of both acids is 12 atoms rather than 14 atoms).

Behenic acid (*HC22A*) and perfluorotetradecanoic acid monolayers phase separate when spread on an aqueous subphase containing dissolved CaCl_2 ⁶⁵. Domains, however, are made of both components, with a partition ratio different from the mixing ratio in the spreading solution, so they are partially miscible rather than completely immiscible.

Mixtures of arachidic acid (*HC20A*) and perfluorotetradecanoic acid (*FC14A*) have been widely investigated with several techniques⁶⁶⁻⁷¹. Total immiscibility⁶⁶ has been proved by pressure/area measurements, analyzed to plot molecular area/molar fraction diagrams, and Langmuir-Blodgett transfer of the monolayers, followed by AFM imaging: *HC20A* domains are visible in a continuous phase of *FC14A*. Infrared spectroscopy has shown that the spreading solution and the LB films had the same composition, and that the orientation of the components did not change upon mixing. Differences in previous accounts found in literature are ascribed by the authors to the type of spreading solvent used. A series of more specific investigations has been carried out by S.E.Qaqish and M.F.Paige: *HC20A* and *FC14A* mixed Langmuir monolayers were studied by Langmuir-Blodgett transfer and AFM⁶⁸. Phase separation is observed: well-defined, hexagonal domains, predominantly made by *HC20A* are found, embedded in a continuous matrix where *FC14A* is predominant. When the LB films are incubated and imaged in *n*-hexane (which is able to selectively dissolve the hydrogenated components), the domains retain their appearance, but their height is lower by the equivalent of the *HC20A* chain length. The matrix is substantially unaltered,

however little holes, absent before treatment, were observed. The authors infer from these data that the domains are purely made of *HC20A*, whereas the matrix is a mixture of 87% *FC14A* and 13% *HC20A*. Further spectroscopic investigations have been made with AFM, X-PEEM (X-ray Photoelectron Emission Microscopy) and SEEM (Secondary Electron Emission Microscopy)⁷², largely confirming the previous results: the discontinuous domains of *HC20A* yield exclusively aliphatic signals, whereas the signal of *FC14A* is primarily located in the continuous, surrounding matrix, and only a small amount is present in the dispersed phase. The mechanism underlying the hexagonal domain formation has been studied by altering the subphase temperature⁶⁷: the surface area occupied by *HC20A* expands when the subphase temperature is raised, whereas the one occupied by *FC14A* is reduced. Higher subphase temperatures allow the formation of a lower number of *HC20A* domains, larger in size.

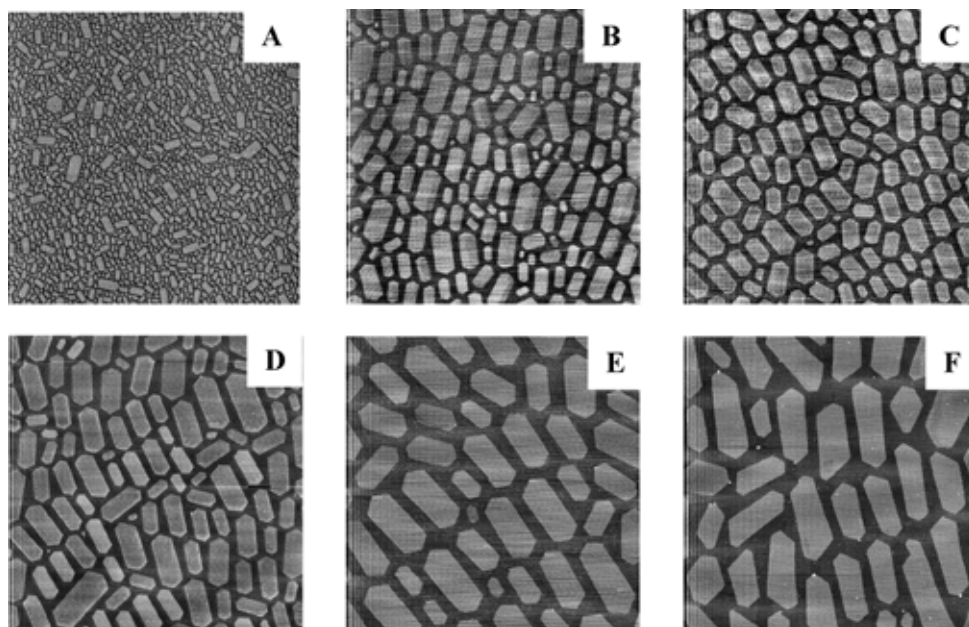


Figure 4. AFM height mode images ($20\ \mu\text{m} \times 20\ \mu\text{m}$) obtained from a 2:1 *HC20A/FC14A* LB film deposited on mica, without shaking the solution mixture, at a surface pressure of $20\ \text{mN m}^{-1}$ and temperatures of (A) 4.4, (B) 10.1, (C) 15.4, (D) 21.4, (E) 25.5, and (F) 31.9 °C. Images were measured using tapping mode in air. Adapted from ref. 67 (figure 2).

The domain growth is caused by a 2D Ostwald ripening process, driven by the minimisation of the phase-boundary area, with an initial nucleation step, confirmed by the observations made when the temperature was varied. Variations in laterally

applied pressure alter the domain morphology too: when films are transferred at low pressures the domains formed are large, almost circular, very distant and low in number; when films are transferred at high pressures the domains formed have a lower size and an elongated hexagonal shape that shows a preferred orientation, their number is higher and they are relatively close to each other. The authors infer that the phase separation process starts already in the spreading solution, which has a concentration higher than the CMC, so probably contains micelles. After spreading at low pressure, the lateral diffusion is large and allows the formation of bigger domains; at high pressure, the lateral diffusion is low and less rearrangements occur. Furthermore, if the spreading solution is vigorously shaken before spreading, domains formed are smaller, circular or indefinite, but not hexagonal. If the shaken solution is left resting for some days, the domains formed are hexagonal again. The rate of domain growth has been studied also as a function of time and temperature⁶⁹, by AFM: a diffusion-limited 2D Ostwald ripening process is recognised as the dominant mechanism of domain growth, according to the Lifshitz-Slyozov model. Some coalescence is observed at low subphase temperatures, combined to short incubation times of the monolayer.

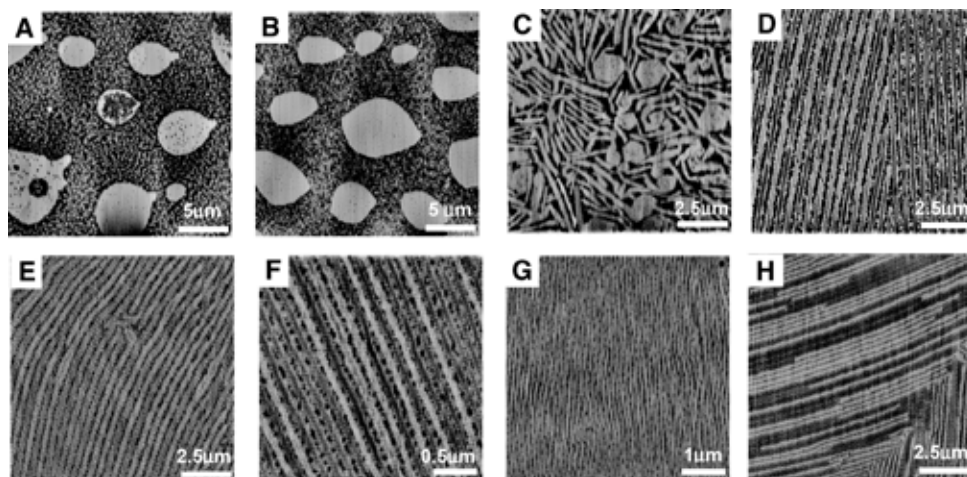


Figure 5. AFM height mode images of HC18A/FC14A 2/1 LB film on mica, deposited at a surface pressure of (A) $1\text{ mN}\cdot\text{m}^{-1}$, (B) $2\text{ mN}\cdot\text{m}^{-1}$, (C) $3\text{ mN}\cdot\text{m}^{-1}$, (D) $4\text{ mN}\cdot\text{m}^{-1}$, (E) $5\text{ mN}\cdot\text{m}^{-1}$ (F), $10\text{ mN}\cdot\text{m}^{-1}$, (G) $20\text{ mN}\cdot\text{m}^{-1}$, and (H) $30\text{ mN}\cdot\text{m}^{-1}$. AFM images were taken in air. Adapted from ref. 70 (figure 3).

An analogous investigation has been carried out on stearic acid (*HC18A*) and *FC14A* mixtures⁷⁰. When the monolayer pressure is kept below 4 mN/m during LB transfer, circular, or branched hydrocarbon domains are formed, surrounded by

smaller *FC14A* deposits. When the pressure is increased a series of parallel lines, almost totally made of *HC18A*, are formed, while the space between the lines is filled by *FC14A*. The suggested mechanism of formation implies a phase separation stage which occurs already in the bulk of the spreading solution. Circular, micrometer-sized domains of *HC18A* form at low pressures, surrounded by numerous, small deposits of *FC14A*. Upon compression *HC18A* forms more complex, linear, or hexagonal structures, densely packed, while *FC14A* begins to form a continuous film. If compression is increased further, the circular or hexagonal domains disperse into linear chains of *HC18A*, with *FC14A* packed in between.

Palmitic acid (*HC16A*) and perfluorooctadecanoic acid (*FC18A*) Langmuir monolayers are also demixed⁷¹: the domain morphology, however, is extremely complex, and *HC16A* is also soluble in the bulk water subphase (the authors used ultrapure water with resistivity of 18.2 MW-cm, without altering its pH). AFM imaging shows hexagonal *FC18A* domains, surrounded by hairy extensions: when the amount of *HC16A* is increased, the extensions become an interdigitated layer that surrounds domains. The *FC18A* molecule is present both in the domains and in the hairy extensions. Fluorescence microscopy and X-PEEM spectroscopy further confirm the composition of the observed structures.

A series of Langmuir monolayers made of partially fluorinated carboxylic acids mixed with their hydrocarbon analogs has been investigated by means of pressure/area isotherms, recorded on a water subphase added with hydrochloric acid (pH=1.9)⁷³. The mixtures used were: 1-(perfluorobutyl)undecanoic acid (*F4C11A*) and pentadecanoic acid (*HC15A*), 1-(perfluorohexyl)undecanoic acid (*F6C11A*) and heptadecanoic acid (*HC17A*), 1-(perfluorooctyl)undecanoic acid (*F8C11A*) and nonadecanoic acid (*HC19A*). The analysis of the isotherms is made by plotting the area/molecule occupied by the partially fluorinated fatty acid versus its molar fraction in the mixture. A linear trend in the data is indicative of an ideally miscible system; however, the same linear trend is also compatible with totally immiscible components³. The analysis performed by the authors shows that all the mixtures display a negative deviation from the ideal mixing behavior, meaning that the interaction between the two components is more attractive than the interaction between molecules of the same type. This behavior is typical of partially miscible components. The miscibility is influenced by the total length of the fatty acids used: *F4C11A* and *HC15A* are significantly mixed, while *F8C11A* and *HC19A* are the least miscible and display an almost linear trend in mixing behavior (which could point either to ideal miscibility or to total immiscibility of

components). The increased length of the fluorinated part of the fatty acid molecule clearly increases repulsive interactions with the totally hydrogenated counterpart.

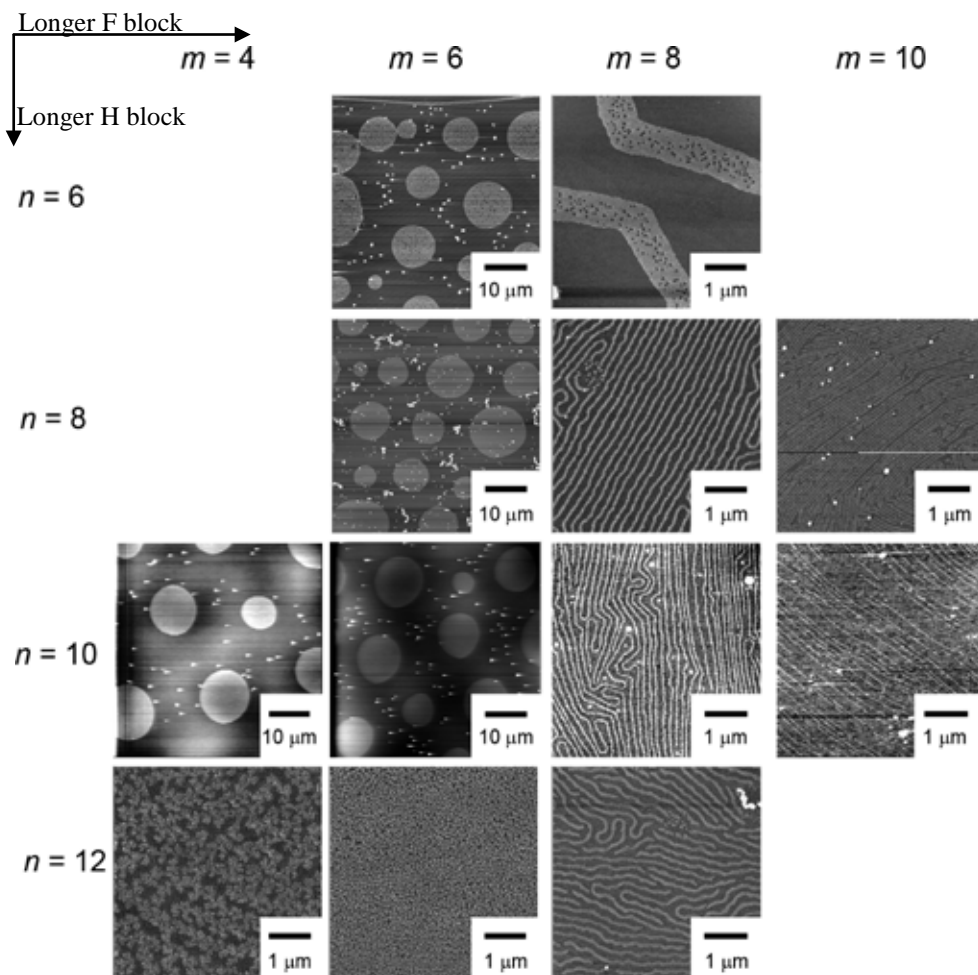


Figure 6. AFM images of the mixed LB films of H17A and *FmHnA* at a molar ratio of 1/1 transferred at $10 \text{ mN}\cdot\text{m}^{-1}$ at 30°C . Adapted from ref. 75 (figure 7).

A series of papers by Matsumoto et al.⁷⁴⁻⁷⁶ investigates phase-separated mixtures made of a fully hydrogenated fatty acid ($\text{C}_k\text{H}_{2k+1}\text{COOH}$, shortened as *HkA*) and a partially fluorinated fatty acid ($\text{C}_m\text{F}_{2m+1}\text{C}_n\text{H}_{2n}\text{COOH}$, shortened as *FmHnA*). Nanowires (average diameter in the order of 100 nm) of controllable

width have been analyzed, changing systematically the m , n , and k parameters of the mixed molecules⁷⁴.

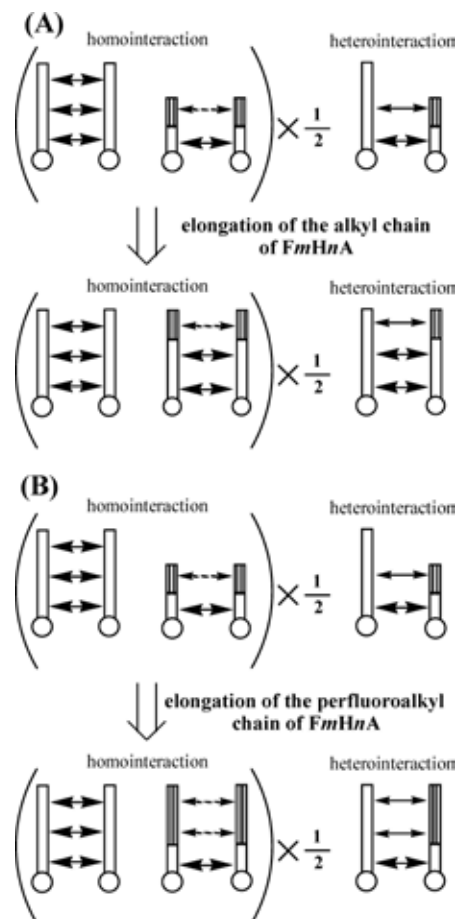


Figure 7. Schematic illustration of changes in the homo- and hetero-interactions in the cases in which the hydrocarbon length (A) and the perfluoroalkyl chain length (B) of FmHnA are elongated. Adapted from ref. 75 (figure 8).

Mixtures of *H17A* and *FmH8A* form disks when m is small, due to the high line tension values; if m is large the domains formed are wires, and their width decreases with increasing m values, due to large dipole-dipole repulsive forces that lower the line tension. When also n is changed in such a way that $m + n \geq 16$, nanostructures are always formed, with the exception of the mixture made of *F6H10* and *H17A*. When the compound *F8H10A* is mixed to different *HkA*

molecules, wires form with compounds that have $17 \leq k \leq 21$, and the width of the wires increases with an increase in the value of k . A second study⁷⁵ further tests how the morphology of the phase-separated domains responds to changes in the molecular parameters k , m , n . *F8H10A* mixed to different *HkA* forms nanowires with widths increasing with k . *H17A* mixed to *FmHnA* yields circular, micrometer-sized domains, when $m + n < 16$, and nanometer-sized domains when $m + n \geq 16$, with the exception of the *F6H10A* compound. If the parameter m has a larger value (the fluorinated chain is longer), the diameter or the width of the domains decreases; if the parameter n has a larger value (the hydrogenated chain is longer), the diameter or the width of the domains also decreases.

A 2D lattice model is introduced in order to calculate the free energy of mixing, in which only the adjacent molecules interact. When k is increased, the homogeneous interactions between hydrogenated parts decrease, ΔG_{mix} and the line tension increase, and the compounds are less miscible. When n is increased, the value of ΔG_{mix} and the line tension decrease, and the compounds become more miscible. The same happens when m is increased. A final, third study investigates the mechanism determining the morphology of the domains⁷⁶, by using *HkA* components with $k = 17, 21$ and *FmH10A* components with $m = 6, 8$. The monolayers are prepared and transferred by the LB technique following two different procedures: an isothermal treatment, and an isobaric thermal treatment. Many different structures are formed, depending on the sample history. In the isothermal treatment of *H17A* and *F6H10A* mixtures, disks form at high transfer temperatures (high line tension), and wires form at low transfer temperatures (low line tension). In the isothermal treatment of *H21A* and *F6H10A* mixtures disks form at high transfer temperatures (high line tension), and polygonal domains form at low transfer temperatures (low line tension). Changes of temperature under isobaric conditions affect only the size of the domains, not the shape, provided that the final temperature reached for the LB transfer is the same as the one used in the isobaric treatment. Mixtures made by *H17A* and *F6H10A*, spread on the subphase at 10 °C, then heated to 20 °C form rods with smaller width than those obtained with isothermal treatment at 20 °C. If they are spread on the subphase at 20 °C and heated to 30 °C, and then transferred, disks are formed, with diameters smaller than disks formed with isothermal treatment at 30 °C. When the isobaric treatment is done by first spreading, and then cooling down the subphase from 30 °C to 20 °C, rods are formed, with larger width than those obtained in isothermal conditions at 20 °C. If the cooling process goes from 30 °C to 10 °C, wires larger than those obtained with the isothermal transfer process at 10 °C are obtained. Clearly, the

temperature at which the LB transfer is carried out determines the final *shape* of the domains, while the history of thermal processing before the LB transfer determines and controls the *size* of the domains. The structure of domains is also affected by the molecular parameters k and m , however changes in k have little consequence for the line tension in the system, and the effects seen are small, while changes in m are more effective in controlling the shape, since the value of the line tension is influenced more by modifications in the length of the fluorinated segment.

5.3 Partially fluorinated amphiphiles mixed with lipids

The miscibility of constituents of cell membranes with fluorinated, or partially fluorinated compounds, has been investigated in several studies^{71,73,77-89}.

Lehmler, Bummer and co-workers have studied the miscibility properties of dipalmitoylphosphatidylcholine (DPPC) with partially fluorinated fatty acids (nonafluoropentadecanoic acid, *F9H6A*, tridecafluoroheptadecanoic acid, *F13H4A*, and heptadecafluorononadecanoic acid, *F17H2A*), and compared them to those measured for mixtures prepared with their fully hydrogenated counterparts (pentadecanoic acid, *H15A*, heptadecanoic acid, *H17A*, and nonadecanoic acid, *H19A*)⁷⁸. The subphase used throughout the work is water acidified with hydrochloric acid to pH= 1.9. The DPPC molecular area/molar fraction diagrams, plotted using pressure/area measurements, show in all mixtures a negative deviation from ideal mixing behavior. All the partially fluorinated compounds have attractive interactions with DPPC and partially mix with the lipid. The pressure of the transition from the liquid-expanded to the liquid-condensed state for all carboxylic acids used changes with composition of the monolayer, supporting the conclusion inferred from the molecular area/molar fraction diagrams, except for *F9H6A*. Headgroup interactions, possibly through hydrogen bonds, might cause the attractions occurring between the mixture components. The miscibility degree is influenced by both the degree of fluorination and the total increase in chain length. More specifically, longer tails, and longer fluorinated sections in the tail reduce the miscibility with DPPC. The overall behavior of partially fluorinated fatty acids in mixtures with DPPC is similar to what is observed with hydrogenated fatty acids. Mixtures of DPPC and two perfluorinated fatty acids (perfluorododecanoic acid, *F12A*, and perfluorotetradecanoic acid, *F14A*, respectively), studied by measuring pressure/area isotherms, are found to be partially miscible, because of their attractive interactions⁷⁷. At low pressures, the mixing behavior has negative deviations from ideality, however if the pressure is raised the miscibility becomes

almost ideal. The properties of Langmuir monolayers made of DPPC and perfluorooctadecanoic acid (*F18A*), spread on either pure water or NaCl solutions up to 0.4 M, are influenced both by salinity and composition ratio⁸⁹. Phase diagrams show that the molecular area occupied by the mixed monolayer is lower than the ideal molecular area. Negative deviations from ideality mean that the two compounds are miscible, since their interactions are attractive and increase the monolayer cohesion. When the salinity is increased, the negative deviations are gradually reduced, the elasticity of the monolayer and the internal cohesion become lower, because the attraction between the negatively charged carboxy group and the zwitterionic lipid is screened more effectively by Na⁺ ions.

A different study deals with several types of phosphatidylcholines (PC), with chain length varying from 14 C atoms to 18 C atoms, mixed to 11-(perfluorohexyl)-undecanoic acid⁷⁹(*F6H5A*). At low pressure all the mixtures have negative deviations from the ideal mixing behavior, whereas at high pressures PC with an even number of C atoms displays negative deviations, and PC with an odd number of C atoms displays a nearly ideal mixing behavior. The pressure at which the phase transition, from a liquid-expanded to a liquid-condensed state, takes place, is dependent on the monolayer composition for all the mixtures containing odd chains PC and DPPC (16 C atoms). The monolayer collapse pressure is dependent on the composition in all the mixtures examined. Only mixtures containing PC with 17 or 18 C atoms in their tails, at medium and high concentration ranges, have an independent collapse pressure. Phase diagrams show immiscibility behavior, which could imply domain formation in the monolayer. Generally, all the studied combinations show partial miscibility of the components.

Shibata and co-workers have realised several miscibility studies using various lipids and fluorinated compounds⁸⁰⁻⁸⁸. DPPC, combined to a series of perfluorinated fatty acids (*F_nA*, with chain length of $n = 12, 14, 16, 18$ C atoms) and spread on water subphase at pH 2, 0.15 M in NaCl, form mixtures that vary from totally miscible (with *F12A*), to partially miscible (with *F14A* and *F16A*, when less than 0.3 in molar fraction) and totally immiscible (*F18A*)⁸⁰. According to miscibility diagrams, the mixtures that are partially miscible are positive azeotropes.

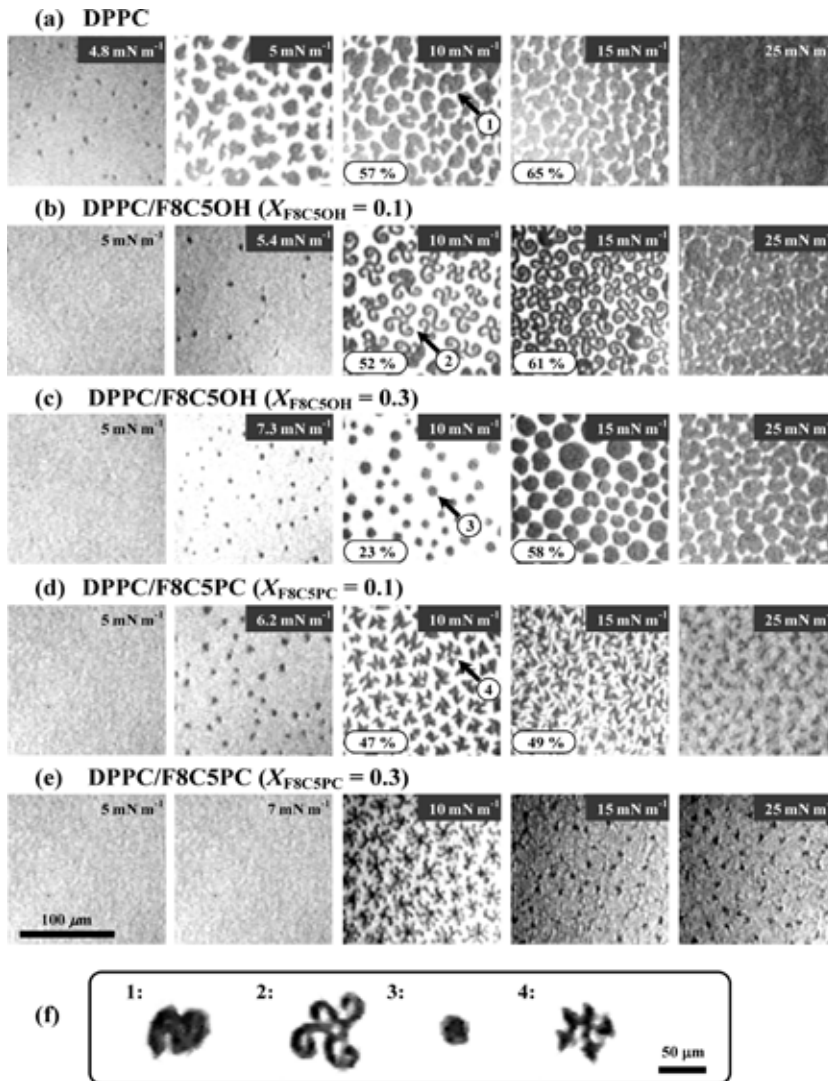


Figure 8. Fluorescence micrographs of (a) pure DPPC, (b) DPPC/F8C5OH ($X_{\text{F8C5OH}} = 0.1$), (c) DPPC/F8C5OH ($X_{\text{F8C5OH}} = 0.3$), (d) DPPC/F8C5PC ($X_{\text{F8C5PC}} = 0.1$), and (e) DPPC/F8C5PC ($X_{\text{F8C5PC}} = 0.3$) monolayers observed at a compression rate of $9.5 \cdot 10^{-2} \text{ nm}^2 \text{ molecule}^{-1} \text{ min}^{-1}$ at 293.2 K on 0.15 M NaCl. In the coexistent phases, the percentage (%) indicated refers to the ordered domains. The monolayer contained 1 mol % fluorescent probe. The scale bar represents 100 μm . The zoomed-in domains indicated by arrows in a–d) at 10 mN m^{-1} are shown in (f), where the scale bar represents 50 μm . Adapted from ref. 82 (figure 7).

The solid-like DPPC domains do not form in combination with *F12A*, and are reduced by the presence of *F14A* or *F16A* (only up to 0.3 molar fraction content). A study that involves (perfluorooctyl)pentylphosphocholine (*F8C5PC*) and (perfluorooctyl)pentanol (*F8C5OH*) monolayers spread on 0.15 M NaCl solution and investigated by pressure/area isotherms, surface potential/area isotherms and dipole moment/area isotherms, shows that the two components are miscible⁸¹. When DPPC is mixed to either *F8C5PC* or *F8C5OH*, the resulting monolayers are also totally miscible⁸². The monolayers are characterized through pressure/area isotherms, surface potential/area isotherms and phase diagrams, which are classified as positive azeotropes. Fluorescence microscopy and BAM show dissolution of DPPC liquid-crystalline domains upon addition of the second component: the DPPC domains alter their morphology and reduce in amount. AFM shows that the miscible monolayer has phase-separated structures on the order of magnitude of nanometers. DPPC mixed to a perfluoroalkylated amphiphile, (perfluoroheptadecyl)-undecyl-dimorpholinophosphate, is totally miscible, and liquid-crystalline domains are not formed anymore⁸³: an ideal mixture is obtained at low pressure; repulsive interactions are present at high pressure; when perfluorooctylbromide is added to the subphase, attractive interactions are found. Also mixtures with (perfluorooctyl)-undecyl-dimorpholinophosphate and DPPC are completely miscible, and fluorescence microscopy confirms the dissolution of liquid-crystalline DPPC domains caused by the amphiphile addition⁸⁴. Other hybrid amphiphiles have been also studied^{85,86}, namely sodium phenyl 1-[(4-perfluorohexyl)-phenyl]-1-hexylphosphate and sodium phenyl 1-[(4-perfluorooctyl)-phenyl]-1-hexylphosphate: they have been spread in combination with DPPC on a 0.13 M NaCl and 0.02 M Tris buffer solution (pH 7.4). Pressure/area measurements and phase diagrams show that the components are miscible; the evidence is supported by fluorescence microscopy characterization. Dipalmitoylphosphatidylglycerol (DPPG) added to perfluorinated fatty acids forms totally miscible monolayers with *F12A* and *F14A*, and immiscible monolayers with *F16A* acid and *F18A*, according to their phase diagrams⁸⁷. Fluorescence microscopy shows that perfluorotetradecanoic acid is only partially miscible, and progressively expelled from DPPG domains when the pressure is increased. Dimyristoylphosphatidylethanolamine, mixed to the same perfluorinated compounds, is immiscible only with perfluorinated fatty acids that have longer tails (*F16A* and *F18A*, with 16 C and 18 C, respectively)⁸⁸. In particular, *F18A* is completely phase-separated, according to AFM characterization. The type of headgroup present in the lipid moiety and its relative polarity influences the

monolayer properties at low pressure. It is generally possible to obtain phase separation upon mixing phospholipids to perfluorinated fatty acids, provided that the fluorocarbon tail is longer than the phospholipid hydrogenated tail.

5.4 Miscellaneous short molecules

Besides perfluorinated or partially fluorinated alkanes and fatty acids, other short, amphiphilic molecules have been studied in mixed Langmuir monolayers, in combination with various compounds. A perfluoropolyether surfactant, $F(CF_2CF_2O)_3CF_2CF_2COOH$, (PFPE), which forms an expanded Langmuir monolayer, has been mixed with a series of carboxylic fatty acids ($n_C = 18, 20, 22, 24$), whose Langmuir monolayers are solid-like: the mixtures, spread on water subphase with Cd^{++} ions, appear immiscible⁹⁰.

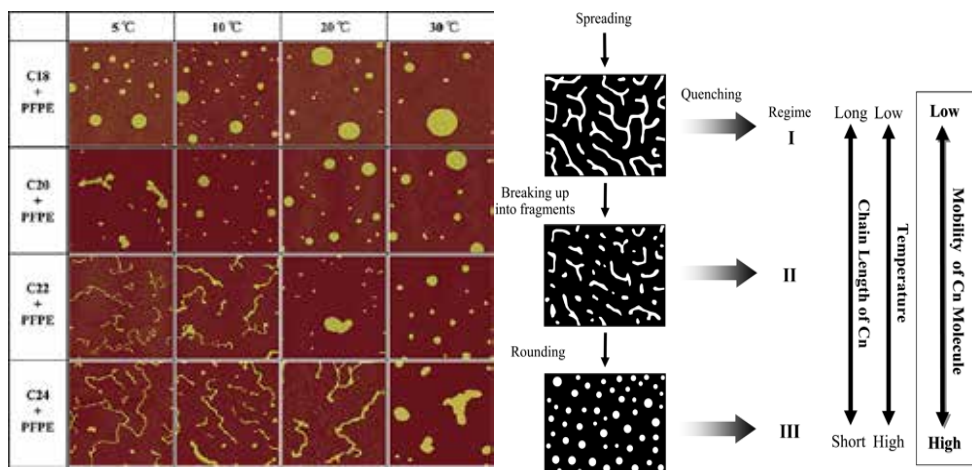


Figure 9. On the left side, $10 \times 10 \mu m^2$ AFM images of mixed monolayers at 5, 10, 20, and 30 °C made of carboxylic fatty acids, C_n /PFPE (2/8) ($n = 18, 20, 22, 24$). The monolayers were transferred on Si wafers at $0.7 \text{ nm}^2 \text{ molecule}^{-1}$.

On the right side, schematic diagram showing the evolution of phase-separated structure in the binary mixed Langmuir monolayer of C_n /PFPE. In the left side cartoons of monolayer surfaces, white and black regions indicate C_n and PFPE phases, respectively. Linearly developed C_n phase domains formed just after monolayer spreading should transform into circular ones in order to minimize the line energy. However, the structural transformation can be stopped by reduced mobility of C_n molecules in their domains; after complete solvent evaporation, the surface structures are frozen at a certain stage of the deformation process (regime I to regime III). The mobility of C_n molecules increases with decreasing chain length of C_n and increasing temperature of the water surface. The transformation process is irreversible; once formed, circular domains are no longer deformed into the elongated ones. Adapted from ref. 90 (figures 4 and 8).

AFM pictures show microscopic, phase-separated domains of a condensed phase, surrounded by an expanded phase. The morphology of domains is influenced by the molecular structure: short fatty acid chains favour the formation of circular domains; long fatty acid chains favour the formation of irregular, branched, elongated domains. Low deposition temperatures yield elongated domains, while high deposition temperatures yield round domains. If spreading is done at low temperature, but LB transfer is done at high temperature, a transition from elongated to round shape is observed; if spreading is done at high temperature, and LB transfer is performed at low temperature, the round shape of domains is retained. Line tension is the key parameter which controls the morphology, however the mobility of molecules determines the stage of morphological evolution at which domains are frozen. Nanoscopic patterns of homogeneous circular domains have been realised mixing an hydrocarbon guanidinium amphiphile to a fluorocarbon carboxylic acid: the very small size of domains obtained is ascribed to the interplay of headgroup interactions (possibility of hydrogen bonding, charged groups, etc.)⁹¹.

Some remarkable examples of phase separation are obtained by using polymerizable molecules, which can be covalently bound after spreading and compression, forming a permanent pattern on the surface of a given substrate⁹²⁻⁹⁴. Amphiphilic silane-coupling agents (SCAs) with perfluorinated alkyl chains, mixed to eicosanoic acid, form phase-separated, micrometer-sized structures⁹³. Several parameters can control size and shape of domains: the trimethoxysilane-based CA favours formation of hexagonal fatty acid domains, while the triethoxysilane and trichlorosilane-based ones yield circular fatty acid domains. An increase in temperature in monolayers formed with the triethoxy SCA, from 10 to 30 °C, causes a considerable increase in domain size. If the fatty acid is replaced with heptadecafluorononadecanoic acid, the domains become 30-60 nm wide nanothreads. Clearly the repulsive interaction between the two different molecules has been lowered by the fluorination of the alkyl chains to energy levels comparable with the interactions present in the homogeneous layer. These LB films are polymerizable, therefore potentially applicable as templates to form nano-patterns with a specific design. Another approach involves biological lipids functionalised with specific moieties: hydrocarbon-based, polymerizable lipids, where the polymerizable functional group is inserted either in the headgroup (methacrylate) or in the tail (diacetylene), have been used in combination with a fluorinated biological lipid, where the headgroup is a glycopeptide⁹⁴. All the mixtures show, at least, a partial miscibility of the components, both at nanometer scale (AFM

pictures) and at micrometer scale (BAM pictures). Finally, perfluorotetradecanoic acid has been mixed to 10,12-pentacosadynoic acid (PCDA), which has a tail that contains a triple C-C bond sensitive to UV illumination, and so easily polymerizable⁹². The Langmuir monolayers form well-defined, phase-separated films, which are easy to transfer through LB technique to a solid substrate. Domains formed by PCDA are irregular, and become thicker upon photopolymerization, yielding most frequently a PCDA bilayer. The mechanism of bilayer formation is not yet clear, however the region of the film which surrounds the thick domains is found to be depleted in PCDA content.

6. Phase-separated systems based on polymers

6.1 Non-fluorinated polymer blends

Preparation of Langmuir monolayers from polymers offers the opportunity to obtain a wide range of new materials, potentially innovative from a technological point of view. Phase-separated mixtures would allow to create materials where the chemical and physical functionalities are controlled at the micrometer, or nanometer scale, by formation of controlled patterns and morphologies. The mixing of homopolymers into two-dimensional blended Langmuir monolayers, though, is not a heavily pursued approach, compared to more complex strategies, where diblock, triblock, or star-like polymers are preferred. Phase separation in polymer blends has been achieved using methacrylate-based polymers that differ by the ester moiety, which has an alkyl chain of different length. Pyrene-labelled poly(isobutyl methacrylate) (PiBMA-Py) and perylene-labelled poly(octadecyl methacrylate) (PODMA-Pe), spread on water, heated to 40 °C, then cooled to 20 °C and transferred on glass, demix in two distinct phases, characterized by AFM and fluorescence scanning near-field optical microscope (SNOM)¹⁸⁻²⁰. The fluorescent labels allow an easy identification of the chemical composition of the domains, and show the total immiscibility of the two polymers. Furthermore, since the excitation energy from pyrene can be transferred to perylene, when they are close to each other, the phase interface can be visualized, and its width measured. The region in which the two polymers are molecularly mixed is 270 nm wide, and the width is independent of the surface pressure at which deposition is done. Before annealing, the PODMA-rich domains contain also PiBMA chains, as the energy-transfer fluorescence imaging shows¹⁸. This is caused by the crystalline nature of PODMA domains at room-temperature, which form solid-like aggregates, trapping PiBMA molecules, during evaporation of the solvent. In this system the repulsive interaction between polymer coils originates from the mismatch in length of the

alkyl moieties connected to the ester group. This mechanism is analogous to the one observed in lipids, discussed in the previous section.

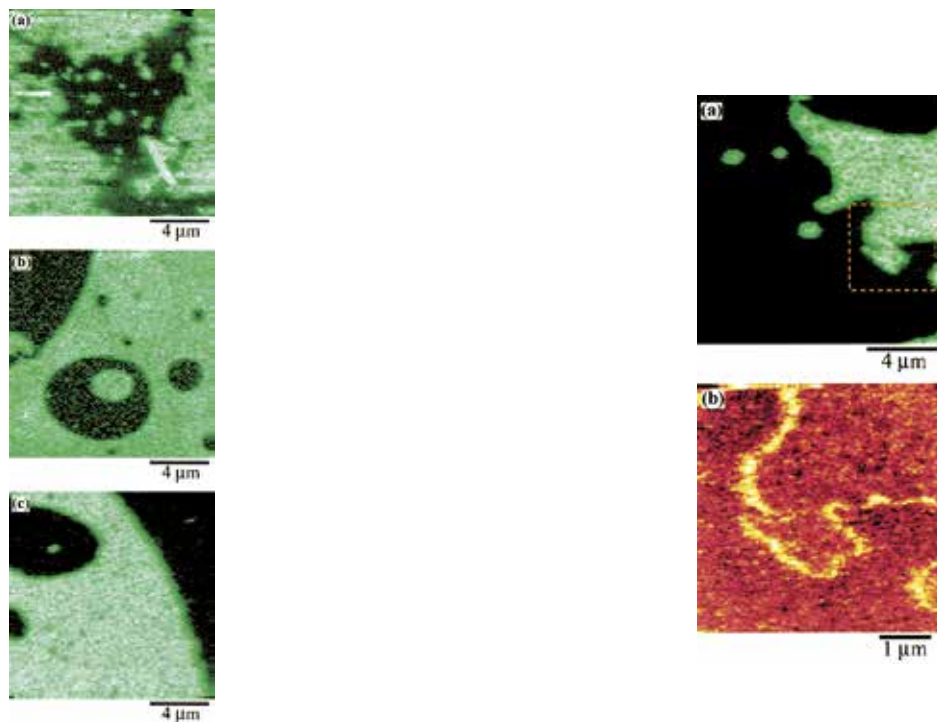


Figure 10. On the left side, perylene fluorescence SNOM images for the PODMA-Pe/PiBMA-Py monolayers with different annealing times: (a) 0, (b) 5, and (c) 60 min. The excitation wavelength was 442 nm, and the fluorescence from perylene was collected through a filter, SC-46 (Fuji). On the right side, perylene fluorescence (a) and energy transfer emission (b) SNOM images of the PODMA-Pe/PiBMA-Py monolayer after annealing. Panel b was obtained by scanning the area indicated as a dashed square in panel a. Adapted from ref. 18 (figures 4 and 6).

Mixtures of poly(methyl methacrylate) (PMMA) and poly-(*n*-nonyl acrylate) (PNA) undergo a reversible, hierarchical phase separation at high surface pressure, which is totally reversible, therefore of a thermodynamic nature. At low surface pressures the monolayer is perfectly miscible⁹⁵. When lateral pressure is increased, the minor component of the monolayer separates on top of the major one, which spreads on the water subphase. Only the mixture composed of PMMA/PNA in the ratio of 25/75 undergoes an inversion of upper and lower layer, while compressed: in the first phase transition, at 17 mN/m, the major component, PNA, is spread on

water and PMMA is pushed on top of it; when the pressure is raised beyond 22 mN/m, inversion takes place and the PMMA monolayer is uniformly spread below PNA domains. Remarkably, this system, although very similar to PODMA/PiBMA, mentioned above, displays a vertical phase separation. Hence, layering already dominates over lateral phase separation when the relative amphiphilicity of the two polymers is slightly different. Blends of polystyrene (PS) and PMMA, in which the relative difference in amphiphilicity is much more significant, are vertically phase separated, with PS domains lying on top of the spread PMMA monolayer⁹⁶. Thus, only a perfect match of the amphiphilicity of the backbone structure in the chosen polymer pair effectively ensures the occurrence of lateral phase separation.

Poly(trimethylene carbonate) and poly-*l*-lactide, both spreadable polymers, turn out to be either miscible or not, depending on the pH of the water subphase⁹⁷. At neutral pH they are mixed, but at pH 10,7 they phase separate. However, both are hydrolysed under these fabrication conditions, and therefore poorly stable. On basic subphase the hydrolysis goes even faster for the blended monolayer, than for the homopolymer monolayers.

Finally, isotactic and syndiotactic PMMA blends phase separate on the water surface, at low pressures, since the former is in an expanded state, while the latter is in a condensed state⁹⁸. If the surface pressure is increased rapidly, the phase separation is preserved, but at low compression rates the phase separation is lost and the stereocomplex is quantitatively formed. Therefore this kind of phase separation is a kinetically induced phenomenon, rather than a stable, thermodynamic state.

6.2 Fluorinated polymer blends

The introduction of partially fluorinated, or perfluorinated, moieties in polymers is a promising approach to obtain phase-separated mixed monolayers. The extensive literature presented in paragraph 5 shows that such an approach would easily introduce lyophobic, repulsive interactions in the mixed monolayer, able to favor the phase segregation of the fluorinated polymer coils from the hydrogenated ones. Furthermore, the fluorinated moieties would add to the polymer film some technologically relevant properties: they are chemically inert, resist to oils and high temperatures, possess good lubrication properties, and finally, have wettability and surface properties different from any other family of polymers. Generally, it is difficult to prepare stable Langmuir Blodgett films directly, because their hydrophobicity and rigidity compromise the transfer of the

Langmuir monolayer to a substrate, so the available literature is modest: molecular design is needed to overcome these intrinsic drawbacks.

Successful incorporation of fluorinated moieties in phase-separated monolayers has been achieved by Fujimori et al., who have based their approach on the synthesis of comb-copolymers with fluorocarbon side chains⁹⁹. The starting monomers are 2-(perfluorodecyl)-ethyl acrylate (FF₁₀EA) and octadecyl acrylate (OA), which are polymerised in bulk reactions. The monolayers are prepared in two different ways: poly-OA and poly-FF₁₀EA are either separately synthesised and then co-spread (ratio 1/1) on the water subphase, or co-polymerised (ratio 1/1) and then spread on the subphase. In the first case a phase-separated binary mixture of two different homopolymers is formed, in which micrometer-sized, circular domains, formed by OA, are surrounded by a fluorinated matrix. In the second case, the monolayer formed by the co-polymer is homogeneous on the micrometer scale, but phase-separated at the nanometer scale, with small, circular, hydrogenated domains of 10-20 nm in diameter. Fourier-transform images show that a 2D hexagonal packing is retained at all length scales by both compounds. When the co-polymer is synthesised from methacrylate monomers¹⁰⁰(OMA and FF₁₀EMA), domains formed have a larger diameter (200-250 nm), due to the different packing hindrance of the methacrylate moiety. However, in this case, the authors did not prepare mixed monolayers from the two different, methacrylate-based homopolymers. When poly-FF₁₀EA is mixed to OA monomer (ratio 1/1), and the monolayer is transferred, forming Z-type Langmuir Blodgett films, domains of 60-100 nm in diameter are observed by AFM¹⁰¹. Also in this case the hydrogenated molecule is localised inside the domains, while the fluorinated polymer forms the surrounding matrix. The composition of domains is confirmed by height measurements done by AFM, and friction coefficient measurements done by FFM. The single-component films of OA have a lower friction coefficient than the films of poly-FF₁₀EA, and domains of the mixed monolayer have a lower friction coefficient than the surrounding matrix. When the mixing ratio is changed, by adding more OA, the domains become more little and dispersed; when more poly-FF₁₀EA is added, the OA domains are deformed. NEXAFS measurements confirm the ordered packing of both types of molecule. Other related works^{102,103}, focused on Langmuir monolayers prepared from a single fluorinated co-polymer, show the influence of molecular architecture on the monolayer morphology and molecular orientation of the comb-polymer chains. If the *w*-position of the side chain contains an F atom instead of an H atom, the orientation and packing properties of the fluorocarbon chain are modified¹⁰⁴. An analogous effect is

obtained by changing the α -methyl group located on the polymer main chain. Even the spreading solvent has an influence on the monolayer morphology¹⁰⁴.

Other approaches to the preparation of stable, transferable fluorinated films are based on the use of poly(*N*-alkylacrylamide)s, functionalised in various ways¹⁰⁵. Their capability to form a hydrogen bonded network between polymer backbones, suggests that a good direction for future investigation in the field might be based on a combined approach, where two polymers are designed so that their repulsive interaction arises from both the hydrophobic moieties (lipophobic-fluorophobic interactions) and the hydrophilic ones (self-recognition through hydrogen-bonding present on only one component in the binary mixture).

7. Line tension

7.1 Definition and experimental measurements

In 2D systems, phases are separated not by surfaces but by lines. So it seems natural to introduce the concept of a linear tension, rather than an interfacial one, that minimises the contact line between phase-separated domains. The line tension, as a concept of surface thermodynamics, seems to have been introduced by Gibbs, who wrote about it in his theory of capillarity¹⁰⁶. Despite that, the investigation of this quantity was not undertaken for many years, and only in these last two decades the topic has gained the attention of many scientists, and several studies and approaches^{107,108} (both theoretical and experimental) have been considered to elucidate the issue. As a matter of fact, the complexity of the topic, the heterogeneous approaches to its investigation, and the debated conclusions reached by different studies, make it very difficult to offer a systematic overview to the reader. At first sight linear phenomena should be simpler than surface phenomena, since the number of dimensions taken into account is lower. This would be true in case we dealt with a true 1D system, when considering a linear boundary in surface thermodynamics. In reality, we always consider 3D systems, even when we deal with surface and line phenomena, but we assign excess thermodynamic quantities to either a surface or a line. This indeed is the cause of the increase of complexity of contact-line phenomena, both in the experimental and in the theoretical realm. The experimental measurement of line tension is made difficult by the typically very small value of this quantity (it is in the order of magnitude of pN), and by the methodology used, which are less easy than those available to measure surface tension. Theoretically, line tension is more complicated than surface tension, since in the latter case, only two bulk phases can meet at a surface, whereas in the former case, several bulk and also surface phases can meet simultaneously at a contact

line. This practically leads to several definitions of line tensions: we do not aim at a detailed and comprehensive treatment of the issue, but rather at an overview of methodologies used in the experimental determination of line tension, which might be applicable to the phase-separated LM.

In the context of a 2D phase-separated system, it is sufficient to specify that phases are separated by lines instead of surfaces, and that interfacial tension becomes linear. In analogy to what is done in 3D systems, the standard approach of defining a Gibbs' dividing line and related linear excess quantities can be easily implemented in 2D systems too. So the line tension is a natural analog of surface tension, and all the basic properties of interfacial tension, derived in a general way, remain valid. In particular, there is an analog of the generalised Laplace equation valid in 2D systems:

$$p^a - p^b = \frac{t}{r} + \frac{\gamma t}{\gamma r} \quad (1)$$

where a and b are the two immiscible phases, p is the two-dimensional pressure, and r is the curvature radius of a dividing line. If the derivative is set to 0 (line of tension, the analog of Gibbs' surface of tension) the equation takes the traditional form of the Laplace equation. In reality the LM is situated between two bulk phases, air and water, and so it is possible to introduce in eq 1 the notion of surface tension:

$$g^b - g^a = \frac{t}{r} + \frac{\gamma t}{\gamma r} \quad (2)$$

The experimental determination is heavily dependent on the instrumental tools used: several methods have been conceived, based on different techniques: surface potential measurements, analysis of Brownian motion of domains, Fourier analysis of capillary waves, analysis of domain relaxation after deformation are the main ones found in literature.

It is usually assumed that the shape of domains is the result of a balance between electrostatic repulsive forces between molecules of the same type, which favor expansion of the domain into the outer phase, and line tension, which minimizes the perimeter of the domain in contact with the outer phase. Rivière et al.¹⁰⁹ use this principle to measure line tension between liquid-expanded and liquid-condensed domains of myristic acid. Their assumptions allow to obtain line tension from the measurement of the surface potential of the two phases, and observation of the shape of the coexisting domains. Their method has the advantage that no assumptions on the dielectric constant or the viscosity of the monolayer are needed. A value of 0.69 pN is given.

Another technique widely used relies on the observation of the dynamics of relaxation of deformed domains. The line tension acts to restore the minimal perimeter of the domain (circular shape), opposed by drag due to viscosity. Mann et al.¹¹⁰ analyze a PDMS monolayer, considering a possible influence of three types of viscosity on the relaxation dynamics: the surface shear viscosity of the polymer monolayer, the shear viscosity of the substrate, and the viscosity between film and substrate. Distorted domains relax according to a characteristic time that depends linearly on the radius of the domains: this is consistent with a main loss mechanism due to surface shear viscosity, while the other two are negligible. These considerations allow to get an estimation of line tension on the order of magnitude of 0.1 pN. However, the same authors extended their work¹¹¹, changing the subphase from pure water to a mixture containing glycerol or glucose: they observed in these circumstances a relaxation rate dependent on the bulk viscosity for domains of moderate size (10-30 nm), and measured a line tension of 1.1 pN, assuming that the regions surrounding the domain are incompressible. A further study^{112,113} elaborates a model to calculate line tension from a closing hole in a PDMS monolayer, which is in agreement with the previous line tension measures. Recently improved experimental techniques¹¹⁴ have led to a refined measure of line tension during hole-closing phenomena in the same system, yielding a value of 0.69 pN for the boundary between the gas/liquid interface.

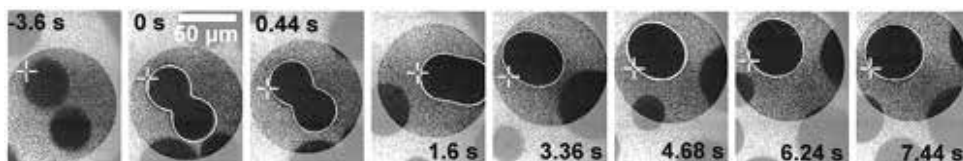


Figure 11. Fluorescence microscopy images of the capture ($t = -3.6$ s) of a domain by the tweezers (white cross) and forced fusion ($t = 0$ s) with a neighboring domain. After fusion, the domain is rotated and translated by the tweezers while concurrently relaxing to a circular shape. Fits according to eq 10 in ref 119 are added as white lines. All images are taken from the same region. Regions far from the domain of interest have been shaded to draw the attention toward the captured domain. Adapted from ref. 119.

Another way to observe domain relaxation dynamics is by deforming it with optical tweezers: Wurlitzer et al. presented a method for force and heat calibration of the tweezers¹¹⁵ and measured¹¹⁶ the line tension of a liquid-expanded/gas phase boundary in a methyl octadecanoate LM at the air/water interface. They manipulated silica spheres immersed in the monolayer with optical tweezers, deforming the domain boundary. Once deformation was achieved, the tweezers

were shut off and the relaxation dynamics, dominated by competition between hydrodynamic resistance and line tension, was recorded.

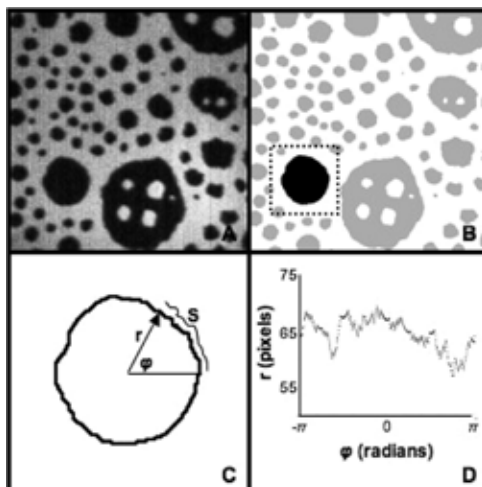


Figure 12. Steps of image processing procedure. Panels A–D illustrate the conversion of captured images to simple functions of r vs. ϕ . (A) Domains are selected on the basis of size and duration in field of view. (B) Thresholding and domain tracking routines are run on sequential images to isolate an individual domain. (C) Images are cropped around domains, and the origin is located at the center of mass. Edge detection routines allow for the isolation of the perimeter. (D) Finally, the domain radius is parameterized in terms of ϕ . Approximately 30–40 configurations (frames) were analyzed per domain, and the line tension was then extracted as described. Adapted from ref. 122.

This method is claimed to allow the observation of faster relaxations, compared to shear flow¹¹⁷, making it possible to investigate low viscous monolayer phases. Contradicting the previous conclusion from Mann¹¹¹, in this work the surface shear viscosity of the LE phase is found to dominate the drag force onto the bead, yielding a line tension value of 7.5 pN instead of 0.5 pN (obtained by neglecting the viscosity of LE phase). In a similar investigation¹¹⁸ two liquid-condensed domains of methyl octadecanoate have been trapped by tweezers and fused together, showing that the viscosity of the LC domains dominates the relaxation process, and the subphase viscosity is negligible (pure 2D flow limit). In the limit of weak deformations¹¹⁹ the electrostatic contribution to the stationary shape of the same system has been evaluated, while in previous works the dipole effect had been neglected.

The large development of fluorescence microscopy visualisation tools has enabled scientist to perform line tension measurements, based exclusively on imaging of phase-separated domains and subsequent analysis of recorded movies¹²⁰⁻¹²³. No external perturbations in this case are needed to obtain data: only custom image processing routines and software, and Model Convolution Microscopy. Especially lipid domains often undulate visibly near transition pressures and critical points. The magnitude of these fluctuations can be directly related to the line tension between coexisting phases, by applying capillary wave theory to the Fourier spectra of boundary fluctuations. The capillary wave treatment neglects the electrostatics, though; nevertheless, agreement of obtained data (within the same order of magnitude) with previous studies has been found.

Less common methods used to study hydrodynamics relaxation are formation of cavitation bubbles in the LM, by local heating with a IR-laser¹²⁴: at high power thermo capillary flow around the laser-induced bubble sets in, caused by a temperature dependence of the gas/liquid line tension. The slope of the line tension with temperature is determined by measuring the thermo capillary flow velocity. Another way is to monitor spontaneous cell coalescence events¹²⁵, similar to the bursting of a soap bubble: an analog of an equation developed by Culick and others to describe the rim velocity of a bursting soap bubble is then used to estimate the line tension. An earlier work used the rate of induced homogeneous nucleation (by high-speed compression), which can be theoretically related to line tension¹²⁶. Finally, an analysis of equilibrium size distribution of circular LC domains has also been suggested as a useful method to estimate line tension¹²⁷.

7.2 Lineactants

So far we have analyzed several 2D systems where different phases coexist, and we have reviewed how it is possible to investigate such systems, both theoretically and experimentally, regarding them as 2D colloids, defining a Gibbs' dividing line, related linear excess quantities, and a linear tension. Now we can extend the analogy one step further. In a 3D system there is a measurable surface tension, which affects the phase separation of immiscible substances into two distinct bulk phases; when a third, surface-active component that partitions at the interface is introduced in small amounts, the surface tension is significantly reduced, and so the interfacial area is significantly increased, and an emulsion is obtained. The two phases are no longer macroscopically phase separated, and the system overall has improved the miscibility. In 2D systems there is a measurable line tension, which governs the shape and morphology of phase-separated domains: it is possible to

hypothesize that the introduction of small amounts of a third component, able to exclusively adsorb at the contact line of domains, causes an effective reduction of the line tension between adjacent phases, favouring an extension of the contact perimeter of domains and forming a 2D emulsion. This line-active compound, analog to the surfactant in the 3D case, is named therefore lineactant, and has a molecular structure that makes it compatible with both the immiscible phases, driving its selective adsorption at the contact line between the domains. First evidence of an effective lineactant activity has been observed by Weis and McConnell¹²⁸ in DPPC monolayers: when a small amount of cholesterol was added to the DPPC, in the phase-coexisting region between LE and LC phases, the LC domain morphology was significantly altered. The almost circular domains became spiral-shaped, increasing significantly the length of their contact line with the surrounding LE region, thereby proving that cholesterol behaves as a lineactant in such a system. Several more accounts of this effect of cholesterol onto lipid LM have been given afterwards⁴⁹. A theoretical proof of the concept has been proposed by Brewster, Safran^{129,130} and Yamamoto¹³¹: they elaborated an analytical model in which a “hybrid” lipid, which has one fully saturated hydrocarbon chain, and one partially unsaturated chain, is added to the typical saturated/unsaturated/cholesterol system. The hybrid preferentially adsorbs at the interface between the two coexisting bulk phases, one composed of mostly saturated lipid, the other composed of mostly unsaturated lipid. The presence of the hybrid at the interface can have a strong effect on the line tension, which can be considerably lowered, down to zero in particular cases. The domain size predicted can range from tens to hundreds of nm. The role of cholesterol is also considered, showing that it causes an increase in domain size when its concentration increases. Hybrid lipids reduce the line tension by reconciling the chain packing incompatibility at the interface between domains.

Hoernberg and Muller devised¹³² a soft, solvent-free, coarse-grained model for lipid bilayer membranes in which the non-bonded interactions take the form of a weighted-density functional that describes the thermodynamics of self-assembly and packing effects of the coarse-grained beads in terms of a density expansion of the equation of state, and weighting functions that regularize the microscopic bead densities, respectively. The model qualitatively reproduces key characteristics (e.g., bending rigidity, area per molecule, and compressibility) of lipid membranes by identifying the length and energy scales via the bilayer thickness and the thermal energy scale. The authors then apply the model to study the main phase transition between the fluid and the gel phase of the bilayer membrane: they locate the phase

coexistence using free energy calculations and also obtain estimates for the bare and the thermodynamic line tension.

Apart from the lipid LM and membranes, effects caused by a lineactant have been reported for other systems by Matsumoto et al.⁷⁴. They prepared phase-separated LM by mixing a partially fluorinated fatty acid to a fully hydrogenated one, and then added an amphiphilic silane-coupling agent to the mixture. Where the binary mixture yielded nanometre-sized stripes, the ternary one yielded spirals. Clearly the morphology is governed by the influence of one of the compounds on the line tension of the system.

An original approach to the issue has been found by Trabelsi et al.¹³³ The authors are the first who specifically designed a molecule to be a lineactant for a suitably phase-separated system. Their system was prepared by mixing hydrogenated and fully fluorinated fatty acid molecules. Two possible lineactants then were synthesised: (i) a single-tail, partially fluorinated phosphonic acid, with the fluorinated block at the end of the tail, (ii) a double-tail phosphonic acid, with a fully hydrogenated tail and a partially fluorinated tail, the latter being identical to the single-tail compound. Line tension was measured by deforming the domains by dragging a needle through the LM, and recording the relaxation dynamics. Line tension decreased systematically as a function of the concentration of lineactant (i) or (ii). Notably, the single-tail lineactant was considerably more efficient than the double-tail one.

Upon increase of lineactant concentration in the system, a consistent reduction of domain size was found for addition of lineactant (ii), and a shape instability was found for addition of lineactant (i). Two different stabilisation mechanisms have been observed: lineactant (i) adsorbs at the phase boundary as individual molecules, while lineactant (ii) forms mesoscale aggregates which then adsorb to the phase boundary as distinct particles: in the latter case ten times higher amount of lineactant is required to achieve the same reduction in line tension.

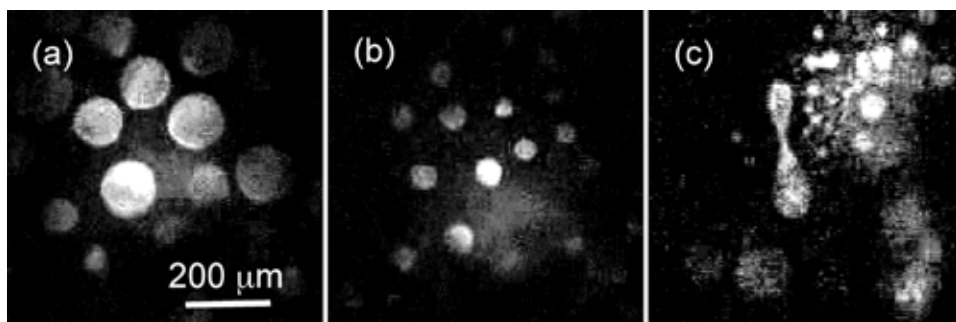


Figure 13. BAM images of two- and three-component monolayers. (a) Two-component monolayer composed of **HC14A** (96.5%) and **FC10A** (3.5%) at $\pi = 6$ mN/m. (b) Three-component monolayer (at $\pi = 6$ mN/m) with the same **HC14A/FC10A** ratio as in (a) but with the addition of $2 \cdot 10^{-4}$ mole fraction of **F10H9PO₃** lineactant. (c) The same composition as in (b) but after the application of interfacial shear. Adapted from ref. 134.

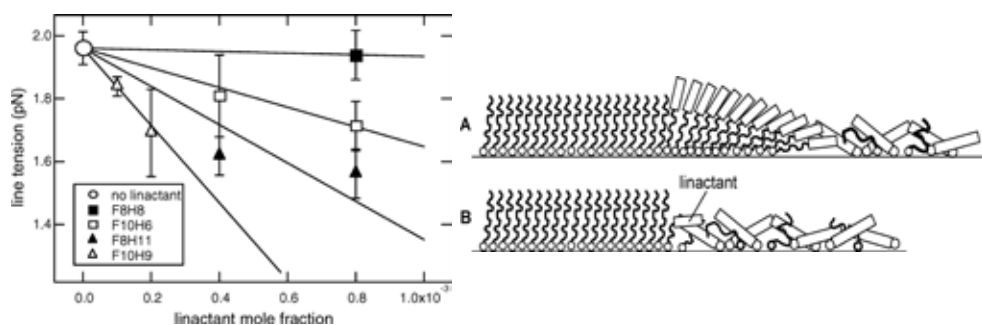


Figure 14. On the left side, measured line tension as a function of lineactant concentration for a monolayer composed of **HC14A** (96.5%) and **FC10A** (3.5%) at $\pi = 6$ mN/m and for monolayers with the same **HC14A:FC10A** ratio with small amounts of additional lineactant. On the right side, proposed arrangement of lineactants at the boundary between a hydrocarbon-rich and fluorocarbon-rich monolayer phase. (a) Hypothetical lineactant arrangement under the conditions of concentrated boundary adsorption. (b) Dilute lineactant adsorption consistent with the isotherms reported here. Adapted from ref. 134 (figures 3 and 7).

The mechanistic correlation between molecular architecture and lineactant efficiency has been further investigated in a second work¹³⁴, where four different partially fluorinated phosphonic acids have been tested: (1)*F8H8*, (2)*F10H6*, (3)*F8H11*, (4)*F10H9*. Couples 1-2 and 3-4 have the same total length, but differ by two $-\text{CF}_2-$ moieties; couples 1-3 and 2-4 have the same amount of fluorinated groups, but differ by three $-\text{CH}_2-$ moieties. The model system consisted of a

mixture of pentadecanoic acid (*HI5A*) and perfluoroundecanoic acid (*F11A*). Monolayers containing the lineactant were qualitatively similar, but with systematically smaller domain sizes; without lineactant the size distribution was heterogeneous over macroscopic length scales. When efficiency was compared between lineactants of same total length, 2 and 4 (with longer fluorinated blocks) were better than, respectively, 1 and 3; lineactants 3 and 4 (the two with the higher total length) were both better than 1 and 2 (the shorter ones). AFM images of domain boundaries show that addition of lineactant dramatically changes the morphology, making the borders much more rough. Moreover, lineactants formed 2D nanometer-sized molecular clusters, whose size seems correlated to the lineactant efficiency. It is hypothesized that lineactant molecules tend to pack in a slightly splayed arrangement, forming a partial cluster structure at the boundary, which maximises the molecular interactions. Self-assembly properties¹³⁵ of lineactants have been further analyzed through AFM, in binary mixtures consisting of a perfluorinated fatty acid and a partially fluorinated lineactant. These mixtures exhibited behavior that was quantitatively consistent with the formation of 2D micelles.

8. General discussion and perspectives

This review aimed at answering whether 2D phases exist as colloidal systems: we presented a vast, though maybe not exhaustive, range of examples of 2D colloids, prepared and characterized in the last years. We shown how it is possible to prepare such systems by using very different compounds, ranging from more traditional amphiphiles, such as lipids and fatty acids, to more unusual ones, e.g. fluoroalkanes, partially fluorinated fatty acids, fluorinated polymers and polymer blends. The overview of lipid-based 2D colloids that we presented aimed at offering a systematic survey of all the chemical and physical properties and variables involved in the phase separation process: the field has been vastly explored in the recent years, and a synthetic but comprehensive review of this subject allows to point out the key factors which must be considered when manipulating these compounds in order to obtain a 2D colloid. In particular, it has been well established how to achieve phase separation through manipulation of tail-to-tail lipid interactions, while headgroup manipulation is less used. Indirect interactions controlled by changing the subphase pH are quite effective in driving phase separation, while the influence of salt counterions dissolved in solution, of head-to-head repulsive forces, or of attractive interactions between the same type

of headgroup are less effective, especially when used alone and not in combination with each other.

A very promising approach has been followed by groups who explored the use of short, fluorinated amphiphiles: several strategies have been adopted. Fluoroalkanes proved to be useful, although in a limited range of conditions, while partially fluorinated fatty acids are very effective in yielding phase-separated systems, in combination with hydrogenated fatty acids. Furthermore, the degree of demixing achievable can be fully controlled by changing the molecular structure (chain length) of the fluorinated and hydrogenated moieties. Partially fluorinated fatty acids are also useful, although they are fully immiscible only in a narrower range of combinations, when the perfluorinated molecule is much shorter than the hydrogenated one added to the mixture. Perfluorinated fatty acids demix also when combined to phospholipids, provided that the fluorinated moiety is, in this case, longer than the hydrogenated one. Generally, these systems are quite versatile and offer a wide range of combinations in which phase separation is easily achieved and controlled. Furthermore, their use allows to introduce specific chemical and physical properties, typical of the fluorinated moieties, into these systems, and so the field has been increasingly explored in the most recent years and represents a very attractive one for future studies.

In contrast, reports on polymers, whether fluorinated or not, are more scarce and poorly systematic: polymer-based systems are very promising for the richness and versatility of compounds that could, potentially, be used to prepare 2D colloids. However, their use, if based on assumptions derived from studies on short amphiphiles, is not straightforward. Studies reviewed here clearly demonstrate how the control of polymer-based 2D colloids is not a trivial task: often polymer monolayers tend to yield phase separation along a direction vertical to the interface on which they have been spread. Lateral phase separation is not easily obtained and requires specific molecular design of the molecules adopted, and a careful selection of the mixture components, in case of non-fluorinated molecules, while in case of use of fluorinated moieties, special attention must be devoted to the molecular structure adopted, in order to be able to successfully transfer the monolayers to a solid support. Further investigations of this field are definitively needed in order to elucidate more in detail which forces are involved in the different phase separation mechanisms, the fundamental properties of these systems, and their potentialities for more applicative purposes.

Investigations on the stability conditions for 2D colloids are also progressively increasing, thanks to the development of optical tools for direct visualisation, and

of several experimental techniques aimed at the measurements of specific thermodynamic quantities, such as the line tension. We offered an overview of several approaches adopted so far, pointing at specific examples in which every technique has been applied.

Finally, we also presented the novel concept of lineactant, showing in which context it was first introduced and successively developed. Recent literature examples are presented, where both theoretical and experimental investigations have been carried out, aimed at establishing which compounds can be used as effective lineactants and what are the structural characteristics necessary to a molecule to display lineactant properties. Some quantitative studies have already been realised, which disclose a new and fascinating direction of research.

We hope that our review will contribute to stimulate further investigations along this direction, as well as into others in the same field of study, enriching even more the knowledge achieved so far by observation and manipulation of these intriguing and fascinating, though rather complex, systems.

Bibliography

- (1) Sahimi, M. *Heterogeneous Materials: Nonlinear and breakdown properties and atomistic modelling*; Springer, 2003.
- (2) Jackson, J. D. *Classical Electrodynamics*; 3rd ed.; Wiley, 1998.
- (3) Dynarowicz-Latka, P.; Dhanabalan, A.; Oliveira, O. N. *Advances in Colloid and Interface Science* **2001**, *91*, 221.
- (4) Kaganer, V. M.; Mohwald, H.; Dutta, P. *Reviews of Modern Physics* **1999**, *71*, 779.
- (5) Ziblat, R.; Leiserowitz, L.; Addadi, L. *Angewandte Chemie-International Edition*, *50*, 3620.
- (6) Mobius, D. *Current Opinion in Colloid & Interface Science* **1996**, *1*, 250.
- (7) Mobius, D. *Current Opinion in Colloid & Interface Science* **1998**, *3*, 137.
- (8) Meunier, J. *Colloids and Surfaces a-Physicochemical and Engineering Aspects* **2000**, *171*, 33.
- (9) Lichtman, J. W.; Conchello, J. A. *Nature Methods* **2005**, *2*, 910.
- (10) Baumgart, T.; Hunt, G.; Farkas, E. R.; Webb, W. W.; Feigenson, G. W. *Biochimica Et Biophysica Acta-Biomembranes* **2007**, *1768*, 2182.
- (11) Lu, Y.; Porterfield, R.; Thunder, T.; Paige, M. F. *Spectrochimica Acta Part a-Molecular and Biomolecular Spectroscopy*, *78*, 216.
- (12) Okonogi, T. M.; McConnell, H. M. *Biophysical Journal* **2004**, *86*, 880.
- (13) Yasuhara, K.; Sasaki, Y.; Kikuchi, J.-i. *Colloids and Surfaces B-Biointerfaces* **2008**, *67*, 145.
- (14) Stockl, M. T.; Herrmann, A. *Biochimica Et Biophysica Acta-Biomembranes*, *1798*, 1444.

- (15) Loura, L. M. S.; Fernandes, F.; Prieto, M. *European Biophysics Journal with Biophysics Letters*, **39**, 589.
- (16) He, H. T.; Marguet, D. *Annual Review of Physical Chemistry*, Vol 62, 62, 417.
- (17) Ito, S.; Aoki, H. *Polymer Analysis, Polymer Theory* **2005**, 182, 131.
- (18) Aoki, H.; Ito, S. *Journal of Physical Chemistry B* **2001**, 105, 4558.
- (19) Aoki, H.; Kunai, Y.; Ito, S.; Yamada, H.; Matsushige, K. *Applied Surface Science* **2002**, 188, 534.
- (20) Aoki, H.; Sakurai, Y.; Ito, S.; Nakagawa, T. *Journal of Physical Chemistry B* **1999**, 103, 10553.
- (21) Connell, S. D.; Smith, D. A. *Molecular Membrane Biology* **2006**, 23, 17.
- (22) Kajiyama, T.; Tanaka, K.; Ge, S. R.; Takahara, A. *Progress in Surface Science* **1996**, 52, 1.
- (23) Overney, R. M.; Meyer, E.; Frommer, J.; Guntherodt, H. J.; Fujihira, M.; Takano, H.; Gotoh, Y. *Langmuir* **1994**, 10, 1281.
- (24) Goodman, T.; Bussmann, E.; Williams, C.; Taveras, M.; Britt, D. *Langmuir* **2004**, 20, 3684.
- (25) Binder, W. H.; Barragan, V.; Menger, F. M. *Angewandte Chemie-International Edition* **2003**, 42, 5802.
- (26) Mercado, F. V.; Maggio, B.; Wilke, N. *Chemistry and Physics of Lipids* **2011**, 164, 386.
- (27) Sovago, M.; Worpel, G. W. H.; Smits, M.; Muller, M.; Bonn, M. *Journal of the American Chemical Society* **2007**, 129, 11079.
- (28) Casillas-Ituarte, N. N.; Chen, X. K.; Castada, H.; Allen, H. C. *Journal of Physical Chemistry B* **2010**, 114, 9485.
- (29) Fang, K.; Zou, G.; He, P. S.; Sheng, X.; Lu, C. H. *Colloids and Surfaces a-Physicochemical and Engineering Aspects* **2003**, 224, 53.
- (30) Silvius, J. R. *Biochimica Et Biophysica Acta* **1986**, 857, 217.
- (31) Viswanath, P.; Suresh, K. A. *Physical Review E* **2003**, 67.
- (32) Brown, R. E. *Journal of Cell Science* **1998**, 111, 1.
- (33) Holopainen, J. M.; Brockman, H. L.; Brown, R. E.; Kinnunen, P. K. J. *Biophysical Journal* **2001**, 80, 765.
- (34) Masserini, M.; Ravasi, D. *Biochimica Et Biophysica Acta-Molecular and Cell Biology of Lipids* **2001**, 1532, 149.
- (35) Kralchevsky, P. A.; Danov, K. D.; Broze, G.; Mehreteab, A. *Langmuir* **1999**, 15, 2351.
- (36) Lucassen.Eh *Journal of Physical Chemistry* **1966**, 70, 1777.
- (37) Hac-Wydro, K.; Jedrzejek, K.; Dynarowicz-Latka, P. *Colloids and Surfaces B-Biointerfaces* **2009**, 72, 101.
- (38) Gardam, M.; Silvius, J. R. *Biochimica Et Biophysica Acta* **1989**, 980, 319.
- (39) Sun, R. G.; Hao, C. C.; Chang, Y. G.; Zhang, J.; Niu, C. L. *Acta Chimica Sinica* **2009**, 67, 1808.
- (40) Angelova, A.; Vanderauweraer, M.; Ionov, R.; Vollhardt, D.; Deschryver, F. C. *Langmuir* **1995**, 11, 3167.

- (41) Knoll, W.; Schmidt, G.; Rotzer, H.; Henkel, T.; Pfeiffer, W.; Sackmann, E.; Mittlerneher, S.; Spinke, J. *Chemistry and Physics of Lipids* **1991**, *57*, 363.
- (42) Silvius, J. R.; delGiudice, D.; Lafleur, M. *Biochemistry* **1996**, *35*, 15198.
- (43) Ahmed, S. N.; Brown, D. A.; London, E. *Biochemistry* **1997**, *36*, 10944.
- (44) Zdravkova, A. N.; van der Eerden, J. P. J. M. *Journal of Crystal Growth* **2007**, *307*, 192.
- (45) Sankaram, M. B.; Thompson, T. E. *Proceedings of the National Academy of Sciences of the United States of America* **1991**, *88*, 8686.
- (46) Smaby, J. M.; Brockman, H. L.; Brown, R. E. *Biochemistry* **1994**, *33*, 9135.
- (47) Su, Y.; Li, Q.; Chen, L.; Yu, Z. *Colloids and Surfaces a-Physicochemical and Engineering Aspects* **2007**, *293*, 123.
- (48) McConnell, H. M.; Vrljic, M. *Annual Review of Biophysics and Biomolecular Structure* **2003**, *32*, 469.
- (49) Marsh, D. *Biochimica Et Biophysica Acta-Biomembranes* **2009**, *1788*, 2114.
- (50) Ramstedt, B.; Slotte, J. P. *Biophysical Journal* **1999**, *76*, 908.
- (51) Goni, F. M.; Alonso, A. *Biochimica Et Biophysica Acta-Biomembranes* **2009**, *1788*, 169.
- (52) Wassall, S. R.; Stillwell, W. *Biochimica Et Biophysica Acta-Biomembranes* **2009**, *1788*, 24.
- (53) Krafft, M. P.; Riess, J. G. *Chemical Reviews* **2009**, *109*, 1714.
- (54) Zhang, G. F.; Marie, P.; Maaloun, M.; Muller, P.; Benoit, N.; Krafft, M. P. *Journal of the American Chemical Society* **2005**, *127*, 10412.
- (55) Lux, C. d. G.; Gallani, J.-L.; Waton, G.; Krafft, M. P. *Chemistry-a European Journal* **2010**, *16*, 7186.
- (56) Maaloum, M.; Muller, P.; Krafft, M. P. *Langmuir* **2004**, *20*, 2261.
- (57) Broniatowski, M.; Nieto-Suarez, M.; Vila-Romeu, N.; Hac-Wydro, K.; Dynarowicz-Latka, P. *Colloids and Surfaces a-Physicochemical and Engineering Aspects* **2004**, *249*, 3.
- (58) Broniatowski, M.; Romeu, N. V.; Dynarowicz-Latka, P. *Journal of Physical Chemistry B* **2006**, *110*, 3078.
- (59) Broniatowski, M.; Dynarowicz-Latka, P. *Langmuir* **2006**, *22*, 2691.
- (60) Broniatowski, M.; Dynarowicz-Latka, P. *Langmuir* **2006**, *22*, 6622.
- (61) Krafft, M. P.; Goldmann, M. *Current Opinion in Colloid & Interface Science* **2003**, *8*, 243.
- (62) Kataoka, S.; Takeuchi, Y.; Endo, A. *Langmuir* **2010**, *26*, 6161.
- (63) Shibata, O.; Yamamoto, S. K.; Lee, S.; Sugihara, G. *Journal of Colloid and Interface Science* **1996**, *184*, 201.
- (64) Rontu, N.; Vaida, V. *Journal of Physical Chemistry C* **2007**, *111*, 9975.
- (65) Yagi, K.; Fujihira, M. *Applied Surface Science* **2000**, *157*, 405.
- (66) Matsumoto, M.; Tanaka, K.; Azumi, R.; Kondo, Y.; Yoshino, N. *Langmuir* **2003**, *19*, 2802.
- (67) Qaqish, S. E.; Paige, M. F. *Langmuir* **2007**, *23*, 10088.

- (68) Qaqish, S. E.; Paige, M. F. *Langmuir* **2007**, *23*, 2582.
- (69) Qaqish, S. E.; Paige, M. F. *Journal of Colloid and Interface Science* **2008**, *325*, 290.
- (70) Qaqish, S. E.; Paige, M. F. *Langmuir* **2008**, *24*, 6146.
- (71) Qaqish, S. E.; Urquhart, S. G.; Lanke, U.; Brunet, S. M. K.; Paige, M. F. *Langmuir* **2009**, *25*, 7401.
- (72) Christensen, S.; Lanke, U. D.; Haines, B.; Qaqish, S. E.; Paige, M. F.; Urquhart, S. G. *Journal of Electron Spectroscopy and Related Phenomena* **2008**, *162*, 107.
- (73) Lehmler, H. J.; Bummer, P. M. *Journal of Colloid and Interface Science* **2002**, *249*, 381.
- (74) Matsumoto, M.; Watanabe, S.; Tanaka, K.; Kimura, H.; Kasahara, M.; Shibata, H.; Azumi, R.; Sakai, H.; Abe, M.; Kondo, Y.; Yoshino, N. *Advanced Materials* **2007**, *19*, 3668.
- (75) Kimura, H.; Watanabe, S.; Shibata, H.; Azumi, R.; Sakai, H.; Abe, M.; Matsumoto, M. *Journal of Physical Chemistry B* **2008**, *112*, 15313.
- (76) Watanabe, S.; Okuda, R.; Azumi, R.; Sakai, H.; Abe, M.; Matsumoto, M. *Journal of Colloid and Interface Science* **2011**, *363*, 379.
- (77) Lehmler, H. J.; Bummer, P. M. *Biochimica Et Biophysica Acta-Biomembranes* **2004**, *1664*, 141.
- (78) Lehmler, H. J.; Jay, M.; Bummer, P. M. *Langmuir* **2000**, *16*, 10161.
- (79) Arora, M.; Bummer, P. M.; Lehmler, H. J. *Langmuir* **2003**, *19*, 8843.
- (80) Nakahara, H.; Nakamura, S.; Kawasaki, H.; Shibata, O. *Colloids and Surfaces B-Biointerfaces* **2005**, *41*, 285.
- (81) Shibata, O.; Krafft, M. P. *Langmuir* **2000**, *16*, 10281.
- (82) Nakamura, S.; Nakahara, H.; Krafft, M. P.; Shibata, O. *Langmuir* **2007**, *23*, 12634.
- (83) Courrier, H. M.; Vandamme, T. F.; Krafft, M. P.; Nakamura, S.; Shibata, O. *Colloids and Surfaces a-Physicochemical and Engineering Aspects* **2003**, *215*, 33.
- (84) Hiranita, T.; Nakamura, S.; Kawachi, M.; Courrier, H. N.; Vandamme, T. F.; Krafft, M. P.; Shibata, O. *Journal of Colloid and Interface Science* **2003**, *265*, 83.
- (85) Hoda, K.; Kawasaki, H.; Yoshino, N.; Chang, C.-H.; Morikawa, Y.; Sugihara, G.; Shibata, O. *Colloids and Surfaces B-Biointerfaces* **2006**, *53*, 37.
- (86) Hoda, K.; Nakahara, H.; Nakamura, S.; Nagadome, S.; Sugihara, G.; Yoshino, N.; Shibata, O. *Colloids and Surfaces B-Biointerfaces* **2006**, *47*, 165.
- (87) Yokoyama, H.; Nakahara, H.; Shibata, O. *Chemistry and Physics of Lipids* **2009**, *161*, 103.
- (88) Yokoyama, H.; Nakahara, H.; Nakagawa, T.; Shimono, S.; Sueishi, K.; Shibata, O. *Journal of Colloid and Interface Science* **2009**, *337*, 191.
- (89) Eftaiha, A. F.; Paige, M. F. *Journal of Colloid and Interface Science* **2011**, *353*, 210.

- (90) Iimura, K.; Shiraku, T.; Kato, T. *Langmuir* **2002**, *18*, 10183.
- (91) Oishi, Y.; Kato, T.; Narita, T.; Ariga, K.; Kunitake, T. *Langmuir* **2008**, *24*, 1682.
- (92) Araghi, H. Y.; Paige, M. F. *Langmuir* **2011**, *27*, 10657.
- (93) Matsumoto, M.; Tanaka, K.; Azumi, R.; Kondo, Y.; Yoshino, N. *Langmuir* **2004**, *20*, 8728.
- (94) Scheibe, P.; Schoenhentz, J.; Platen, T.; Hoffmann-Roeder, A.; Zentel, R. *Langmuir* **2010**, *26*, 18246.
- (95) Sasaki, Y.; Aiba, N.; Hashimoto, H.; Kumaki, J. *Macromolecules* **2010**, *43*, 9077.
- (96) Pohjakallio, M.; Aho, T.; Kontturi, K.; Kontturi, E. *Soft Matter* **2011**, *7*, 743.
- (97) Moon, H. K.; Choi, Y. S.; Lee, J.-K.; Ha, C.-S.; Lee, W.-K.; Gardella, J. A., Jr. *Langmuir* **2009**, *25*, 4478.
- (98) Aiba, N.; Sasaki, Y.; Kumaki, J. *Langmuir* **2010**, *26*, 12703.
- (99) Masuya, R.; Ninomiya, N.; Fujimori, A.; Nakahara, H.; Masuko, T. *Journal of Polymer Science Part B-Polymer Physics* **2006**, *44*, 416.
- (100) Fujimori, A.; Kobayashi, S.; Masuya, R.; Masuko, T.; Ito, E.; Hara, M.; Kanai, K.; Ouchi, Y.; Seki, K.; Nakahara, H. *Macromolecular Symposia* **2006**, *245*, 215.
- (101) Fujimori, A.; Nakahara, H. *Chemistry Letters* **2003**, *32*, 2.
- (102) Fujimori, A.; Araki, T.; Nakahara, H.; Ito, E.; Hara, M.; Ishii, H.; Ouchi, Y.; Seki, K. *Chemical Physics Letters* **2001**, *349*, 6.
- (103) Fujimori, A.; Araki, T.; Nakahara, H. *Journal of Colloid and Interface Science* **2002**, *247*, 351.
- (104) Fujimori, A.; Nakahara, H.; Ito, E.; Hara, M.; Kanai, K.; Ouchi, Y.; Seki, K. *Journal of Colloid and Interface Science* **2004**, *278*, 184.
- (105) Aminuzzaman, M.; Mitsuishi, M.; Miyashita, T. *Polymer International* **2010**, *59*, 583.
- (106) Gibbs, J. W. *The Scientific Papers*; Longmans: New York, 1928.
- (107) Rusanov, A. I. *Surface Science Reports* **2005**, *58*, 111.
- (108) Babak, V. G. *Reviews in Chemical Engineering* **1999**, *15*, 157.
- (109) Riviere, S.; Henon, S.; Meunier, J. *Physical Review Letters* **1995**, *75*, 2506.
- (110) Mann, E. K.; Henon, S.; Langevin, D.; Meunier, J. *Journal De Physique Ii* **1992**, *2*, 1683.
- (111) Mann, E. K.; Henon, S.; Langevin, D.; Meunier, J.; Leger, L. *Physical Review E* **1995**, *51*, 5708.
- (112) Alexander, J. C.; Bernoff, A. J.; Mann, E. K.; Mann, J. A.; Wintersmith, J. R.; Zou, L. *Journal of Fluid Mechanics* **2007**, *571*, 191.
- (113) Alexander, J. C.; Bernoff, A. J.; Mann, E. K.; Mann, J. A.; Zou, L. *Physics of Fluids* **2006**, *18*.
- (114) Zou, L.; Bernoff, A. J.; Mann, J. A.; Alexander, J. C.; Mann, E. K. *Langmuir*, *26*, 3232.

- (115) Wurlitzer, S.; Lautz, C.; Liley, M.; Duschl, C.; Fischer, T. M. *Journal of Physical Chemistry B* **2001**, *105*, 182.
- (116) Wurlitzer, S.; Steffen, P.; Fischer, T. M. *Journal of Chemical Physics* **2000**, *112*, 5915.
- (117) Lauger, J.; Robertson, C. R.; Frank, C. W.; Fuller, G. G. *Langmuir* **1996**, *12*, 5630.
- (118) Steffen, P.; Wurlitzer, S.; Fischer, T. M. *Journal of Physical Chemistry A* **2001**, *105*, 8281.
- (119) Wurlitzer, S.; Steffen, P.; Wurlitzer, M.; Khattari, Z.; Fischer, T. M. *Journal of Chemical Physics* **2000**, *113*, 3822.
- (120) Esposito, C.; Tian, A.; Melamed, S.; Johnson, C.; Tee, S. Y.; Baumgart, T. *Biophysical Journal* **2007**, *93*, 3169.
- (121) Honerkamp-Smith, A. R.; Cicuta, P.; Collins, M. D.; Veatch, S. L.; den Nijs, M.; Schick, M.; Keller, S. L. *Biophysical Journal* **2008**, *95*, 236.
- (122) Stottrup, B. L.; Heussler, A. M.; Bibelnieks, T. A. *Journal of Physical Chemistry B* **2007**, *111*, 11091.
- (123) Stottrup, B. L.; Nguyen, A. H.; Tuzel, E. *Biochimica Et Biophysica Acta-Biomembranes*, *1798*, 1289.
- (124) Muruganathan, R. M.; Khattari, Z.; Fischer, T. M. *Journal of Physical Chemistry B* **2005**, *109*, 21772.
- (125) Roberts, M. J.; Teer, E. J.; Duran, R. S. *Journal of Physical Chemistry B* **1997**, *101*, 699.
- (126) Muller, P.; Gallet, F. *Physical Review Letters* **1991**, *67*, 1106.
- (127) Mulder, W. H. *Journal of Colloid and Interface Science* **2003**, *264*, 558.
- (128) Weis, R. M.; McConnell, H. M. *Journal of Physical Chemistry* **1985**, *89*, 4453.
- (129) Brewster, R.; Pincus, P. A.; Safran, S. A. *Biophysical Journal* **2009**, *97*, 1087.
- (130) Brewster, R.; Safran, S. A. *Biophysical Journal*, *98*, L21.
- (131) Yamamoto, T.; Brewster, R.; Safran, S. A. *Epl*, *91*.
- (132) Homberg, M.; Muller, M. *Journal of Chemical Physics*, *132*, 18.
- (133) Trabelsi, S.; Zhang, S.; Lee, T. R.; Schwartz, D. K. *Physical Review Letters* **2008**, *100*.
- (134) Trabelsi, S.; Zhang, Z.; Zhang, S.; Lee, T. R.; Schwartz, D. K. *Langmuir* **2009**, *25*, 8056.
- (135) Malone, S. M.; Trabelsi, S.; Zhang, S.; Lee, T. R.; Schwartz, D. K. *Journal of Physical Chemistry B*, *114*, 8616.

Chapter 3

Polymers at the Water/Air Interface

Surface Pressure Isotherms and Molecularly Detailed Modeling

Abstract

Surface pressure isotherms at the air/water interface are reproduced for four different polymers, poly-L-lactic acid (PLLA), poly(dimethylsiloxane) (PDMS), poly(methyl methacrylate) (PMMA), and poly(isobutylene) (PiB). The polymers have the common property that they do not dissolve in water. The four isotherms differ strongly. To unravel the underlying details that are causing these differences we have performed molecularly detailed self-consistent field (SCF) modeling. We describe the polymers on a united atom level, taking the side groups on the monomer level into account. In line with experiments, we find that PiB spreads in a monolayer which smoothly thickens already at a very low surface pressure. PMMA has an autophobic behavior: a PMMA liquid does not spread on top of the monolayer of PMMA at the air/water interface. A thicker PMMA layer only forms after the collapse of the film at a relatively high pressure. The isotherm of PDMS has regions with extreme compressibility which are linked to a layering transition. PLLA wets the water surface and spreads homogeneously at larger areas per monomer. The classical SCF approach features only short-range nearest-neighbor interactions. For the correct positioning of the layering and for the thickening of the polymer films, we account for a power-law van der Waals contribution in the model. Two-gradient SCF computations are performed to model the interface between two coexistent PDMS films at the layering transition, and an estimation of the length of their interfacial contact is obtained, together with the associated line tension value.

1. Introduction

Fabrication of nanostructured materials is crucial in the thin film technology realm: the use of polymeric monolayers, combined to techniques such as the Langmuir–Blodgett (LB) deposition, represents a very promising strategy. In order to be able to control the assembly of these structures, fundamental knowledge of the physical behavior of polymer monolayers is crucial, and an accurate insight into the structure of both homopolymer thin films and mixed polymeric monolayers at the air/water interface is required.

In this work we have studied four polymers, potentially suitable for preparation of mixed polymeric Langmuir monolayers, which are chemically stable, are water-insoluble, and behave as liquids on the water surface, so that easily reach the equilibrium state after spreading, namely poly(dimethylsiloxane) (PDMS), poly(methyl methacrylate) (PMMA), poly-L-lactic acid and poly(isobutylene) (PiB).

Some time ago, pure PDMS monolayers at the air/water interface were investigated by pressure/area isotherms studies¹ and measures of rheological properties.^{2–4} Early hypotheses on the possible configurations of the polymer chains¹, which would unfold at low concentration in order to expose the polar groups to the water surface, then collapse into surface-parallel helices at close-packing, have been questioned in more recent years.^{5–7} Mann and Langevin⁷ combined the use of surface pressure, ellipsometry and surface rheological experiments and observed that pure PDMS forms islands at very small surface concentrations and a homogeneous thin layer above a critical concentration. Subsequently, the thin layer of PDMS turns into a thick layer when a second critical concentration value is reached. The authors concluded that the configuration changes previously proposed were less progressive than suggested. Their observations with neutron reflectivity⁸ shown that PDMS is able to form stable molecular layers on water, of thickness unrelated to the molecular weight, and densities and thicknesses of layers have been determined. Brewster angle microscopy (BAM) pictures⁹ taken in the submonolayer surface concentration region, as well as in the collapse region of the pressure/area isotherm, show inhomogeneous patterns on the water surface, with different relative thicknesses: PDMS covers the water subphase with very big domains, coexisting with bare water regions, at low surface coverage, and stratifies into discrete layers when the collapse regime is approached. End-group effects on monolayers of functionally

terminated poly(dimethylsiloxane)s has been investigated by Lenk et al.:¹⁰ in the pressure/area isotherms, they could distinguish between monomer-dependent transitions, typical of non-functionalized PDMS, and transitions involving orientation of the whole chains, dependent on the type of chosen end-group, on the molecular weight, and on the nature of the subphase. Reflectance infrared spectroscopy and epifluorescent microscopy investigations¹¹ proved the coexistence of two different phases in the plateau region of the isotherm at 9 mN/m, although they did not prove definitively their structural nature, being unable to discriminate between a layering transition or the formation of horizontal helices. A recent study¹² based on sum frequency generation spectroscopy found random conformation of the PDMS coils in the diluted regime, and monolayers with one methyl group close to the surface normal and the other close to the surface in the semi-diluted region. Conformation in the plateau region remains under debate, whether it consists of helices laying on top of the monolayer or odd-numbered horizontal layers. Instead, transition to horizontal helices is ruled out. In particular conditions, PDMS can also form a 2D-foam analog at the air/water interface¹³ when spread on both water and AOT subphases, although the polymer is more stable on the former, due to the larger electrostatic repulsion forces.

Poly(methyl methacrylate)s have also been studied with a wide range of experimental techniques: pressure/area isotherms,^{14–17} surface light scattering,^{2,18–20} ellipsometry,^{21–23} neutron reflectometry,²⁰ rheology.²⁴ Homopolymer thin films are found to be inhomogeneous at low pressure areas by different experimental approaches.^{22,23} The PMMA forms island-like structures on the water surface, mixed with water molecules,²² and the thickness of the monolayer has been determined by ellipsometry. Analysis of the scaling behavior by different authors^{25,26} has shown that the air/water interface behaves as a poor solvent close to theta conditions, so that the polymeric film is scarcely hydrated and displays an increase in friction due to direct contact between segments. Accordingly, the viscoelastic behavior is the one of nearly incompressible films.^{19,20} It has also been shown that polymer tacticity^{16,27} has a strong influence on the interfacial behavior: isotactic PMMA in particular shows a rather different pressure/area isotherm when compared to atactic or syndiotactic polymer monolayers, with the former being more expanded than the latter. It also shows a transition upon compression which has been attributed to the formation of double-helical structures at the water surface, similar to those proposed for the bulk crystalline material.

Poly-L-lactic acid Langmuir monolayers have critical behavior in two dimensions: they exhibit a liquid expanded-to-condensed phase transition at low surface pressure, in which the molecules form well-ordered structures, dependent on both temperature and molecular weight changes.²⁸ The monolayers are degraded in alkaline conditions;²⁹ kinetic of interfacial enzymatic degradation has also been reported in a few studies.^{30,31}

Poly(isobutylene) monolayers are seldom reported in the literature: a study of Cox et al.³² reports the spreading behavior of variously end-functionalized polyisobutylene derivatives, while other investigations are focused on its amphiphilic derivatives.^{33,34}

The work presented in this chapter has been aimed at assessing the suitability of model systems composed of (atactic) PMMA, PDMS, PLLA and PiB for the development of an effective modeling technique, which can support experimental evidence and data interpretation in both pure and mixed polymeric Langmuir monolayers. Developing a theoretical description of polymer monolayers, with a good correspondence with experimental data, might allow a more systematic investigation of the behavior of mixed polymeric Langmuir monolayers, addressing issues such as 2D phase separation and partitioning in these systems with a combined theoretical and experimental approach.

In this context, we have investigated PMMA, PDMS, PLLA, and PiB pure monolayer formation through pressure/area isotherms and Brewster angle microscopy, and interpreted our findings by SCF calculations: in more detail, we will forward models where the monomeric features of the polymers are represented on the united atom level; we will determine the orientation at the interface of the hydrophobic and hydrophilic moieties of the polymer coils from the volume fraction distribution profiles; and we will analyze, in the light of these findings, their calculated pressure/area isotherms. We will also investigate how the presence of long-range van der Waals interaction forces between the polymer coils and the interface affects the calculated isotherms, both qualitatively and quantitatively, allowing a better correspondence between calculated and experimental results. It must be noted that the SCF models cannot account for subtle details, due to the tacticity of the polymers, that cause helix conformations or cooperative ordering phenomena. Hence, transitions such as liquid expanded (LE) to liquid condensed (LC) will not be seen. Instead, the focus is on transitions driven by the solvency effects. As it turns out, and in line with experimental results, even a small

difference in local amphiphilicity of the polymer coils on the monomeric level has major consequences for the predicted pressure/area isotherms.

2. Experimental Results

Pressure/area isotherms measured for the pure homopolymer monolayers are shown in Figure 1. They are in good agreement with previously published data.^{7,9,28,35} Further details about the experiments, materials and methods adopted are available in the Supporting Information.

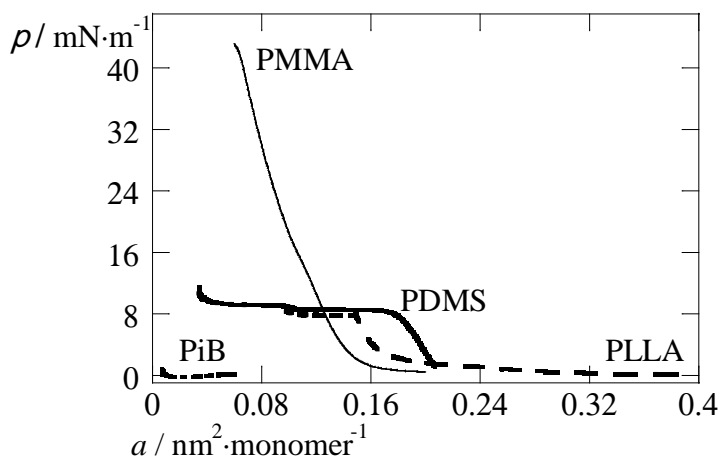


Figure 1: Pressure/area isotherms of Langmuir monolayers constituted of PMMA (thin line), PDMS (thick line), PLLA (long-dashed line), and PiB (short-dashed line). Surface area is expressed in units per monomer.

3. Theoretical Considerations

Here we will elaborate on the use of the self-consistent field theory (SCF) to model polymers at interfaces. In particular, we will apply the freely jointed chain and the lattice approximations, in the spirit of the Scheutjens and Fleer SCF (SF-SCF) approach using a united atom-like model. The classical application of SF-SCF is appropriate for polymers at interfaces, in good solvent conditions. Our aim is to consider polymers at interfaces in the regime that the polymer components are immiscible with the solvent.

In general, the situation of an adsorbing compound which has a miscibility gap in the bulk solution is the domain of wetting theory.^{36,37} The key quantity of interest is the adsorbed amount of the wetting component (adsorbing species) $G^\#$ when the concentration of this component in the bulk reaches the bulk binodal value, that is, the saturation value. Basically, there are two scenarios. Either this adsorbed amount is finite (partial wetting) or it is infinite (complete wetting). In the former case, a macroscopic amount of the adsorbed species will form a droplet on the surface with a finite contact angle. Transitions from partial to complete wetting have received ample attention in the literature. Again, there are two basic scenarios.³⁸ When the transition occurs not too far from the bulk critical point, one usually expects a second order wetting transition. The signature of this transition is that the adsorbed amount at coexistence $G^\#$ diverges smoothly and continuously when going from partial to complete wetting. Much more frequently, the wetting transition is first order. In this case, $G^\#$ is finite (usually a microscopically low value) below the wetting transition and it jumps to infinity at the wetting transition. This situation is expected for polymers in selective solvents under most conditions.

Associated to a first-order wetting transition is a prewetting step in the adsorption isotherm. At the prewetting step, a well-defined jump in adsorbed amount is found from a microscopic, dilute gaslike value, to some larger, that is, mesoscopic value, which occurs when the concentration of the wetting component in the bulk is subsaturated. The position of the prewetting step can be very far from coexistence, in the case that the wetting component is polymeric. It is reasonable to take a prewetting step in a particular system as an indication that the system is in the wet state, that is, above the wetting transition.

The above scenarios follow from a simple Landau theory for the case in which there are short-range interactions (with the surface) only. From the more recent literature,³⁹ it is clear that there are more complex scenarios in systems with complex interactions at the surface, such as systems which have a prewetting step in the adsorption isotherm and remain in the partial wetting regime, having a finite saturation value $G^\#$. From a Landau theoretical perspective, one can then argue that, apparently, there are interactions on multiple length scales. We will argue below that for polymers a complex wetting scenario is the rule rather than the exception, as, on a monomeric level, the interactions with the surface are nontrivial due to hydrophobic and hydrophilic subunits in the chains.

In our set of polymers, PiB, having only C and H atoms, is the most homogeneous in its surface interactions. In the others, we can distinguish between amphiphilicity in the backbone (as in PDMS or PLLA) or amphiphilicity in a dangling side group (as in PMMA). Our goal is to relate the molecular structure of the polymers to the observed different interfacial behaviors. Possible different wetting scenarios are briefly summarized below.

A system is known to be autophobic when the molecules that form a compact monolayer are not wetted by a drop of the same molecules. Surfactant systems⁴⁰ are autophobic on most surfaces. In polymer systems, autophobicity is much less well documented. In another wetting scenario, the thickness of the wetting layer grows stepwise upon increasing the bulk concentration up to the binodal value. The discrete thicknesses of the film occur through a series of layering transitions. A first layer of the molecules is formed, by way of a prewetting step, at the surface, as a result of favorable interactions with the substrate. Due to a weak autophobic effect, the adsorbed layer cannot grow smoothly in thickness and the formation of a second monolayer is suppressed. Then, when the bulk concentration of the polymer is closer to the bulk binodal, a second layer forms abruptly on top of the first one. This process can, in principle, repeat itself. A power-law decay of the van der Waals forces may be part of the underlying physics. From our experimental findings, it seems that PDMS on the air/water interface has features relating to this phenomenon.

From the above, it is clear that for a match between theory and experiment it is important to elaborate on molecularly realistic models. The approach of Scheutjens and Fleer, which we name SF-SCF theory, is well-suited for this.

4. Molecular Detailed SF-SCF Approach with Long-Range van der Waals Interactions

In numerical solutions of the SCF equations, one has to introduce a discretization scheme. Here we follow Scheutjens and Fleer^{41,42} who suggested the

use of a lattice with discrete layers of lattice sites parallel to an impenetrable surface. The surface mimics the sharp air/water interface; below, we choose parameters such that the surface has hydrophobic features. In classical models, the polymer chains are considered as a string of equally sized, spherical segments. In this rather coarse-grained representation, the effective size of the segment may be as large as 0.5 nm. We will adopt as our model a flexible backbone flanked by side groups; that is, we can view the chains as a comb-polymer with precisely positioned polar and apolar united atoms. The molecular details of the models will be discussed in a separate section. In the following paragraph, we will briefly review the SCF machinery utilized.

Unlike in computer simulations such as Monte Carlo or molecular dynamics, in SCF theory, we adopt a mean-field free energy functional $F[\varphi, u, \alpha]$ that needs to be minimized with respect to the volume fraction profiles $\varphi_k(\mathbf{r})$, and maximized with respect to the conjugated molecular fields, which are better known as the self-consistent potentials, or in short the potentials, $u_k(\mathbf{r})$, and the Lagrange field $\alpha(\mathbf{r})$ that takes care of the compressibility condition:

$$\frac{F}{k_B T} = -\ln Q(N, T, u) - \sum_k \sum_{\mathbf{r}} u_k(\mathbf{r}) \varphi_k(\mathbf{r}) + \frac{F^{\text{int}}(\varphi)}{k_B T} + \sum_{\mathbf{r}} \alpha(\mathbf{r}) \left[\sum_k \varphi_k(\mathbf{r}) - 1 \right] \quad (1)$$

where \mathbf{r} refers to the discrete spatial coordinates. Below, we will use two types of coordinate systems, a one-gradient and a two-gradient system. The latter is needed when we want to consider lateral inhomogeneities. The extremisation leads to the so-called self-consistent field equations. (i) The optimization with respect to the volume fractions leads to

$$\frac{\partial F}{\partial \varphi_k(\mathbf{r})} = 0 \Rightarrow \frac{u_k(\mathbf{r})}{k_B T} = \alpha(\mathbf{r}) + E_k(\mathbf{r}) \quad E_k(\mathbf{r}) = \frac{\partial F^{\text{int}} / k_B T}{\partial \varphi_k(\mathbf{r})} \quad (2)$$

which may be referred to as rule 1. In other words, in order to optimize the free energy, we need to compute the potentials as defined by rule 1. (ii) The maximization with respect to the segment potentials leads to:

$$\frac{\partial F}{\partial u_k(\mathbf{r})} = 0 \Rightarrow \varphi(\mathbf{r}) = -k_B T \frac{\partial \ln Q}{\partial u_k(\mathbf{r})} \quad (3)$$

which may be referred to as rule 2. If we compute the segment distributions as in rule 2, we thus maximize the free energy functional (strictly speaking, we have to inspect the second derivative to prove that a local maximum is found, which we will not do here). (iii) The maximization with respect to the parameter $\alpha(\mathbf{r})$ leads to:

$$\frac{\partial F}{\partial \alpha(\mathbf{r})} = 0 \quad \Rightarrow \quad \sum_{\mathbf{k}} \varphi_{\mathbf{k}}(\mathbf{r}) = 1 \quad (4)$$

which may be referred to as rule 3. If at each coordinate the sum of the volume fractions equals unity, we have maximized the free energy.

Finding a saddle point of the free energy is numerically not an easy task, and therefore, the numerical strategies focus exclusively on rules 1–3. For the i th guess for the segment potentials $u_{\mathbf{k}}^{(i)}(\mathbf{r})$ we can compute the i th guess of the volume fractions $\varphi_{\mathbf{k}}^{(i+1)}(\mathbf{r})$ with rule 2. We can check whether rule 3 is obeyed. Deviations of the latter rule will guide the change of the Lagrange field $\alpha^{(i+1)}(\mathbf{r}) = \alpha^{(i)}(\mathbf{r}) + \left[\sum_{\mathbf{k}} \varphi_{\mathbf{k}}^{(i+1)}(\mathbf{r}) - 1 \right]$. Then with rule 1 we first find a new guess for $E_{\mathbf{k}}^{(i+1)}(\mathbf{r})$ and then recompute $u_{\mathbf{k}}^{(i+1)}(\mathbf{r})$. The so-called fixed point is defined by the requirement that $u_{\mathbf{k}}^{(i+1)}(\mathbf{r}) = u_{\mathbf{k}}^{(i)}(\mathbf{r})$ and $\alpha^{(i+1)}(\mathbf{r}) = \alpha^{(i)}(\mathbf{r})$. For such fixed point, it can be shown that the distributions are also stationary $\varphi_{\mathbf{k}}^{(i+1)}(\mathbf{r}) = \varphi_{\mathbf{k}}^{(i)}(\mathbf{r})$. Solutions with at least 7 significant digits can be obtained routinely.

A more extended description of the implementation of rules 1–3 is reported in Appendix A, where we account for the type of interactions occurring in short subsections, while in Appendix B we focus on the treatment of architecturally complex molecules.

5. Parameters and molecular model

The air/water interface is represented in our model by a solid, impenetrable, flat surface in contact with a fluid phase, composed of segment units $k = S$. This

assumption is justified by the sharp nature of the air/water interfacial region: the width of this interface is comparable to the size of a water molecule. A liquid–liquid interface has, on top of this, capillary waves. These lateral fluctuations are out of the scope of our model and are expected to be of minor influence, especially for very thin adsorption layers. Moreover, the presence of a dense polymer film may suppress the small wavelength capillary waves.

The polymers are modeled by two simple types of segments, a united C atom, which mimics the methylene/methyl unit $-\text{CH}_2-/-\text{CH}_3$ and hydrophobic end groups, and an oxygen atom. In order to account for the bigger volume occupied by carboxy groups in PMMA and PLLA, we have introduced two connected oxygen

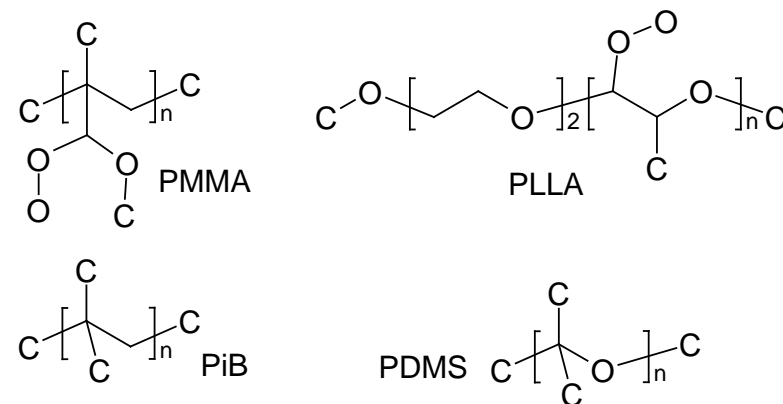


Figure 2: Structures of the homopolymers as modeled in our calculations. The architecture follows closely the chemical details of the real polymer molecules. Small modifications of these structures are motivated by the fact that these models are implemented on a lattice in which the volume of a site coincides with the volume of the building unit of the molecules.

atoms instead of only one. The Si atom is modeled as a C atom, as the differences between the parameters which describe either the Si or C interaction with all the other components in the system are very small: more specifically, O atoms can form strong hydrogen bonds with the solvent, due to the presence of two lone electron pairs, while both Si and C have no lone pairs able to strongly interact with water molecules, and, in this sense, they display a very similar behavior. The chemical structures adopted are reported in Figure 2.

Each polymer, unless mentioned otherwise, consists of $n = 100$ monomer units, close to the size of the compounds studied in the experiments. The number of segments N in the chain is given by the number of monomers times the number of segments in each monomer (which differs for each of the polymers), plus some end segments.

The fluid phase is constituted of water, modeled as a four-armed star, which occupies five lattice sites: the reason for using this object instead of a monomeric unit is that for free water monomers the translational entropy is overestimated.⁴³ It is known that water is a strongly associative liquid, due to its molecules' ability to form hydrogen bonds, and this behavior reduces the free mobility of water molecules. The star-shaped model captures this self-associative property of water molecules in our system.

The Flory-Huggins parameters needed for such a system are five in total: two for the interaction between C or O units and water molecules, two for the interaction between C or O units and the surface, and one for the interaction between C and O units in the polymers. The interaction parameters χ are chosen so that the hydrophobic C units display repulsion toward water molecules and O units, and a strong attraction toward the surface, while the O units are modeled as neutral toward both the solvent and the surface. Here we have used the following values:

$$\chi_{c.w} = 1, \chi_{c.o} = 1.5, \chi_{c.s} = -1.9, \chi_{o.w} = 0, \chi_{o.s} = 0.$$

Similar values have already been used in molecularly detailed modeling of non-ionic surfactant adsorption on silica surface by Postmus et al.⁴³ van der Waals interactions between the C unit and the surface have been introduced in the model in a second stage, as a decaying function of the lattice site distance from the surface ($\chi_{c.s} = c \cdot z^{-3}$, $c = -0.3, z > 1$); the interaction parameter in the first layer has been reduced in all cases to one-third of the original value $\chi_{c.s} = -1.9$.

6. Results and Discussion

In this section, we will first analyze the typical conformations of the polymers that were studied, in the regime where the monolayer is formed. After this, we

consider the adsorption and surface pressure isotherms and quantities that can be derived from those, with some emphasis placed on the effect of the strength of the van der Waals contribution to the adsorption of the chains. In the end of this section, we present two–gradient SCF results focusing on the thin–thick coexistence (layering) predicted for the PDMS film.

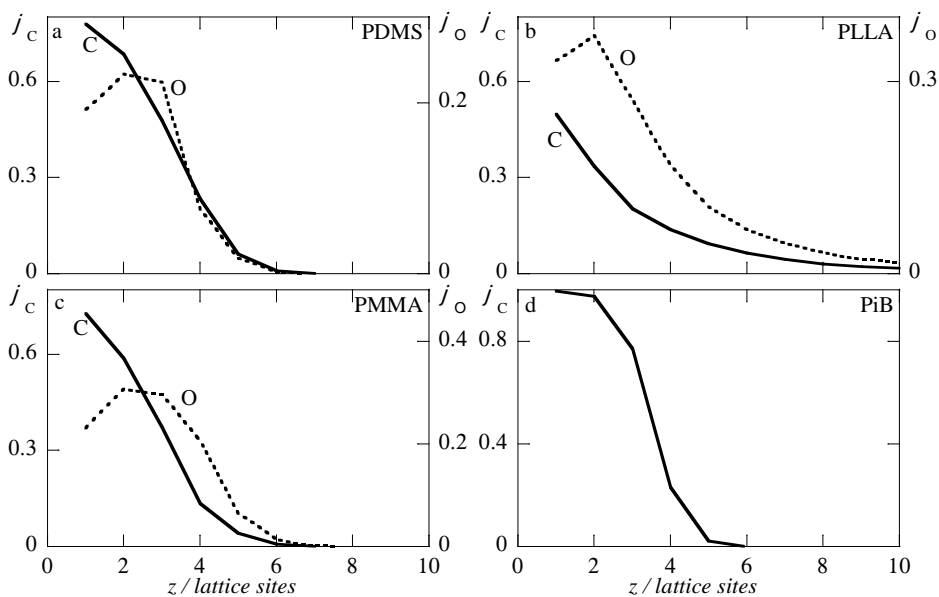


Figure 3: Volume fraction distribution profiles for the polymer systems studied, plotted versus the distance z from the surface, expressed in lattice sites; the volume fraction distribution of the C united atoms is plotted on the left axis (solid line), while the volume fraction distribution of the O united atoms is plotted on the right axis (dashed line): (a) PDMS, (b) PLLA, (c) PMMA, (d) PiB.

The volume fraction distribution profiles for the polymers studied are presented in Figure 3. Considering the fact that the monomer structure differs, there are significant quantitative differences for these density profiles. In each graph the volume fraction $\varphi_k(z)$ for the C and O united atoms are reported, as a function of the distance z from the surface into the water, expressed in lattice sites. The distribution profiles have been calculated for all the polymers at the same surface excess concentration, which corresponds to 2.5 equivalent monolayers ($\mathcal{G}_p = 2.5$), according to the definition given in equation (18), at the point where the chemical potential is close to the bulk coexistence value: in these conditions, each polymer

has formed a thin layer (compact monolayer) at the interface, and the thickness of these layers is comparable for all of them.

The distribution profiles show that the polymers are confined to the layers close to the surface (positioned at $z = 0$), and their concentration diminishes very rapidly with the distance, so that the water subphase (at large z -values) is free from the polymer to a very good approximation. The model thus reproduces the typical experiment of spreading of an insoluble polymer solution at the air/water interface, with the formation of a so-called Langmuir monolayer.

The plots of the separate volume fraction distributions for C and O atoms, for each polymer considered, allow to estimate the degree of orientation of the polar moieties in the monomers with respect to the surface plane: all the polymers display monotonic curves for the C atoms distribution, indicating a preferred orientation of the hydrophobic moieties in the polymer molecule toward the surface (which mimics the vapor phase), whereas the O atom profiles always have a maximum localized in the second (lattice) layer, followed by a monotonic decrease, which indicates a tendency of the hydrophilic moieties to avoid the surface (vapor). The qualitative trend in the volume fraction profiles is very similar for PDMS, PMMA, and PiB, indicating that a strong localization at the surface is occurring, while the density profile is smoother for PLLA and reaches negligible values at greater distances from the surface, implicating a weaker localization at the surface and a looser adsorption with small loops; this is because the PLLA has a higher content in O atoms, which are neither attracted nor repelled by both the surface and the solvent, according to our parameters, so we expect a weaker interaction of this polymer with the surface with respect to all the others. Moreover, both the C and O distribution profiles decrease monotonically, without any crossover until negligible concentration values, indicating that the monomer units have no preferred orientation toward the surface. This is indeed expected, since the molecular structure has hydrophilic and hydrophobic parts in both the backbone and in the side groups, which precludes a strong preferred conformation. In contrast, PiB, which is constituted only of C atoms, displays a distribution profile strongly confined in the first 6 layers of the lattice, pointing at the formation of compact, hydrophobic layers.

The distribution profile of the O atoms of PDMS indicates a high concentration in the second and third layers, followed by a rapid decrease; at the fourth layer, the C and O profile cross over, and they merge again further away. The polymer chains

appear to be oriented only weakly in the close proximity of the surface, whereas at slightly larger distances no preferred orientation is displayed. Apparently, the arrangement of the hydrophilic backbone structure of the PDMS molecules is affected only when they are directly exposed at the interface.

In the case of PMMA, we observe a stronger effect of the surface on the orientation of the polymer coils: the distribution of the O atoms is decreasing more slowly with distance, and the overlap with the C distribution profile is located further away from the surface, at almost negligible concentrations, indicating that, in the thin film formed by the polymer, the coils orient their hydrophilic side groups preferentially toward the fluid phase, whereas the hydrophobic backbone is strongly confined at the surface. The higher mobility of the hydrophilic parts of the polymer, located exclusively in the dangling side groups, allows the orientation of the coils to persist up to a greater distance from the interface.

The difference in orientation between PMMA and PDMS in a Langmuir layer is reflected in the respective adsorption isotherms, namely, partial wetting by the former and a layering transition and complete wetting for the latter: that is, PMMA behaves clearly as a polymeric amphiphile, whereas PDMS has only marginal amphiphilicity.

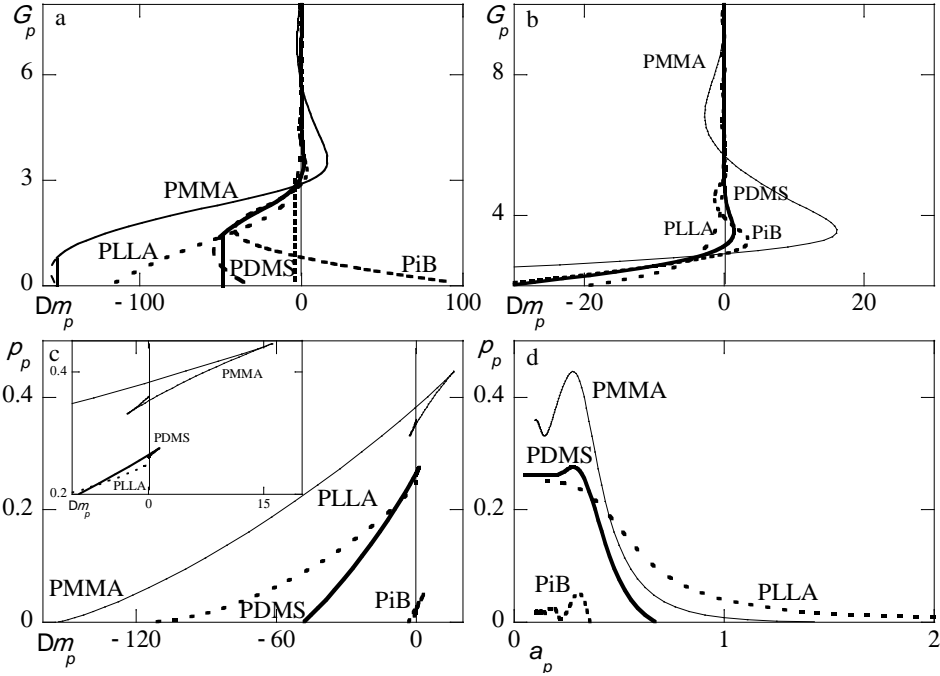


Figure 4. (a) Adsorption isotherms for PDMS, PMMA, PLLA and PiB ($n = 100$), plotted as surface excess concentration G_p versus normalized chemical potential $\Delta\mu_p = \mu_p - \mu_p^\#$; prewetting steps for PMMA, PDMS and PiB are shown as dashed lines, while the observable trend is marked by the vertical lines; (b) enlargement of (a) close to the $\mu_p^\#$ region; (c) surface pressure π_p versus normalized chemical potential $\Delta\mu_p$; (d) π_p / a_p calculated isotherms. Parameters have the default value and only short-range interactions are considered (that is, the long range van der Waals contribution is set to zero).

The calculated adsorption isotherms for PLLA, PDMS, PMMA, and PiB polymers are presented in Figure 4a, b. In these graphs the adsorbed amount, defined as

$$\Gamma_1 = \sum_Z (\varphi_1(z) - \varphi_1^b), \quad (5)$$

is given in equivalent monolayers and presented as a function of a normalized chemical potential defined by:

$$\Delta\mu_i = \left(\frac{\mu_i - \mu_i^\#}{k_B T} \right) \quad (6)$$

where $\mu_i^\#$ is the chemical potential at the bulk binodal (saturation). The chemical potentials follow from the Flory–Huggins theory and can be written as:

$$\frac{\mu_i - \mu_i^*}{k_B T} = \ln \varphi_i^b + 1 - N_i \sum_j \frac{\varphi_j^b}{N_j} + \frac{N_i}{2} \sum_A \sum_B \left(\varphi_A^b - \frac{N_{Ai}}{N_i} \right) \chi_{AB} \left(\varphi_B^b - \frac{N_{Bi}}{N_i} \right) \quad (7)$$

In this equation μ_i^* is the chemical potential in the reference phase for which the pure component is taken, and N_{Ai} / N_i is the ratio of segments of type *A* in molecule *i*. From eqns. (6) and (7) it follows that the chemical potentials can be computed explicitly from the equilibrium bulk volume fractions of the polymers in the system.

The PLLA isotherm (diagram c) shows that this polymer forms a film in the complete wetting regime; the surface concentration grows smoothly, without any abrupt change in thickness, until the coexistence chemical potential is reached and a macroscopically thick film forms. A prewetting step, which marks the transition from the dilute gaslike film to a compact film, is not observed. The molecular structure of this polymer is the most hydrophilic in the series: the chain has hydrophilic O atoms in both the backbone and the side groups. Hence, the polymer spreads easily on the water surface, and the resulting monolayer is in a disordered, liquid–expanded state.

The PDMS isotherm displays a prewetting step at low surface coverage, consistent with data reported by Mann et al.⁹ and Lee et al.,⁸ followed by the formation of a dense monolayer: further layering appears inhibited, as the second transition occurs already beyond the binodal, so that this system remains in the partial wetting regime up to coexistence. The molecular structure of PDMS is that of a hydrophilic backbone decorated by hydrophobic side groups: a weak orientation at the air/water interface is expected, consistent with data obtained from sum frequency generation spectroscopy applied to PDMS monolayers in the semi-diluted regime,¹² so that layering is inhibited. However, we do not expect a strong inhibition of this phenomenon, as from experimental evidence we know that a

layering transition might occur^{11,12} in the plateau region of the pressure/area isotherm, and at higher surface coverage layer formation has been reproduced in our experiments, accordingly with observations of Mann et al.;⁹ long-range interaction forces may play a relevant role in this layering process, and so we will introduce below a power-law decay of the van der Waals forces in the interaction parameter, which accounts for C atoms interactions with the surface, in order to comply with the experimentally found layering transition.

PMMA also shows the occurrence of a prewetting step at low surface concentrations, followed by the monolayer growth; also in this case, the growth of further polymer layers is inhibited and the coexistence chemical potential is reached when the surface coverage is still finite; that is, the film is still microscopically thin. The structure of the PMMA chain is hydrophobic in the backbone and hydrophilic in the side groups, therefore, a higher capability to orient at the surface is expected. This high degree of orientation in the polymer coils causes the occurrence of an autophobic effect. Indeed, the first PMMA layer readily spreads on the water surface and forms a strongly anisotropic monolayer. This layer gradually becomes more compact with increasing values of surface coverage and is anisotropic, due to the orientation of the hydrophilic side groups on the chain; therefore, the formation of a second layer on top of it is inhibited.

PiB is the most hydrophobic polymer in our collection, as its chain does not contain any hydrophilic moiety, and it is the most homogeneous polymer considered, with respect to its surface interactions. The adsorption isotherm shows a prewetting step occurring at surface coverage already close to the binodal value. The isotherm indicates that this system is weak in the partial wetting regime.

SCF calculation allow to evaluate straightforwardly the free energy of the system. From this free energy it is possible to extract other thermodynamic potentials, such as the grand potential:

$$\Omega = F - \sum_{\mathbf{i}} \mu_{\mathbf{i}} n_{\mathbf{i}} \quad (8)$$

There are closed expressions for the grand potential in terms of the volume fraction and segment potential distributions. Without losing generality, we can write the grand potential as $\Omega = \sum_{\mathbf{r}} L(\mathbf{r}) \omega(\mathbf{r})$, where the grand potential density is given

by:

$$\frac{\omega(\mathbf{r})}{k_B T} = -\frac{(\varphi_1(\mathbf{r}) - \varphi_1^b)}{N_i} - \alpha(\mathbf{r}) - \frac{1}{2} \sum_{A'} \sum_{B'} \chi_{AB} (\varphi_A(\mathbf{r}) \langle \varphi_B(\mathbf{r}) \rangle - \varphi_A^b \varphi_B^b) \quad (9)$$

In this equation the primes on the summations indicate that the surface component is not included in the summation. Hence the van der Waals term is not needed in this formula. Of course the van der Waals term influences the distributions and by this way has an obvious effect on the grand potential density. Moreover, the factor $\frac{1}{2}$ in eq. (22) shows that we have distributed the pair interaction evenly over the two components involved in the interactions. This choice does not influence the value of observables, such as the surface tension or line tension in the system. In the one–gradient systems we focus on the grand potential per unit area which is interpreted as the surface tension $\gamma = \Omega / A$.

Figure 4c displays the surface pressure calculated as $\pi_p = \gamma_p^0 - \gamma_p$ (where γ_p^0 stands for the surface tension of the pristine surface) of the spread polymer monolayers as a function of the chemical potential. Whereas there is no layering transition occurring for PLLA, PDMS, and PMMA display phase transitions occurring beyond the chemical potential of the coexistence value, that is, for $\Delta\mu_i > 0$.

The calculated pressure/area isotherms, corresponding to the adsorption curves in Figure 4,a and b, are reported in Figure 4d. The area per molecule has been obtained from the inverse of the surface excess of adsorbed polymer, $a_i = 1 / \Gamma_i$. We observe that a qualitative correspondence between the experimental (Figure1) and the calculated isotherms is achieved.

The PLLA pressure/area isotherm grows very smoothly from large areas, much larger than those for the other polymers, as it is also found in the experimental data here reported. However, the small kink at low pressure, clearly visible in the experimental isotherm, is not reproduced by the SCF calculations. This signature has been assigned to the ordering transition from a liquid–expanded phase to a liquid–condensed phase; this kind of ordering transition cannot be reproduced in a mean–field model. We also do not find any layering occurring at higher pressure values, whereas in the experimental isotherm we observe a plateau region in the lower areas, which could be attributed to the layering phenomenon, occurring after the formation of the ordered, liquid–condensed phase.

The PDMS isotherm shows a steeper increase in pressure at lower areas and a final pressure value very close to, but slightly higher than the one calculated for PLLA, which corresponds to our experimental observations. Furthermore, the two isotherms cross each other at pressure values next to the plateau values, both in the experiment and in the calculations.

The PMMA isotherm, compared to the previous ones, reaches much higher values for the collapse pressure, both in the calculations and in the experiment. This is also in agreement with data found in literature, where the PMMA monolayer is found incompressible.^{19,20} The PMMA pressure begins to rise at lower area values than those found for PLLA and grows smoothly until the collapse value is reached; however, in the experiment, the curve crosses both the PLLA and PDMS isotherms, while in the calculations there is no crossover between the PDMS and PMMA isotherms. Finally, the PiB isotherm displays both in experiments and in calculations very low pressure values, at much lower areas than those shown by all the other polymers.

Figure 5 reports the result obtained on the same polymeric systems, but now in the presence of a long-range van der Waals interaction force. The interaction parameter related to the interactions of C atoms with the surface has been modified by introducing a power-law decay of the van der Waals force, a function of the distance Z of the lattice sites from the surface. The pre-factor, which modulates the strength of the van der Waals interaction, has been varied in order to optimize the results with respect to our experimental data.

Comparison between the adsorption isotherms calculated with the long-range van der Waals interaction and those previously shown displays that the introduction of a slightly stronger attraction of the polymer chains for the surface leads to a shift of all the curves to lower chemical potentials. All the prewetting transitions occur at slightly more negative chemical potentials, and the PDMS layering transition now occurs just before the coexistence value is reached. The PDMS adsorption isotherm is the most sensitive to the introduction of the long-range interaction force. Now there is even a qualitative change. Inspection of Figure 5b proves that a first-order layering step occurs and the system has transformed, from being in the partial wetting regime to being in the complete wetting regime. All the other polymers only show minor quantitative changes.

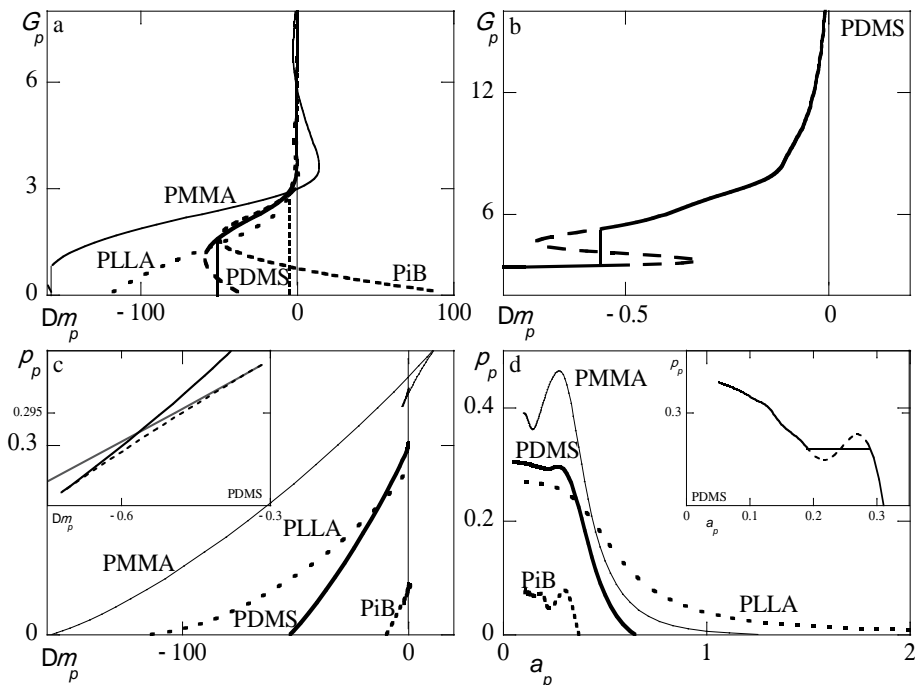


Figure 5. (a) Adsorption isotherms of PDMS, PMMA, and PiB ($n = 100$), plotted as surface excess concentration G_p versus normalized chemical potential $\Delta\mu_p = \mu_p - \mu_p^\#$, calculated from long-range interaction forces between polymer and surface; prewetting steps for PMMA, PDMS, and PiB are shown as dashed lines; (b) enlargement which shows the occurrence of the phase transition in the PDMS adsorption isotherm, next to the coexistence chemical potential (the transition region is marked with a dashed line; the observable trend of the adsorption curve is indicated by the solid line); (c) surface pressure π_p of the polymers versus normalized chemical potential $\Delta\mu_p$: the inset displays the phase transition region for PDMS (grey line, thin film region; dashed line, unstable region; black line, thick film region); (d) pressure/area isotherms calculated with long-range van der Waals interaction forces; the inset shows the region of the PDMS isotherm in which the phase transition (dashed line) occurs, and where the plateau is experimentally observable (solid line).

In Figure 5c, where the surface pressure of the polymer films is plotted versus their chemical potentials, it is again noticed that only the PMMA system is still in the partial wetting regime, whereas the other systems are very close to, or in the complete wetting regime. More specifically, the PDMS system is now clearly in

the complete wetting regime, which is seen by the fact that the surface pressure is a continuously increasing function until the chemical potential hits the binodal value.

The calculated pressure/area isotherms are shown in Figure 5d. The rise in the collapse pressure value for all the curves, due to the increased interaction with the surface, is apparent, especially for PiB and PDMS isotherms, which are more sensitive to the change of the C–surface interaction parameter than those of PMMA or PLLA, due to their higher content of C atoms per segment. Furthermore, the pressure raises earlier, at higher area values, for the same reason. In the inset, the enlargement of the final part of the PDMS isotherm is reported. Now it is clearly visible that the pressure versus the area has a plateau region analogous to the experimentally observed one. The length of this plateau region in the experimental data has been used to optimize the pre-factor applied in the power–law decay of the van der Waals attraction force. From our experimental data, we can see that the area reduces by approximately a factor of 2, consistent with the report of Hahn et al.,¹¹ during the monolayer compression in the plateau region; the pre-factor value has been adjusted accordingly in our calculations, as it also shown in Figure 6.

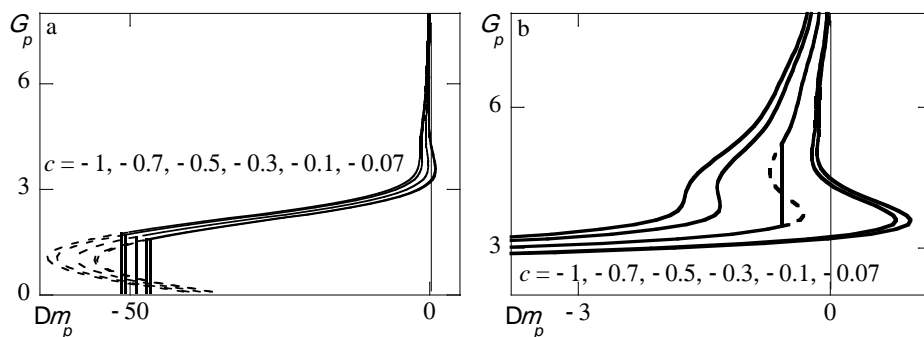


Figure 6. (a) Adsorption curves of PDMS obtained varying the long–range van der Waals interaction force between the C atoms in the polymer chain and the surface; (b) enlargement which shows the transition from a supercritical behavior to a first–order wetting transition for PDMS adsorption isotherms, when the pre-factor of the long range interaction potential is changed from -1 to -0.07 .

The effect of the molecular weight on the position and the length of the plateau region in the PDMS isotherm has been found negligible in previous experiments on methyl–terminated linear PDMS.¹⁰ Also in our calculations, this phase transition has proved to be hardly sensitive to the change in the polymer chain length, as it is shown in Figure 7.

Surface Pressure Isotherms and Molecularly Detailed Modeling

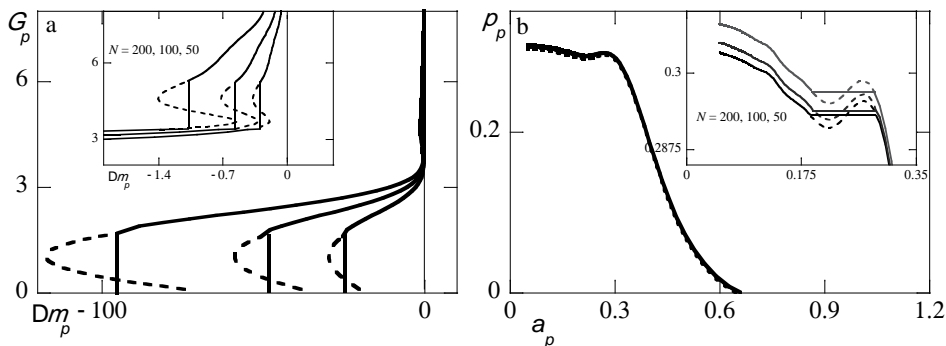


Figure 7. (a) Effect of PDMS chain length variation on the adsorption isotherms calculated with long-range interaction forces; (b) corresponding pressure/area isotherms for PDMS ($n = 200$, bottom line; 100, middle line; 50, upper line).

The length of the plateau region in the pressure/area isotherms is unmodified by the alteration of the chain length, while the pressure reached at the end of the compression is subjected to negligible variations.

Since the model shows good correspondence with the experimental findings, particularly in the modeling of the PDMS behavior and its layering transition, we have deepened the investigation of the latter one, performing two-gradient (2G) calculations in the phase coexistence region; indeed, as there is only one direct observation¹¹ of the layering phenomenon, the SCF calculations provide new insights into this transition. Briefly, in these calculations, the coordinate systems are expressed by $\mathbf{r} = (x, z)$, where x is a coordinate parallel to the surface and z is the coordinate perpendicular to the surface. The mean-field averaging is performed in the y -direction (along the surface perpendicular to the x -direction).

In Figure 8, we report the results obtained when performing a 2G analysis of the PDMS film at the phase coexistence conditions. Figure 8a shows the density profile of the PDMS film in a contour plot in the $x-z$ plane, calculated in the phase coexistence region; the profile shows the coexistence of a thin PDMS film layer with a thicker PDMS film, separated by an interfacial contact region which extends along the direction parallel to the surface.

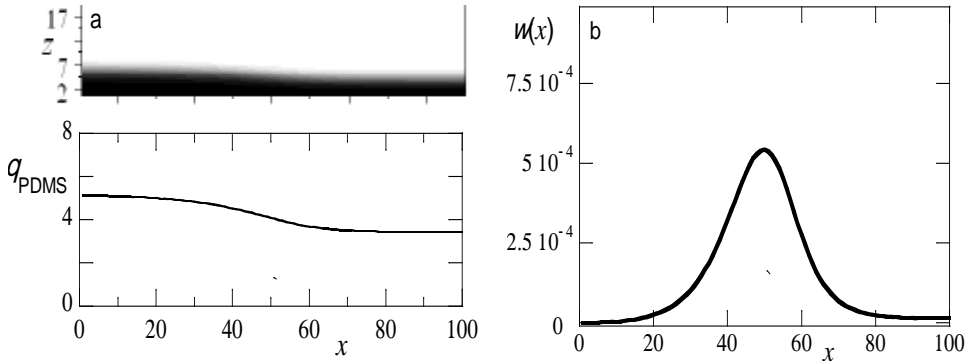


Figure 8. (a) Equal density distributions in color shades (top), in the z and x plane, for a PDMS film in the phase coexistence region and the amount of PDMS θ as a function of the x -coordinate (bottom); (b) grand potential $w(x)$ calculated along the x axis direction; the integrated area below the function is the line tension \mathbf{t} associated with the interfacial contact line between thick and thin PDMS film domains.

In the lower diagram, we also give the amount of PDMS per unit length in the y -direction computed as

$$\theta_1(x) = \sum_z (\varphi_1(x, z) - \varphi_1^b) \quad (10)$$

The $\theta_1(x)$ profile in Figure 8a (bottom) is particularly useful to show the extent of the interface between thin and thick of the PDMS film that undergoes the layering transition.

The interface which separates the two films of different thicknesses is remarkably wide: considering a typical lattice site dimension in our model of about 0.2–0.3 nm in length, the interface associated with this layering transition is more than 12 nm long. Of course, this can be attributed to the fact that the van der Waals loop that is associated to the layering transition is not very pronounced. In other words, the layering transition is close to its critical point.

In analogy with the three-dimensional case, where the interfacial area, which separates two different bulk phases, is associated to a typical value of the surface tension, we can compute a line tension \mathbf{t} , associated to the contact line of the thick–thin PDMS films at coexistence. Since the interfacial region is remarkably wide, the estimation of the line tension must yield very low values: we have

Surface Pressure Isotherms and Molecularly Detailed Modeling

estimated the line tension associated to the interfacial contact line in Figure 8b by plotting the grand potential $w(x) = \int_z \dot{a} w(x,z)$ along the x axis direction and integrating the area bounded by the function: as expected, the calculated value of $t = 0.013 \text{ kT} / \text{nm}$ is extremely low. More specifically, this result means that one needs a line of order $b/0.013 \gg 23 \text{ nm}$ length before the free energy associated to this line reaches the value of $k_B T$. We can estimate a value of $t \sim 0.05 \text{ pN}$ in the phase coexistence region of the isotherm. Such a low line tension implies significant fluctuations in the borders between thin and thick PDMS films and an intrinsic difficulty to visualize domains of either one phase or the other, when performing an experiment on this peculiar system.

Line tension measurements in the gas/liquid region of the isotherm have been reported by Mann et al.,⁴⁴ which estimate a value of $1.1 \pm 0.3 \text{ pN}$ by studying domain relaxation over time. Observing holes closure of the dense polymer film in the same submonolayer regime, Alexander et al.⁴⁵ reported a line tension value of $0.65 \pm 0.03 \text{ pN}$, while Zou et al.⁴⁶ measure a value of $0.69 \pm 0.02 \text{ pN}$. Our prediction is reasonably consistent with these values, as the interfacial contact region between a liquid and a gaseous phase is sharper. It is also known an estimation, in the high density collapsed regime, of 0.1 pN as the upper limit of the line tension value, reported by Mann et al.,⁹ which further corroborates the results obtained by our calculations.

The analysis of the conformation of both thick and thin PDMS layers at coexistence is shown in Figures 9 and 10: the volume fraction distribution profiles $\varphi_k(z)$ of both C and O united atoms are plotted as a function of the distance z from the surface for three different coordinates along the x direction, corresponding to the thin layer (a), in the interfacial zone (b), and the thick layer region (c) in Figure 9. The thin film density profiles reported in Figure 9a show the formation of a weakly, anisotropically oriented monolayer, analogous to what has already been observed in Figure 3. The hydrophobic segments of the polymer chain are preferentially oriented toward the air, while the most hydrophilic ones prefer to orient toward the water phase.

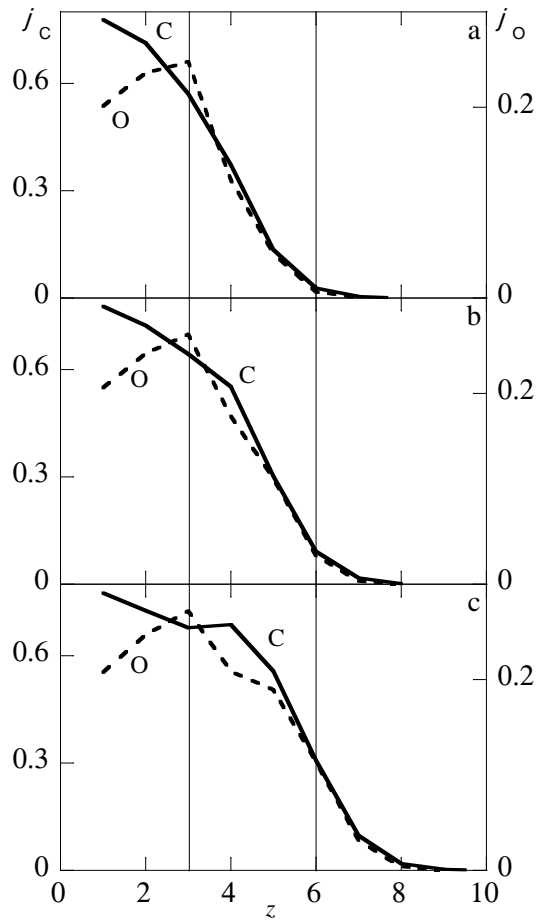


Figure 9. Volume fraction distribution profiles of C and O united atoms plotted versus the distance z from the surface, expressed in lattice sites, for the PDMS thin-thick system at coexistence; the volume fraction distribution of the C united atoms is plotted on the left axis (solid line), while the volume fraction distribution of the O united atoms is plotted on the right axis (dashed line); (a) thin film region, (b) interfacial contact region, (c) thick film region.

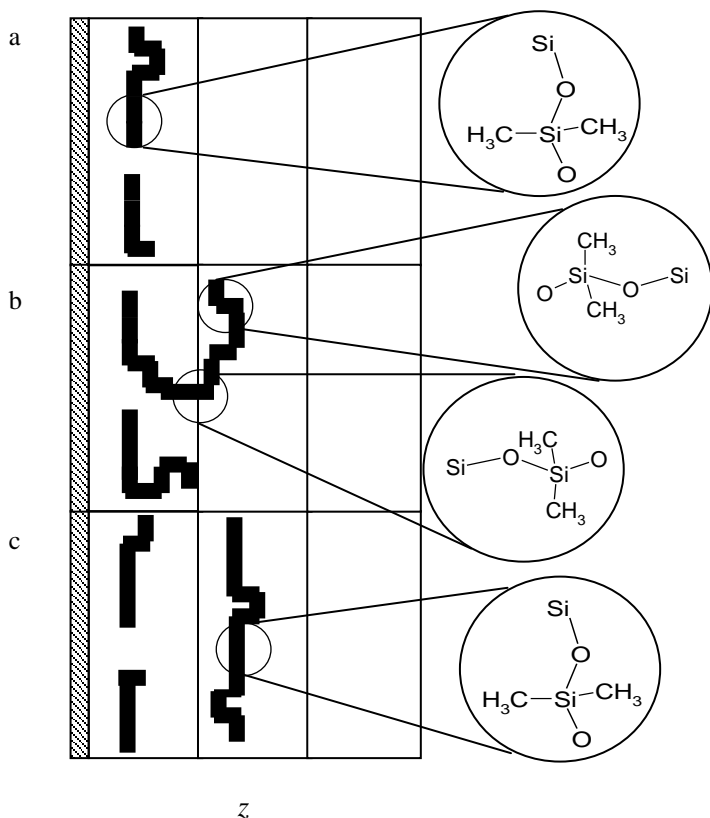


Figure 10. Schematic illustration of the corresponding preferred coil orientations in the layers; vertical segments are aligned to the air/water interfacial plane. When segments align to the surface (case a and c) anisotropy can arise spontaneously from the polymer architecture, as hydrophobic units ($-\text{Si}-$, $-\text{CH}_3$) are preferentially oriented toward the air and oxygen atoms face the water subphase. In the transition (case b) toward the second layer formation, at the interfacial contact between thick and thin film, coils might have loops orienting randomly into the water subphase, which account for the more isotropic state found in the corresponding volume fraction distribution profile.

In Figure 10a, we show how the preferential orientation of the polymer coils along the surface (in the x direction) allows for a spontaneous segregation of C and O atoms in the monolayer, consistent with the volume fraction distribution profile. Our result is consistent with the model presented by Kim et al.¹² for the

semi-diluted regime in the PDMS isotherm. In the thick film region, shown in Figure 9c and 10c, the formation of a second PDMS layer is also accompanied by a partial rearrangement of both hydrophobic and hydrophilic segments toward the air and water phases, respectively; again, this segregation can spontaneously occur when the coils in the thick layer orient preferentially along the surface, leading to the partial segregation of the hydrophobic and hydrophilic moieties in the polymer chain. Again, the odd-numbered, horizontally folded layers model, proposed by Kim et al. for the plateau region in the isotherm, reasonably agrees with our results. The second layer formation is preceded by an intermediate state in which the polymer chains show no preferential orientation; that is, the layer is isotropic at intermediate thicknesses. As shown in the profiles of Figure 9b and in Figure 10b, in the transition region from the thin phase toward the thick one, there is no preferred orientation of either hydrophobic or hydrophilic segments: the coils assume more random configurations, so that the polymer chains display no preferred orientation on average, and the anisotropy is absent. Such a transition state is energetically disfavored and discourages the occurrence of the layering phenomenon.

7. Conclusion

The SF-SCF molecularly detailed modeling of PLLA, PDMS, PMMA, and PiB monolayers, spread at the air/water surface, has proven to be consistent with experimental data: the incorporation in the model of a detailed molecular description of the monomeric features of the four compounds examined here has been crucial in reproducing the features of the adsorption and pressure/area isotherms. These isotherms are totally determined by the different molecular architecture of the polymers at the monomeric level and their consequent preferred orientation when spread at the air/water interface.

The calculations have allowed us to forward a new interpretation of the spreading phenomena occurring at the air/water interface, in terms of wettability of the interface by the spread polymer. In particular, PMMA has proved to be autophobic, due to the anisotropic orientation of its monomers on the water surface, which prevents the growth of multiple layers upon compression. On the other hand PDMS has shown the occurrence of a layering phase transition, also experimentally observed. This process is largely caused by long-range interaction forces between the surface and the polymer segments. The correspondence between modeled and experimental pressure/area isotherms for PDMS has allowed to achieve new

insights into the phenomenon of the layering transition: an estimation of the extension of the interfacial region between thick and thin PDMS film domains and the associated line tension have been obtained through two–gradient calculations.

The molecularly detailed approach has proved its general validity in the description of homopolymers with totally different spreading behavior; as a further work, we intend to apply the same approach also to the description of polymer mixtures spread at the air/water interface, aiming at the analysis of topics such as 2D phase separation and partitioning in mixed polymeric Langmuir monolayers.

Appendix A: Detailed Implementation the SF–SCF Approach with Long–Range van der Waals Interactions.

(1) *The minimization of the mean field free energy (eq. 1) with respect to the segment volume fractions resulted in eq. (2) which was referred to as Rule 1. In the classical approach the interaction–contribution, $E_k(\mathbf{r})$, (eq. 2 in this chapter) is given by the Flory–Huggins interaction energy in which the nearest–neighbor interactions are specified by the Flory–Huggins exchange parameters, $\chi_{k,l}$, for the unlike contacts between segments k and l and in which the Bragg–Williams mean–field approximation is applied.*

$$E_k^{(FH)}(\mathbf{r}) = \sum_l \chi_{k,l} (\langle \varphi_l(\mathbf{r}) \rangle - \varphi_l^b) \quad (\text{A1})$$

In this equation, the angular brackets are needed because the volume fractions are not constant but spatially varying. More specifically, the so–called site fraction is defined as

$$\langle \varphi(\mathbf{r}) \rangle = \sum_{\mathbf{r}'} \lambda(\mathbf{r}, \mathbf{r}') \varphi(\mathbf{r}') \approx \varphi(\xi) + \lambda \nabla_{\mathbf{r}} \varphi(\xi) \quad (\text{A2})$$

wherein ξ is the spatial coordinate in continuous space. From the right–end side of eq. (A2) it is easily seen that the site fraction accounts for both the local volume fraction and the curvature effects. The implementation of eq. (A2) depends on the coordinate system, for which the step probabilities $\lambda(\mathbf{r}, \mathbf{r}')$ are specified.

Here we will consider the situation that a flat solid surface (mimicking a sharp air/water interface) at $z = 0$ is placed next to a series of parallel layers numbered $z = 1, 2, \dots, M_z$. In the one–gradient approach, all inhomogeneities inside the layer are ignored by applying the mean field approximation. Hence, in this case, \mathbf{r} simply is replaced by z . Now we have only three step probabilities per layer, $\lambda(z, z - 1)$, $\lambda(z, z)$, and $\lambda(z, z + 1)$. The three probabilities add up to unity. In a two–gradient approach, we introduce the x –coordinate as a direction parallel to the surface. The mean field approximation is applied in the y –direction, and now we have nine step probabilities per site (x, z) , $\lambda(x; z, x'; z')$, as $x' = x - 1, x, x + 1$ and

$z' = z - 1, z, z + 1$. Again the sum over all transition probabilities equals unity:

$$\sum_x \sum_{z''} \lambda(x; z, x'; z') = 1$$

Below, we will argue that, in addition to the classical approach here outlined, we need to account for a long-range van der Waals contribution experienced by a segment k a distance z away from the surface.

$$E_k^{(\text{vdW})}(z) = \begin{cases} 0 & z < 2 \\ E_k^{(\text{vdW})}(0)z^{-3} & z > 1 \end{cases} \quad (\text{A3})$$

Hence, in this approach we have both a short-range contribution with the surface, using the parameter χ_{Sk} , and a distance-dependent contribution specified by

$$u_k^{(\text{vdW})}(0).$$

Summarizing, the total interactions are given by $E_k(z) = E_k^{(\text{FH})}(z) + E_k^{(\text{vdW})}(z)$.

To implement rule 1 we need a guess for the Lagrange field which will be discussed below in more detail.

(2) *The Maximization of the Mean-Field Free Energy (eq. 1) with Respect to the Segment Potentials Resulted in eq. (3) Which Was Referred to as Rule 2.* The implementation of rule 2 depends strongly on the chain model that is used. For a given chain model, one should generate conformations of individual chains, determine the statistical weight for each conformation, and then arrive at the partition function. Having statistical weights for each conformation allows the evaluation of the density distributions without the explicit need to differentiate to the potentials as required by rule 2. For self-avoiding chains, this route is possible but computationally very demanding. For freely jointed chains, however, there exists an extremely efficient way to compute the volume fractions which is making use of the propagator formalism. Here we outline the approach for linear chains first. For linear chains of type i with segments $s = 1, 2, \dots, N_i$ we may introduce two complementary end-point distributions $G_i(\mathbf{r}, s | 1)$ and $G_i(\mathbf{r}, s | N)$ with the interpretation that these contain the statistical weight of all possible and allowed conformations of chain fragments that have the segment s_i at coordinate \mathbf{r} , provided this segment is connected through $s - 1$ links to segment number 1_i or with $N_i - s$

links to segment number N_i , respectively. Here the position of the first and last segments are not specified, which implies that all starting positions are allowed (are summed over). We will show below how these can be computed, but first we mention that the combination of the two gives the volume fraction distribution of segment s :

$$\varphi_i(\mathbf{r},s) = C_i \frac{G_i(\mathbf{r},s|1)G_i(\mathbf{r},s|N)}{G_i(\mathbf{r},s|\mathbf{r},s)} \quad (\text{A4})$$

where C_i is a normalization constant which fixes the total number of chains in the system, n_i ,

$$C_i = \frac{n_i}{\sum_{\mathbf{r}} G_i(\mathbf{r},1|N)} \quad (\text{A5})$$

In this equation, the denominator is identified as the single-chain partition function. It is also easily seen that $C_i = \frac{\varphi_i^b}{N_i}$, which can be used to compute the volume fraction in the bulk of the system. In eq. (A4), the denominator specifies the statistical weight of a walk from segment s to s , or in other words, of a single segment. This quantity is simply given by the Boltzmann weight

$$G_i(\mathbf{r},s|\mathbf{r},s) = \exp\left(-\frac{u_i(\mathbf{r},s)}{k_B T}\right) \quad (\text{A6})$$

At this point, we should realize that eq. (A6) features a segment potential which depends on the segment ranking number. From rule 1, we know that this quantity depends also on the segment type, which may vary along the chain. For this reason, we introduce a chain architecture operator $\delta_{s,i}^k$, specific for chains with a non-trivial sequence, which is fully specified by the monomer sequence of the polymer chains of type i : it assumes the value unity when segment s of molecule i is of type k and zero otherwise. Hence,

$$u_i(\mathbf{r},s) = \sum_k \delta_{s,i}^k u_k(\mathbf{r}) \quad (\text{A7})$$

The end–point distributions are generated by a pair of complementary propagator equations:

$$\begin{aligned} G_i(\mathbf{r},s | 1) &= G_i(\mathbf{r},s | \mathbf{r},s) \sum_{\mathbf{r}'} \lambda(\mathbf{r},\mathbf{r}') G_i(\mathbf{r}',s-1 | 1) \\ G_i(\mathbf{r},s | N) &= G_i(\mathbf{r},s | \mathbf{r},s) \sum_{\mathbf{r}'} \lambda(\mathbf{r},\mathbf{r}') G_i(\mathbf{r}',s+1 | N) \end{aligned} \quad (\text{A8a,b})$$

which once again make use of the *a priori* step probabilities $\lambda(\mathbf{r},\mathbf{r}')$. The propagators are started at the free ends of the molecule, that is, $G_i(\mathbf{r},1 | 1) = G_i(\mathbf{r},1 | \mathbf{r},1)$ and $G_i(\mathbf{r},N | N) = G_i(\mathbf{r},N | \mathbf{r},N)$, respectively. Applying the procedure for a monomeric solvent is straightforward:

$$\varphi_W(\mathbf{r}) = C_i G_W(\mathbf{r}) \quad (\text{A9})$$

and because the weights G are normalized to unity in the bulk, we have $C_i = \varphi_W^b$. Hence, in practice, the bulk volume fraction of the solvent is needed for this normalization, and typically this value is computed from the compressibility relation $\sum_k \varphi_k^b = 1$.

In passing, we may point to the opportunity that when the solvent is monomeric, one can use eq. (A9).

(3) *The Maximization of the Mean–Field Free Energy (eq. 1) with Respect to the Lagrange Field Resulted in Rule 3.* In the Scheutjens–Fleer SCF formalism, the lattice sites are taken to fit the monomeric species in the system. The macromolecules are assumed to be built up from these monomeric species. In this special case, that the monomeric volume per segment is fixed to b^3 , where b is the monomer length; the Lagrange contribution $\alpha(\mathbf{r})$ to the segment potential is independent of the monomer type.

To apply rule 2, we need the volume fraction distribution collected per segment type. These are found by

$$\varphi_k(\mathbf{r}) = \sum_i \sum_{s=1}^{N_i} \delta_{s,i}^k \varphi_i(\mathbf{r},s) \quad (\text{A10})$$

Appendix B: Architecturally Complex Molecules

It is relatively easy to see how the propagator formalism should be generalized for molecules that consist of sequences of monomers that are not *per se* organized in a linear fashion. The strong molecular specificity found in the experimental pressure/area isotherms clearly points to the necessity that the structure of the chain on a monomeric level should be accounted for. Here we will illustrate the procedure for a molecule with one branch point, and thus with three chain ends, and trust that the generalization to molecules with multiple branching point is straightforward.

Consider a molecule with three arms connected to a branching segment, e.g., $(A)_5(B)_1[(A)_{10}](A)_6$, where the chain fragment between the square brackets is the sub-chain that is linked to the central B segment as a side chain. $s = 1, 2, \dots, 12$ may be the ranking numbers of the main chain and the branching unit is, in this example, at $s = 6$. The remaining segments are numbered $s = 13, 14, \dots, 22$, where $s = 13$ sits next to the branching segment and $s = 22$ is the free end. The first point is that, in this case, there are three end-point distribution functions, which are found from starting at one free end and propagating to the branch point: $G_1(\mathbf{r}, s | 1)$, which can be computed for $s = 1, 2, \dots, 6$, $G_1(\mathbf{r}, s | 12)$ for the fragment $s = 12, 11, \dots, 6$ and $G_1(\mathbf{r}, s | 22)$ for the side moiety $s = 22, 21, \dots, 13, 6$. Here we recall that segment 13 is the segment next to $s = 6$. Combining two of these end-point distributions at the branching point allows one to propagate from a branch point to one of the ends. The combination rule reads:

$$G_1(\mathbf{r}, 6 | 1; 12) = \frac{G_1(\mathbf{r}, 6 | 1)G_1(\mathbf{r}, 6 | 12)}{G_1(\mathbf{r}, 6 | \mathbf{r}, 6)} \quad (\text{A11})$$

for the propagation toward the end of the side group. The division by the free segment distribution is necessary because the segment weight for segment $s = 6$ should occur just once. For the segments $s = 13, 14, \dots, 22$ the volume fraction distribution follows from

$$\varphi_1(\mathbf{r},s) = C_i \frac{G_i(\mathbf{r},s | 1;12)G_i(\mathbf{r},s | 22)}{G_i(\mathbf{r},s | \mathbf{r},s)} \quad (\text{A12})$$

Analogous eqs (A10,A12) apply for the volume fraction of segments in the other two chain fragments. Finally, the volume fraction distribution of the branch point follows from:

$$\varphi_1(\mathbf{r},s) = C_i \frac{G_i(\mathbf{r},s | 1)G_i(\mathbf{r},s | 12)G_i(\mathbf{r},s | 22)}{G_i(\mathbf{r},s | \mathbf{r},s)^2} \quad (\text{A13})$$

Appendix C: supporting information

Materials and methods

The polymers Polydimethylsiloxane, (M_n 14800, M_w 16900, PDI 1.14), here named PDMS, Poly(methylmethacrylate), (M_n 21500, M_w 30000, PDI 1.4), here named PMMA, Poly(L-lactic acid), (M_n 15000, M_w 20200, PDI 1.35) here named PLLA and Polyisobutylene, (M_n 13900, M_w 23800, PDI 1.7) here named PiB, have been purchased from Polymer Source Inc. and used as received. All the glassware was soaked into KOH 2 M ethanol solution and rinsed thoroughly with demineralized water before use. Stock solutions were prepared in chloroform (Aldrich, > 99.9%, HPLC grade). A few microlitres of these solutions were spread with the aid of an 10 μl Hamilton syringe on water demineralized ($R > 18.2 \text{ MW}$) using an EasypureUV machine from Barnstead; no special test for the presence of amphiphilic impurities were performed on it.

Langmuir isotherms were measured with a MicroTroughXL apparatus, purchased from Kibron Inc. The trough was thoroughly flushed with ethanol and acetone solutions, and then rinsed with demineralized water before every use. The equipment was kept at constant temperature of 20 °C for the whole experiment by connection to a waterbath. The water subphase was cleaned thoroughly by compression and suction of the water, until the surface pressure was less than 0.1 mN/m in the whole compression cycle. Then the solution (usually around 10 μl) was spread with a microsyringe and the solvent was allowed to evaporate in the next 20 minutes, before performing any compression. Unless mentioned otherwise, compression rate is fixed to 5 mm/min.

Brewster angle microscopy (BAM) was performed fixing the Langmuir trough equipment under a Multiskop apparatus purchased from Optrel GBR.

Experimental results

Pressure/area isotherms measured for the pure homopolymer monolayers are shown in Figure A1. They are in good agreement with previously published data^{7,9,28,35}.

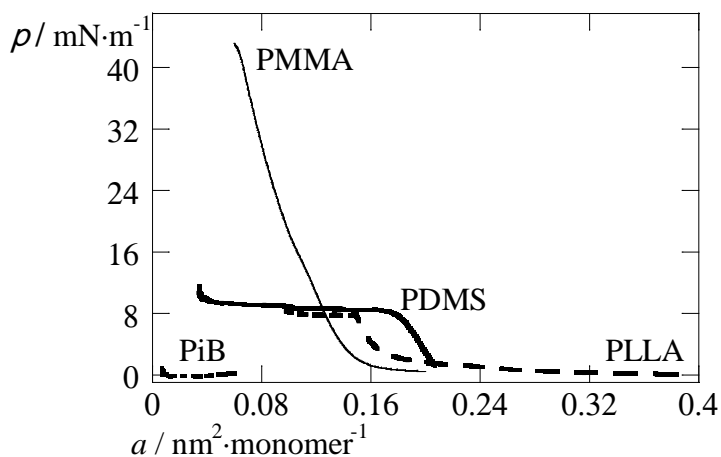


Figure A1. Pressure/area isotherms of Langmuir monolayers constituted of PMMA (thin line), PDMS (thick line), PLLA (long-dashed line) and PiB (short-dashed line). Surface area is expressed in units per monomer.

The purpose of the experiments here described is to have a consistent set of data, acquired in homogeneous conditions, which can be fruitfully compared to the model developed.

While PMMA surface pressure increases smoothly with decreasing area, the PDMS isotherm exhibits a remarkably long and flat plateau region, at $\rho = 8.4$ mN/m. A small feature at $a = 0.10$ nm²/monomer is apparent, where the surface pressure slightly increases to $\rho = 9$ mN/m and then remains constant until very low molecular areas. PLLA isotherm shows a smooth increase in pressure up to $a = 0.23$ nm²/monomer, where the phase transition region starts, then at $a = 0.17$ nm²/monomer a steep increase in the pressure values denotes formation of a

compressed layer, which collapses at $a = 0.15 \text{ nm}^2/\text{monomer}$, $\rho = 8 \text{ mN/m}$, yielding a flat plateau region at $\rho = 7.8 \text{ mN/m}$. The PiB isotherm has $\rho < 1 \text{ mN/m}$ through the whole compression cycle.

BAM pictures of the homopolymer monolayers have been taken during the compression cycles. PMMA is the only polymer here that does not show any particular feature: the brightness of the monolayer steadily increases through the compression along with the measured pressure. PDMS monolayer also does not show any relevant feature in the first stages of compression, and in the whole plateau region, while in the final stages of compression some very bright domains appear, which subsequently increase in diameter. These bright spots tend to increase in area also when the compression is stopped for 30 minutes or more. Similar observations have been done by Mann et al. at the same surface coverage with concentrated spreading solutions, and their results are consistent with our findings.⁷ They have also observed very complex morphologies at submonolayer concentrations, while they do not report any BAM pictures in the region of the isotherm where the pressure increases and reaches the plateau value. Our experiments did not focus on the submonolayer region of the isotherm, where surface pressure is negligible, so we were not able to see these complex domain patterns. From ellipsometric data by Lee et al.⁸ inhomogeneities in the film thickness are present both at submonolayer concentrations and at high surface coverage, confirming the formation of discrete layers close to the collapse pressure, as BAM pictures also suggest. PLLA pictures taken in the isotherm region where the LE/LC phase transition occurs show circular, brighter domains, while in the

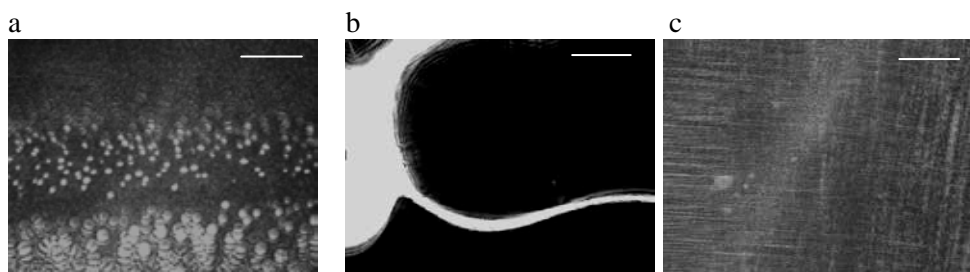


Figure A2. a) PDMS monolayer at 9.6 mN/m , $0.09 \text{ nm}^2/\text{monomer}$; b) PiB monolayer at 0 mN/m , $0.25 \text{ nm}^2/\text{monomer}$; c) PLLA monolayer in the phase transition region, 1.7 mN/m , $0.19 \text{ nm}^2/\text{monomer}$. Scale-bar corresponds to 150 nm .

more compressed region these domains disappear and the brightness of the monolayer increases. The PiB monolayer shows fluid-like, structureless or circular features, very bright and heterogeneous in size, in all the stages of the compression cycle.

Bibliography

- (1) Fox, H. W.; Taylor, P. W.; Zisman, W. A. *Ind. Eng. Chem.* **1947**, *39*, 1401–1409.
- (2) Hard, S.; Neuman, R. D. *J. Colloid Interf. Sci.* **1987**, *120*, 15–29.
- (3) Jarvis, N. L. *J. Phys. Chem.* **1966**, *70*, 3027–&.
- (4) Garrett, W. D.; Zisman, W. A. *J. Phys. Chem.* **1970**, *74*, 1796–&.
- (5) Granick, S. *Macromolecules* **1985**, *18*, 1597–1602.
- (6) Granick, S.; Clarson, S. J.; Formoy, T. R.; Semlyen, J. A. *Polymer* **1985**, *26*, 925–929.
- (7) Mann, E. K.; Langevin, D. *Langmuir* **1991**, *7*, 1112–1117.
- (8) Lee, L. T.; Mann, E. K.; Langevin, D.; Farnoux, B. *Langmuir* **1991**, *7*, 3076–3080.
- (9) Mann, E. K.; Henon, S.; Langevin, D.; Meunier, J. *J. Phys. II* **1992**, *2*, 1683–1704.
- (10) Lenk, T. J.; Lee, D. H. T.; Koberstein, J. T. *Langmuir* **1994**, *10*, 1857–1864.
- (11) Hahn, T. D.; Hsu, S. L.; Stidham, H. D. *Macromolecules* **1997**, *30*, 87–92.
- (12) Kim, C.; Gurau, M. C.; Cremer, P. S.; Yu, H. *Langmuir* **2008**, *24*, 10155–10160.
- (13) Mann, E. K.; Primak, S. V. *Phys. Rev. Lett.* **1999**, *83*, 5397–5400.
- (14) Crisp, D. J. *J. Coll. Sci.* **1946**, *1*, 161–184.
- (15) Crisp, D. J. *J. Coll. Sci.* **1946**, *1*, 49–70.
- (16) Brinkhuis, R. H. G.; Schouten, A. J. *Macromolecules* **1991**, *24*, 1487–1495.
- (17) Capan, I.; Capan, R.; Tanrisever, T.; Can, S. *Mater. Lett.* **2005**, *59*, 2468–2471.
- (18) Kawaguchi, M.; Sauer, B. B.; Yu, H. *Macromolecules* **1989**, *22*, 1735–1743.
- (19) Esker, A. R.; Zhang, L. H.; Sauer, B. B.; Lee, W.; Yu, H. *Colloids Surf. A* **2000**, *171*, 131–148.
- (20) Gissing, S. K.; Richards, R. W.; Rochford, B. R. *Colloids Surf. A* **1994**, *86*, 171–183.
- (21) Kawaguchi, M.; Tohyama, M.; Mutoh, Y.; Takahashi, A. *Langmuir* **1988**, *4*, 407–410.
- (22) Kawaguchi, M.; Tohyama, M.; Takahashi, A. *Langmuir* **1988**, *4*, 411–413.
- (23) Sauer, B. B.; Yu, H.; Yazdanian, M.; Zograf, G.; Kim, M. W. *Macromolecules* **1989**, *22*, 2332–2337.

Surface Pressure Isotherms and Molecularly Detailed Modeling

- (24) Maestro, A.; Ortega, F.; Monroy, F.; Kragel, J.; Miller, R. *Langmuir* **2009**, *25*, 7393–7400.
- (25) Vilanove, R.; Rondelez, F. *Phys. Rev. Lett.* **1980**, *45*, 1502–1505.
- (26) Vilanove, R.; Poupinet, D.; Rondelez, F. *Macromolecules* **1988**, *21*, 2880–2887.
- (27) Hsu, W. P.; Lee, Y. L.; Liou, S. H. *Appl. Surf. Sci.* **2006**, *252*, 4312–4320.
- (28) Ni, S. L.; Lee, W.; Li, B. B.; Esker, A. R. *Langmuir* **2006**, *22*, 3672–3677.
- (29) Jo, N. J.; Iwata, T.; Lim, K. T.; Jung, S. H.; Lee, W. K. *Polym. Degrad. Stab.* **2007**, *92*, 1199–1203.
- (30) Numata, K.; Finne–Wistrand, A.; Albertsson, A. C.; Doi, Y.; Abe, H. *Biomacromolecules* **2008**, *9*, 2180–2185.
- (31) Kim, E. Y.; Lee, J. K.; Lee, W. K. *J. Nanosci. Nanotechnol.* **2008**, *8*, 4830–4833.
- (32) Cox, A. R.; Vincent, B.; Harley, S.; Taylor, S. E. *Colloids Surf. A* **1999**, *146*, 153–162.
- (33) Ghaicha, L.; Leblanc, R. M.; Villamagna, F.; Chattopadhyay, A. K. *Langmuir* **1995**, *11*, 585–590.
- (34) Reynolds, P. A.; McGillivray, D. J.; Gilbert, E. P.; Holt, S. A.; Henderson, M. J.; White, J. W. *Langmuir* **2003**, *19*, 752–761.
- (35) Labbauf, A.; Zack, J. R. *Journal of Colloid and Interface Science* **1971**, *35*, 569–&.
- (36) Schick, M. *Introduction to wetting phenomena, in Liquids at interfaces–Les Houches–Session XLVIII 1988*, Elsevier Science Publishers, Amsterdam 1990.
- (37) de Gennes, P. G. *Rev. Mod. Phys.* **1985**, *57*, 827.
- (38) Schick, M. *Prog. Surf. Sci.* **1981**, *11*, 245–292.
- (39) MacDowell, L. G.; Muller, M. J. *Chem. Phys.* **2006**, *124*, 13.
- (40) Kuragane, S.; Fujii, T.; Ban, T.; Shioi, A. *Colloids Surf. A* **2007**, *311*, 16–25.
- (41) Scheutjens, J.; Fleer, G. J. *J. Phys. Chem.* **1979**, *83*, 1619–1635.
- (42) Scheutjens, J.; Fleer, G. J. *J. Phys. Chem.* **1980**, *84*, 178–190.
- (43) Postmus, B. R.; Leermakers, F. A. M.; Stuart, M. A. C. *Langmuir* **2008**, *24*, 3960–3969.
- (44) Mann, E. K.; Henon, S.; Langevin, D.; Meunier, J.; Leger, L. *Phys. Rev. E* **1995**, *51*, 5708–5720.
- (45) Alexander, J. C.; Bernoff, A. J.; Mann, E. K.; Mann, J. A.; Zou, L. *Phys. Fluids* **2006**, *18*, 10.
- (46) Zou, L.; Bernoff, A. J.; Mann, J. A.; Alexander, J. C.; Mann, E. K. *Langmuir* **2010**, *26*, 3232–3236.

Chapter 4

PMMA Highlights the Layering Transition of PDMS in Langmuir Films

Abstract

We report a system consisting of a mixed Langmuir monolayer, made of water-insoluble, spreadable, fluid-like polymers polydimethylsiloxane (PDMS) and polymethylmethacrylate (PMMA) with a minority P(DMS-*b*-MMA) copolymer. We have performed both Langmuir trough pressure/area isotherm measurements and Brewster angle microscopy (BAM) observations and complement the experiments with molecularly detailed self-consistent field (SCF) calculations. PDMS undergoes a layering transition that is difficult to detect by BAM. Addition of PMMA gives contrast in BAM, now showing a two-phase system: if this would consist of separate two-dimensional (2D) PMMA and PDMS phases, a PDMS-PMMA diblock should accumulate at the phase boundary. However, the diblock copolymer of PDMS-PMMA failed to show the expected “lineactant” behavior, i.e., failed to accumulate at the phase boundary. The calculations point to a nontrivial arrangement of the polymer chains at the interface: in mixtures of the two homopolymers, in a rather wide composition ratio, we find a vertical (with respect to the air/water interfacial plane) configuration, with PMMA sitting preferably at the PDMS/water interface of the thicker PDMS film, during the PDMS layering phase transition. This also explains why the diblock copolymer is not a lineactant. Both PMMA and P(DMS-*b*-MMA) are depleted from the thin-thick PDMS film interface, and the line tension between the phases is, consequently, increased, in the binary mixtures as well as in the ternary ones.

1. Introduction

Thin polymeric films have been widely investigated because of their relevance in the technological development of advanced materials and coatings; in order to achieve full control of this technology, it is crucial that the fundamental physics underlying the thin films behavior is known. A critical aspect in thin film fabrication is the control over the structure at the microscopic level, especially when polymer mixtures are to be used.^{1,2} Bulk behavior of polymer blends does not provide relevant information, as the behavior of polymer chains confined to a surface differs strongly.³ Langmuir monolayers, then, become a suitable model system in order to address issues such as polymeric thin film structural organization, and the lateral phase separation at the air/water interface of polymer mixtures.

In our work we report a model system consisting of a mixed Langmuir monolayer, made of polydimethylsiloxane (PDMS) and polymethylmethacrylate (PMMA): both of them are water-insoluble, spreadable, fluid-like polymers, with a very well-known surface behavior,⁴⁻¹² potentially able to yield lateral phase separation, due to the different chemical structure at the segment level. Should this indeed occur, one expects a diblock copolymer of PDMS-PMMA to specifically accumulate at the phase boundaries, as a “lineactant”. We have performed both Langmuir trough pressure/area isotherm measurements and BAM observations on this binary mixture. The experimental results, surprisingly, could not be explained in terms of a two-dimensional (2D) biphasic system, with separate PDMS and PMMA domains on the water surface. Moreover, the PDMS-PMMA diblock copolymer did not show any lineactant behavior. Clearly, the mixed system PDMS/PMMA must be viewed differently. We therefore invoked theoretical calculations, based on a self-consistent field (SCF), molecularly-detailed model that we had developed in a previous work.¹³ As we shall show below, it is the third dimension that had to be taken into account.

2. Materials and Methods

The polymers PDMS, Poly(dimethylsiloxane), (M_n 14800, M_w 16900, PDI 1.14), PMMA, Poly(methyl methacrylate), (M_n 21500, M_w 30000, PDI 1.4), and P(DMS₁₀₈-*b*-MMA₂₀₀), Poly(dimethylsiloxane-*b*-methyl methacrylate), (M_n 8000-*b*-20000, PDI 1.20), were purchased from Polymer Source Inc. and used as

received. All the glassware was soaked in a KOH 2 M ethanol solution and rinsed thoroughly with demineralized water before use. Stock solutions were prepared in chloroform (Aldrich, > 99.9%, HPLC grade), and the appropriate amounts were mixed in order to prepare the polymer solutions in the desired proportion. All the polymer mixtures compositions are expressed in weight ratios. A few microliters of these solutions were spread using a 10 mL Hamilton syringe on the subphase, constituted by water ($R > 18.2$ MW) demineralized using an EasypureUV machine from Barnstead; no special tests for the presence of amphiphilic impurities were performed on it.

Langmuir isotherms were measured at room temperature (20 °C) with a MicroTroughXL apparatus, purchased from Kibron Inc. The trough was thoroughly flushed with ethanol and acetone solutions, and then rinsed with demineralized water before every use. The equipment was kept at a constant temperature of 20 °C for the whole experiment by connection to a water bath. The water subphase was cleaned by compression and suction of the air/water surface, until the surface pressure was less than 0.1 mN/m in the whole compression cycle. Then the solution (usually around 10 mL) was spread with a microsyringe, and the solvent was allowed to evaporate in the next 20 min, before performing any compression. Unless mentioned otherwise, the compression rate was fixed at 5 mm/min.

Brewster angle microscopy (BAM) was performed fixing the Langmuir trough equipment under a Multiskop apparatus purchased from Optrel GBR.

3. Experimental Results

Thin, films of pure PDMS⁴⁻⁶ and PMMA^{7-12,14,15} homopolymers on water have been extensively studied, and our data agree with the available literature. PMMA shows a condensed-type pressure/area isotherm: its surface pressure increases steeply during the compression, until a collapse value is reached. On the contrary, PDMS has an expanded isotherm type, with a remarkably long and flat plateau region, at $p = 8.4$ mN/m. A small feature at $a = 0.10$ nm²/monomer is apparent, where the surface pressure slightly increases to $p = 9$ mN/m and then remains constant until very low molecular areas are reached in the compression cycle.

This plateau has been subjected to several investigations, in order to clarify the nature of the occurring phase transition. Early hypotheses¹⁶ interpreted it as a process of progressive folding into closed-packed horizontal surface helices; more recently, several investigations performed with a wide range of techniques,^{4-6,17} proved the existence of a layering transition, occurring when the surface concentration exceeds a critical value situated in the final part of the plateau region. Infrared reflectance spectroscopy and epifluorescent microscopy investigations¹⁸ proved the coexistence of two different phases in the plateau region, although they did not prove definitively their structural nature, being unable to discriminate between a layering transition or the formation of horizontal helices. Instead, the transition to horizontal helices was ruled out in a more recent study,¹⁹ based on sum frequency generation spectroscopy, although the authors could not unequivocally determine the nature of the PDMS film in the transition phase: the conformation in the plateau region could consist either of helices laying on top of the PDMS monolayer, or of odd-numbered horizontal layers.

We have recently developed an SCF model,¹³ in which we interpret the spreading phenomena occurring at the air/water interface, in terms of wettability of the interface by the spread polymer; in this study we concluded that PDMS undergoes a layering phase transition, largely driven by long-range interaction forces between the surface and the polymer segments. On the other hand PMMA was found to be autophobic, due to the anisotropic orientation of its monomers on the water surface, which prevents the growth of multiple layers upon compression. From these results we expected that a binary mixture of PDMS and PMMA could also laterally phase separate, when spread on the water surface, and form a biphasic film in the semi-dilute region of the pressure/area isotherm.

In the mixed films, we observed phase coexistence between two differently contrasted phases, by means of BAM. However, the nature of these phases is not immediately obvious: they could be the expected separate PDMS and PMMA phases, or they could, somehow, be related to the layering transition of PDMS. In the case of a lateral phase separation occurring between the two different polymers, the diameters of the domains are expected to be dependent on the ratio of the components in the mixture. Moreover, the introduction of a third component into the mixture, such as a diblock copolymer of the type P(DMS-*b*-MMA), should cause a dramatic modification of the morphology observed, as it is expected to localize preferentially along the contact line separating PDMS and PMMA domains. If this occurs, then the line tension at the phase boundaries would be

reduced, and the extent of the PDMS/PMMA contact might increase, leading to a more complex domain morphology and to a reduction of their average diameter. On the other hand, if PDMS is dictating the domain formation, the observed morphology should be insensitive to any composition changes. In this case, it is not clear what the fate of PMMA and the diblock copolymer is. Also, the fact that the contrast between domains is much larger than in the case of pure, biphasic PDMS, has to be accounted for.

Pressure/area isotherms of PDMS and PMMA binary mixtures are displayed in Figure 1; the graph clearly shows that the 90% w/w PDMS mixture isotherm has a very close resemblance to the pure PDMS one and retains the plateau region at the same surface pressure; from 70% PDMS content onward, the plateau region is no longer present, and the shape of the pressure/area curves becomes progressively similar to the pure PMMA isotherm. BAM pictures (Figure 2) from the 90% PDMS mixture clearly show a phase coexistence, which occurs, during the compression, only when the plateau region is reached: at the beginning of the plateau region, small domains, slightly brighter than the surrounding medium, appear: they grow during the compression, until they touch and start to merge, forming a uniform brighter layer, when the pressure slightly increases with a small step along the curve. At the end of the compression, at very small areas, very bright spots appear on top of the gray background, as shown in Figure 2c. These brighter domains are also present when a pure PDMS monolayer is compressed to very small areas; we tend to attribute them to the formation of multi-layering regions⁵ on the very compact polymer film. Occasionally, as shown in Figure 2a, a phase inversion can occur and darker domains appear, surrounded by a brighter matrix. Such an observation (i.e., easy phase inversion) would be justified by a low line tension value, with a very weak curvature dependence, pertaining to this system. None of the remaining mixtures (with more PMMA) show this phase coexistence and, when observed with the BAM, appear homogeneous throughout the whole compression. So, the presence of a plateau region in the mixture isotherms is directly connected to the appearance of the reflecting domains in the BAM in that same region.

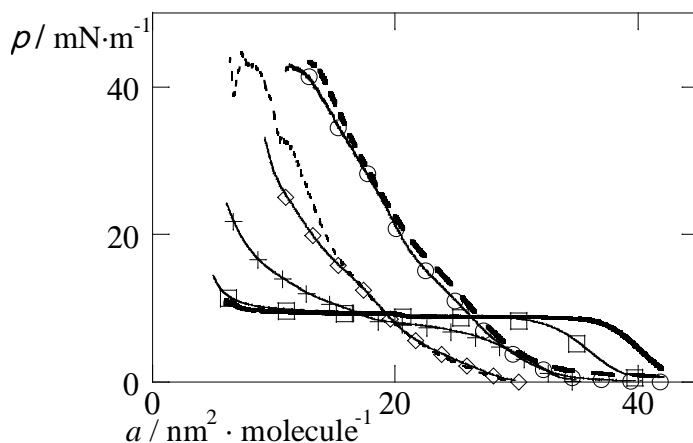


Figure 1. Pressure/area isotherms of mixed Langmuir monolayers constituted of PMMA and PDMS in different weight ratios. PDMS content: 100% thick solid line, 90% solid line with open squares, 70% solid line with crosses, 50% solid line with open diamonds, 30% thin dashed line, 10% solid line with open circles, 0% thick dashed line.

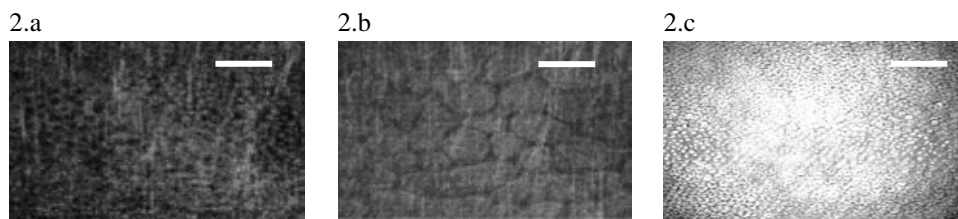


Figure 2. BAM pictures of 90% PDMS/10% PMMA mixture; (a) $p = 7.4$ mN/m, $a = 22$ nm² · molecule⁻¹; (b) $p = 8.0$ mN/m, $a = 15.7$ nm² · molecule⁻¹; (c) $p = 12.5$ mN/m, $a = 5.5$ nm² · molecule⁻¹. The scale bar is 150 nm. The vertical bright stripes sometimes visible are artifacts.

The observed correlation, between the appearance of the domains and the presence of the pressure plateau at the typical pressure of the PDMS layering transition, would suggest that PMMA does not form its own domains, but somehow acts as a “reporter” of the PDMS layering transition. Indeed, the change of the composition ratio, to a minimal extent, does not cause any correlated change in the size of the domains, while the increase of the amount of PMMA beyond 20% leads to the disappearing of the plateau in the isotherm. As the PMMA monolayer can bear much higher pressure, at the same area/molecule value, than PDMS, it probably displaces the latter from the water surface, when present in excess.

In order to verify this hypothesis, we have performed some experiments with ternary mixtures composed of PMMA, PDMS, and a diblock copolymer of the type PDMS-*b*-PMMA. The most significant isotherms measured in the experiment series are reported in Figure 3.

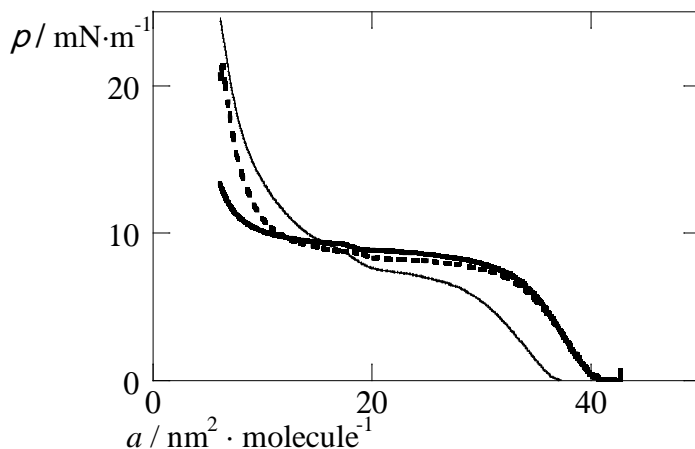


Figure 3. Pressure/area isotherms of mixed Langmuir monolayers constituted of PMMA and PDMS in different weight ratios, plus 5% of P(DMS₁₀₈-*b*-MMA₂₀₀) diblock copolymer. PMMA content: 20% solid, thin line, 10% dashed line, 5% solid, thick line.

In ternary mixtures composed of 5% P(DMS₁₀₈-*b*-MMA₂₀₀) and a variable amount of PMMA (from 5 to 20%) and PDMS (from 75 to 92%) the formation of domains occurs only in the mixtures containing 85% of PDMS or more, as shown in some examples reported in Figure 4. In other cases, the film looks homogeneous throughout the whole compression cycle. So the P(DMS-*b*-MMA) addition has almost the same effect as pure PMMA: it does not change the range of concentration where domains become visible, and does not alter the pressure at which the plateau in the isotherm is observed.

Moreover, in those cases where the formation of visible domains occurs, we have also noticed that their morphology is completely insensitive to the amount of diblock copolymer added, and to its change in relative concentration (from 3 to 8% of the total polymer spread). The domains always appear when the plateau region in the PDMS isotherm is approached, first as very tiny dots, slightly brighter than the surrounding medium, and then they gradually grow in size, until they fuse, at the point where the surface pressure starts to rise again.

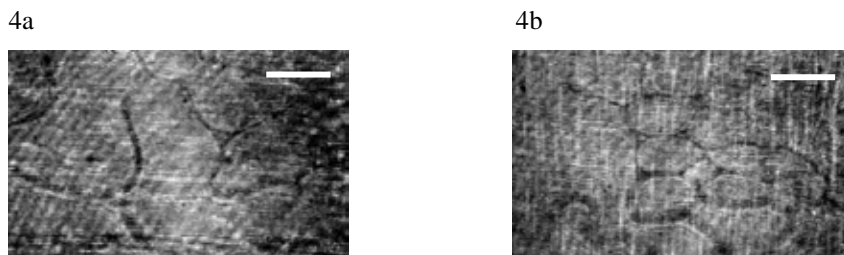


Figure 4. (a) BAM pictures of a ternary mixture containing 5% P(DMS₁₀₈-*b*-MMA₂₀₀), 5% PMMA, and 90% PDMS during a compression cycle, at 19.5 nm². (b) Ternary mixture containing 5% P(DMS₁₀₈-*b*-MMA₂₀₀), 10% PMMA, and 90% PDMS, same experimental conditions, at 20.4 nm². The scale bar is 150 nm.

Our experimental findings are an indication that what we actually see might be the coexistence of two PDMS films of different thicknesses during a layering phase transition. To account for the mixture results, we must assume that one of the phases is selectively “highlighted” either by PMMA, or by the diblock copolymer partitioning. When pure PDMS films are observed, we should expect the appearance of domains, but hardly any difference in contrast can be seen at the BAM, likely because of the very small difference in relative thicknesses. However, if a second component, which can partition differently over the two coexisting films, is added to the PDMS monolayer, it would be possible to enhance the contrast of one phase with respect to the other, and so the domains would become observable at the BAM.¹⁸ We hypothesize that a small amount of PMMA or diblock copolymer might act, indeed, as a contrast enhancer in these series of experiments. Figure 5 displays a schematic drawing that illustrates the possible hypotheses we have examined in the Experimental Results section.

A series of experiments, in which we have studied binary mixtures, containing PDMS and a diblock copolymer in variable amounts, supports the hypothesis of the partition of small quantities of a second polymer between the two coexisting PDMS films of different thicknesses, during the observed layering transition. As shown by the BAM pictures in Figure 6, the addition of P(DMS₁₀₈-*b*-MMA₂₀₀) to the PDMS monolayer causes the formation of domains only in the plateau region of the isotherm, which is limited to a concentration range below 10% of the diblock copolymer content.

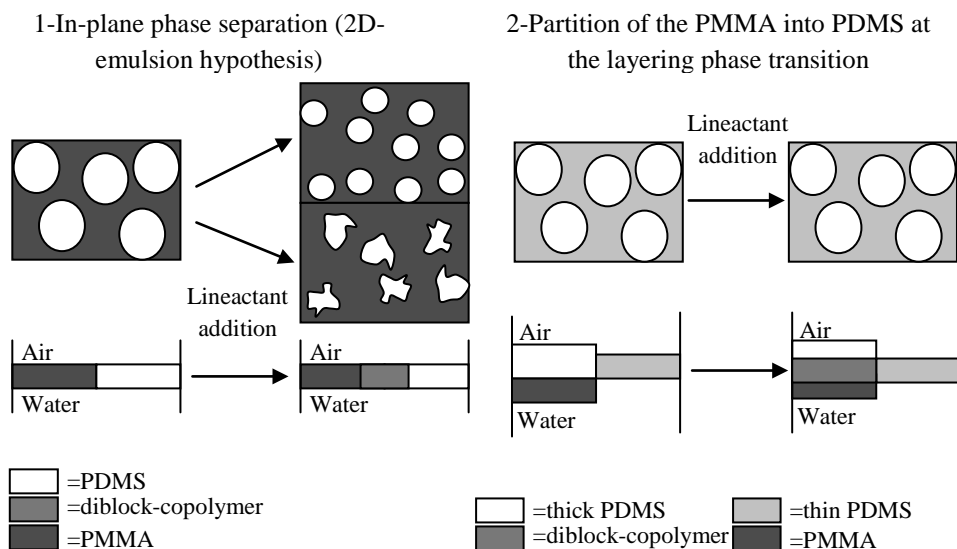


Figure 5. Schematic summary of the possible arrangements of the mixed monolayers as hypothesized in the Experimental Results section. On the left side we represent the case of a 2D-emulsion formation: the left above diagram shows the possible changes in size and/or shape of the domains expected upon lineactant addition, when looking at the monolayer from the top; the lower left diagram depicts the monolayer structure as seen from the side. On the right side (above, top view; below, side view) we depict the partition of the PMMA into the PDMS thick domains, when the PDMS layering phase transition occurs: the contrast enhancement allows one to visualize domains at BAM: however no alteration of the domains can be induced by the addition of the diblock-copolymer, as it partitions unevenly in the two PDMS phases as well.

The overall effect that diblocks have on the PDMS film is coincident with what is observed in the PDMS+PMMA mixed monolayers. Therefore, from all the experimental evidence that we have collected, we deduce that PMMA homopolymer, when added in small quantities to a PDMS monolayer, acts as a contrast enhancer of the layering phase transition of the PDMS. This is a most unexpected result, requiring very subtle differences in interaction between spread PMMA on one hand, and thin or thick PDMS films on the other. In order to underpin our conclusions, we made SCF calculations on these systems, which are presented in the following section.

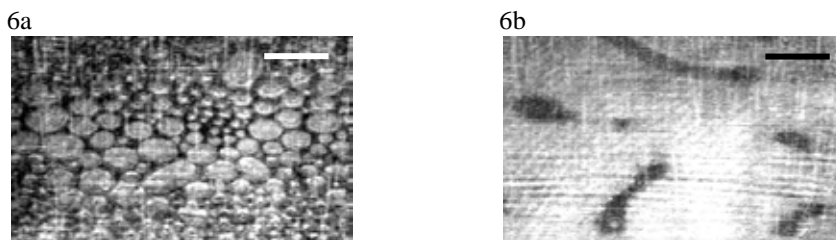


Figure 6. BAM pictures of a binary mixture containing 5% P(DMS₁₀₈-*b*-MMA₂₀₀), and 95% PDMS during a compression cycle: (a) 11.8 nm², (b) 9.5 nm². The scale bar is 150 nm. The bright stripes sometimes visible are artifacts due to scattering from the trough bottom surface or interference fringes.

4. Modeling

In order to deepen our knowledge of the systems investigated in our experiments, and possibly clarify the interpretation of the results so far displayed, we have developed a model representation of the studied binary and ternary mixed polymeric films, using the SCF approximation method, as developed by Scheutjens and Fleer (SF-SCF). A molecularly detailed description (on a united atom level) of the polymeric chains is implemented. Statistical weights of all freely-jointed chains are computed using the Bragg-Williams mean-field approximation, parameterized by Flory-Huggins interaction parameters and complemented by long-range van der Waals interaction potentials. More details about the theoretical background, the model parameters used¹³ and the calculation of the observable parameters are given as Supporting Information. In this paragraph, we will first describe the nature of the pure monolayers of the homopolymers considered here, in the phase coexistence conditions. Then, we will consider a simple mixed Langmuir monolayer, composed of PDMS and PMMA, in a ratio close to the one in which domains have been experimentally visualized (PDMS/PMMA approximate ratio 9/1). We will subsequently consider a binary mixture made of PDMS and a diblock copolymer in the appropriate ratio (PDMS/diblock copolymer approximate ratio 9/1), and verify the diblock effect on the PDMS layer, compared to the PMMA effect.

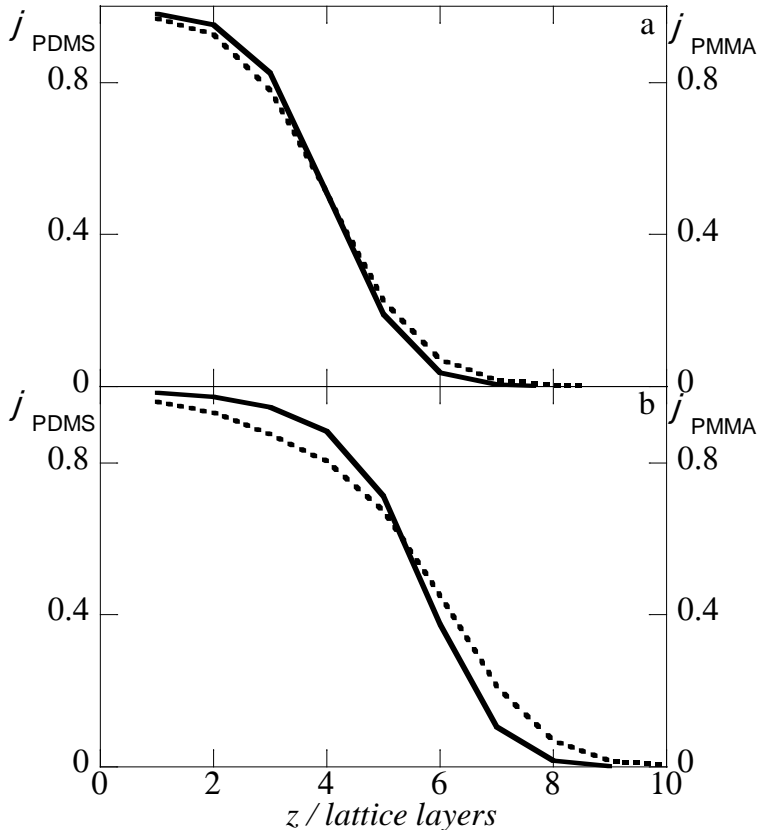


Figure 7. Volume fraction distribution profiles along z (direction normal to the air/water interface) of PDMS (continuous curve) and PMMA (dashed curve) homopolymers monolayers, at equal surface coverage, correspondent to (a) the beginning and (b) the end of the PDMS layering phase transition.

Finally, we will model a ternary mixture composed of PDMS, PMMA, and diblock copolymer (PDMS/PMMA+diblock approximate ratio 9/1), observe the related distribution profiles, and calculate the relevant parameters of the system, constantly relating our data interpretation to the experimental evidence we have already shown.

Figure 7 presents the volume fraction distribution profiles in the z direction (perpendicular to the water surface) for PDMS and PMMA homopolymer monolayers, respectively adsorbed at the air/water interface, at equal surface coverage. In both cases the bulk concentrations of the polymers are near, but below

their saturation values. Two profiles for each polymer are shown: in Figure 7a the surface coverage for each homopolymer is lower than the value at which PDMS undergoes the layering process. Clearly, both polymers behave as amphiphilic molecules which readily spread at the interface, forming insoluble, very compact layers. The lattice sites occupied are only those in the very proximity of the surface. Their interfacial behavior is very similar, as the two profiles show: PMMA, which has a slightly more hydrophilic structure, with two oxygen atoms per monomer, appears to be slightly less compact than PDMS, which takes up a little less water. This tendency is marginal in this case: however, when the surface coverage is progressively increased, until the value corresponding to the end of the layering region is reached, the distribution of the two polymers becomes progressively different. As shown in Figure 7b, at increased surface coverage, both PDMS and PMMA layers have become thicker; however, the latter has a more expanded structure and a stronger tendency to orient toward the air/water interface than the former one.

An example of density contour plots in the $x - z$ plane, for PDMS and PMMA in the binary mixture at phase coexistence, are reported in Figure 8. PDMS is in the layering transition region: two films of different thicknesses coexist at the same surface pressure value. The thin/thick contact line, which separates the thick film from the thin one, extends along the y direction, parallel to the air/water interface. This contact line is remarkably wide, along the x direction, like the one we have already calculated for the homopolymer mixture, on the order of 10 nm. A very low line tension, t , is associated with this phase boundary; we found a value $t \sim 0.013 kT / \text{nm}$ for the pure PDMS film. The PMMA distribution over the thin and thick films is not homogeneous; PMMA displays a slight preference for the thin one: PMMA is quite homogeneously mixed with PDMS in the thin phase, whereas it accumulates preferentially next to the PDMS/water interfacial contact in the thick phase.

In Figure 9, the volume fraction distribution profiles along the z axis are reported, in the bulk thick and thin phases (a and b, respectively), for both PMMA and PDMS: the distribution of the polymers in the thin and thick domains differs considerably.

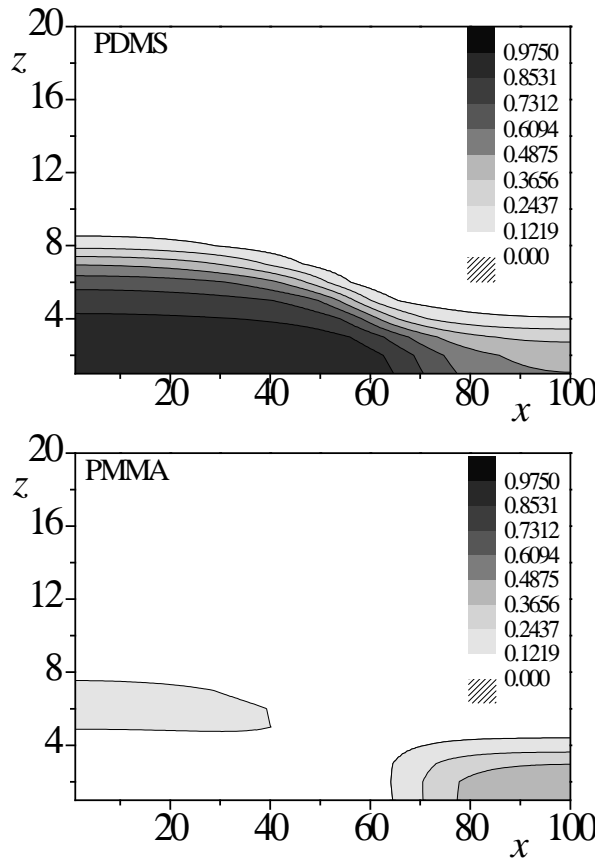


Figure 8. Surface contour plot of the volume fraction distribution density of PDMS and PMMA, in a binary mixed film (approximate PDMS/PMMA ratio is 9/1), during the PDMS layering phase transition. The volume fraction density distributions in this plot correspond to a value of $\eta_{\text{PMMA}} = -24.363$.

PMMA and PDMS are homogeneously mixed in the thin region, as indicated by almost identical z profiles. The PMMA layer appears slightly more oriented toward the water phase than PDMS, but this tendency is marginal and totally equivalent to the behavior displayed by the homopolymer thin layers shown above (Figure 7).

In contrast, the volume fraction profiles in the thick film reveal a remarkably different partition. Instead of forming a homogeneous, thicker layer, where both polymers are completely mixed, PMMA chains tend to localize preferentially in between the PDMS film and water, and they are depleted from the PDMS/air interface.

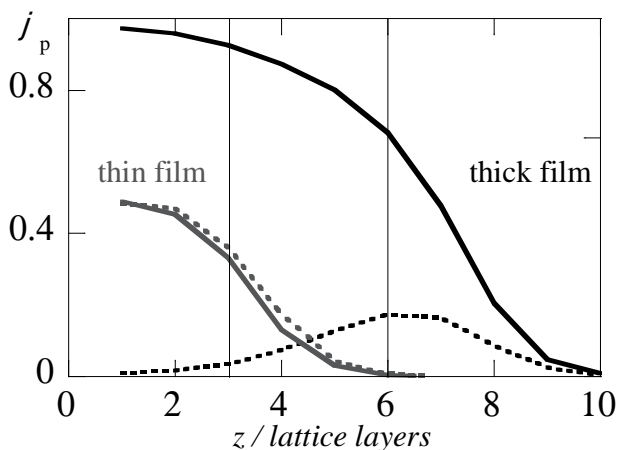


Figure 9. Volume fraction distribution profiles of PMMA and PDMS in a binary mixed Langmuir monolayer, at the thin/thick PDMS film phase coexistence region, plotted along the direction vertical to the air/water interface. Profiles of both polymers inside thin film domain are provided as gray lines (PDMS, solid gray line; PMMA, dashed gray line), and as black lines inside the thick film domain (PDMS, solid black line; PMMA, dashed black line).

Apparently, its more amphiphilic nature drives the PMMA coils to this preferential localization. Once the PMMA and PDMS are present in sufficient amounts, they separate from each other in the z -direction with a modest mixing zone (the interface is narrow). Another relevant feature is that the PMMA, although preferentially localized between PDMS and water, still appears fairly well mixed with the PDMS coils, rather than forming a distinct second layer. Clearly, the affinity between PDMS and PMMA coils in the thin film is maintained, even though in a smaller region inside the thicker film.

Figure 10 presents the variation in composition of the thick and thin film domains, as a function of PMMA chemical potential, when more PMMA is added to PDMS, in the binary mixture at phase coexistence. The trends in variation of the composition of the two kinds of domains are significant: here it is possible to see that both the interfacial fraction in the thick and in the thin film increase along with the increase of the PMMA chemical potential; however, the increase of PMMA content in the thin domains is more pronounced than in the thick ones.

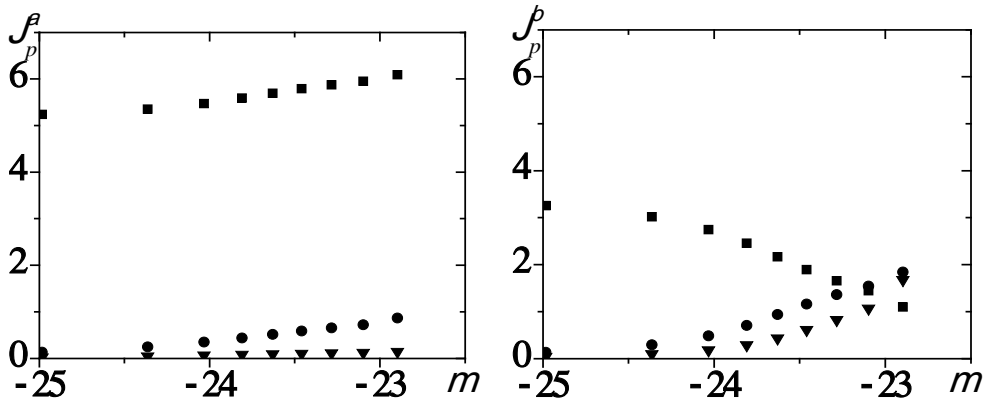


Figure 10. Adsorbed amount of polymers, versus PMMA chemical potential: on the left side, interfacial concentrations in the bulk thick film domains (J^{α}_{PDMS} , black squares; J^{α}_{PMMA} , black circles; $J^{\alpha}_{PMMA} / J^{\alpha}_{PDMS}$, black inverted triangles); on the right side, interfacial concentrations in the bulk thin film domains (J^{β}_{PDMS} , black squares; J^{β}_{PMMA} , black circles; $J^{\beta}_{PMMA} / J^{\beta}_{PDMS}$, black inverted triangles).

It appears that PMMA preferentially partitions in the thin film region when its overall content in the system increases. Strikingly, the PDMS interfacial fraction present in the thin regions undergoes a considerable decrease when the PMMA chemical potential increases, whereas that in the thick film increases. The overall increase in PMMA content at the interface causes the displacement of the PDMS coils from the thin domains, and, consequently, their accumulation in the thick phase. As a result, the PMMA/PDMS ratio in the thick phase is almost constant with the PMMA chemical potential, whereas the thin phase becomes progressively richer in PMMA. This trend would explain the disappearance of the PDMS plateau region in experiments where the PMMA content of the mixture is increased: the enriching of the thin film in PMMA content would totally displace the PDMS coils from it, and so the phase coexistence would be lost, in favor of the formation of a homogeneous mixed monolayer, on top of which the residual excess of PDMS can nucleate in droplets, not wet by the water subphase.

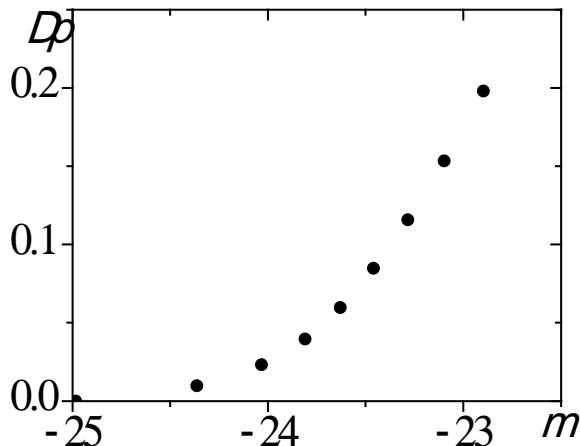


Figure 11. Pressure variation in the film layer, as a function of the PMMA chemical potential.

We recall that the situation reproduced in the calculations is slightly different from that in the experiments: in a single, experimental compression cycle, the composition ratio between polymers is kept constant, while their total surface amount increases progressively, but in the calculations, the total adsorbed amount of polymers is kept constant, and the ratio of the two components is changed. So, in order to be consistent when a comparison is made between the results from the model and the experiments, we refer to the trends shown across compression cycles carried out at different relative compositions. One of the observed experimental trends is the sensitivity of the layering phase transition to variations in the PMMA amount present in the mixture. For pure PDMS, the transition region is marked, in the pressure/area graph, by a remarkably long plateau region. When 10% of PMMA is present in the mixture, the plateau length decreases by 1/3, and, when the PMMA amount is 30%, the plateau has almost disappeared. An analogous sensitivity has been found in our model, as can be seen from the variation in the surface pressure, as a function of the PMMA chemical potential, in Figure 11.

A surprising result shown by the 2D profiles in Figure 8 deserves further exploration in our analysis: as it can be easily noticed, PMMA avoids the thin/thick phase boundary region. We can quantify this effect, (using eq 10; see Appendix A) as a negative contact line excess. Moreover, it must be associated with an increase

of the line tension, with respect to the pure PDMS film, (which can be estimated too, using eq 8; see Appendix A).

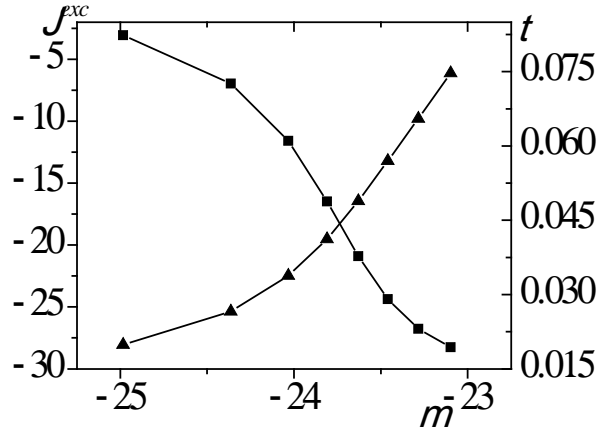


Figure 12. PMMA line excess (black squares, values on the left axis) and line tension (black triangles, values on the right axis) plotted versus PMMA chemical potential.

The PMMA line excess and the line tension, as a function of the PMMA chemical potential in the system, are shown in Figure 12: the calculated line excess, accordingly to our expectations, is negative for all the PMMA/PDMS ratios used in the calculation; furthermore, the line tension value in the film binary mixture increases too, up to 5 times higher values than the one estimated for the pure PDMS film, when the PMMA overall amount is increased.

In line with the experimental evidence shown in the preceding paragraph, we have observed the same behavior and trends of a binary mixture made of PDMS and PMMA homopolymers in a binary mixture of PDMS and PDMS-*b*-PMMA polymers.

Figure 13 shows that the same trends of composition variation in both the thick and thin PDMS layers are obtained when the diblock copolymer is added instead of the PMMA homopolymer: more specifically, the thinning of the PDMS film in phase b is enhanced by diblock copolymer addition as much as by PMMA homopolymer addition, whereas the tendency toward a different partitioning between the two phases is less pronounced for the diblock copolymer, than for the PMMA.

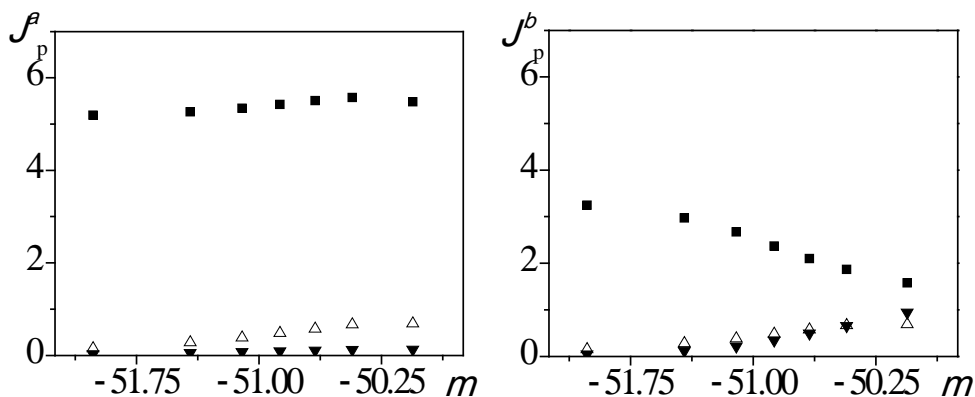


Figure 13. Adsorbed amount of PDMS and PDMS-*b*-PMMA, versus PDMS-*b*-PMMA chemical potential: on the left side, interfacial concentrations in the bulk thick film domains (J_{PDMS}^{α} , black squares; $J_{\text{PDMS-}b\text{-PMMA}}^{\alpha}$, open triangles; $J_{\text{PDMS-}b\text{-PMMA}}^{\alpha} / J_{\text{PDMS}}^{\alpha}$, black inverted triangles); on the right side, interfacial concentrations in the bulk thin film domains (J_{PDMS}^{β} , black squares; $J_{\text{PDMS-}b\text{-PMMA}}^{\beta}$, open triangles; $J_{\text{PDMS-}b\text{-PMMA}}^{\beta} / J_{\text{PDMS}}^{\beta}$, black inverted triangles).

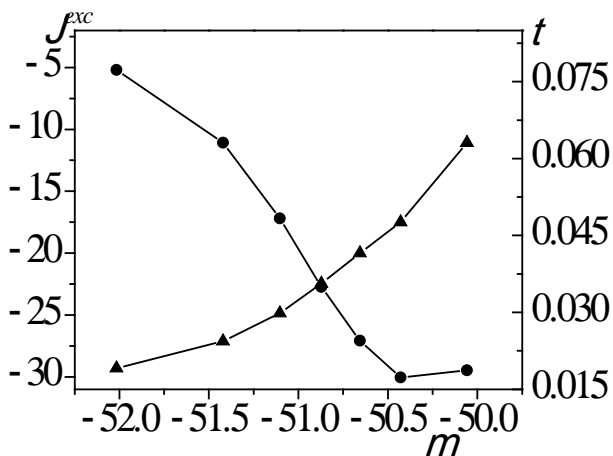


Figure 14. PDMS-*b*-PMMA line excess (black circles, values on the left axis) and line tension (black triangles, values on the right axis) plotted versus PDMS-*b*-PMMA chemical potential.

Figure 14 displays the variation in the line excess of diblock copolymer and line tension of the systems, as a function of the diblock copolymer chemical potential: again the trends previously observed in the homopolymers mixture are analogous to the ones shown here. The diblock copolymer interfacial excess is negative, and it becomes even more negative with the addition of more polymer to the system, as the partitioning in the bulk phases, rather than in the contact line region, is more favorable. Accordingly, the line tension value increases with the increase of diblock copolymer in the system. The order of magnitude of both quantities is the same for both the homopolymer binary mixture and the PDMS+diblock copolymer binary mixture; however, both the interfacial depletion phenomenon and the line excess increase appear to level off slightly more rapidly in the case of diblock copolymer addition, than in the case of pure homopolymer addition. This increase is consistent with the experimental observations illustrated in the Experimental Results section. When the surface coverage is decreased through the compression of the monolayer, the surface concentration of the diblock copolymer increases; the BAM pictures show that such an increase in diblock surface concentration is not accompanied by a decrease in size of the circular domains, as expected when the diblock copolymer behaves as a lineactant. On the contrary, the circular domains grow in size progressively, until they fuse together, consistently with an “anti-lineactant” effect of the diblock copolymer, as predicted in these calculations.

In order to investigate a system composed of PDMS and a small amount of both PMMA and diblock copolymer, we have implemented a model where the interfacial total amount of PDMS was fixed, together with the bulk concentration of PMMA, while the diblock copolymer interfacial concentration was progressively increased.

The volume fraction density distribution profiles of the three components are shown in the contour plot in Figure 15. The distribution profile of PDMS is unchanged, while we can observe that the PMMA tendency to avoid the interfacial contact line between the coexisting phases is decreased, when compared to the binary mixture case. On the other side, the diblock copolymer preferably partitions in the bulk phases, and avoids the contact region even more than the PMMA homopolymer, reproducing the same behavior observed in the binary mixture with PDMS.

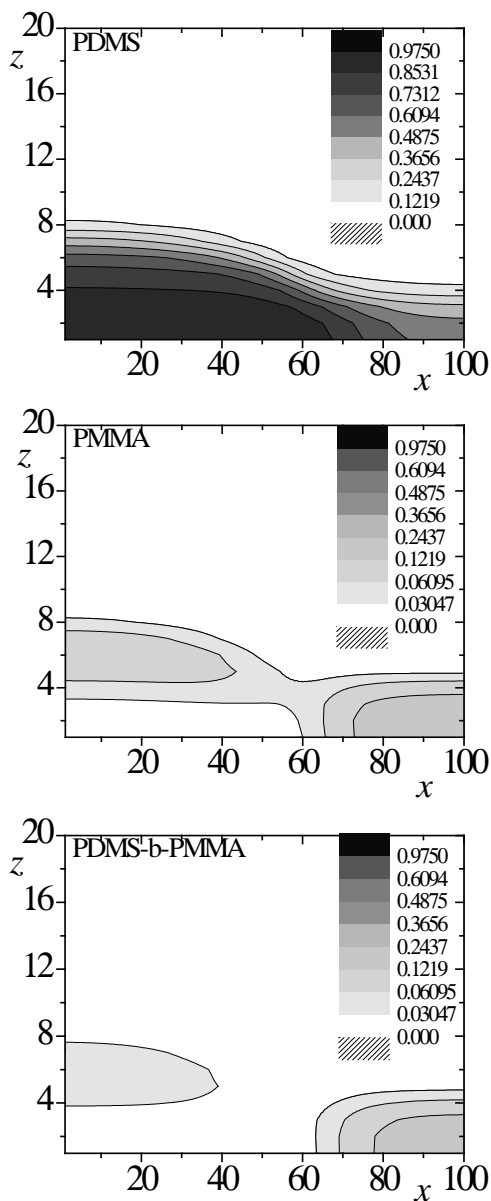


Figure 15. Surface contour plot of the volume fraction distribution density of PDMS, PMMA, and PDMS-*b*-PMMA, in a ternary mixed film, during the PDMS layering phase transition (approximate PDMS/PMMA ratio is 9/1). The volume fraction density distributions in this plot correspond to a value of $m_{\text{PDMS-}b\text{-PMMA}} = -51.312$ and $m_{\text{PMMA}} = -23.809$.

This trend is clearly visible also in Figure 16, where the variations in the composition of both thick and thin PDMS phases are displayed as a function of the increasing diblock copolymer chemical potential. The PDMS amount in the thick phase increases very slightly, while, at the same time, the PDMS amount in the thin phase reduces. The PMMA amount decreases at the same time in both bulk phases, while the diblock quantity increases considerably; PMMA coils are displaced from the bulk of the domains toward the interfacial region, and replaced by the adsorbing diblock copolymer coils.

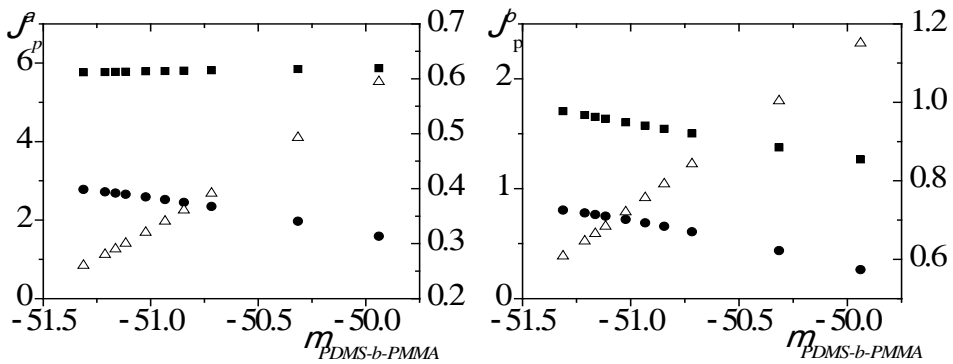


Figure 16. Adsorbed amount of PDMS, PMMA and PDMS-*b*-PMMA, versus PDMS-*b*-PMMA chemical potential: on the left side, interfacial concentrations in the bulk thick film domains (J_{PDMS}^{α} , black squares, values on left axis; $J_{\text{PDMS-}b\text{-PMMA}}^{\alpha}$, open triangles; J_{PMMA}^{α} , black circles, values on the right axis); on the right side, interfacial concentrations in the bulk thin film domains (J_{PDMS}^{β} , black squares, values on the left axis; $J_{\text{PDMS-}b\text{-PMMA}}^{\beta}$, open triangles; J_{PMMA}^{β} , black circles, values on the right axis).

In agreement with these observations, the interfacial excess of PMMA homopolymer, shown in Figure 17, increases with the diblock copolymer addition, even though it always remains negative. Consistently, at the same time, the interfacial excess of diblock copolymer becomes more negative, indicating an increased depletion of this compound from the contact region between domains, when its overall quantity is progressively increased. The effect of these partitioning phenomena on the line tension value is an overall increase, analogous to the one that has been observed in all the model cases displayed so far.

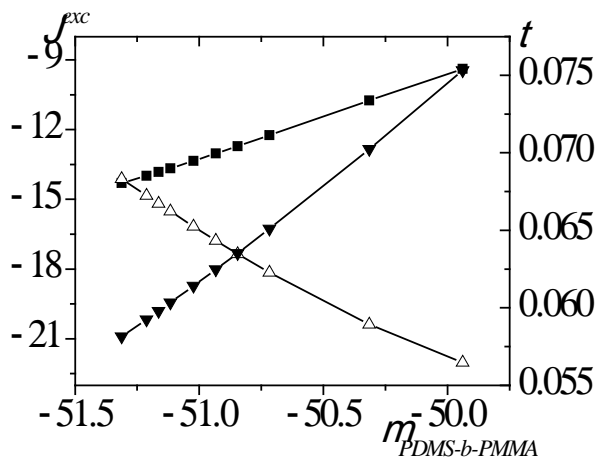


Figure 17. PMMA (black squares) and PDMS-*b*-PMMA (open triangles) line excess (values on the left axis) and line tension (black inverted triangles, values on the right axis) plotted versus PDMS-*b*-PMMA chemical potential.

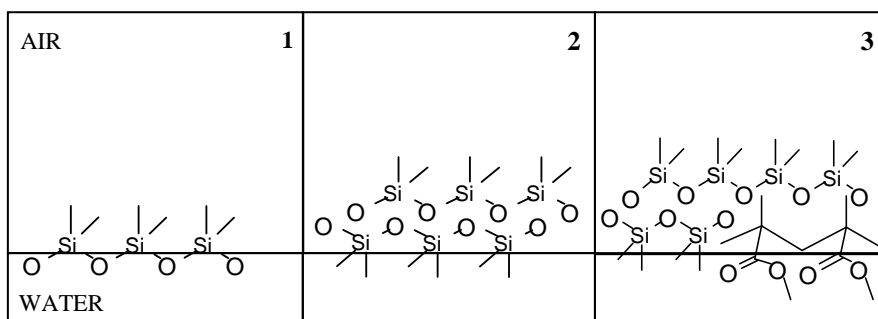


Figure 18. Schematic drawing of the possible polymeric coil orientations in the films studied: (1) thin PDMS domains at phase coexistence: polymer segments are horizontally aligned to the surface, with oxygen atoms preferentially pointing toward the water subphase; (2) thick PDMS domains at phase coexistence: polymer segments are horizontally aligned to the surface; however, in this case, oxygen atoms can also face the air phase, as they can be stabilized by dipolar interaction with oxygen atoms from other layers; (3) thick PDMS domains at phase coexistence, in a binary mixture made of PDMS+PMMA homopolymers; PMMA coil interpenetrate the PDMS layer closer to the surface, and, due to their higher amphiphilicity, help decreasing the interfacial tension.

In Figure 18 we suggest a possible arrangement of the polymer coils, compatible with our findings from the model results, reported above in Figure 11. In boxes 1 and 2 the pure PDMS film is considered in the phase coexistence region: PDMS coils in the thin region (case 1) are horizontally aligned to the surface, and point the oxygen atoms in the backbone preferentially toward the water phase, whereas in the thick film (case 2) the oxygen atoms can also point toward the air phase. This configuration would be energetically more unfavorable, due to the increase in the film hydrophobicity, caused by the methyl groups pointing at water; however, other oxygen atoms from the layers can form pairs, thanks to their dipolar interaction, and compensate the energy increase. A model based on sum frequency generation studies, which is compatible with the arrangement suggested above, has been proposed by Kim et al.¹⁹ for PDMS films at the air/water interface, at high surface coverages. When PMMA coils are added to the film (case 3), they preferentially mix, in the thick domains, with the PDMS layer closer to the water phase, and contribute to the lowering of the interfacial tension between the thick film and water, as their nature is more amphiphilic and they can screen more effectively PDMS/water unfavorable interactions.

5. Conclusion

We have proven, both experimentally and with the aid of SCF modeling techniques, that a small amount of PMMA homopolymer, added to a PDMS monolayer spread at the air/water interface, acts as a contrast enhancer of the PDMS layering transition. We have ruled out that the bright domains observed by BAM in mixed polymeric monolayers, during the PDMS phase transition, are due to a phase segregation phenomenon occurring between PMMA and PDMS coils. We produced experimental evidence for that, showing that a diblock copolymer added to the mixture does not modify the formation of the domains or their morphology. We further corroborated our hypothesis with model calculations, using an SCF molecularly detailed model that we previously developed for polymer monolayers at the air/water interface.

The results shown in this chapter prove that gaining an accurate control over thin film structures at the microscopic level is far from a trivial task, and the acquisition of fundamental knowledge is necessary in order to interpret experimental data in an appropriate way.

Appendix A: Supporting Information

Theoretical Background

Insoluble polymers that spread on the air/water interface may be regarded as residing in “flat land”. In a previous publication, where we considered several such systems, among which PDMS and PMMA, we proved that, within the self-consistent field theory, and, in particular, using a molecular model with specified chains, having segments with a non-trivial architecture, we could elucidate the relationship between chemical structure and various observables in these systems. Below we will use the same theory and exactly the same molecular models as before, and apply the model to polymer mixtures. The air/liquid interface is sharp, and for this reason we may model such boundary by an impenetrable Fresnel surface: all conformations that ‘visit’ the vapor phase are so unlikely that they can be excluded from our considerations. Conceptually, one could take the level of approximation one step further and also prevent conformations that protrude inside the water phase, making the system purely two-dimensional. We argue that this is not a good idea, because such an approach cannot account for molecular-dependent orientational features, on the local (monomeric) scale, features which make one polymer distinctly different from another. Therefore, we consider the case where there is, adjacent to the boundary, a water-phase, which is a poor solvent for the polymeric species. As a result, our modeling is not strictly a two-dimensional one, even though the polymer films that we will consider have a thickness that is of the order of the segment size. We will prove that this quasi two-dimensional model allows, in line with experimental findings, for non-trivial distributions of its molecular species.

In the previous chapter, we considered systems composed of just one polymer species. Even then, biphasic systems are possible; PDMS provides an example, undergoing a “layering” transition. Here, we consider polymer mixtures. Polymers readily demix, and therefore the phase behavior in this quasi two-dimensional system becomes of key importance. This calls for a two-gradient calculation scheme, where it is possible to account for polymer density gradients, both *normal* to the Fresnel interface, and *parallel* to it. We already introduced such two-gradient systems in our previous publication, to explore the properties of the PDMS system, when it undergoes its layering transition. We studied the lateral phase boundary (or contact line) between two film thicknesses, that differed only by a factor of two. It was found that a remarkably wide interface separates the two

regions, and the associated line tension, though extremely low, was calculated. Here, we consider this system once again, but now we focus on what happens when PMMA is added to it. We note that the molecular models for both polymers are identical to the ones used before, and the model and parameters are briefly outlined below. Here, we will only schematically describe the two–gradient SCF method and its approximations.

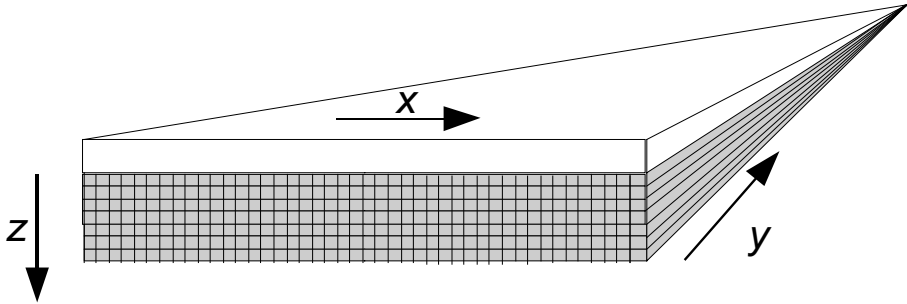


Figure A1. The two–gradient coordinate system used in SCF calculations. The gray region is the part that is considered in the calculations. It sits next to the impenetrable vapor phase (white). Normal to the vapor phase we have $z = 1, 2, \dots, z_M$ flat lattice layers (numbers are not indicated). Within each layer there are straight lines of lattice sites numbered $x = 1, 2, \dots, x_M$. Along the y –direction the mean field averaging is implemented (therefore no lattice sites are indicated). End–effects are ignored, implying that the system is infinitely long in the y –direction. Reflecting boundaries are chosen at z_M and $x=1$ and $x = x_M$ locations.

The SCF theory makes use of the mean field approximation. As explained, our interest is in a two–gradient version. Referring to Figure 1, we introduce the directions x (along the interface), and z (perpendicular to the interface), so that the mean–field approximation is applied in the remaining y –directions (along the interface). The exact location of segments, with respect to the y –coordinate, is not specified for a given location $\mathbf{r} = (x,z)$. Instead, we focus on the volume fraction $\varphi(\mathbf{r}) \equiv \varphi(z,x)$. Here, the volume fraction is the dimensionless concentration, specified by the number of segments at coordinates (z,x) , times the molar volume, divided by the volume that is available in the y –direction. Equivalently, it is the ratio of the number of segments and number of available lattice sites. We have such a distribution for each segment type (generically referred to by the sub-index A). Conjugated to the segment volume fractions $\varphi_A(\mathbf{r})$, there are segment potentials $u_A(\mathbf{r})$. The SCF approach starts with the mean–field free energy, which

is a functional of the volume fractions and potentials, subject to a compressibility condition. More specifically, we choose the system to be locally incompressible:

$$\sum_A \varphi_A(\mathbf{r}) = 1 \quad (\text{A1})$$

where the summation runs over all molecular components; this equality is imposed for each coordinate \mathbf{r} . A saddle point of the free energy function represents a physically observable situation. This leads to the SCF scheme, which we denote as:

$$\varphi[u(\mathbf{r})] \mathcal{F} u[\varphi(\mathbf{r})] \quad (\text{A2})$$

In words, eq A2 says that, within the SCF framework, the volume fractions can be computed from the segment potentials (left hand side), and vice versa (right hand side). A chain model is needed to compute the volume fractions. Here, we have implemented a freely-jointed chain model, for which there is a very efficient method (the propagator method) to compute the volume fraction profiles on a lattice. We need to specify the interactions to compute the potentials. We implemented the Bragg–Williams approximation, to include binary interactions, similarly as in the Flory–Huggins theory, using the Flory–Huggins parameters:

$$\chi_{AB} = \frac{Z}{2k_B T} [2U_{AB} - U_{AA} - U_{BB}] \quad (\text{A3})$$

From this definition, we see that these parameters are made dimensionless by the thermal energy $k_B T$. We likewise present all the results in dimensionless form. In eq 3, a combination of interaction energies U specifies the value of the c . When the cross-contribution U_{AB} is lower than the average of the U_{AA} and U_{BB} , a negative FH value is found, and then the two segments like to mix. Thus, a positive c gives a tendency for demixing. Whether demixing occurs in reality depends also on the mixing entropy. Compared to monomeric species, polymers have little translational entropy per unit mass, and therefore, a small positive value ($c > 0.5$) may already lead to demixing.

From eq A3, it is obvious that only the unlike contacts have a non-zero c -value. The Bragg–Williams approximation is used to estimate the probability for unlike contacts. Here, the *a priori* number of contacts is just given by the product of the respective volume fractions. In systems where there are density gradients (here, these occur in both the x and z directions), one has to implement a local

averaging of the volume fractions. This averaging takes place over all neighboring cells, such that all the cells contribute equally to the local average. This leads to non-local contributions in the segment potentials. These non-local contributions result in some complications in the numerical algorithm that searches for the solution of eq A2. However, in order to have a proper account of interfaces between various polymer phases, these non-local contributions are essential.

Interactions with the substrate (here the vapor phase) are also accounted for, again using relevant Flory–Huggins parameters. As these interactions are strictly short-range, there is only an interaction with the substrate when the segment is in layer $z = 1$. Indeed, this essentially implies that long-range effects, such as van der Waals forces, are not covered by the F–H parameters, rendering the theory with only contact interactions incomplete. In our previous work¹ it was shown that a van der Waals-like interaction was crucial to account for the layering of PDMS. Therefore, we added a term obeying to a power-law decay as a function of the distance of the segment from the vapor phase, to the short-range segment potential, for one type of the segments. Details will be given below.

Numerical solutions of the SCF equations directly lead to an optimized free energy functional. Other thermodynamic quantities follow from this free energy functional. At this stage, it is important to mention that it is possible to compute the grand potential of the system from

$$\Omega = F - \sum_i n_i \mu_i = \sum_z \sum_x \omega(x, z) \quad (\text{A4})$$

which is evaluated per unit length in the y -direction. In eq 4 the summation over i is over all molecule types in the system, n is the number of molecules per unit length in the y -direction, and μ is the chemical potential for the specified molecular component. Finally, in eq A4, ω is the grand potential density (again per unit length in the y -direction). Below, we will use the grand potential density to compute the lateral pressure of a particular system and the line tension of the interface between two coexisting phases. For the grand potential density, we employ an equation in terms of volume fraction and segment potential profiles.

Parameters and Molecular Model

The model implemented here has been developed in a previous work, based on experimental data obtained for four different homopolymers. In this model, the air/water interface is represented by a solid, impenetrable, flat surface, composed of segment units $k = S$ in contact with a fluid phase. The fluid phase is constituted of water, modeled as a four-armed star, which occupies five lattice sites: the reason for using this object, instead of a monomeric unity, is that for free water monomers the translational entropy is overestimated.² The star-shaped model reduces the free mobility of the solvent molecules in our system, therefore mimicking the ability of water molecules to form hydrogen bonds.

The polymers are modeled by two simple types of segments: a united C atom, which mimics the methylene/methyl unit, $-\text{CH}_2-/-\text{CH}_3$, and hydrophobic end groups, and an oxygen atom. In order to account for the bigger volume occupied by the carboxy groups in PMMA, we have introduced two connected oxygen atoms, instead of only one. The Si atom is modeled as a C atom, as the differences between the parameters which describe either the Si or C interaction with all the other components in the system are very small. O atoms can indeed form strong hydrogen bonds with the solvent, *via* two lone electron pairs; in contrast, both Si and C have no lone pairs able to strongly interact with water molecules, and, in this sense, they display a very similar behavior. The chemical structures adopted are reported in Figure A2.

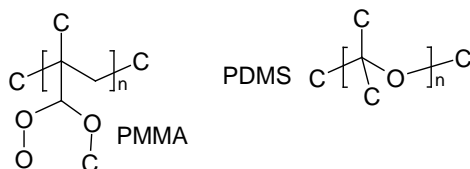


Figure A2. Structures of the homopolymers as modeled in our calculations. The architecture follows closely the chemical details of the real polymer molecules. Modifications of the actual molecular structures are motivated by the fact that these models are implemented on a lattice, in which the volume of a site coincides with the volume of the building unit of the molecules.

Each polymer, unless mentioned otherwise, consists of $n = 100$ monomer units. The number of segments N in the chain is given by the number of monomers, times the number of segments in each monomer (which differs for each of the polymers), plus some end segments.

The Flory–Huggins parameters needed for such a system are five in total: segments C and O interacting with the surface and with the solvent, and one for the interaction between C and O units within the polymers. The interaction parameters χ are chosen such that the hydrophobic C units display repulsion towards water molecules and O units, and a strong attraction towards the surface, while the O units are modeled as neutral towards both the solvent and the surface. Like in our previous calculations, we have used the following values:

$$\chi_{c.w} = 1, \chi_{c.o} = 1.5, \chi_{o.w} = \chi_{o.s} = 0.$$

Van der Waals interactions between the C unit and the surface have been introduced, as a decaying function of the lattice site distance from the surface ($\chi_{c.s} = c \cdot z^{-3}, c = -0.3, z > 1$); the interaction parameter in the first layer ($z = 1$) has the following value: $\chi_{c.s} = -0.63$.

The calculations lead to various volume fraction profiles as well as to the distribution of the grand potential density. From these, various observables can be extracted. In these calculations, the coordinate systems are expressed by $\mathbf{r} = (x, z)$, where x is a coordinate parallel to the surface and z is the coordinate perpendicular to the surface. Mean–field averaging is performed in the y –direction (along the surface, perpendicular to the x –direction).

From the calculated volume fractions, it is possible to compute the excess volume fraction $\Phi_i(x, z)$ of the polymer i adsorbed at the interface, per unit length, in the x, z –plane, with the following:

$$\Phi_i(x, z) = \varphi_i(x, z) - \varphi_i^b \quad (\text{A5})$$

where φ_i^b is the volume fraction in the bulk (water) phase, that is far away from the air–water interface. In this way we obtain a 2D distribution profile of the polymer interfacial concentration, averaged along the y –direction. When this quantity is integrated over the direction normal to the interface, we obtain the adsorbed amount of component i per unit length in the y –direction, $\theta_i(x)$

$$\theta_i(x) = \sum_z \Phi_i(x, z) \quad (\text{A6})$$

The total adsorbed amount follows from the subsequent summation over the x -coordinate:

$$\theta_1 = \sum_x \theta_1(x) \quad (\text{A7})$$

Below our interest is in a laterally inhomogeneous distribution of the molecules at the interface. More specifically, we will have two coexisting phases a and b positioned at low values of x (that is near $x = 1$) and high values of x (that is near $x = x_M$), respectively, along the surface. The adsorbed amounts in the homogeneous parts are referred to by q_i^a and q_i^b .

It is possible to evaluate the line tension corresponding to the line between the phases a and b without the need for a precise definition of the position of this line. Let us first evaluate the local interfacial tension $g(x) = \mathring{a} \int_z w(x, z)$. The tension, in the homogeneous regions far from the line, does not depend on the phase, that is, it is given by $g^a = g^b$. Therefore, the line tension t , which is the excess grand potential that can be assigned to the line, may be computed from:

$$t = \mathring{a} \int_x (g(x) - g^a) = W \cdot x_M g^a \quad (\text{A8})$$

To quantify the adsorbed amount of components at the line, it is necessary to specify the Gibbs' interfacial plane x^{Gibbs} . (Here we must use the classical nomenclature of a Gibbs' plane, rather than a Gibbs' line). One of the components that are involved with the formation of the two phases, is used to determine this plane. Here we use the PDMS component. The idea is that there is a value for x^{Gibbs} such that the excess of PDMS is zero, that is, $J_{PDMS}^{exc} = 0$. It is easily checked that:

$$x^{Gibbs} = \frac{q_{PDMS} - x_M q_{PDMS}^b}{q_{PDMS}^a - q_{PDMS}^b} \quad (\text{A9})$$

Using the Gibbs' plane, we can compute the Gibbs excess of component i at the line by:

$$J_i^{exc} = \mathring{a} \int_{x=1}^{x^{Gibbs}} (q_i(x) - q_i^a) + \mathring{a} \int_{x=x^{Gibbs}}^{x_M} (q_i(x) - q_i^b) \quad (\text{A10})$$

which may also be written as $J_i^{exc} = q_i - x^{Gibbs} q_i^a - (x_M - x^{Gibbs}) q_i^b$. In analogy with the Gibbs' law for adsorption on a classical two-dimensional interface, we may write a Gibbs' law for adsorption of a component k on the line between the phases a and b as:

$$\frac{\gamma t}{\gamma m_k} = - \frac{J_k^{exc}}{N_k} \quad (\text{A11})$$

Where N_k is the number of segments in molecule k . From this we see that a positive value for J_k^{exc} leads to a reduction of the line tension and *vice versa*.

Additional Experimental Data

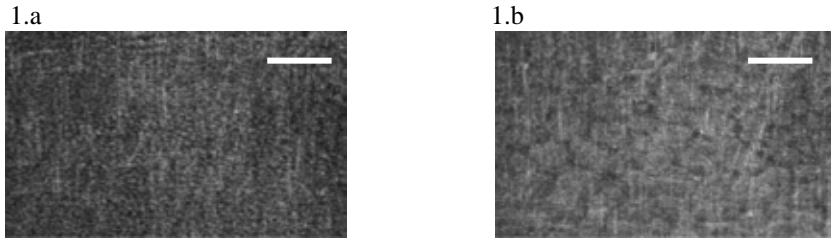


Figure 1. BAM pictures of 90% PDMS – 10% PMMA mixture; (a) $p = 7.7$ mN/m, $a = 22$ nm² · molecule⁻¹ (after a pause of the compression of 30 minutes); (b) $p = 8$ mN/m, $a = 15.9$ nm² · molecule⁻¹; The scale bar is 150 nm.

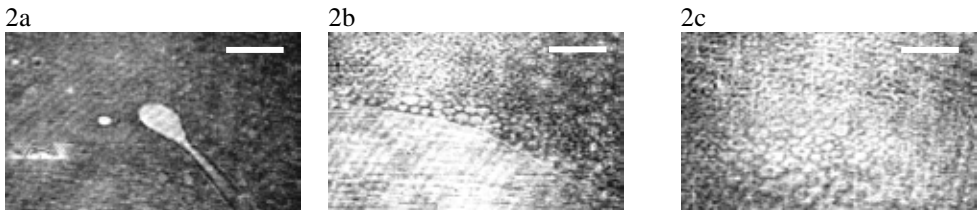


Figure 2. BAM pictures of a ternary mixture containing 5% P(DMS₁₀₈-b-MMA₂₀₀), 5% PMMA and 90% PDMS during a compression cycle; (a) 34,4 nm², (b) 23.3 nm². Ternary mixture containing 5% P(DMS₁₀₈-b-MMA₂₀₀), 10% PMMA and 90% PDMS, same experimental conditions, at 27.5 nm². The scale bar is 150 nm. The bright stripes sometimes visible are artifacts due to scattering from the bottom surface or interference fringes.

Bibliography

- (1) Cox, J. K.; Eisenberg, A.; Lennox, R. B. *Curr. Opin. Colloid Interface Sci.* **1999**, *4*, 52.
- (2) Fasolka, M. J.; Mayes, A. M. *Ann. Rev. Mater. Res.* **2001**, *31*, 323.
- (3) Krausch, G. *Mater. Sci. Eng. R-Rep.* **1995**, *14*, 1.
- (4) Mann, E. K.; Langevin, D. *Langmuir* **1991**, *7*, 1112.
- (5) Mann, E. K.; Henon, S.; Langevin, D.; Meunier, J. *Journal De Physique Ii* **1992**, *2*, 1683.
- (6) Lee, L. T.; Mann, E. K.; Langevin, D.; Farnoux, B. *Langmuir* **1991**, *7*, 3076.
- (7) Crisp, D. J. *Journal of Colloid Science* **1946**, *1*, 161.
- (8) Beredjick, N.; Ahlbeck, R. A.; Kwei, T. K.; Ries, H. E. *Journal of Polymer Science* **1960**, *46*, 268.
- (9) Beredjick, N.; Ries, H. E. *Journal of Polymer Science* **1962**, *62*, S64.
- (10) Labbauf, A.; Zack, J. R. *Journal of Colloid and Interface Science* **1971**, *35*, 569.
- (11) Kuan, S. W. J.; Frank, C. W.; Fu, C. C.; Allee, D. R.; Maccagno, P.; Pease, R. F. W. *J. Vac. Sci. Technol. B* **1988**, *6*, 2274.
- (12) Kawaguchi, M.; Tohyama, M.; Mutoh, Y.; Takahashi, A. *Langmuir* **1988**, *4*, 407.
- (13) Bernardini, C.; Stoyanov, S. D.; Stuart, M. A. C.; Arnaudov, L. N.; Leermakers, F. A. M. *Langmuir* **2010**, *26*, 11850.
- (14) Brinkhuis, R. H. G.; Schouten, A. J. *Macromolecules* **1991**, *24*, 1496.
- (15) Pireaux, J. J.; Gregoire, C.; Caudano, R.; Rei Vilar, M.; Brinkhuis, R.; Schouten, A. J. *Langmuir* **1991**, *7*, 2433.
- (16) Fox, H. W.; Taylor, P. W.; Zisman, W. A. *Industrial and Engineering Chemistry* **1947**, *39*, 1401.
- (17) Mann, E. K.; Lee, L. T.; Henon, S.; Langevin, D.; Meunier, J. *Macromolecules* **1993**, *26*, 7037.
- (18) Hahn, T. D.; Hsu, S. L.; Stidham, H. D. *Macromolecules* **1997**, *30*, 87.
- (19) Kim, C.; Gurau, M. C.; Cremer, P. S.; Yu, H. *Langmuir* **2008**, *24*, 10155.

Chapter 5

Polymer Compatibility in Two Dimensions

Modeling of Phase Behavior of Mixed Polymethacrylate Langmuir Films

Abstract

We analyze the possibility of polymer blends to undergo phase separation in two dimensions. To this end we investigate a model system consisting of water-supported Langmuir monolayers, obtained from binary polyalkyl methacrylate mixtures (PXMA, where X stands for any of the type of ester side groups used: M, methyl-; E, ethyl-; B, butyl-; H, hexyl-; O, octyl-; L, lauryl-methacrylate), by means of Self Consistent Field (SCF) calculations.

In particular, we address the conditions which determine demixing and phase separation in the two-dimensional system, showing that a sufficient chain length mismatch in the ester side group moieties is able to drive the polymer demixing. When the difference in length of the alkyl chain of the ester moieties on the two types of polymers is progressively reduced, from 11 carbon atoms (PMMA/PLMA) to 4 carbons only (POMA/PLMA), the demixing tendency is also reduced. The polymer/subphase interactions affect more the distribution of the polymer coils in the POMA/PLMA blend monolayer. Mixing of the two polymers is observed, but also a partial layering along the vertical direction.

We also add, to a PMMA/PLMA blended monolayer, a third component, namely a symmetrical diblock copolymer of the type PLMA-*b*-PMMA. We observe adsorption of the diblock copolymer exclusively at the contact line between the two homopolymer domains, and a concomitant lowering of the line tension. The line tension varies with chemical potential of the diblock copolymer according to the Gibbs' law, which demonstrates that PLMA-*b*-PMMA can act as a "lineactant" (the equivalent of a surfactant in two-dimensional systems) in the binary demixed PMMA/PLMA Langmuir monolayer.

1. Introduction

Polymer monolayers are an attractive subject of research, since they allow to fabricate highly controlled thin films¹⁻⁴. The use of amphiphilic molecules for preparation of Langmuir monolayers, together with the Langmuir-Blodgett deposition technique, allows to achieve a remarkable control over the film thickness, however the strategies to control the formation of structures parallel to the interface are less systematically explored. One possibility lies in the realization of a monolayer made of a blend of incompatible polymers.

Polymer blends in two-dimensional systems are much less investigated than their equivalents⁵ in the bulk. Particularly the conditions which determine demixing and phase separation^{6,7} are not addressed in a systematic way.

We addressed the issue with both experiments and Self Consistent Field (SCF) calculations, trying to obtain polymer blends from PDMS and PMMA polymers⁸, both spreadable, amphiphilic and unambiguously immiscible in a three dimensional system. However we found that the same polymers, spread on water, formed mixed domains. Apparently, upon confinement of the polymer coils to a strictly two-dimensional environment, the system becomes much more sensitive to the polarity differences displayed by the type of molecules used. Indeed, since Langmuir films are not isotropic but oriented, differences in the relative amphiphilicity of the components may hamper demixing at the air/water interface. In the case of PDMS/PMMA binary mixtures, the polarity mismatch of the two components turns out to favor a layering along the direction normal to the water surface, so that lateral phase separation is not found.

In order to achieve lateral phase separation in Langmuir monolayers a more suitable model system would be a mixture made of components which belong to the same polymer family, so that polarity does not vary considerably among the different members. An example of such a system is represented by polyalkylmethacrylates blends⁹⁻¹¹ and one of these has been experimentally investigated by Aoki *et al.* In their accounts a critical parameter for achieving lateral phase separation at the air/water interface seems to be the lateral chain mismatch between the ester groups pending from the methacrylate polymer skeleton. Demixing due to chain mismatch is a well documented phenomenon in the lipid monolayers field¹²⁻¹⁵, but no systematic accounts are available in the polymer field.

We previously developed a SCF model¹⁶, calibrated on a set of experimental data collected in our group, to analyze the behavior of PDMS/PMMA blends spread at the water surface. In this work we apply the same modeling approach to the analysis of the behavior of polyalkyl methacrylates blends, in order to explore, in a systematic fashion, the influence of the ester side group chain length mismatch on the demixing phenomenon. Furthermore, we test the possibility to modify the miscibility of the components of the binary mixture by the addition of a symmetric diblock copolymer, based on alkyl methacrylates blocks, which also have different ester alkyl groups. The diblock structure should favor its partitioning at the contact line between the domains of the demixed polymers, thereby lowering the line tension between the two phases and favoring their emulsification. Such a compound would act as the equivalent of a surfactant in a two-dimensional environment, therefore it is named “lineactant”. Experimental¹⁷⁻¹⁹ and theoretical²⁰⁻²² studies where lineactants have been tested for efficacy have been carried out. The model systems used were either a mixture of lipids, or lipids added to modified fluorocarbon lipids. The lineactant adopted was, respectively, either a hybrid lipid, with alkyl tails of different lengths, or a partially fluorinated lipid molecule. In this work we aim at testing the generality of these approaches by the use of SCF modeling, extending the “lineactant” concept, born in the lipid monolayers realm, to the polymer thin film research field.

2. Method

A brief outline of the SCF approach is provided in the Appendix. Here we describe how we compute the thermodynamic quantities, which are later presented in the results paragraph, in the investigated system.

2.1 Observables and thermodynamic quantities computed in the system

The free energy functional obtained from the numerical solution of the SCF set of equations allows to calculate the grand potential of the system, according to

$$\Omega = F - \sum_i n_i \mu_i = \sum_z \sum_x \omega(x, z) \quad (1)$$

which is evaluated in the y -direction per unit length. The sum over i is calculated over all the molecule types in the system, n is the number of molecules per unit length in the y -direction, and μ_i is the chemical potential for the specified molecule. Ω is the grand potential density, also expressed per unit length in the y -direction.

Several observables of interest can be extracted: when we study the behavior of homogeneous monolayers, consisting of one polymer, in the one-gradient models, the adsorbed amount at the air/water interface is the relevant quantity given by:

$$\Gamma_i = \sum_z (\varphi_i(z) - \varphi_i^b) \quad (2)$$

As usual, this quantity is presented as the function of the normalized chemical potential, defined by:

$$\Delta\mu_i = \left(\frac{\mu_i - \mu_i^\#}{k_B T} \right) \quad (3)$$

where $\mu_i^\#$ is the chemical potential at the bulk binodal (saturation). The equation to calculate chemical potentials is given in the Appendix.

In order to model the pressure/area isotherms we calculate the surface tension as the grand potential per unit area, following:

$$\gamma = \Omega / A \quad (4)$$

From eq 4 the surface pressure is readily computed as:

$$\pi_p = \gamma_p^0 - \gamma_p \quad (5)$$

where γ_p^0 stands for the surface tension of the pristine surface.

The area per molecule is obtained from the inverse of the surface excess of adsorbed polymer:

$$a_i = 1 / \Gamma_i \quad (6)$$

When binary mixtures of homopolymers are modeled, the excess volume fraction of the polymer i per unit length, in the x, z plane, adsorbed at the interface $\Phi_1(x, z)$, is calculated according to:

$$\Phi_1(x, z) = \varphi_1(x, z) - \varphi_1^b \quad (7)$$

where φ_1^b is the volume fraction in the bulk (water) phase. This parameter represents the 2D distribution profile of the interfacial concentration of the polymer: its integration over the z -direction, normal to the interface, results in the adsorbed amount of component i per unit length in the y -direction $\theta_1(x)$

$$\theta_1(x) = \int_z \Phi_1(x, z) \quad (8)$$

The total adsorbed amount follows immediately upon subsequent integration over the x coordinate

$$\theta_1 = \int_x \theta_1(x) \quad (9)$$

As we study laterally inhomogeneous polymer phases, we will find in the results paragraph two coexisting polymer phases, denoted as a (near $x = 1$) and b (near $x = x_M$; see Figure 2 below for a drawing of the model implemented); the interfacial adsorbed amount in the homogeneous parts is indicated as q_i^a and q_i^b .

The local interfacial tension of the system is obtained as follows:

$$g(x) = \int_z \mathring{a} w(x, z) \quad (10)$$

The interfacial tension tends to a well defined limit, which is the same in both the a and the b phase, since the system is in equilibrium.

It is also possible to calculate the excess grand potential at the point of contact between the two phases, known as the line tension, by:

$$t = \int_x \mathring{a} (g(x) - g^a) = W - x_M g^a \quad (11)$$

where \mathcal{G}^a is the local interfacial tension in the bulk phase (away from the contact line) and x_M is the number of layers in the x-direction.

The position of the interfacial Gibbs' plane x^{Gibbs} (according to classical terminology, we keep this nomenclature rather than defining a Gibbs' line in the system) is determined by selecting one of the polymers present in the mixture as reference, generically denoted by the subscript A , according to the following equation:

$$x^{Gibbs} = \frac{q_A - x_M q_A^b}{q_A^a - q_A^b} \quad (12)$$

The Gibbs' interfacial excess of molecule A is now set to 0 by definition. Using the Gibbs' plane, it is possible to obtain the excess of the other components i at the line by:

$$J_i^{exc} = \mathring{a}_{x=1}^{x^{Gibbs}} (q_i(x) - q_i^a) + \mathring{a}_{x=x^{Gibbs}}^{x_M} (q_i(x) - q_i^b) \quad (13)$$

or, alternatively, by:

$$J_i^{exc} = q_i - x^{Gibbs} q_i^a - (x_M - x^{Gibbs}) q_i^b \quad (14)$$

In analogy with the Gibbs' law of adsorption in a classical two-dimensional interface, we may write a Gibbs' law for the adsorption at the contact line between the phases a and b

$$\mathring{t} = - \mathring{a}_i \frac{J_i^{exc}}{N_i} \mathring{t} \eta \quad (15)$$

for all the components i made of N_i segments, for which the total amount in the system has been fixed. From eq 15 we see that a positive value of J_k^{exc} leads to a reduction in \mathring{t} and vice versa.

2.2 Parameters and molecular model

The model adopted here has been developed and successfully implemented in two previous works^{8,16} by the same authors, where a detailed description is provided. Here we provide a very short summary of its relevant features.

The air/water interface is represented by a solid and impenetrable flat surface (vapor phase), in contact with a fluid surface (water phase). The polymers are modeled by the use of two simple type of segments: a united C atom, which stands for the hydrophobic functional groups of the polymer molecule ($-\text{CH}_2-$ / $-\text{CH}_3$), and a united O atom, which represents the hydrophilic functionalities. The architecture of the modeled monomers is showed in Figure 1, and a sketch of the model box that we have used for our calculations is given in Figure 2.

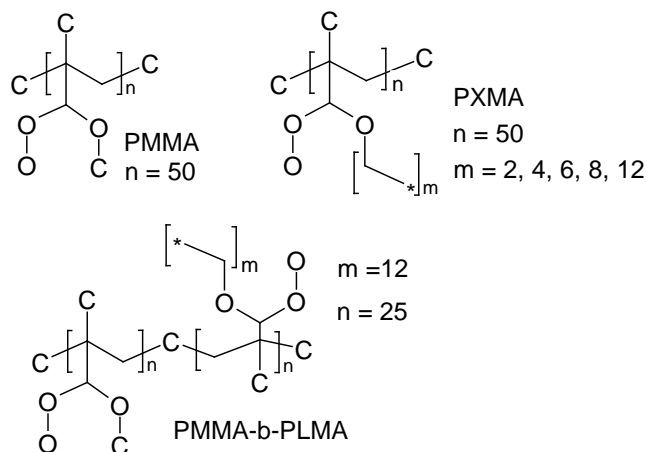


Figure 1. Structures of the polymers as modeled in our calculations; the architecture follows closely the real chemical structure of the molecules. Small modifications are motivated by the fact that the volume of a site coincides with the volume of the building segment of the molecule in the lattice on which the model has been implemented.

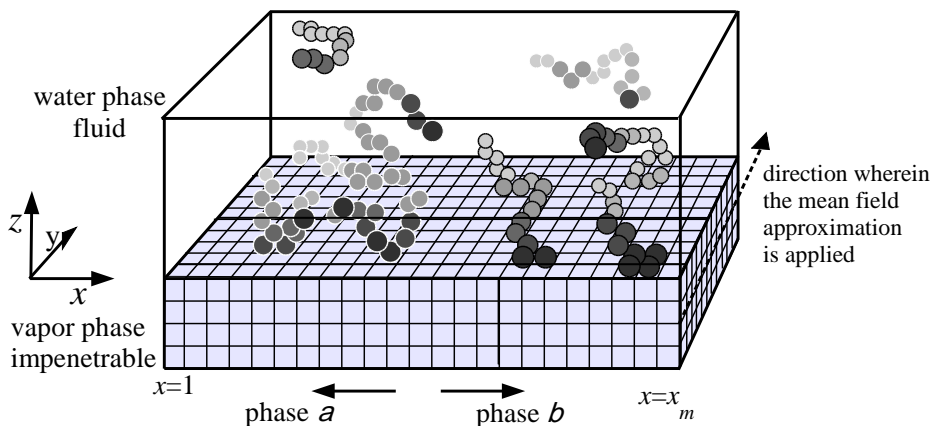


Figure 2. Representation of the model used throughout our calculations: the water phase, fluid, is located in the upper part of the box; the air phase is represented by the impenetrable solid surface at the bottom. The grey region is not considered in the calculations, although the lattice sites have been drawn on it for clarity of the picture. In the fluid phase we have $z = 1, 2, \dots, z_M$ flat lattice layers: each layer is divided into lattice sites numbered $x = 1, 2, \dots, x_M$. Along the y -direction the system must be considered infinitely long. Reflected boundaries are chosen at $x = 1, x = x_M$ and $z = z_M$ sites. When polymers form two coexisting distinct phases, the one on the left side is denoted as a (near $x = 1$), while the other, on the right side of the box, is indicated by the letter b (near $x = x_M$).

Parameters have been chosen so that C units display a strong repulsion towards water molecules and O units, and attraction for the surface, while O units are neutral towards both the solvent and the surface. Like in our previous works, we have used the following values:

$$\chi_{c.w} = 1, \chi_{c.o} = 1.5, \chi_{o.w} = \chi_{o.s} = 0.$$

3. Results and discussion

In the following section we discuss the conditions which determine polymer incompatibility at the air/water interface, as they result from our model system. We first analyze the spreading properties of single, pure, homopolymer monolayers of the alkyl-methacrylate polymer family, which later will constitute the single components of our model mixtures. Then we focus on binary mixtures of different

types of alkyl–methacrylates, where the two components have different side chain pending groups: both of them are alkyl groups, but their length is different. We progressively reduce the difference in the side chain length and we observe how the polymer architecture ultimately reflects onto their reciprocal miscibility in a two–dimensional environment. After that we examine a more complex system, in which we introduce into the binary demixed polymer monolayer a diblock copolymer: the two blocks of the latter one are identical to the mixture components. The structure of the diblock copolymer favors its partitioning at the interfacial contact line between the two demixed phases, hence it acts as a lineactant (the equivalent of a surfactant in a two–dimensional system). We study how the introduction of the lineactant affects the line tension of the system under investigation, and to what extent the lineactant molecular architecture influences its adsorption at the contact line of the two polymer phases.

3.1 Behavior of homopolymer polyalkyl-methacrylate Langmuir monolayers.

In this study we address the spreading behavior of polymers belonging to the polyalkyl–methacrylate family. We have based the selection of such a system on a previous work¹⁶ from the same authors, where we investigated experimentally and by SCF modeling the spreading properties of a series of water–insoluble polymers at the air/water interface.

In that work we proposed a new interpretation of the spreading phenomena occurring at the air/water interface, discussing the experimental findings in terms of wettability of the surface by a given polymer. PMMA, in particular, was found to be autophobic, due to the presence of hydrophilic moieties as lateral pending groups on the polymer skeleton: the anisotropic orientation of its monomers on the water surface confers to the monolayer the observed autophobicity, which prevents the growth of multiple layers upon compression. Therefore, the combination of these two characteristics (the good spreadability and the autophobicity) made PMMA and its alkyl–derivatives the best candidates to be selected in order to study polymer incompatibility in a strictly two–dimensional environment.

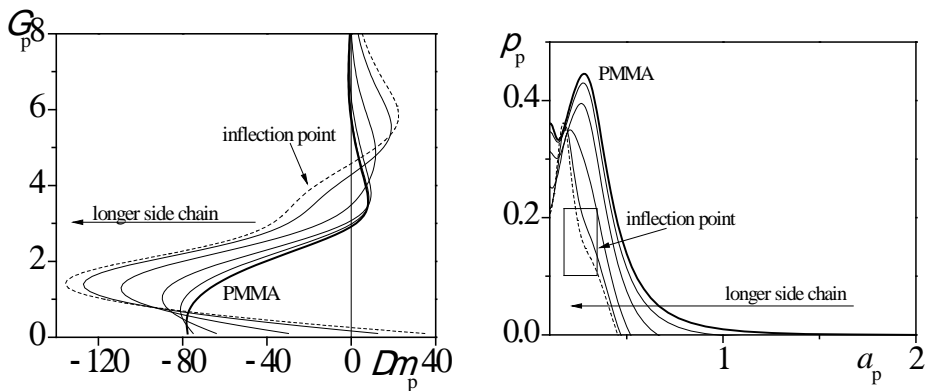


Figure 3. On the left panel, adsorption isotherms for the polyalkyl-methacrylate polymers, plotted as surface excess concentration G_p versus the normalized chemical potential Dm_p . On the right panel, calculated pressure/area isotherms for the same polymers. The thick continuous line shows the PMMA isotherm, the thin lines show the variation occurring when the ester group becomes longer ($n^{\#}_{C \text{ atoms}} = 2, 4, 8, 12$). The dashed line corresponds to the isotherm of poly-tetradecyl-methacrylate.

The wetting properties and the spreading behavior of polyalkyl-methacrylates is shown in Figure 3, as a function of the alkyl lateral chain length. The left panel shows the calculated adsorption isotherms at the air/water interface, plotted versus the normalized chemical potential. All the polymers are in the partial wetting regime. PMMA shows the occurrence of a “pre-wetting step” at low surface concentrations, followed by the monolayer growth; the growth of further polymer layers is inhibited (anisotropic behavior) and the chemical potential of coexistence is reached when the surface coverage is still finite (the film is microscopically thin). The corresponding pressure/area isotherm (right panel) shows how the spread monolayer resists to layering when an external lateral pressure is applied to it, becoming progressively more compact, in agreement with experimental evidence.

When the length of the alkyl side chain is increased progressively, from methyl- (1 C atom), to myristic- (14 C atoms) side chain, we notice the corresponding occurrence of a more marked “pre-wetting step” in the adsorption isotherm; longer, more hydrophobic, lateral pendant groups enhance the tendency of the polymer coils to form compact “pancakes”, in equilibrium with an extremely diluted gas-like phase, on top of the water surface. Only PMMA, where the side chain is constituted by a methyl group, is able to spread efficiently on the water subphase at low surface coverage values (large molecular areas), whereas polymer

with longer alkyl side chains require an increasing value of surface coverage, hence very low molecular areas, before they can form a compact monolayer, which fully covers the water subphase. The autophobicity observed in the case of PMMA is well preserved through the series; however, a tendency towards layering phenomena (indicated by the appearance of an inflection point, see arrow in Figure 3) is observed in the cases of the longest side chains (12 C and 14 C atoms).

3.2 Langmuir monolayers made of PXMA/PLMA mixtures.

Chain length mismatch has been correlated to the occurring of phase separation phenomena in Langmuir monolayers in several systems^{12,13} consisting of mixtures made of different types of lipids. The same behavior has been observed in polyalkyl-acrylates Langmuir monolayers: poly(isobutyl methacrylate) and poly(octadecyl methacrylate) blends phase separated at the air/water interface have been thoroughly characterized with many experimental techniques⁹⁻¹¹.

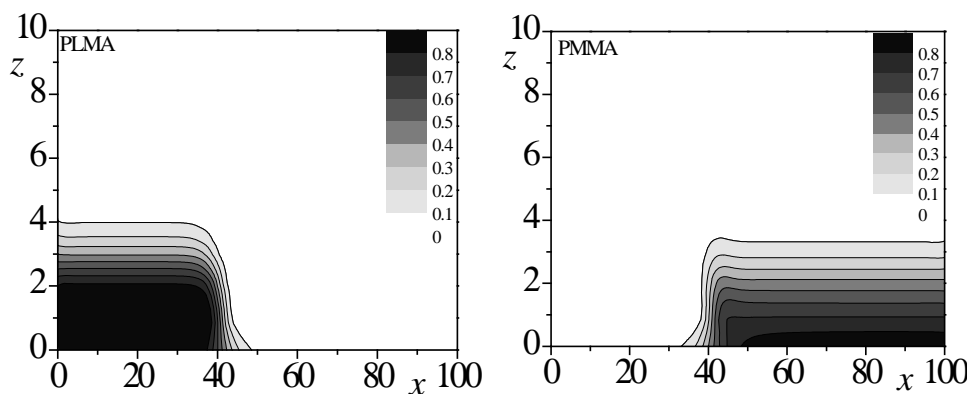


Figure 4. Surface contour plot of the volume fraction distribution density of PMMA and PLMA, in a binary mixed film. The approximate ratio of the polymers is 1/1.

In our previous work on PDMS/PMMA polymer blends spread at the air/water interface, we concluded that differences in relative amphiphilicity between the two polymers favored the occurring of layering along the direction normal to the water surface, rather than a lateral phase separation in polymer mixed Langmuir monolayers.

Therefore, basing our reasoning on the experimental findings mentioned above and our own considerations, we decided to study mixtures of polymers belonging to the same family (polyalkyl–methacrylates, in our case) with an adequate amphiphilicity degree, but different pending alkyl side groups, to see whether any pair would favor the lateral phase separation, or rather, the previously found tendency towards layering.

In Figure 4 we report the typical volume fraction distribution profiles found for a binary mixture made of polymethyl–methacrylate (PMMA, see right diagram) and polylauryl–methacrylate (PLMA, see left diagram). The two polymers modeled differ in their lateral pending groups by 11 carbon atoms.

As we expected, the two polymers are immiscible. When equal amounts of both polymers are allowed to spread, and the surface coverage of both is high enough to obtain a homogeneous monolayer, PMMA, which spreads more easily on top of the water surface, forms the continuous phase and embeds compact domains of PLMA. The difference in compressibility between PMMA and PLMA shown in Figure 3 (right panel), allows to speculate that the PLMA constitutes the dispersed phase, when both polymers coexist at the air/water surface at a given surface pressure. The interface between the two polymer phases is sharp; negligible quantities of one polymer appear to dissolve in the bulk phase of the other one.

We then examined the effect of the side chain length variation on the possibility to obtain well defined phase separated mixtures, addressing the following cases: PXMA/PLMA binary mixtures, with X = E(ethyl-), B(butyl-), H(*n*-hexyl-), where the total length of the alkyl ester lateral pending groups is progressively increased. For each PXMA polymer, we performed calculations where the interfacial concentration of PXMA in the system was progressively increased, while the PLMA interfacial amount was kept constant.

In Figure 5 we observe the variation in thickness of the bulk phases *a* and *b* when the PXMA polymer is progressively added to the PLMA monolayer. As we can see from the plot, the thickness of the bulk phase *a*, rich in PLMA content, increases linearly with the addition of the other component, independently of the nature of the latter one. This is consistent with a scenario where the two phases mix negligibly and the water surface is fully covered by the demixed polymer film.

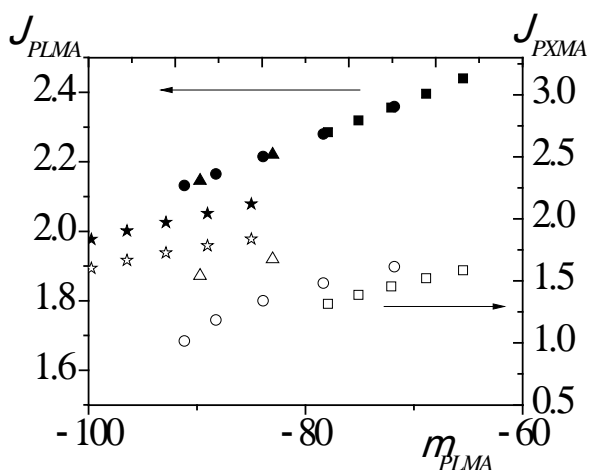


Figure 5. Interfacial adsorbed amount of polymers plotted versus PLMA chemical potential: on the left axis, the interfacial PLMA concentrations in the bulk of the PLMA film domains (phase *a*) are shown for all the binary mixtures studied (black squares, PMMA/PLMA mixture; black circles, PEMA/PLMA mixture; black triangles, PBMA/PLMA mixture; black stars, PHMA/PLMA mixture). On the right axis, interfacial PXMA concentrations (open squares, PMMA; open circles, PEMA; open triangles, PBMA; open stars, PHMA) in the bulk of the PXMA film domains (phase *b*).

The PLMA interfacial amount does not change considerably when the other polymer is added, however the thickness of the PLMA rich phase is increasing with the load of more PXMA because the latter one subtracts surface to the former, squeezing the PLMA domains and making them more compact and slightly thicker. Since the PLMA compressibility is the same, whatever second (immiscible) component is added, the same linear increase in film thickness is seen for all the binary mixtures studied, except for the PHMA/PLMA mixture. The type of PXMA polymer added does not influence how much the thickness of the PLMA domain changes, as long as both components are negligibly miscible.

The thickness of phase *b*, richer in PXMA polymer, varies differently when the X group is changed. The longer the X side group is, the thicker phase *b* appears, when the same surface coverage is attained. This is consistent with the molecular structure of the PXMA polymer: longer X groups make the molecules bigger and so the thickness of the film is larger at the same surface coverage values.

The PHMA/PLMA mixture case is the only one which does not follow the trend illustrated above: the PLMA rich phase (phase *a*) becomes thicker with the

addition of PHMA, although the thickness is lower than the one observed for other mixtures at comparable chemical potentials. The PHMA rich phase is also thicker than the other PXMA rich phases, consistently with the more bulky molecule here modeled. The compressibility of the two types of molecules, displayed in Figure 3 (right panel), is rather similar; at a given surface coverage, the two films have similar surface pressure values, which might favor a better mixing. All these factors point to a slightly higher miscibility of PHMA and PLMA, due to their reduced chain mismatch in their respective lateral ester side chains.

Figure 6 shows the typical volume fraction distribution profile obtained when the PHMA/PLMA mixture is studied, confirming the higher miscibility of these two polymers. The interfacial contact line is much broader than the one observed between PMMA and PLMA. As we can see from the profiles, the PHMA polymer seems to be slightly soluble in the PLMA bulk phase, while PLMA does not seem to penetrate into the bulk of PHMA phase: this is in line with the general finding that it is energetically more unfavorable to dissolve long molecules in a thin layer made of shorter ones rather than the opposite. Triglycerides binary mixtures show a similar behavior¹².

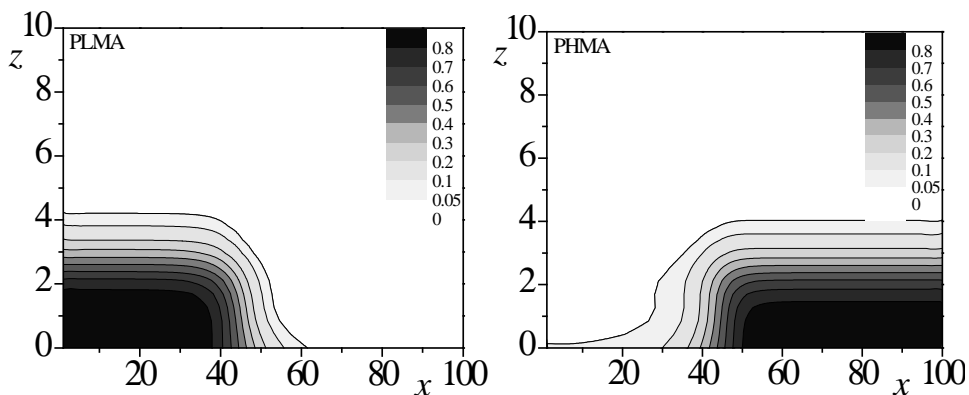


Figure 6. Surface contour plot of the volume fraction distribution density of PLMA (left panel) and PHMA (right panel), in a binary mixed film. The approximate ratio of the polymers is 1/1.

According to eq 11 we can measure a line tension between the bulk phases a (PLMA) and b (PXMA); the variation of the line tension as a function of PLMA chemical potential in the different binary mixtures is shown in Figure 7.

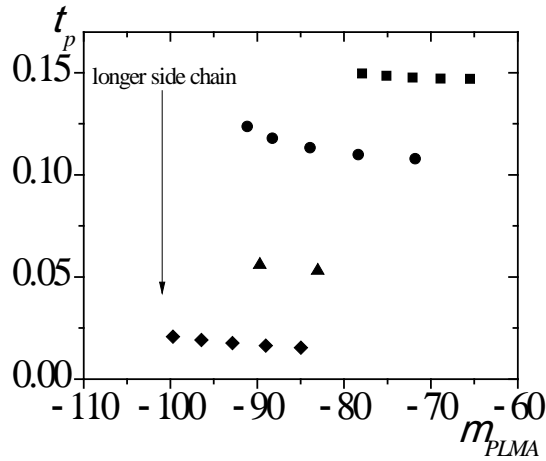


Figure 7. Line tension plotted versus PLMA chemical potential, for different PXMA/PLMA mixtures (black squares, PMMA/PLMA mixture; black circles, PEMA/PLMA mixture; black triangles, PBMA/PLMA mixture; black diamonds, PHMA/PLMA mixture).

When the amount of PXMA is increased progressively, and the thickness of PLMA is made larger (increased value of the PLMA chemical potential), the line tension does not seem to change appreciably, and fluctuations in its value are very little in the range of PLMA chemical potentials considered. Hence we can compare the limiting values of the line tension in different binary mixtures, even though the chemical potential of PLMA is slightly different for every case.

It is also apparent that a change in the side group chain length affects considerably the line tension of the system: in particular, the line tension of the PHMA/PLMA mixture is almost one order of magnitude lower than the one calculated for the PMMA/PLMA mixture. The calculated line tension for the mixture displayed in Figure 4, according to eq 11, is $0.147 kT/\text{lattice site}$, which corresponds to a value of approximately 0.11 pN (considering the dimension of a single lattice site approximately 0.3 nm). This value is consistent with the data calculated with the same model for the PDMS monolayer, in the region of coexistence between the thick and thin phases (0.05 pN)¹⁶. In case of demixing, we expect to get an interface sharper and, consequently, a line tension higher for the polyalkyl-acrylates binary mixture, compared to the value obtained for the interface between thick and thin PDMS, during the layering phase transition. Several papers²⁵⁻²⁸ have measured the experimental values of the line tension at the

gas/liquid phase boundary in PDMS monolayers: the range of values found (from 0.65 to 1.1 pN) has the same order of magnitude of our estimate; furthermore, a line tension between a gas/liquid interface is expected to be higher than in a liquid/liquid interface, due to the much sharper boundary region, and our calculated value is lower than the ones listed above, as expected.

Figure 8 shows more clearly the changes occurring at the interfacial contact line of the binary mixtures when the side group chain length is modified. On the left side we observe the change in the interfacial concentration per unit length $\theta_p(x)$ of PXMA polymer, as a function of the x -coordinate in the system: the variation of the interfacial concentration, from the bulk value of phase b to the negligible amounts in phase a , is very sharp in the PMMA case, and progressively more gradual when the side chain length is increased.

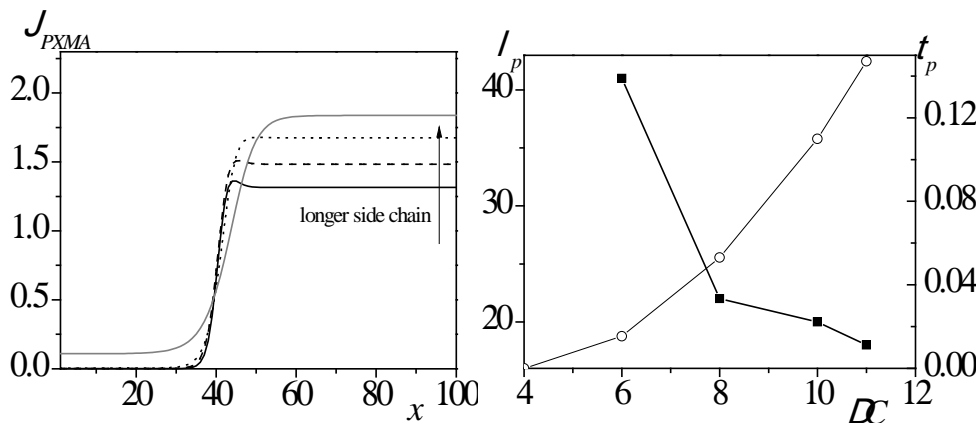


Figure 8. On the left panel, interfacial adsorbed amount of PXMA polymer, $J_p(x)$, plotted as a function of the x -coordinate of the model system (PMMA, black continuous line; PEMA, dashed line; PBMA, dotted line; PHMA, grey continuous line). On the right panel, interfacial thickness l_p (left axis, black squares) and line tension t_p (right axis, open circles), plotted versus the difference in length of the ester side group chains $DC = X_{PLMA} - X_{PXMA}$ of the considered polymers, expressed in $n^\#$ of C atoms.

In case of PHMA the interfacial concentration in the bulk b phase is not negligible anymore. On the right side we plot the limit value of the line tension calculated for every mixture, and the thickness of the interfacial contact line, as functions of the side chain mismatch, $DC = n_{C(PLMA)} - n_{C(PXMA)}$, between the two mixed polymers. The interfacial thickness of the contact line is computed in

number of lattice sites along the x -coordinate, where the difference in the interfacial concentration between two adjacent sites, $J(x+1) - J(x)$, is higher than 0.001 units. We observe a progressively diminishing line tension when the \mathcal{DC} parameter decreases, whereas the interfacial length of the contact line changes in a less linear fashion, increasing slightly, and then abruptly, with the decrease of the \mathcal{DC} parameter. When the side chain mismatch is reduced further, as in the binary mixture made of polyoctyl-methacrylate and polylauryl-methacrylate, POMA/PLMA ($\mathcal{DC} = 4$), phase separation no longer occurs: the line tension vanishes and the two polymers mix in a single domain, where the POMA distributes homogeneously inside the PLMA domain far from the contact line, and just adsorbs onto the PLMA boundary line (which is a 1D interface).

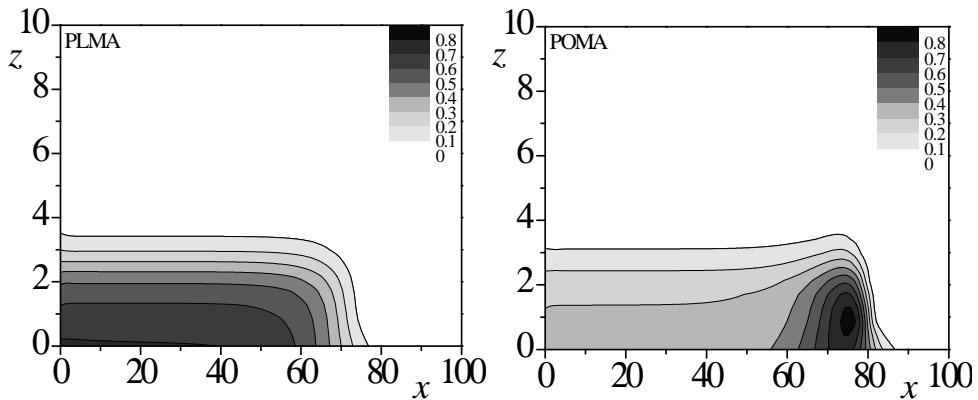


Figure 9. Surface contour plot of the volume fraction distribution density of PLMA (left panel) and POMA (right panel), in a binary mixed film. The approximate ratio of the polymers is 1/1.

Indeed, as it is shown in the volume fraction distribution profiles reported in Figure 9, PLMA forms a compact pancake in equilibrium with an extremely diluted gas-like phase, at the air/water interface. POMA also forms a compact pancake in equilibrium with the diluted gas-like phase, but, instead of sitting next to the PLMA domain, it mixes with it. As a remnant of two-dimensional demixing, we see also some extra accumulation of POMA at the edge of the mixed domain (see Figure 9, right panel). Such a layering phenomenon along the z -axis, occurring inside the PLMA domain, has been reported also in our previous work concerning the mixtures of PDMS and PMMA polymers. A summarizing scheme of all the

structural configurations observed in the various binary mixtures is provided in Figure 10.

The distribution of the polymer coils in a mixed Langmuir monolayer is a very complex phenomenon, subjected to the interplay of various forces, acting both along the air/water interface and in the direction normal to it. Therefore, the confinement of polymer chains to a strictly two-dimensional environment appears rather difficult to achieve, since not only chemical differences in the polymer coils are crucial, but their relative polarity too. Even though the difference in side chain length is of 4 C atoms, which is usually enough to yield demixing in lipid-based systems¹², polarity mismatch is also acting on the POMA/PLMA system, favoring the layering over phase separation.

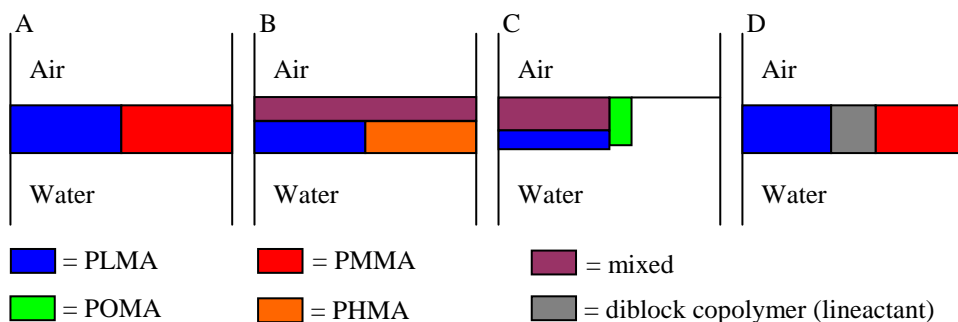


Figure 10. The drawing represents the four scenarios illustrated in the results section: (a) PLMA/PMMA laterally phase-separated mixture; (b) PLMA/PHMA mixture: the interpenetration of the homopolymers starts from the region in contact with air, while next to water the phase separation is still prevailing; (c) PLMA/POMA are mixed, and only at the edge of the mixed domain there is some extra-accumulation of POMA, as a remnant of 2D demixing; (d) PLMA/PMMA added with diblock copolymer: the latter acts as a lineactant and adsorbs selectively at the contact line between homopolymer domains, forming a 2D emulsion.

3.4 Use of a diblock copolymer as lineactant in PMMA/PLMA Langmuir monolayers.

In this paragraph we aim at showing that it is possible to modify the miscibility of the components of the phase separated binary mixture by the addition of a symmetric diblock copolymer, based on alkyl methacrylates blocks which have different ester alkyl groups, selected in order to match those present in the

homopolymer domains. In order to do so, we focused our analysis on the system made of PMMA and PLMA homopolymers, mixed in the same proportions. PLMA-*b*-PMMA has been used as the diblock copolymer. Its architecture is sketched in Figure 1. We perform calculations for a ternary mixture where the interfacial adsorbed amount of PMMA homopolymer is fixed (that is, the chemical potential is kept constant by fixing a bulk PMMA concentration), while the amount of PLMA is kept constant, and, at the same time, a progressively higher amount of diblock copolymer is introduced into the system. An example of the volume fraction distribution profiles obtained is reported in Figure 11.

We can see from the profiles that the homopolymers are demixed, like in the binary mixture case. The diblock copolymer added is adsorbed exclusively at the contact line between the PLMA and the PMMA domains. Therefore the architecture adopted is highly effective in favoring the adsorption process at the contact line: the diblock copolymer acts as a lineactant, the analog of a surfactant in the classic three-dimensional scenario.

The adsorption process at the contact line of the two homopolymer domains is illustrated in Figure 12. On the left axis, the graph shows how the calculated interfacial Gibbs' excess of the lineactant molecule (denoted with l) increases when the total amount of diblock copolymer is increased (higher chemical potential values). Correspondingly, on the right axis, the values of the calculated line tension are plotted versus the lineactant chemical potential: as expected, these values are monotonically decreasing with the addition of lineactant to the system. The maximum lowering of line tension achieved in our calculation is roughly around 28 % of the starting value calculated in the binary mixture.

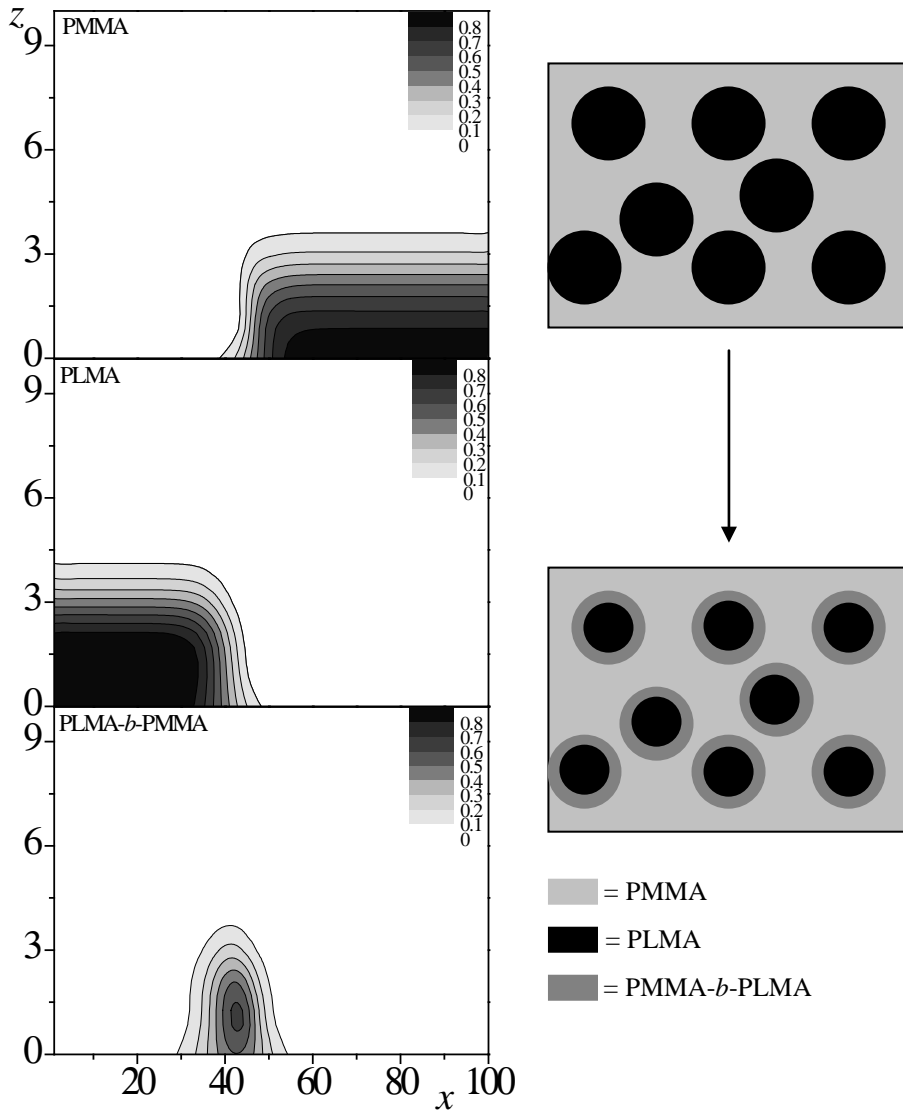


Figure 11. On the left, surface contour plot of the volume fraction distribution density of PMMA, PLMA, and PLMA-*b*-PMMA diblock copolymer in a film made of a ternary polymer mixture. The approximate ratio of the homopolymers is 1/1. On the right, a cartoon which represents the system, as seen from the top of the water surface, before and after addition of the diblock copolymer (lineactant).

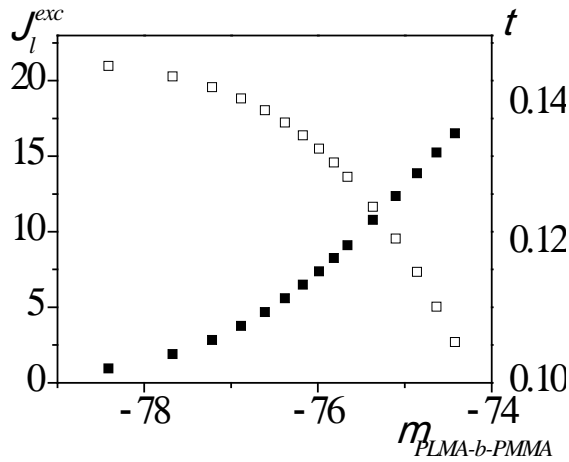


Figure 12. On the left axis, interfacial Gibbs' excess of lineactant adsorbed at the contact line plotted versus the lineactant chemical potential (black squares). On the right axis, line tension of the ternary mixture plotted versus the lineactant chemical potential (open squares).

In order to verify if the decreasing trend of line tension obeys to the Gibbs' law, we plot the data set, according to eq 15, linearized as follows:

$$\frac{\nabla t}{\nabla m} = - \frac{J_l^{exc}}{N_l} - \frac{J_{PLMA}^{exc}}{N_{PLMA}} \frac{\nabla m_{PLMA}}{\nabla m} \quad (16)$$

in Figure 13.

The plot is linear and the calculated values of both the slope and the intercept are in good agreement with the Gibbs' law. Therefore our initial hypothesis is verified, and the diblock copolymer adopted in our calculations displays a behavior which is fully compatible with the expected lineactant action on the components of the binary mixture.

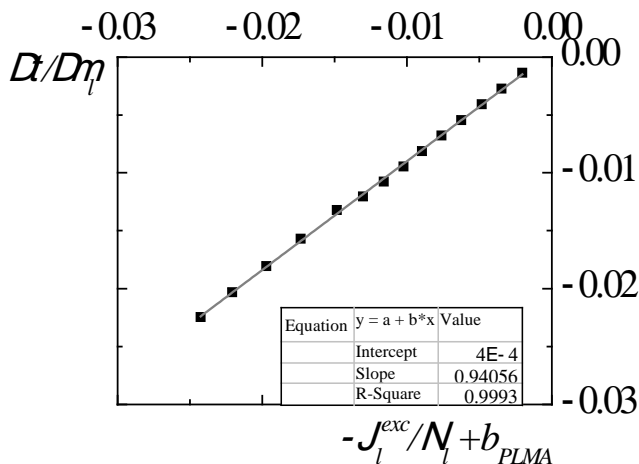


Figure 13. Linearized Gibbs' law calculated according to eq 16 with the data set obtained for the ternary mixture PMMA + PLMA + PLMA-*b*-PMMA polymers. The contribution of PLMA to the equation is indicated by $b_{PLMA} = -\frac{J_{PLMA}^{exc}}{N_{PLMA}} \frac{\eta_{PLMA}}{\eta}$ on the right axis. PMMA has been chosen as the reference molecule, and its chemical potential is kept constant throughout the calculations, therefore its contribution to eq 15 vanishes.

4. Conclusion

In this chapter we have analyzed, through SCF calculations, the requirements needed to achieve polymer blend demixing in a Langmuir monolayer: spreadable, insoluble polymers, with the same amphiphilicity degree, combined to a certain chemical mismatch of the side moieties are necessary in order to cause demixing at the air/water interface. The polyalkyl methacrylate example investigated here, represents a suitable model system, since the methacrylate backbone guarantees that the different polymers have the same affinity towards the water subphase, while the different ester moieties drive the occurrence of lateral demixing. We have shown the dependency of the lateral demixing on the difference in length between the two ester side groups chosen. We suggest that a rather complex interplay of forces regulates the distribution of the polymer coils in the monolayer: subtle alterations of this complex balance might favor the dewetting of the mixture in a

single domain, together with the layering of the blended polymers along the direction normal to the air/water interface, as well as accumulation of one polymer at the domain edge, instead of the occurrence of the lateral phase separation.

Furthermore, we have proven the possibility to control emulsification of two-dimensional demixed polymer blends by use of a diblock copolymer, which acts as a lineactant (the two-dimensional analog of a surfactant), adsorbing at the contact line of the polymer domains. We demonstrate, through our calculations, the possibility to extend the lineactant concept, first elaborated in the context of lipid membrane investigations, to the polymer thin films field of study. The development of polymer-based systems where lineactants are applicable discloses opportunities to develop novel ways of regulating structuring and self assembly of complex structures in thin films.

Future research directions in this topic might be experimental tests aimed at verifying the conclusions achieved through our model, and further deepening, through SCF calculations, of the relationship between lineactant efficiency and molecular architecture of the diblock copolymer adopted.

Appendix

1. Overview of the Self Consistent Field theory

In this paragraph we outline briefly the SCF (Self Consistent Field) method, used to model the behavior of mixed polyalkyl-methacrylate Langmuir films.

The SCF theory relies on the use of the so called mean field approximation. In this specific study we are interested in the behavior of polymer Langmuir monolayers, therefore we focus on the interactions which occur along the z -axis, normal to the air/water interface, where the spread insoluble polymers are localized. However, as we are interested in the behavior of mixed polymeric monolayers, we also study the lateral interaction between these films, occurring along the x -axis. As a consequence, we need to implement a two-gradient version of the SCF method, where we apply the mean field approximation in the remaining y -direction, along the air/water interface (see Figure 2 in Section 2 - Methods). Any given location in the system is defined by the vector $\mathbf{r} = (x,z)$.

The polymer segments are not localized individually in the system; instead, we focus on the overall volume fraction $\varphi_A(\mathbf{r}) \equiv \varphi_A(z, x)$, which is a dimensionless concentration, obtained from the number of segments of coordinates (x, z) , times the molar volume, divided by the volume that is available in the y -direction. In other words, it is the ratio between the number of segments and the number of available lattice sites. Every segment type has its own distribution, generically denoted by the index A . Each segment volume fraction is associated to a segment potential .

The mean-field free $u_A(\mathbf{r})$ energy of the system is expressed as a functional of these two profiles, the volume fractions and the potentials, and it is constrained by making the system locally incompressible

$$\sum_A \varphi_A(\mathbf{r}) = 1 \quad (1)$$

for every coordinate \mathbf{r} . Then the functional is optimized iteratively: a saddle point of the free energy function represents a valid solution, corresponding to a physically observable situation. The iteration is performed according to the following scheme:

$$\varphi[u(\mathbf{r})] \mathcal{f} u[\varphi(\mathbf{r})] \quad (2)$$

where the segment potentials are computed from a starting value (initial or subsequent guesses) of the volume fractions, and vice versa, until convergence is reached.

In order to calculate the volume fraction of our polymer segments, we implement the freely-jointed chain model and use the propagator method to compute the volume fraction profiles on the lattice^{23,24}.

Potentials are determined by defining, for each segment type, its interaction with the other segments of the system through the Bragg-Williams approximation, using the Flory-Huggins parameters:

$$\chi_{AB} = \frac{Z}{2k_B T} [2U_{AB} - U_{AA} - U_{BB}] \quad (3)$$

From eq 3 we see that the interaction parameters are dimensionless, as they are all divided by the thermal energy $k_B T$, so that every result presented here is expressed in dimensionless form. We also see that in case the interaction potential U_{AB} between a segment A and a segment B is lower than the average of the interaction potentials between similar segments, (U_{AA} and U_{BB}) a negative c parameter is

found, and the two segments tend to mix. On the contrary, a positive c indicates a tendency towards demixing. In case of polymer segments, generally the demixing occurs at lower c values than with monomers, because polymers have a reduced translational entropy per unit mass. The interactions with the vapor phase are also accounted for, through an appropriate parameter value, and occur only when the segments are located in the layer $z = 1$, since they are strictly short-rangeⁱ (the air/water interface is indeed very sharp, since its width is in the order of magnitude of $1 \cdot 10^{-10}$ m).

The numerical solution of the SCF equations leads directly to the optimized free energy functional. Further thermodynamic quantities can be computed, as shown in paragraph 2.1 of this chapter.

The chemical potentials used in the results paragraph follow from the Flory-Huggins theory and can be written as:

$$\frac{\mu_i - \mu_i^*}{k_B T} = \ln \phi_i^b + 1 - N_i \sum_j \frac{\phi_j^b}{N_j} + \frac{N_i}{2} \sum_A \sum_B \left(\phi_A^b - \frac{N_{Ai}}{N_i} \right) \chi_{AB} \left(\phi_B^b - \frac{N_{Bi}}{N_i} \right) \quad (4)$$

In this equation μ_i^* is the chemical potential in the reference phase for which the pure component is taken, and N_{Ai} / N_i is the ratio of segments of type A in molecule i .

ⁱ Note that in our previous papers (ref 8 and 16) we also accounted for an external van der Waals-like potential. This long range potential was needed to get the layering transition for PDMS in accordance with experiments. In the current chapter we did not include this external potential because our interest is not in small shifts of layering features in the adsorption isotherm. In other words the results in this chapter will not change significantly when a long range external van der Waals interaction is added or not. Hence, we opted for the simple option and decided not to include the extra van der Waals contribution in the current analysis.

Bibliography

- (1) Fasolka, M. J.; Mayes, A. M. *Ann. Rev. Mater. Res.* **2001**, *31*, 323.
- (2) Cox, J. K.; Eisenberg, A.; Lennox, R. B. *Curr. Opin. Colloid Interface Sci.* **1999**, *4*, 52.
- (3) Krausch, G. *Mater. Sci. Eng. R-Rep.* **1995**, *14*, 1.
- (4) Forster, S.; Plantenberg, T. *Angew Chem Int Edit* **2002**, *41*, 689.
- (5) de Gennes, P. G. *Scaling Concepts in Polymer Physics*; Cornell University: Ithaca, New York, 1979.
- (6) Kumaki, J.; Hashimoto, T. *Journal of the American Chemical Society* **1998**, *120*, 423.
- (7) Yuba, T.; Yokoyama, S.; Kakimoto, M.; Imai, K. Y. *Advanced Materials* **1994**, *6*, 888.
- (8) Bernardini, C.; Stoyanov, S. D.; Stuart, M. A. C.; Arnaudov, L. N.; Leermakers, F. A. M. *Langmuir* **2011**, *27*, 2501.
- (9) Aoki, H.; Sakurai, Y.; Ito, S.; Nakagawa, T. *Journal of Physical Chemistry B* **1999**, *103*, 10553.
- (10) Aoki, H.; Ito, S. *Journal of Physical Chemistry B* **2001**, *105*, 4558.
- (11) Aoki, H.; Kunai, Y.; Ito, S.; Yamada, H.; Matsushige, K. *Applied Surface Science* **2002**, *188*, 534.
- (12) Zdravkova, A. N.; van der Eerden, J. P. J. M. *Journal of Crystal Growth* **2007**, *307*, 192.
- (13) Hagen, J. P.; McConnell, H. M. *Biochimica Et Biophysica Acta-Biomembranes* **1997**, *1329*, 7.
- (14) Kimura, H.; Watanabe, S.; Shibata, H.; Azumi, R.; Sakai, H.; Abe, M.; Matsumoto, M. *Journal of Physical Chemistry B* **2008**, *112*, 15313.
- (15) Binder, W. H.; Barragan, V.; Menger, F. M. *Angew Chem Int Edit* **2003**, *42*, 5802.
- (16) Bernardini, C.; Stoyanov, S. D.; Stuart, M. A. C.; Arnaudov, L. N.; Leermakers, F. A. M. *Langmuir* **2010**, *26*, 11850.
- (17) Trabelsi, S.; Zhang, S.; Lee, T. R.; Schwartz, D. K. *Physical Review Letters* **2008**, *100*.
- (18) Trabelsi, S.; Zhang, Z.; Zhang, S.; Lee, T. R.; Schwartz, D. K. *Langmuir* **2009**, *25*, 8056.
- (19) Zhang, Z.; Trabelsi, S.; Schwartz, D. K.; Lee, T. R. *Abstracts of Papers of the American Chemical Society* **2008**, 235.
- (20) Brewster, R.; Pincus, P. A.; Safran, S. A. *Biophysical Journal* **2009**, *97*, 1087.
- (21) Brewster, R.; Safran, S. A. *Biophysical Journal* **2010**, *98*, L21.
- (22) Yamamoto, T.; Brewster, R.; Safran, S. A. *Epl* **2010**, *91*.
- (23) Scheutjens, J.; Fleer, G. J. *Journal of Physical Chemistry* **1979**, *83*, 1619.
- (24) Scheutjens, J.; Fleer, G. J. *Journal of Physical Chemistry* **1980**, *84*, 178.
- (25) Alexander, J. C.; Bernoff, A. J.; Mann, E. K.; Mann, J. A.; Zou, L. *Phys. Fluids* **2006**, *18*, 10.

- (26) Mann, E. K.; Henon, S.; Langevin, D.; Meunier, J. *Journal De Physique Ii* **1992**, 2, 1683.
- (27) Mann, E. K.; Henon, S.; Langevin, D.; Meunier, J.; Leger, L. *Physical Review E* **1995**, 51, 5708.
- (28) Zou, L.; Bernoff, A. J.; Mann, J. A.; Alexander, J. C.; Mann, E. K. *Langmuir* **2010**, 26, 3232.

Chapter 6

Summary and General Discussion

1. Summary of the thesis

The possibility of preparing 2D stable emulsions through mixing of homopolymers in a Langmuir monolayer is the core topic of this thesis. While colloid science has achieved well established results in the study of bulk dispersed systems, accounts on properties of mixed monomolecular films are fewer, and seldom systematic. The aim of this investigation is to contribute to a deeper understanding of the subject, in order to gain insight into fundamental science of 2D colloids, and to explore opportunities to apply the acquired knowledge to the fabrication of technologically relevant materials. In particular, this study focused on an innovative strategy which might be applicable to the manipulation of the morphology and the patterning of mixed Langmuir monolayers: the possibility to stabilize and control a dispersion of homopolymers through the addition of a lineactant (the equivalent of a surfactant in three dimensional systems), able to adsorb preferentially at the interfacial contact line of polymer domains, thereby lowering the interfacial energy (line tension) in the system and favoring an effective dispersion of one component into the other.

The state of the art of the preparation and investigation of 2D colloids is the subject of **Chapter 2**, which is a comprehensive review on several systems able to yield phase-separated Langmuir monolayers. This chapter includes a complete introduction of the field of research dealt with in this thesis: a general definition of the concept of a 2D colloid is provided, followed by a section that summarizes the most relevant instrumental techniques and experimental tools available for the investigation of these systems. The next sections extensively summarize several systems suitable for preparing 2D colloid dispersions, ranging from lipid-based systems (the first and most widely investigated), to short fluorinated amphiphiles and fluorinated and non-fluorinated polymer-based mixtures. The concept of lineactant is then introduced in a general way, and several examples, both experimental and theoretical, are presented, in which compounds acting as lineactants have been investigated. This review clearly shows that the polymer-based mixtures are a poorly explored subject, when compared to amphiphiles of natural origin, and so the rest of the thesis has been devoted to the investigation of polymer-based Langmuir monolayers.

This investigation has been carried out with two parallel approaches: classical experiments at the Langmuir trough and morphological characterization of the Langmuir monolayers with the Brewster Angle Microscope have been performed,

along with Self-Consistent Field modeling of the same systems. In order to do so, some reference experiments had to be carried out, so that the SCF model could be implemented on the basis of the results collected in these experiments. The setup of the SCF model and comparison of SCF calculation with experimental data from the reference experiments are dealt with in **Chapter 3**. Surface pressure isotherms at the air/water interface were reproduced for four different polymers, poly-*l*-lactic acid (PLLA), poly (dimethylsiloxane) (PDMS), poly (methyl methacrylate) (PMMA), and poly (isobutylene) (PiB). The polymers are all insoluble in water, but display a different degree of amphiphilicity; therefore the four isotherms differed strongly. To unravel the underlying details that caused these differences, molecularly detailed self-consistent field (SCF) modeling was performed. The polymers were described on a united atom level, taking the side groups on the monomer level into account. In line with experiments, the model shown that PiB spread in a monolayer which smoothly thickened at a very low surface pressure and area/monomer value. The monolayer made of PMMA had an autophobic behavior: a PMMA liquid did not spread on top of the monolayer of PMMA at the air/water interface. A thicker PMMA layer only formed after the collapse of the film at a relatively high pressure. The isotherm of PDMS had regions with extreme compressibility which were linked to a layering transition. Finally, PLLA wetted the water surface and spread homogeneously at larger areas per monomer. The classical SCF approach features only short-range, nearest-neighbor interactions. For the correct positioning of the layering and for the thickening of the polymer films, a power-law van der Waals contribution was taken into account in this model. Two-gradient SCF computations were performed to model the interface between two coexistent PDMS films at the layering transition, and an estimation of the length of their interfacial contact was obtained, together with the associated line tension value. The SF-SCF molecularly detailed modeling of PLLA, PDMS, PMMA, and PiB monolayers, spread at the air/water surface, has proven to be consistent with experimental data: the incorporation in the model of a detailed molecular description of the monomeric features of the four compounds examined has been crucial to reproducing the features of the adsorption and pressure/area isotherms. These isotherms were totally determined by the different molecular architecture of the polymers at the monomeric level and their consequent preferred orientation when spread at the air/water interface. The calculations support a new interpretation of the spreading phenomena occurring at the air/water interface, in terms of wettability of the interface by the spread polymer. In particular, PMMA has proved to be autophobic, due to the anisotropic orientation of its monomers on

the water surface, which prevented the growth of multiple layers upon compression. On the other hand, PDMS featured the occurrence of a layering phase transition, also experimentally observed. This process could be modulated by long-range interaction forces between the surface and the polymer segments. The correspondence between modeled and experimental pressure/area isotherms for PDMS has allowed to obtain new insights into the phenomenon of the layering transition: an estimation of the extension of the interfacial region between thick and thin PDMS film domains and the associated line tension have been obtained through two-gradient calculations. The molecularly detailed SCF approach has proved its general validity in the description of homopolymers with totally different spreading behavior.

In **Chapter 4**, the same approach was applied to the description of polymer mixtures spread at the air/water interface. The aim of this chapter was to analyze topics such as 2D phase separation and partitioning in mixed polymeric Langmuir monolayers. Two of the four polymers studied in Chapter 3 were selected in order to obtain a mixed Langmuir monolayer. A system consisting of water-insoluble, spreadable, fluid-like polymers was prepared. The polymers were polydimethylsiloxane (PDMS) and polymethylmethacrylate (PMMA), combined, in some cases, with a minority of PDMS-*b*-PMMA copolymer. Both Langmuir trough pressure/area isotherm measurements and Brewster angle microscopy (BAM) observations were performed, and complemented with molecularly detailed self-consistent field (SCF) calculations. It was shown that PDMS undergoes a layering transition that is difficult to detect by BAM. Addition of PMMA enhanced contrast in BAM, showing a two-phase system: if this consisted of separate two-dimensional (2D) PMMA and PDMS phases, a PDMS-PMMA diblock should accumulate at the phase boundary. However, the diblock copolymer of PDMS-PMMA failed to show the expected “lineactant” behavior, i.e., failed to accumulate at the phase boundary. The calculations pointed to a non-trivial arrangement of the polymer chains at the interface: in mixtures of the two homopolymers, in a rather wide composition ratio, a *vertical* (with respect to the air/water interfacial plane) configuration was found, with PMMA sitting preferably at the PDMS/water interface of the thicker PDMS film, during the PDMS layering phase transition. This also explained why the diblock copolymer was not a lineactant. Both PMMA and PDMS-*b*-PMMA were depleted from the thin-thick PDMS film interface, and the line tension between the phases consequently *increased* in the binary mixtures, as well as in the ternary ones. In this chapter it has been proven, both experimentally and with the aid of SCF modeling techniques, that a small amount

of PMMA homopolymer, added to a PDMS monolayer spread at the air/water interface, acts as a contrast enhancer of the PDMS layering transition. It was ruled out that the bright domains observed by BAM in mixed polymeric monolayers, during the PDMS phase transition, could be due to a phase segregation phenomenon occurring between PMMA and PDMS coils. Experimental evidence for that was obtained, showing that a diblock copolymer added to the mixture does not modify the formation of the domains or their morphology. Furthermore this hypothesis was corroborated with model calculations, using the SCF molecularly detailed model previously developed for polymer monolayers at the air/water interface, in Chapter 3. The results shown in this chapter proved that gaining an accurate control over thin film structures at the microscopic level is a far from trivial task, and the acquisition of fundamental knowledge is necessary in order to interpret experimental data in an appropriate way.

As a consequence, in **Chapter 5** an investigation based solely on SCF modeling was carried out, in order to analyze which polymer blends could have the possibility to undergo lateral phase separation in two dimensions. Specifically, the model system investigated consisted of water-supported Langmuir monolayers, obtained from binary polyalkyl methacrylate mixtures (PXMA, where X stands for any of the type of ester side groups used: M, methyl-; E, ethyl-; B, butyl-; H, hexyl-; O, octyl-; L, lauryl-methacrylate). In particular, the conditions which determined demixing and phase separation in the two-dimensional system were addressed, showing that a sufficient chain length mismatch in the ester side group moieties is able to drive the polymer demixing. When the difference in length of the alkyl chain of the ester moieties on the two types of polymers was progressively reduced, from 11 carbon atoms (PMMA/PLMA) to 4 carbons only (POMA/PLMA), the demixing tendency was also reduced; it vanished, indeed, for POMA/PLMA. In the latter case the polymer/subphase interactions affected more the distribution of the polymer coils in the blend monolayer: mixing of the two polymers was observed, but also a partial layering along the vertical direction.

Lineactancy was also considered, by selecting the mixture in which phase separation was best achieved: a third component, namely a symmetrical diblock copolymer of the type PLMA-*b*-PMMA, was added to a PMMA/PLMA blended monolayer. Adsorption of the diblock copolymer was observed exclusively at the contact line between the two homopolymer domains, together with a concomitant lowering of the line tension. The line tension varied with chemical potential of the diblock copolymer according to the Gibbs' law, which demonstrated that PLMA-

b-PMMA indeed acted as a lineactant (the two-dimensional analog of a surfactant) in the model system made of a binary demixed PMMA/PLMA Langmuir monolayer. In conclusion, the requirements needed to achieve polymer blend demixing in a Langmuir monolayer are the following: *spreadable, insoluble* polymers, with *the same amphiphilicity degree*, combined to a *certain chemical mismatch* of the side moieties *are necessary* in order to cause *lateral demixing* at the air/water interface. The polyalkyl methacrylate example investigated in the chapter represented a suitable model system, since the methacrylate backbone guarantees that the different polymers have the same affinity towards the water subphase, while the different ester moieties drive the occurrence of lateral demixing. The dependency of the lateral demixing on the difference in length between the two ester side groups chosen was demonstrated. A rather complex interplay of forces regulates the distribution of the polymer coils in the monolayer: subtle alterations of this complex balance might favor the dewetting of the mixture in a single domain, together with the layering of the blended polymers along the direction normal to the air/water interface, as well as accumulation of one polymer at the domain edge, instead of the occurrence of the lateral phase separation. Furthermore, the possibility to control emulsification of two-dimensional demixed polymer blends was proven. This was achieved by use of a diblock copolymer, which acted as a lineactant by adsorbing at the contact line of the polymer domains. The calculations demonstrated the possibility to extend the lineactant concept, first elaborated in the context of lipid membrane investigations, to the field of study of polymer thin films.

2. General Discussion and Outlook

The development of polymer-based systems where lineactants could be applicable would disclose opportunities to develop novel ways of regulating structuring and self assembly of complex structures in thin films. This thesis represents the first attempt to direct research on polymer-based Langmuir films towards this new direction. Future research directions in this topic might be experimental tests aimed at verifying the conclusions achieved through our model of polymethylmethacrylates, and further deepening, through SCF calculations, of the relationship between lineactant efficiency and molecular architecture of the diblock copolymer adopted.

In order to generalize the use of lineactants as a tool to regulate self-assembly in thin films, it is needed to investigate, in a systematic way, the molecular and structural characteristics of the homopolymers required to guarantee that phase separation of the polymer blend occurs exclusively along the interfacial air/water plane. This thesis has shown that so far this aspect has been largely neglected. Since the concept of lineactancy was born in the field of lipid-based Langmuir monolayers, its generalization and extension to the polymer realm is not a straightforward procedure. A crucial property which must be taken into consideration is the amphiphilicity of the chosen molecule: in systems based on natural lipid mixtures, or on synthetic short amphiphiles, such as fluorinated fatty acids, the amphiphilicity of molecules is mostly dependent on the type of polar headgroup present. In many cases these headgroups are the same, or very similar ones (mainly phosphate and carboxylate anions), and the molecular amphiphilicity is therefore also very similar. In these cases the formation of multilayers is easily prevented, in a sufficiently wide range of surface pressures, by a strong anchoring of the molecule polar headgroup to the water surface. Besides that, the fact that natural, or synthetic lipids are rather short molecules, reduces significantly the number of possible conformations and orientations assumed by the molecules in the monolayer. Overall, these properties undoubtedly make it simple to control the behavior of these systems directly.

When the type of control achieved by using lineactants in lipid-based monolayers must be translated to the context of polymer monolayers, and in particular to uncharged polymers, difficulties inevitably emerge, which are connected to the two issues of amphiphilicity and length of the molecules chosen. While lipids have a single polar extremity (often charged) anchored to the water surface, which largely drives the orientation of the rest of the molecule, polymers have multiple anchoring polar groups distributed along the chain, and therefore the conformations assumed by polymer coils at the surface are less predictable. In fact, polymers may already display a degree of amphiphilicity at the monomer level. If two types of polymers are mixed in a monolayer, the amphiphilicity of their coils depends on a complex ensemble of variables: number, type and spatial distribution of anchoring polar groups along the chain, overall orientation assumed by the coils on the water surface, interaction of the different functional groups of the two polymer types with each other and with the air/water interface. Different polymers will very rarely display exactly the same degree of amphiphilicity, due to the interplay of all these variables, and so they will not phase separate exclusively in the lateral direction, forming a 2D emulsion. This aspect restricts the possibility to

use polymer blends to form 2D colloids quite substantially, as a general approach towards nano-patterned films fabrication.

Nevertheless, in this work it has been shown that it is possible to overcome this substantial drawback, and prepare 2D colloids, by blending polymers that belong to the same chemical family: this provides the required matching of amphiphilicity. Phase separation can be driven, then, analogously to what happens with films made of short molecules, by using, on each type of polymer, lateral pending groups that are reciprocally incompatible: here it has been shown that a simple mismatch in the alkyl side chain length is sufficient to achieve phase separation. This possibility has been demonstrated here only through calculations, but it is successfully validated with some experimental data found in the literature. The successful use of a lineactant has been proven in the model, not in experiments, and the proof of these conclusions through experiments is the first and most important objective to be achieved for future research in this field. Successful experiments will have to overcome several technical difficulties: first, since the chemical nature of the polymer blend used is pretty similar, the BAM as a characterization tool becomes useless: no contrast between the two phases is obtainable if the refractive indexes are very similar. A good strategy might be the chemical functionalization of the polymers with fluorescent labels, combined to an *in situ* characterization performed directly at the air/water interface with adequate instrumentation. This would enable the study of dynamics of 2D colloids as a function of lineactant concentration and molecular structure, a largely unexplored, very interesting subject of research. Moreover, it would undoubtedly be interesting to investigate systematically which other chemically incompatible side groups might be introduced onto the polymer coils, to achieve phase separation: chain mismatch is a rather simple solution, but more complex strategies could be envisaged, such as π -stacking of aryl lateral groups, repulsions due to steric hindrance, non-covalent attractive interactions among groups of the same nature, such as H-bonds, or, finally, the use of lyophobic functional groups, such as (partially) fluorinated moieties.

The advantage of pursuing a patterning strategy based on lineactants is the possibility to avoid the exclusive use of diblock copolymers, or polymers with even more sophisticated architectures, to direct self-assembly into complex morphologies. However, from this thesis, it is concluded that a careful choice of the molecular structure, along with a certain amount of manipulation of the molecular architecture of polymers, is needed to obtain a successful outcome. Therefore this strategy is not so generally and widely applicable, but anyway it

represents a reasonable alternative to other approaches proposed up to now, which is worthy of further investigation, also for the sake of advancing fundamental science.

Notes

Samenvatting

Dit proefschrift onderzocht de mogelijkheid dat gestabiliseerde tweedimensionale (2D) emulsies kunnen worden gevormd door mengsels van homopolymeren in Langmuir films. Terwijl kolloidkunde gewone kolloidale systemen grotendeels bevredigend kan beschrijven, zijn eigenschappen van mengsels van homopolymeren in Langmuir films onvoldoende begrepen. Het doel van dit proefschrift is een diepere, fundamentele analyse van 2D kolloïden, en het onderzoeken van mogelijkheden voor praktische toepassingen, bijvoorbeeld als “smart” materialen. Wij hebben een innovatieve strategie geanalyseerd om gemengde Langmuir laagjes te patroneren door het toevoegen van een “contactlijn-actieve stof” (het equivalent van een oppervlakte actieve stof in 3D systemen), die kan worden geadsorbeerd aan de fasengrens tussen homopolymeerdomeinen. De lijnspanning kan worden verminderd door de lijn-actieve stof, waardoor een homopolymeer kan worden gedispergeerd in monolaag van het andere polymeer.

Hoofdstuk 2 behandelt de bereiding en studie van 2D kolloïden. Het hoofdstuk geeft een definitie van het concept van een 2D kolloïd, gevolgd door een uitvoerig overzicht van de methoden en de experimentele instrumenten gebruikt voor de studie van deze systemen. Daarna worden verscheidene systemen gepresenteerd die geschikt zijn voor de bereiding van een 2D kolloïd: lipiden-gebaseerde systemen (de eerste en meest populaire), korte gefluorineerde amfifielen, en ook combinaties van gefluorineerde polymeren met andere soorten van polymeren. Ten slotte wordt het concept van de lijn-actieve stof geïntroduceerd, met zowel theoretische als praktische voorbeelden. Dit overzicht laat duidelijk zien dat Langmuir laagjes gebaseerd op polymere mengsels minder zijn bestudeerd dan op lipiden gebaseerde mengsels. Daardoor onderzoeken we in dit proefschrift alleen Langmuir films van polymeer mengsels.

Twee methodes zijn gebruikt: Langmuir trog en Brewster Angle Microscope (BAM) experimenten, samen met Self Consistent Field (SCF) modelberekeningen aan dezelfde systemen. **Hoofdstuk 3** gaat over de opzet van de SCF berekeningen en de vergelijking met experimentele gegevens, verkregen via de referentie experimenten. De oppervlakedruk isothermen van vier homopolymeren zijn gemeten: poly-*L*-lactic acid (PLLA), poly (dimethylsiloxane) (PDMS), poly (methyl methacrylate) (PMMA), and poly (isobutylene) (PiB). De vier polymeren zijn onoplosbaar in water, maar verschillen in amphifiliciteit. De vier isothermen zijn daardoor heel verschillend. De functionele polymeergroepen zijn geïntroduceerd in de modelberekening, door middel van een “united-atom” aanpak.

De berekeningen komen goed overeen met de referentie experimenten: PiB spreidt in een monolaag die geleidelijk dikker wordt. De monolaag van PMMA is autofoob: Vloeibaar PMMA spreidt niet boven een PMMA monolaag. Een dikkere PMMA laag wordt alleen gevormd als de film instort, wat pas bij hogere druk gebeurt. De PDMS isotherm verhoont een gebied van hoge samendrukbaarheid: dat bewijst dat er een overgang is naar dikkere lagen. PLLA tenslotte bevochtigt de lucht/water grensvlak geheel, en spreidt homogeen wanneer het oppervlak per monomeer groot is. Het klassieke SCF model kent alleen korte afstand, nabuur wisselwerking interacties, maar Van der Waals interactie is nodig om een correcte positie van de PDMS overgang te krijgen. Twee-gradiënt SCF berekeningen zijn gedaan om de grens tussen een dikke PDMS laag en een dunne PDMS laag te modelleren. Een schatting van de lengte van de contactlijn en de betrokken lijnspanning gekregen werd. Het verdisconteren van van elk polymeer in het model is noodzakelijk om de druk/oppervlak isothermen en adsorptie isothermen te reproduceren, omdat de kenmerken van de isothermen afhankelijk zijn van de verschillende moleculaire structuren van de monomeren. Deze verschillende moleculaire structuren beslissend zijn voor de oriëntatie van de hele homopolymeer, wanneer het gespreid is op het lucht/water grensvlak. De resultaten van het model ondersteunen een nieuwe interpretatie van het spreiden op het lucht/water grensvlak, in termen van bevochtiging van het grensvlak door het gespreide polymeer. Het nieuwe SCF model met geïncorporeerde functionele groepen van monomeren, heeft zijn algemene geldigheid bewezen voor de beschrijving van homopolymeren met erg verschillende spreidingskenmerken.

In **hoofdstuk 4** is dezelfde strategie gebruikt om laagjes van mengsels van polymeren gespreid op het lucht/water grensvlak te beschrijven. Het doel van dit hoofdstuk is het analyseren van 2D fasescheiding in gemengde Langmuir polymeerlaagjes. Twee van de vier homopolymeren beschreven in hoofdstuk 3 werden hiervoor geselecteerd. De geselecteerde polymeren waren PDMS en PMMA. Soms worden beide polymeren gemengd met een kleine hoeveelheid van een derde co-polymeer, PDMS-*b*-PMMA. Zowel Langmuir trog experimenten als BAM experimenten werden uitgevoerd, met SCF berekeningen van dezelfde mengsels als complement. Wij lieten zien dat PDMS een overgang naar dikkere lagen maakt. Deze overgang is moeilijk te detecteren door BAM. Als PMMA wordt toegevoegd, wordt het contrast van de BAM afbeeldingen verbeterd en een 2D fasescheiding wordt zichtbaar. Als de PDMS en PMMA fasen zouden scheiden, zou de copolymeer PDMS-*b*-PMMA accumuleren op the grenslijn. Maar in de experimenten gebeurde dat niet. De SCF berekeningen toonden aan dat de

polymeren een bijzondere rangschikking hebben op het lucht/water grensvlak. Een *verticale* rangschikking van de polymeren (ten opzichte van het lucht/water grensvlak) werd gevonden: tijdens de PDMS overgang naar een dikkere laag zit PMMA op het PDMS/water grensvlak onder de gebieden met dikkere PDMS film. Dit is gevonden voor verschillende verhoudingen van PDMS en PMMA in het mengsel. Dit kan verklaren dat het copolymeer niet een lijn-actieve stof was in dit mengsel. De lijnspanning tussen de domeinen van dikke PDMS en de domeinen van dunne PDMS *verhoogde* beide mengsels met twee en drie polymeren, want zowel PMMA en PDMS-*b*-PMMA vermijden de grenslijn tussen de domeinen van dikke PDMS en domeinen van dunne PDMS. De resultaten van dit hoofdstuk hebben laten zien dat controle over de microscopische structuur van een gemengde Langmuir laag niet een gemakkelijke opgave is. Meer fundamentele wetenschappelijk onderzoek is nodig om de experimentele resultaten correct te verklaren.

Voortbouwend op deze conclusie presenteert **hoofdstuk 5** een studie waarin alleen SCF berekeningen zijn gebruikt om te ontdekken welke mengsels van polymeren geschikt zijn voor de bereiding van een 2D kolloïd. Een essentiële vereiste is dat de polymeren fasescheiden ten opzicht van het lucht/water grensvlak. We hebben een model gemaakt van gemengde Langmuir laagjes gespreid op water. De polymeren die wij gebruikt hebben in de modellen zijn polyalkyl methacrylate mengsels (PXMA, waar X staat voor elk van de types van de ester zij-groepen die gebruikt zijn: M, methyl-; E, ethyl-; B, butyl-; H, hexyl-; O, octyl-; L, lauryl-methacrylate). Wij hebben onderzocht welke voorwaarden nodig waren om horizontale 2D fasescheiden te krijgen, en hebben laten zien dat, als de ester groepen voldoende verschillende lengten hebben, de polymeren de gewenste fasescheiding kunnen geven. Als het lengtverschil tussen de estergroepen gereduceerd wordt, van 11 koolstofatomen (PMMA/PLMA) naar 4 koolstofatomen (POMA/PLMA), wordt de fasescheiding onderdrukt; POMA/PLMA vertoonde geen fasescheiding. In dit systeem hadden de interacties tussen het polymeer en het water grote invloed op de soort mengsel dat gevormd werd: menging van de polymeren werd waargenomen, maar ook een gedeeltelijke verticale segregatie. We keken ook naar lijn-activiteit, waarvoor we het sterkts fasescheidende mengsel kozen. Aan dat mengsel van PMMA en PLMA hebben wij een symmetrisch diblock copolymeer toegevoegd, PLMA-*b*-PMMA. Het copolymeer bleek uitsluitend geadsorbeerd op de grenslijn tussen de PLMA en PMMA domeinen. De lijnspanning werd tegelijkertijd minder. De lijnspanning nam af met stijgende

chemische potentiaal, volgens de wet van Gibbs, wat bewijst dat de PLMA-*b*-PMMA copolymeer inderdaad een lijn-actieve stof voor dit mengsel is.

We kunnen ten slotte concluderen dat de volgende vereisten nodig zijn om 2D fasescheiding binnen Langmuir films te krijgen: de polymeren moeten *onoplosbaar* zijn in water, ze moeten *spreiden op* het oppervlak van water, ze moeten *eveneens amfifiel* zijn, en ze moeten voldoende *verschillende chemische zijgroepen* hebben om fasescheiding te waarborgen. Een vrij ingewikkeld stelsel van interacties regelt de verdeling van verschillende polymeren binnen de monolaag. Subtiele veranderingen in dit evenwicht van interacties kan leiden tot “dewetting” van het mengsel en de oprichting van een enkel polymeerdomein, gepaard met de vorming van gescheiden lagen van verschillende polymeren in verticale richting, dan wel segregatie van een polymeer op de grenslijn van het andere polymeerdomein, in plaats van echte 2D fasescheiding. Bovendien hebben wij laten zien dat emulgeren van gemengde Langmuir polymeerlaagjes door het toevoegen van een lijn-actieve stof mogelijk is. De SCF modellen hebben gedemonstreerd dat ook het begrip “lijn-actieve stof”, dat aanvankelijk was ontworpen voor lipide membranen, kan worden uitgeheid tot Langmuir polymeerfilms.

Riassunto

Questa tesi esplora la possibilità di riuscire a preparare emulsioni su una superficie rigorosamente bidimensionale (ossia il cui spessore sia dell'ordine di grandezza di un singolo strato di molecole, un "monostrato"). Per raggiungere tale scopo, è necessario preparare un monostrato composto da una miscela binaria di polimeri, mediante un apparecchio denominato "bilancia di Langmuir", il quale consente di preparare e manipolare con sufficiente precisione film composti da un singolo strato di molecole, regolando a piacimento la densità del film e l'impaccamento delle molecole.

La scienza dei colloidali ha da tempo esplorato il tema della preparazione e stabilizzazione delle emulsioni, tuttavia, le proprietà dei film monomolecolari composti da miscele di sostanze fra loro insolubili non sono state oggetto di ampi e sistematici studi. Lo scopo di questa tesi è fornire un contributo in tal senso, in modo tale da delineare un percorso di ricerca di base che approfondisca il trattamento sistematico delle miscele colloidali in sistemi rigorosamente bidimensionali. Inoltre, si è cercato di stabilire se sia possibile applicare tali conoscenze allo sviluppo di nuove tecnologie atte a fabbricare materiali ad alto contenuto tecnologico. In particolare questa tesi ha voluto esplorare una strategia innovativa per l'eventuale manipolazione della morfologia e delle caratteristiche strutturali dei monostrati di Langmuir costituiti da miscele binarie di composti insolubili. Nel campo della scienza dei colloidali si ricorre all'uso di composti specifici per la stabilizzazione di un'emulsione, i cosiddetti "surfattanti", molecole dalle caratteristiche chimiche e strutturali speciali, le quali sono compatibili con entrambe le fasi, reciprocamente insolubili, che compongono una emulsione. Data la loro peculiare compatibilità, i surfattanti sono adsorbiti all'interfase delle due sostanze reciprocamente immiscibili, e in tal modo coadiuvano il processo di emulsificazione, rendendo possibile il mescolamento di sostanze altrimenti incompatibili. In questa tesi si è voluto provare a verificare se un meccanismo del tutto analogo può funzionare con altrettanta efficacia nel caso del monostrato bidimensionale, ossia se un cosiddetto "lineattante", dalla struttura compatibile con entrambi i componenti del film monomolecolare misto, può essere adsorbito lungo il perimetro dei domini di uno dei due componenti, agevolandone il mescolamento con l'altro.

Lo stato dell'arte nella preparazione e studio chimico-fisico di miscele colloidali bidimensionali é oggetto di esposizione nel **Capitolo 2**, una rassegna completa ed esaustiva di tutti i sistemi sperimentali in grado di formare miscele bifasiche, se distribuiti in film sottili all'interfase aria/acqua, corredata anche da una sezione esplicativa delle principali tecniche strumentali e sperimentali in uso per lo studio di tali sistemi. Inoltre viene definito in maniera generale il concetto di "colloide bidimensionale" e quello di "lineattante", con l'illustrazione di esempi, sia teorici sia pratici, presenti in letteratura. Dalle considerazioni finali di questo capitolo emerge chiaramente come i film sottili composti da miscele polimeriche siano scarsamente studiati, e necessitino di un'esplorazione piú accurata, al fine di stabilire se sono utilizzabili come colloidali bidimensionali, anche a scopo applicativo.

Il resto della tesi dunque si fonda sullo studio di monostrati di Langmuir a base polimerica, strutturato secondo due direzioni parallele: la preparazione sperimentale é infatti affiancata da un'indagine teorica effettuata mediante modelli computazionali. I parametri necessari per costruire il modello, secondo l'approccio detto del "Self Consistent Field", sono stati ottenuti mediante lo svolgimento di alcuni esperimenti di riferimento, cui sono stati comparati i risultati di diverse simulazioni, fino ad ottenere risultati coincidenti. Questo studio costituisce l'ossatura del **Capitolo 3**; la pressione di superficie é stata misurata, in condizioni isoterme, all'interfase aria/acqua, per quattro diversi polimeri di riferimento, con crescente grado di affinitá verso la fase acquosa: poli-isobutilene (PiB), polidimetilsilossano (PDMS), poli-metil-metacrilato (PMMA) e, infine, acido poli-lattico (PLLA). Le simulazioni eseguite al computer sono state effettuate seguendo il metodo di Self Consistent Field sviluppato da Scheutjens-Fleer (SF-SCF): i polimeri vengono descritti a livello di "raggruppamenti atomici", definendo parametri che descrivono le interazioni reciproche dei singoli gruppi funzionali all'interno del monomero che forma la molecola stessa. I risultati ottenuti mediante l'ottimizzazione dei parametri che regolano l'interazione dei vari gruppi funzionali presenti nei polimeri esaminati, coincidono a livello qualitativo con le isoterme misurate sperimentalmente. Il PiB forma un monostrato che aumenta di spessore in modo omogeneo solo quando é compresso fino a raggiungere valori di area/monomero disponibile molto ridotti, a bassa pressione superficiale. Il PMMA ha un comportamento "autofobico" ossia forma un monostrato sul quale ulteriori gocce di PMMA liquido non sono in grado di spandersi, bagnandolo. Solo a valori

di pressione di superficie molto elevati il monostrato di PMMA collassa su se stesso, formando multistrati. Il PDMS ha regioni di comprimibilità molto elevata, indice del verificarsi di una transizione da un monostrato a un multistrato. Infine, il PLLA ha elevata affinità con l'acqua e si spande in modo omogeneo su di essa, formando un monostrato uniforme, a valori di area/monomero molto elevati. Nel modello SCF classico le interazioni dei "raggruppamenti atomici" sono a corto raggio, e avvengono solo con i più vicini "raggruppamenti atomici" circostanti. Per ottenere la riproduzione della transizione da monostrato a multistrato del PDMS è stato necessario considerare un ulteriore contributo a queste interazioni, nella forma di una forza di interazione con decadimento esponenziale in funzione della distanza, di tipo analogo alle interazioni di van der Waals. Calcoli a doppio gradiente sono stati usati per modellizzare l'interfase fra il film sottile (monostrato) di PDMS e quello spesso (multistrato), in coesistenza, durante la transizione. Una stima della lunghezza della regione di contatto interfasale è stata ottenuta, e con essa si è calcolata la tensione di linea (analogo alla tensione di superficie) fra il perimetro dei domini di monostrato e di multistrato di PDMS in contatto reciproco. Perché la coincidenza fra modello e esperimento sia adeguata, è cruciale riprodurre i diversi polimeri nei loro dettagli strutturali, ponendo attenzione alle differenti caratteristiche chimiche dei gruppi funzionali che formano le unità monomeriche.

Nel **Capitolo 4** si è applicato lo stesso procedimento alla descrizione di monostrati costituiti da una miscela binaria di PDMS e PMMA. Lo scopo di questo capitolo è di analizzare la possibilità di ottenere una emulsione bidimensionale, mescolando dapprima questa coppia di polimeri, e usando poi la miscela ottenuta per effettuare la preparazione di un monostrato di Langmuir. I due polimeri selezionati sono stati scelti sulla base dei risultati illustrati nel precedente capitolo, in quanto entrambi sono insolubili in acqua, possono formare un monostrato all'interfase aria/acqua, e sono reciprocamente immiscibili. Gli esperimenti condotti alla bilancia di Langmuir, corredati da osservazioni effettuate mediante il Brewster Angle Microscope (BAM), hanno dimostrato che la transizione da monostrato a multistrato del PDMS è di difficoltosa osservazione mediante questo tipo di microscopia. L'aggiunta di PMMA invece consente di aumentare il contrasto, ed al microscopio è chiaramente visibile un sistema bifasico: se questo sistema fosse una emulsione bidimensionale di PDMS e PMMA, l'aggiunta di un polimero formato da due blocchi coniugati PDMS-*b*-PMMA, dovrebbe causare l'emulsificazione dei componenti, causando la scomparsa delle due fasi visibili al

microscopio. Tuttavia il sistema oggetto di studio é rimasto bifasico anche in seguito all'aggiunta del "lineattante" PDMS-*b*-PMMA, che evidentemente non si é adsorbito efficacemente lungo il perimetro dei domini osservati. Le simulazioni effettuate hanno mostrato che la distribuzione dei polimeri PDMS e PMMA nella miscela binaria é totalmente differente da quanto ipotizzato all'inizio dell'esperimento. In realtà i due polimeri, anziché ripartirsi in due fasi distinte all'interno di un monostrato, formano un multistrato misto, sovrapponendosi l'uno all'altro, il quale coesiste con un monostrato di PDMS. Il lineattante, in questa configurazione, si localizza all'interno dei domini del multistrato, e non sul perimetro fra il monostrato ed il multistrato. Per questo motivo l'emulsificazione non può aver luogo. In questo capitolo si dimostra dunque quanto il controllo a livello molecolare della struttura di film sottili a base polimerica é sperimentalmente difficile da ottenere, in quanto le interazioni reciproche fra i polimeri che compongono la miscela non sono state mai oggetto di indagine sistematica: é pertanto necessario che la ricerca in questo campo sia approfondita ulteriormente, prima di poter essere in grado di utilizzare questi materiali a fini applicativi.

Di conseguenza, nel **Capitolo 5** si illustra uno studio teorico, basato sui modelli precedentemente elaborati, teso a determinare quali sono le condizioni necessarie a garantire che una miscela di polimeri formi un monostrato, nel quale i componenti della miscela diano luogo a una separazione di fase esclusivamente lungo la direzione parallela all'interfase aria/acqua, senza stratificarsi lungo la direzione normale all'interfase aria/acqua. In base a dati di letteratura ed alle osservazioni fatte durante lo studio delle miscele binarie PDMS/PMMA, si é deciso di simulare il mescolamento di coppie di polialchil-metacrilati (PXMA, dove X rappresenta un qualsivoglia dei seguenti gruppi funzionali usati, M, metil-, E, etil-, B, butil-, H, esil-, O, ottil- o L, lauril-metacrilato a seconda dei singoli casi). Si dimostra dunque che le miscele binarie di metacrilati danno luogo a separazione di fase, formando due fasi distinte e adiacenti all'interno del monostrato, qualora le catene alchiliche dei gruppi pendenti laterali siano di lunghezza sufficientemente dissimile. Quando la differenza di lunghezza dei gruppi pendenti -COOR viene progressivamente ridotta, da 11 atomi di carbonio (miscela di PMMA/PLMA) a 4 (miscela di POMA/PLMA), la separazione di fase é meno netta, fino a scomparire nel caso della miscela POMA/PLMA. In quest'ultimo sistema, le interazioni tra polimero e fase acquosa influenzano la distribuzione

complessiva delle catene polimeriche all'interfase molto più delle repulsioni fra i due tipi di polimeri che si verificano all'interfase stessa. I due polimeri, POMA e PLMA, si dissolvono l'uno nell'altro, e danno luogo a una parziale stratificazione lungo la direzione normale all'interfase aria/acqua. L'aggiunta di un lineattante alla miscela PMMA/PLMA, la quale forma la migliore emulsione bidimensionale, è stata simulata nei calcoli, introducendo un terzo componente, ossia un polimero a blocchi di tipo PMMA-*b*-PLMA, simmetrico. Tale polimero si adsorbe esclusivamente lungo il perimetro dei domini di PLMA, dispersi in una fase continua formata da PMMA, e diminuisce in maniera apprezzabile la tensione di linea del sistema. In particolare, la variazione della tensione di linea rispetto al potenziale chimico del lineattante obbedisce all'equivalente dell'equazione di Gibbs in sistemi bidimensionali. Resta dunque dimostrato, in via teorica, che è possibile ottenere un colloide bidimensionale, in cui due polimeri immiscibili si organizzano rigorosamente in un monostrato dove la separazione fra le due fasi distinte avviene esclusivamente lungo una direzione parallela all'interfase aria/acqua. Tale sistema colloidale è stabilizzato dall'aggiunta di un agente emulsificante, il lineattante, la cui struttura di polimero a blocchi garantisce piena compatibilità con entrambe le fasi tra loro immiscibili, e il suo esclusivo adsorbimento lungo la linea di confine fra tali fasi.

In conclusione, i *requisiti indispensabili* perché una miscela binaria di polimeri dia luogo a *separazione di fase all'interno di un monostrato di Langmuir* sono i seguenti: i polimeri scelti, seppur *insolubili in acqua*, debbono *essere in grado di bagnare la superficie acquosa*, espandendosi su di essa fino a formare un monostrato, ed *entrambi essere caratterizzati dallo stesso grado di anfifilicità*, ossia devono avere la stessa affinità per l'acqua. *Quest'ultimo parametro è cruciale per impedire la loro sovrapposizione e stratificazione lungo la direzione normale all'interfase aria/acqua*. Infine, *entrambi debbono avere gruppi funzionali che garantiscano un certo grado di repulsione fra i due tipi di catena polimerica*. Questo parametro è *fondamentale perché all'interno del monostrato stesso abbia luogo la separazione di fase*. L'esempio dei polialchil-metacrilati qui presentato rappresenta una felice combinazione di tutti i requisiti sopra esposti. Qualora i requisiti siano tutti soddisfatti, è possibile formare un colloide bidimensionale e stabilizzarlo con l'aggiunta di un lineattante, come è stato dimostrato nel capitolo 5. Finora nessuno ha mai provato la validità di un tale principio in sistemi costituiti da film sottili di miscele di polimeri. I calcoli presentati in questa tesi

Riassunto

rappresentano la prima dimostrazione scientifica di tale principio, che in futuro potrebbe trovare una definitiva conferma sperimentale.

Curriculum Vitae

Cecilia Bernardini was born in Como in 1983, the first of her family unfortunate enough to have been born north of the 45°N. Following in the footsteps of one of the most famous natives of Como, Alessandro Volta, she attended the homonymous *liceo classico* (secondary school for classical languages), Como's most renowned secondary school, located in a historic building featuring original Roman columns (always covered with students' graffiti) and a church dedicated to Saint...Cecilia, of course. After successfully sitting the final exams in the sultry June 2002 (a three-day ordeal including the translation of an excerpt of Cicero's *De amicitia*), Cecilia hung up her full mark (100/100) diploma and chose to try her hand at something different from Latin and Greek. Caught in the dilemma over what university course to follow, she finally opted for Chemistry at the *Università degli Studi di Milano*. Despite her non-scientific background, Cecilia was able to overcome the first year's student-killers (Math, Physics, Chemistry) and the heat wave of June 2003 (35°C in the Organic Chemistry lab, sheathed in a haze of solvent vapours) to get on track to obtain her BSc degree. Her final thesis was completed under the supervision of Prof. P.R. Mussini and dealt with the "*Combined voltammetric and capacitive study of specific adsorption of halide anions on surface-controlled polycrystalline silver electrode in paradigmatic organic solvents*". Cecilia presented her thesis at the final viva in October 2005 and was awarded the BSc degree with full marks (110/110) *cum laude*. Then, she went on to attend the MSc Chemistry course; however, she grew tired of the boring everyday routine, and so she successfully applied for an *Erasmus* scholarship, flying out to the Netherlands to join Dr. A. Kros' research group SMC (Soft Matter Chemistry) at Leiden University in January 2006. The six-month research project was focussed on "*The peptides' coiled-coil motif in self-assembly*" and let Cecilia become familiar with peptide synthesis, supramolecular chemistry and TEM microscopy. Once she returned to Italy, she resumed the regular course, without going astray as many Erasmus students do, and joined Prof. E. Selli's group for a one-year research project, investigating the "*Effect of structural properties of titanium dioxide on its photocatalytic activity in aqueous phase*". After countless flashes of UV light through the photochemical reactor, she successfully defended her thesis and obtained her MSc degree with full marks (110/110) *cum laude* in December 2007. Afterwards, Cecilia took no heed of the voices trying to talk her out of a PhD project and moved to the Netherlands again, first to Unilever R&D in Vlaardingen for a three-month training internship, then to Wageningen to start her PhD, an opportunity to escape from Milan's infamous suspended particulate matter and photochemical smog. Her project was aimed at redefining the concept of 3D emulsification via surface-active agents on a 2D scale. You can read the results of this work in the hundreds of pages that precede this CV...

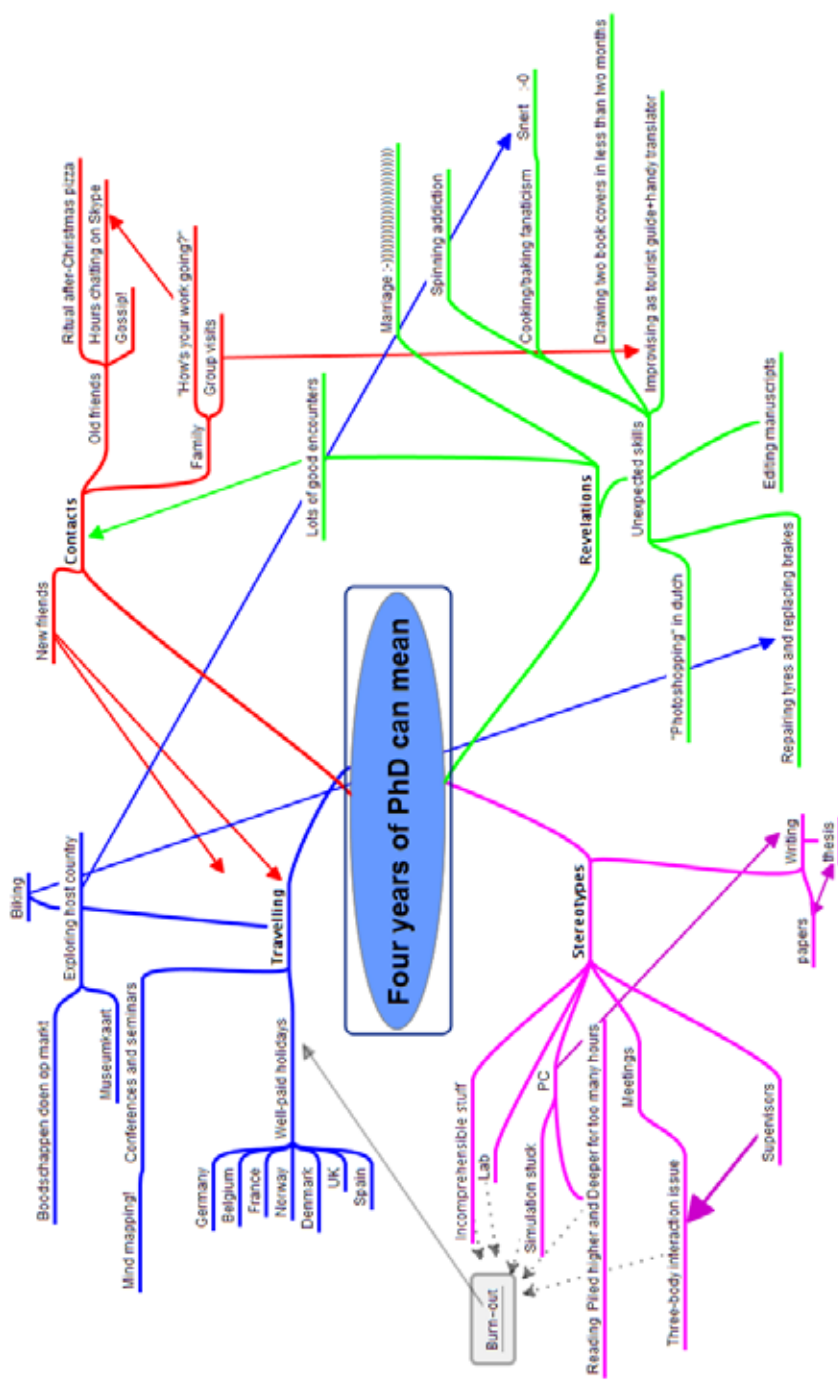
List of publications

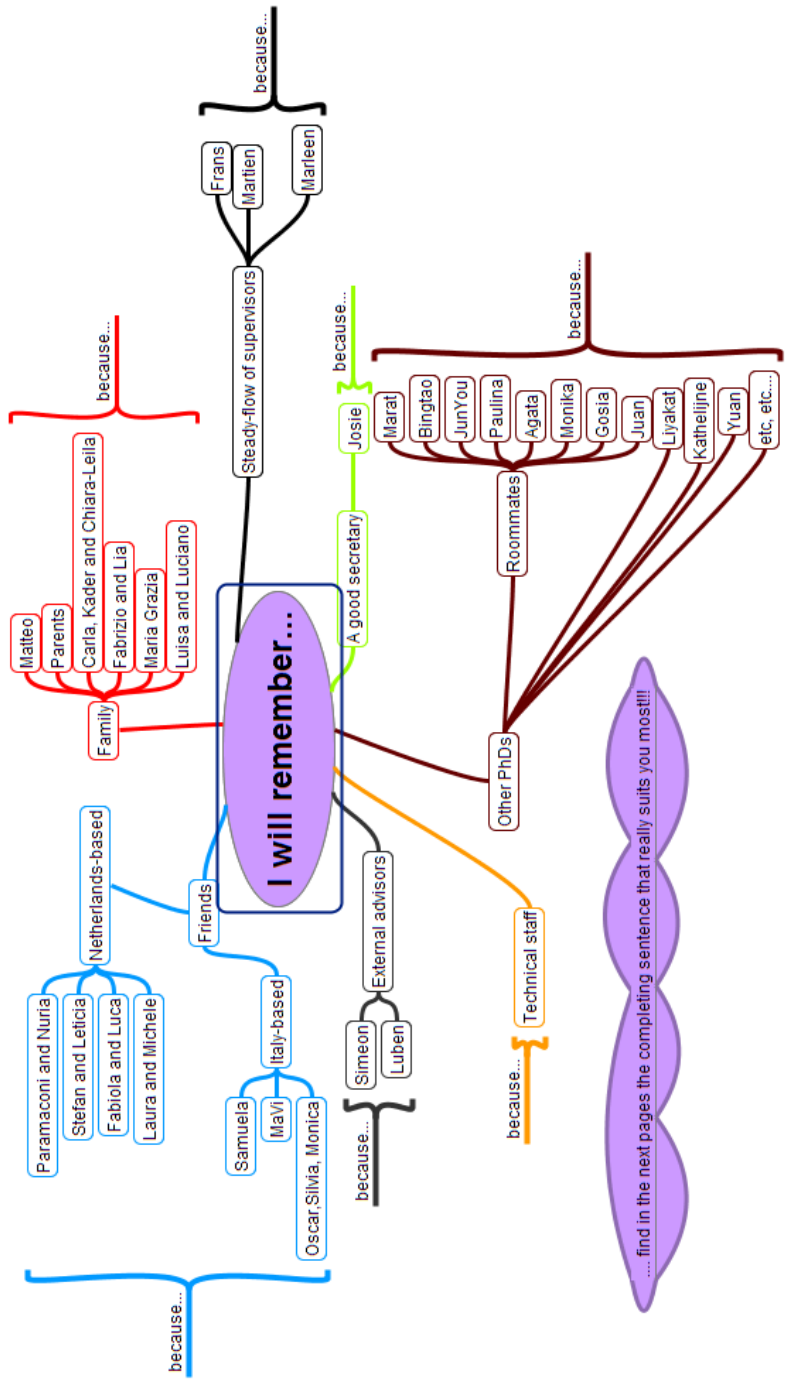
- Ü Bernardini C., Cappelletti G., Dozzi M. V., Selli E., “Photocatalytic degradation of organic molecules in water: photoactivity and reaction paths in relation to TiO₂ particles features”, *Journal of photochemistry and photobiology A-chemistry* **2010**, *211*, 185-192. **DOI:** 10.1016/j.jphotochem.2010.03.006
- Ü Bernardini, C., Stoyanov, S. D., Stuart, M. A. Cohen, Arnaudov, L. N., Leermakers, F. A. M., “Polymers at the Water/Air Interface, Surface Pressure Isotherms, and Molecularly Detailed Modeling”, *Langmuir* **2010**, *26*, 11850-11861. **DOI:** 10.1021/la101003c
- Ü Bernardini, C., Stoyanov, S. D., Stuart, M. A. Cohen, Arnaudov, L. N., Leermakers, F. A. M., “PMMA Highlights the Layering Transition of PDMS in Langmuir Films”, *Langmuir* **2011**, *27*, 2501-2508. **DOI:** 10.1021/la104285z
- Ü Bernardini, C., Stuart, M. A. Cohen, Stoyanov, S. D., Arnaudov, L. N., Leermakers, F. A. M., “Polymer Compatibility in Two Dimensions: Modeling of Phase Behavior of Mixed Polymethacrylate Langmuir Films”, accepted for publication in *Langmuir*. **DOI:** 10.1021/la2040642
- Ü Bernardini, C., Stoyanov, S. D., Stuart, M. A. Cohen, “Two-Dimensional Colloids: Preparation, Characterization and Research Perspectives”, in preparation.

Afterword

I was at a loss for words.....

And then somebody told me: “A picture is worth one thousand words.”





you shared with me lots of funny and wonderful moments during our MSc internship, and afterwards too, besides having the courage to get through a PhD in Italy...

your kindness and your discrete friendship as a PhD colleague and roommate

of a portable Chinese-English translator that made very funny trying to talk with you!

we have shared together experiences as PhD students, good moments when living in the Netherlands, and even our marriages!

we chatted about work and life as PhD colleagues

you have given invaluable support to Matteo over these years, and sincere friendship to both of us: muchas gracias querido!

you have been a really good friend to both Matteo and me, taking part in some of the most memorable moments of our life in these four years

your enigmatic smile when talking about my project, forecasting all the troubles I would have gone through in these four years, and your passion for De Andrè songs

of your kindness and friendship, and your availability when I needed advice over my work-related troubles

of your constant reminding me that having an husband is more important than getting a PhD

you have patiently beared the almost infinite “cahier de doléances” of 3 different PhD students around you without getting crazy: instead we had group therapy based on 1)talking about Japanese cartoons of the ‘80s, 2)wii competitions, 3)lasagne or risotto lunches!

even though you had to deal with the classical “aap op de schouder” issue, you made it with a smile and a supportive and encouraging approach

you have been always so close to my heart and so empathic!!! Or, (as they like to say about you) you can be the human version of a dog that wags its tail...:-D

You provided me with humane support and you have shown interest in me as a person and not just as a working student

You provided me with a living example of the Schrödinger’s cat paradox...

you have shown me
where extreme ambition
might lead...

your kindness and
sensitivity, and your
trustful and friendly
approach to people,
besides your willingness
to be my paranymph!

you constantly keep in
touch with us despite
the long distance and
the years gone by

of your politeness, the chats at
coffee-breaks, and your patience
in walking me through the never-
ending corridors of the Louvre

of shared group-
meetings, coffee-
breaks, PhD trips,
or beers and chats
during a party

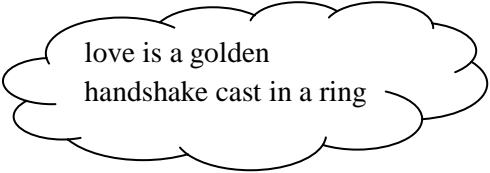
you palmed off a FIAT on me
(Fix It And Toil), instead of a
BMW...

you were so trustful in a positive
outcome of my work and your
self-confidence and positive
attitude have been inspiring to me

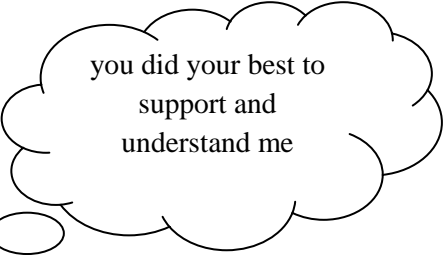
of your energy and enthusiasm for
your research, your italian charm,
and your cheerfulness!

you showed me
mistakes I'll try to
avoid

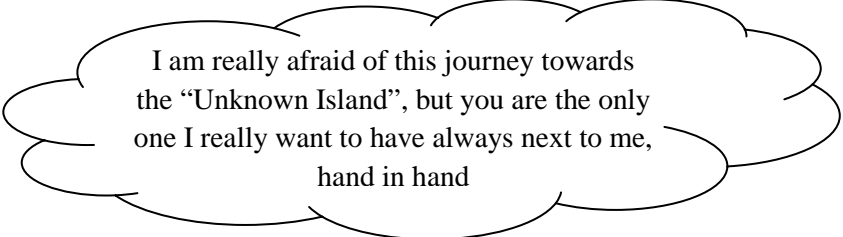
your friendship is a safe shelter across the border,
when everybody around me speaks a language I
don't understand



love is a golden
handshake cast in a ring



you did your best to
support and
understand me



I am really afraid of this journey towards
the “Unknown Island”, but you are the only
one I really want to have always next to me,
hand in hand

Overview of completed training activities

Discipline-specific Courses

Han-sur-Lesse winterschool "Physical Chemistry", Belgium, 2008

COST school on surface analytical techniques, Dresden, 2009

Conferences and Meetings

ESA EU Foam conference, Leiden, The Netherlands, 2008

Symposium "Dynamics in self-organised systems", Wageningen, The Netherlands, 2009

ECIS conference Antalya, Turkey, 2009

KNCV Symposium Energy and Polymers, Wageningen, The Netherlands, 2009

Delft discussion on Soft Matter, The Netherlands, 2010

8th Soft Matter Meeting Wageningen, The Netherlands, 2010

FOM Symposium "Women in science" –Arnhem, The Netherlands, 2010

Willem Norde farewell symposium, Wageningen, The Netherlands, 2010

9th Soft Matter Meeting Leiden, The Netherlands, 2010

NWO - Veldhoven meeting, The Netherlands, 2011 [#]

2nd COST action meeting on biological adhesives, Mons, Belgium, 2011 ^{*}

Frontiers in polymer science, Lyon, France, 2011 ^{*}

General Courses

ELCAT Meeting "Gender issues and interviewing skills" –Reading, UK, 2010

KNCV Career Advice Activity-Amsterdam, The Netherlands, 2010

Course Communication with the media and the general public, 2010

Career Assessment, 2010

Course Effective behaviour in the workplace, 2010

Philosophy and Ethics in Food Science and Technology, 2011

Interpersonal Communication for PhD students, 2011

Career perspectives, 2011

Techniques for Writing and Presenting a Scientific Paper, 2011

Scientific publishing, 2011

Other Activities

PhD trip, Switzerland and France, 2009

Advanced Soft Matter course, 2009

Group meetings 2008-2010

[#] Oral contribution

^{*} Poster contribution

The research described in this thesis was financially supported by NWO through an ECHO grant.

Cover idea and design by Cecilia Bernardini

“Loosening the Third Dimension”, inspired by “Fontana Monumentale” in Piazza Camerlata (Como), by Cesare Cattaneo and Mario Radice.

Printed in Ede by GVO | Ponsen & Looijen, March 2012